Function and Pharmacological Modulation of the Epilepsy-Associated $K_{Na}1.1$ (*KCNT1*) Potassium Channel

Bethan Aimee Cole

Submitted in accordance with the requirements of the degree of Doctor of Philosophy

The University of Leeds
School of Biomedical Sciences

September 2021

The candidate confirms that the work submitted is her own, except where work which has formed part of jointly authored publications has been included. The contribution of the candidate and the other authors to this work has been explicitly indicated below. The candidate confirms that appropriate credit has been given within the thesis where reference has been made to the work of others. This copy has been supplied on the understanding that it is copyright material and that no quotation from the thesis may be published without proper acknowledgement.

Chapter 1 contains work from one jointly-authored review paper:

Cole, B.A., Clapcote, S.J., Muench, S.P., and Lippiat, J.D. 2021. Targeting K_{Na}1.1 channels in *KCNT1*-associated epilepsy. *Trends in Pharmacological Sciences* **42**(8), p.700-713.

The candidate wrote the initial draft of the manuscript and was involved in the subsequent editing. J.D. Lippiat assisted in writing and editing the manuscript and producing figures, and all authors were involved in proof-reading of the manuscript.

Chapter 3 contains work from one jointly-authored paper published as a pre-print in 2021:

Cole, B.A., Pilati, N., and Lippiat, J.D. 2021 Epilepsy-causing *KCNT1* variants increase K_{Na}1.1 channel activity by disrupting the activation gate. *BioRxiv* [preprint].

The candidate conducted all experimental work and molecular biology, produced all figures except for Figure 1., and drafted the manuscript with J.D. Lippiat. J.D. Lippiat produced Figure 1. J.D. Lippiat and N. Pilati supervised and helped conceptualise the project, and helped with proof-reading and editing the manuscript.

Chapter 5 contains work from one jointly-authored paper published in 2020:

Cole, B.A., Johnson, R.M., Dejakaisaya, H., Pilati, N., Fishwick, C.W.G., Muench, S.P., and Lippiat, J.D. Structure-Based Identification and Characterization of Inhibitors of the Epilepsy-Associated KNa1.1 (*KCNT1*) Potassium Channel*. iScience* **23**(5), p.101100 (2020).

The candidate carried out electrophysiology work, cytotoxicity assays, mutagenesis to create epilepsy-causing pathogenic variants, and subcloning of channel pore mutants into pcDNA6 vector. R.M. Johnson carried out virtual high throughput screening of small molecule compound library and short-listed compounds, J.D. Lippiat carried out *in silico* docking of existing inhibitors and identified possible binding residues, and H. Dejakaisaya carried out mutagenesis to create pore mutants. Other authors supervised and helped conceptualise the project, and helped with reviewing and editing the manuscript.

Acknowledgements

Firstly I would like to thank my supervisor, Jon Lippiat, for providing me with the opportunity to work on this project, all of the support over the last few years and for being a very patient electrophysiology mentor. Thanks to Nadia Pilati, Ste Muench, Steve Clapcote and Sue Deuchars for all of your help and advice that has been essential for this thesis and my development as a scientist.

Thank you to BBSRC and Autifony Therapeutics Ltd. for funding this work.

Thanks to past and present members of the Lippiat lab; Catherine, Laura, Dan, Emma and Matt, for putting up with and understanding the many highs and lows that come with being an electrophysiologist, and providing constant entertainment (and emotional support) in the lab.

To Maia, Maddie and Louise, for the lunchtimes in the Miall social space, Little Tokyo trips and more recently the support group chat that kept me going through writing this thesis- I am so proud of us for getting to this point in our PhDs in one piece.

Thanks to my parents, who support and inspire me throughout everything I do in life, and are always there to pick up the pieces/ the phone in times of stress and feign interest in ion channels so well (and kindly moved to Cornwall, enabling me to write this thesis by the sea!). To my siblings, Rhiannon and Ieuan- you bring me back down to Earth regularly. To all of my beautiful-souled friends in and out of Leeds who make life fun outside of work and never fail to ask “how are your cells doing?”.

Finally, to Harry Wing Young. For your belief in me, without which this thesis may have never been completed. For all the love and support you give me every day, your unparalleled ambition and excitement for our future adventures.

Abstract

Gain-of-function missense pathogenic variants of *KCNT1,* the gene encoding the sodium-activated potassium channel subunit $K_{Na}1.1$, are associated with intractable early-onset epilepsies. Variants in diverse regions of the channel are hypothesised to interfere with channel gating, although the mechanisms of gating are poorly defined. Patients are heterozygous and there is a lack of information about how pathogenic variants increase channel activity and also the behaviour of heterotetrametric channels comprised of wildtype and variant subunits. Inhibition of hyperactive $K_{Na}1.1$ channels with class I antiarrhythmic quinidine has had variable success in patients due to low potency, non-selectivity and poor blood-brain-barrier penetration.

Seven disease-causing variants were selected from across the spectrum of disorders and involving different protein domains. Whole cell electrophysiology was used to characterise homomeric and heteromeric $K_{Na}1.1$ channel assemblies carrying epilepsy-causing variants expressed in CHO cells. We found that all disease-causing $K_{Na}1.1$ variants lowered the energetic barrier associated with the sodium-dependent activation gate by destabilising the inactivated channel conformation. Some variants also had effects on selectivity filter gating. Using the previously determined cryo-EM structure of $K_{Na}1.1$ and mutational analysis, we identified how quinidine binds within the intracellular pore vestibule. Using *in silico* methods and whole cell electrophysiology, six small molecule compounds and four FDA-approved drugs were identified that inhibit $K_{Na}1.1$ channels with low- and sub-micromolar potency. Finally, using mutagenesis and whole cell electrophysiology, six residues involved in Na^+-activation were identified, located on the cytoplasmic RCK (regulators of conductance of K^+) domains.

The results provide a common mechanism for how disease-causing variants cause gain-of-function. In addition to providing more information about the gating of $K_{Na}1.1$, identification of the Na^+-activation mechanisms will aid development of alternative drug modalities in future. We have identified potential therapeutic drugs that could be repurposed for treating *KCNT1*-related epilepsies, or possible pharmacophores that could be starting points for developing potent and selective inhibitors.

Table of contents

List of figures

List of tables

List of abbreviations

(AD)SHE	Autosomal-dominant or sporadic sleep-related hypermotor epilepsy
AA	Arachidonic acid
ADR-1	Activated disease resistance protein 1
AHP	Afterhyperpolarisation
ALS	Amyotrophic lateral sclerosis
AMPA	α-amino-3-hydroxy-5-methyl-4-isoxazolepropionic acid
ANS	Autonomic nervous system
ASM	Arterial smooth muscle
ASO	Antisense oligonucleotide
ATP	Adenosine-5'-triphosphate
BBB	Blood-brain-barrier
CADD	Computer-aided drug discovery
cDNA	Complementary DNA
CDS	Coding sequence
CHO	Chinese hamster ovary
CNS	Central nervous system
COX-2	Cyclooxygenase-2
Cryo-EM	Cryogenic electron microscopy
CSF	Cerebrospinal fluid
DEE	Developmental and epileptic encephalopathy
DMEM	Dulbecco's Modified Eagle's Medium
DMSO	Dimethyl Sulfoxide
DRG	Dorsal root ganglion
DTT	1,4-dithiothreitol
EC_{50}	Half-maximal effective concentration
ECG	Electrocardiogram
EDTA	Ethylenediaminetetraacetic acid
EGTA	Ethylene glycol-bis(β-aminoethyl ether)-N,N,N′,N′-tetraacetic acid
EIMFS	Epilepsy of infancy with migrating focal seizures
EYFP	Enhanced yellow fluorescent protein
fAHP	Fast afterhyperpolarisation
FDA	Food and Drug Administration
FMRP	Fragile X mental retardation protein
GABA	Gamma-aminobutyric acid
GC	Guanine-cytosine
GHK	Goldman-Hodgkin-Katz
GIRK	G-protein coupled inwardly-rectifying
GOF	Gain-of-function
GPCR	G protein-coupled receptor
HEK	Human embryonic kidney
HEPES	4-(2-hydroxyethyl)-1-piperazineethanesulfonic acid
hERG	Human *ether-à-go-go*
HMG-CoA	3-hydroxy-3-methyl-glutaryl-coenzyme A
HRP	Horseradish peroxidase
IC_{50}	Half-maximal inhibitory concentration
IED	Interictal epileptiform discharge
INap	Persistent inward Na^+ current
iPSC	Induced pluripotent stem cell
K2P	Two-pore or tandem-pore K^+ channel
KO	Knockout
LOF	Loss-of-function

MD	Molecular dynamics
MEA	Multi-electrode array
MNTB	Medial nucleus of the trapezoid body
mRNA	Messenger RNA
MSR	Macrophage scavenger receptor
nAChR	Nicotinic acetylcholine receptor
NAD^+	Nicotinamide adenine dinucleotide
NALCN	Non-voltage-activated Na^+ channels
NMR	Nuclear magnetic resonance
PAINS	Pan assay interference
PBS	Phosphate buffered saline
PCR	Polymerase chain reaction
PIP_2	Phosphatidylinositol bisphosphate
PKA	Protein Kinase A
PKC	Protein Kinase C
PMA	Phorbol 12-myristate 13-acetate
P_o	Probability of opening
PP1	Protein phosphatase 1
PTZ	Pentylenetetrazole
RCK	Regulators of conductance of K^+
RMP	Resting membrane potential
SDS	Sodium dodecyl sulfate
T2A	Thosea asigna virus 2A
TAE	Tris-acetate-EDTA
TEA^+	Tetraethylammonium ions
TPA	12-O-Tetradecanoylphorbol-13-acetate
TRAAK	TWIK related arachidonic acid activated K^+ channel
TREK	TWIK related K^+ channel
TWIK-1	Tandem of pore domains in a weak inward rectifying K^+ channel
UTR	Untranslated region
VSD	Voltage-sensing domain
WST-1	Water-soluble tetrazolium-1
WT	Wildtype

1 General introduction

1.1 Potassium channels

Potassium channels are the most diverse of the ion channel family, encoded for by 80 genes in mammals, and are characterised by their strong selectivity for K^+ ions. They enable K^+ ion permeation across the plasma membrane along their electrochemical gradient by moving between active, resting and inactive states, and are critical in the propagation of action potentials. The asymmetrical gradient of K^+ concentration across the plasma membrane in excitable cells means that K^+ channels usually have an equilibrium potential of ~-90 mV, determined by the Nernst equation, and upon opening efflux of K^+ ions results in hyperpolarisation; shifting membrane potential away from the threshold for Na^+ channel opening (Hille, 2001). Structurally, all members of the K^+ channel family possess a pore-forming region which is largely conserved, and diversity arises from regulatory domains which enable the channels to respond to external stimuli such as voltage or ligands (Coetzee et al., 1999; Gonzalez et al., 2012).

1.1.1 How K^+ selectivity and permeation arises

K^+ channels have selectivity in the order of; $K^+ \approx Rb^+ > Cs^+$ and negligible Na^+ and Li^+ selectivity. Whilst K^+ channels show great structural diversity between families, almost all share a common selectivity filter amino acid motif within the pore-forming region (TVGY/FG) that confers their high K^+ ion selectivity (Heginbotham et al., 1994; Doyle et al., 1998). Some variation in the selectivity filter sequence can be tolerated; for example the sequence in human *ether-à-go-go* (hERG) channels is SVGFG (Wang and MacKinnon, 2017). The selectivity filter motif was first identified by mutational analysis based on sequence comparisons between voltage-gated K^+ channels and cyclic nucleotide-gated channels, which are not K^+ selective (Heginbotham et al., 1994). This motif was later corroborated by the first crystal structure of a K^+ channel, KcsA, from *Streptomyces lividans,* and is located at the interface of four subunits in a tetramer. Selectivity filter-lining carbonyl groups point into the pore-forming cavity, forming four consecutive K^+ binding sites (S1-4). It was proposed that selectivity arises as hydroxyl oxygens on the carbonyl backbone of the selectivity filter replace the shell of six H_2O molecules bound to each fully hydrated K^+ ion serially, as they pass through the S1-4 binding sites (Doyle et al., 1998). The ions become hydrated again once they exit the selectivity filter. A “soft knock-on” permeation mechanism later became the

widely accepted model, wherein two K^+ ions occupy two of the four selectivity filter occupancy sites, but are separated by a co-permeating water molecule, moving through the selectivity filter with a water:ion ratio of 1. K^+ ions either occupy S1 and 3 or S2 and 4, and a K^+ ion arriving at the start of the chain pushes the ions occupying the selectivity filter through, resulting in outward K^+ flux. It was thought that since Na^+ is too small to be coordinated by the selectivity filter, binding is thermodynamically unfavourable due to its smaller diameter (Morais-Cabral et al., 2001; Doyle et al., 1998; Zhou et al., 2001).

Recent advances have provided a new possible explanation for how K^+ channels maintain both high selectivity and permeation rates. Through atomistic molecular dynamics (MD) simulations and re-analysis of KcsA crystallography data, it was revealed that K^+ ions permeate through the selectivity filter completely desolvated. Electrostatic repulsion between adjacent ions causes a “direct knock-on” effect (Kopec et al., 2018; Kopfer et al., 2014). Whilst it was previously thought that each K^+ ion was accompanied by one water molecule in the selectivity filter, the recent findings demonstrated that water co-permeating in the pore would in fact reduce conduction efficiency. A study using solid-state nuclear magnetic resonance (NMR) to probe the selectivity filter of NaK2K, an engineered K^+-selective channel, also highlighted that the S1-4 binding sites are devoid of water under physiological conditions (Oster et al., 2019). It is more likely that the K^+ ions form pairs at neighbouring binding sites, enabling the coulombic “knock-on” permeation. The strong interactions between the desolvated K^+ ions prevent permeation of competing Na^+ ions, giving rise to high K^+ selectivity (Kopec et al., 2018).

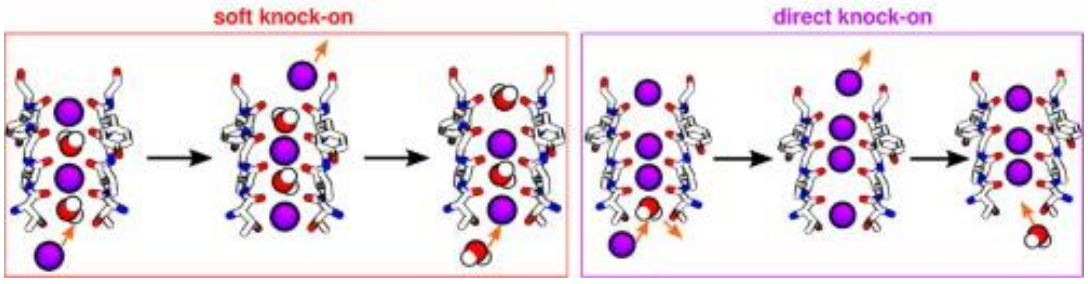

Figure 1.1: The two proposed permeation mechanisms for potassium channels. The soft knock-on (left) mechanism involves K^+ ions moving through the selectivity filter separated by co-permeating water molecules. Two of the four selectivity filter binding sites are occupied at any one time. The hard knock-on (right) mechanism involves K^+ ions moving through the selectivity filter desolvated, with electrostatic repulsion between adjacent ion enabling movement (Mironenko et al., 2021).

1.1.2 Members of the K^+ channel family

K^+ channels are usually grouped into three main structural classes based upon topology of the alpha subunit; subunits with two, four, and six transmembrane (TM) domains. Within these structural classes there are five main subfamilies; K_{ir} (2-TM domains), K2P (4-TM domains and two pores) and K_v, SK, and SLO channels (all 6-TM domains). K^+ channel subunits assemble to form tetramers composed of four monomeric alpha subunits, or in the case of K2P channels, two pseudo-dimeric subunits (Coetzee et al., 1999; Gonzalez et al., 2012).

K_{ir} channel subunits have two transmembrane domains flanking the pore-forming region and are characterised by inward rectification following membrane depolarisation. This is a result of an open-channel block by blocking ions or linear polyamines such as spermine, that penetrate into the pore to limit K^+ conduction following release from a shallow cation binding site (Hibino et al., 2010). K2P (two-pore or tandem-pore) channels possess, as the name implies, two pore-forming regions per subunit, and four transmembrane domains. They are modulated by numerous stimuli, such as pH, temperature and stretch, and are important in setting RMP and regulating excitability (Enyedi and Czirják, 2010). K_v channels, or voltage-gated channels, are the largest subfamily of K^+ channel subunits, spanning from K_v1.x-K_v12.x. Channels belonging to the K_v subfamily have six transmembrane domains and possess an excess of positively charged residues on their S4 domain, forming the voltage-sensing domain (VSD). The fourth subfamily of K^+ channels is the high-conductance SLO subfamily, one member of which forms the basis of this thesis and is discussed in detail in the following sections.

1.1.3 The Slo subfamily of potassium channels

K^+ channels belonging to the SLO subfamily display unusually high conductance and are encoded for by four genes in mammals. The Slo1 channel (K_{Ca}1.1 or BK_{Ca}) for example, has a unitary conductance of 250 pS in symmetrical 100 mmol/L K^+ concentrations (Table 1.1). Whilst these channels bare some similarities to delayed rectifier K_v channels, SLO channels are modified by other factors such as Ca^{2+}, Na^+, Cl- and pH, distinguishing them from other voltage-gated channels (Salkoff et al., 2006).

K_{Ca}1.1 was the first identified member of the SLO subfamily and is activated both by intracellular Ca^{2+} and voltage. This channel possesses a seventh transmembrane domain, termed S0, meaning its N-terminus lies on the cytosolic side of the cell

membrane. Slo2.1 (K_{Na}1.2) and Slo2.2 (K_{Na}1.1) are closely related and are activated primarily by intracellular Na^+ and weakly by voltage. These two channels underlie Na^+-activated K^+ currents (IK_{Na}). Unlike K_{Ca}1.1 and pH sensitive K_{Ca}5.1 (Slo3) subunits, K_{Na}1.1 and K_{Na}1.2 lack a canonical VSD defined by positively charged residues on their S4 domains (Kaczmarek, 2013).

Table 1.1: Four members of the SLO K^+ channel family.
[Adapted from (Salkoff et al., 2006)].

Channel	Names	Gene	Chromosomal location	Unitary conductance
Slo1	BK, K_{Ca}, K_{Ca}1.1, maxi-K	*KCNMA1*	10q22	100-270 pS
Slo2.1	Slick, K_{Na}1.2, K_{Ca}4.2	*KCNT2*	1q31.3	60-140 pS
Slo2.2	Slack, K_{Na}1.1, K_{Ca}4.1	*KCNT1*	9q34.3	100-180 pS
Slo3	K_{Ca}5.1	*KCNU1*	8p11.2	70-100 pS

1.2 Slo2.2

KCNT1 is the gene encoding the largest known K^+ channel subunit, K_{Na}1.1 (previously K_{Ca}4.1) , which forms tetrameric Na^+-activated K^+ channels otherwise known as Slo2.2 or Slack ('Sequence like a Ca^{2+}-activated K^+ channel') (Joiner et al., 1998). At least 60 *de novo* and inherited missense pathogenic *KCNT1* variants are associated with severe, pharmacoresistant epilepsies in children; that are accompanied by psychomotor and intellectual disabilities (Bonardi et al., 2021). Epilepsy of infancy with migrating focal seizures (EIMFS) and autosomal-dominant or sporadic sleep-related hypermotor epilepsy ((AD)SHE) are two examples, but a number of other developmental and epileptic encephalopathies (DEE) have also been identified (Barcia et al., 2012; Heron et al., 2012). Channelopathies of K^+ channels arise from both loss- and gain-of-function pathogenic variants in a number of epilepsies (Villa and Combi, 2016), although DEE-causing *KCNT1* variants appear to cause significantly more severe clinical phenotypes. There is an increasingly large phenotypic spectrum associated with *KCNT1* pathogenic variants and no specific antagonists acting on the channel, making both prediction of disease outcome and treatment difficult (Bonardi et al., 2021).

1.3 Structure and properties of $K_{Na}1.1$ channels

$K_{Na}1.1$ subunits have structural similarities to $K_{Ca}1.1$ channels, the high conductance Ca^{2+}-activated K^+ channels from which their name is derived; although the channels in fact only have ~7 % sequence homology. $K_{Na}1.1$ subunits also share some structural similarities with the K_v family of K^+ channels, which are voltage-gated. Each $K_{Na}1.1$ subunit possesses six transmembrane alpha helices (S1-6) and a re-entrant pore loop between the S5 and 6 domains containing the selectivity filter (Hite et al., 2015; Hite and MacKinnon, 2017).

The channel is weakly voltage-gated, with current amplitude recorded in whole cell patch clamp experiments increasing with depolarisation. The mechanisms underlying this are yet to be resolved since, unlike $K_{Ca}1.1$ and K_v channels, $K_{Na}1.1$ does not possess an excess of positively charged residues located on the S4 domain conferring voltage sensitivity. In contrast to the mobile S4 helix that enables voltage-sensing of K_v channels, structures of the chicken $K_{Na}1.1$ channel show that the S4 domain is in contact with the pore-forming region, and is in a different orientation despite having a similar helical structure (Hite et al., 2015; Hite and MacKinnon, 2017). There are six fewer residues on the S4 domain of $K_{Na}1.1$ channels (Santi et al., 2006), and in place of the positively charged residues present in other voltage-gated channels, $K_{Na}1.1$ channels have two positively and two negatively charged residues. Mutation of the equivalent residues in $K_{Na}1.2$ had no effect on voltage-dependence of the channel (Dai et al., 2010), therefore it is likely that another mechanism enables voltage-activation.

Other K^+ channels lacking an excess of positively charged residues on the S4 domain have been shown to have voltage sensitivity; for example, two-pore K^+ channels (K2P) such as TREK-1, TREK-2 (TWIK related K^+ channel 1 and 2) and TRAAK (TWIK related arachidonic acid activated K^+ channel). These channels were previously thought to be purely ‘leak’ channels (Lesage and Lazdunski, 2000), and the non-linear outwardly rectifying current-voltage relationship was thought to arise from the large K^+ gradient across cell membranes according to the Goldman-Hodgkin-Katz (GHK) equation (Goldman, 1943; Hodgkin and Katz, 1949). However, the channels also show some voltage and time-dependent gating. It has been proposed that voltage-sensing is tightly coupled to the electrochemical gradient, evidenced by a shift in the half-maximal activation voltage in parallel with changes in reversal potential. Changes in transmembrane voltage force K^+ ions into the selectivity filter ion occupancy sites, causing the channel to be in an “ion-occupied” state. This state is unstable and leads to

outward K^+ flux, and the permeating state is voltage-independent. Outward movement of K^+ ions leads to channel opening, and inward movement inactivates the channel (Schewe et al., 2016).

$K_{Na}1.1$ has a large intracellular C-terminal domain containing two RCK domains (regulators of conductance of K^+), a characteristic of all SLO subfamily members, and multiple putative sites for phosphorylation by protein kinase C (PKC), which is potentially a regulator of the channel (Santi et al., 2006; Bhattacharjee et al., 2003; Barcia et al., 2012). The C-terminal domain also contains a nicotinamide adenine dinucleotide (NAD^+) binding domain that is believed to be involved in modulating channel function (Tamsett et al., 2009). Whilst $K_{Na}1.1$ channels are weakly voltage-sensitive, the primary activator of these channels is intracellular Na^+. The EC_{50} for Na^+-activation is 40 mM in symmetrical K^+ solutions (Bhattacharjee et al., 2003), and in the absence of Na^+, WT $K_{Na}1.1$ channels show almost no activity in whole cell patch clamp experiments (Bhattacharjee and Kaczmarek, 2005; Rizzo et al., 2016). The EC_{50} values reported are measured in excised patch experiments however, and therefore NAD^+ was missing from the intracellular solution. When NAD^+ was applied to the cytoplasmic face of channels excised from rat dorsal root ganglion (DRG) neurons, an increase in probability of opening (P_o) was seen, and a decrease in the EC_{50} for Na^+-activation from 50 to 17 mM (Tamsett et al., 2009).

The RCK domains of $K_{Na}1.1$ have importance in conferring Na^+-sensitivity of the channel, and mutation of residues located on these domains has been shown to alter Na^+-sensitivity of the channel (Zhang, Z. et al., 2010). Rat (r)H823 and rD818 [human (h)H844 and hD839] are part of a putative Na^+ binding motif, DXRXXH (where X can be any amino acid), which is conserved with that of G protein-coupled inwardly-rectifying K^+ (GIRK) channels (Zhang et al., 2010; Whorton and MacKinnon, 2011). It is likely that other residues are involved however, since a small amount of Na^+ sensitivity is retained when these residues are mutated (Zhang et al., 2010). Furthermore, the model proposed for Na^+-activation does not align with the later resolved cryo-EM structure of the chicken $K_{Na}1.1$ channel (Hite and MacKinnon, 2017).

$K_{Na}1.1$ channels can be identified by large, outwardly rectifying macroscopic currents, and display an instantaneous component followed by a time dependent component (Bhattacharjee et al., 2003). The channels have varying reported unitary conductance of 88-180 pS in heterologous expression systems, although they can enter into multiple subconductance states (Brown et al., 2010; Bhattacharjee et al., 2003; Bhattacharjee

and Kaczmarek, 2005). It is believed that their unusually high K^+ conductance arises from a funnel of negatively-charged glutamate and aspartate sidechains lining the pore-forming region, making the inner surface of the gating ring formed by RCK1 and 2 domains highly electronegative (Hite et al., 2015). This is similar to the molecular basis of high conductance of $K_{Ca}1.1$ channels (Tao et al., 2017).

1.4 Localisation and role of $K_{Na}1.1$ in normal physiology

1.4.1 Central Nervous System

$K_{Na}1.1$ and $K_{Na}1.2$ have distinct patterns of expression throughout the central nervous system (CNS) but can form heteromeric assemblies in regions where their expression is overlapping. In normal physiology, K_{Na} channels have been implicated in three different roles. K_{Na} channels have been shown as being involved in generating the slow afterhyperpolarisation (AHP) that follows single action potentials, both in rat hippocampal CA1 pyramidal cells (Liu, X. and Stan Leung, 2004) and intrinsically bursting neurons in slices of the rat sensorimotor cortex (Franceschetti et al., 2003). In principle neurons of the medial nucleus of the trapezoid body (MNTB), K_{Na} channels generate an AHP following bursts of action potential firing, regulating inter-burst timing and accuracy of firing (Yang et al., 2007).

$K_{Na}1.1$ channels are widely distributed throughout the CNS of rodents. In the mouse brain the highest levels of immunoreactivity for a non-specific pan-Slack antibody were seen in the olfactory bulb, the lateral septal nuclei, basal ganglia, midbrain, brainstem and the cerebellar cortex (Rizzi et al., 2016). In the rat brain there were some differences, though an antibody for only one amino-terminal isoform of the channel, Slack-B, was used. The highest levels of expression were seen in the olfactory bulb, frontal cortex, forebrain, thalamus, midbrain, deep cerebellar nuclei and brainstem (Bhattacharjee et al., 2002).

1.4.2 Peripheral Nervous System

Despite being imperative in generating the slow AHP in many neuron types, outside of the CNS K_{Na} channels are important in stabilising the resting membrane potential in a number of excitable cells. $K_{Na}1.1$ is almost ubiquitously expressed in the somata and axonal tracts of small, medium and large diameter DRG neurons (Tamsett et al., 2009),

and in K_{Na} KO mice, threshold for action potential generation of dissociated DRG neurons is reduced, and action potential firing is elevated (Martinez-Espinosa et al., 2015). In mouse cochlear spiral ganglion neurons, K_{Na} channels contribute at subthreshold voltages and hold the resting membrane potential at hyperpolarised potentials (Lee et al., 2019; Reijntjes et al., 2019).

1.4.3 Cardiovascular System

$K_{Na}1.1$ expression has been demonstrated in rat ASM cells and K_{Na} channels were first identified in guinea pig cardiomyocytes (Kameyama et al., 1984). K_{Na} channels are potentially the most important determinant of resting membrane potential and intrinsic excitability of arterial smooth muscle (ASM) cells; a role that has been overlooked. In K_{Na} knockout (KO) mice, resting K^+ conductance of ASM cells is reduced, which leads to a higher probability of response to excitatory stimuli such as sympathomimetic drugs. Upon administration of phenylephrine, the KO mice show a large increase in blood pressure compared to WT mice. When the ASM cells are studied in the current clamp mode, Ca^{2+}-dependent action potentials are more easily evoked; again suggesting that the resting K^+ conductance is reduced, and implicating K_{Na} channels as a regulator of excitability (Li et al., 2019).

1.5 Na^+-activation of $K_{Na}1.1$

Intracellular Na^+ is an absolute requirement for $K_{Na}1.1$ activation, although the concentration of Na^+ required to activate channels is considerably higher than that found in the cytoplasm at rest (Tamsett et al., 2009). Considering the abundance of evidence associating $K_{Na}1.1$ with the resting K^+ conductance of a number of cell types (Lee et al., 2019; Reijntjes et al., 2019) (Martinez-Espinosa et al., 2015; Li et al., 2019) there must be a Na^+ supply enabling activation of these channels at rest.

Outside-out excised patch recordings from the soma of mitral cells from the rat olfactory bulb have demonstrated a coupling between $K_{Na}1.1$ channels and a persistent inward Na^+ current (INap) mediated by re-opening voltage-gated Na^+ channels. It has been proposed that this persistent Na^+ current occurs even at rest, and results in higher Na^+ concentration locally to $K_{Na}1.1$ channels compared to the bulk cytoplasmic Na^+ concentration (Hage and Salkoff, 2012). In line with this, in murine ASM cells, a persistent Na^+ leak current is thought to arise from non-voltage-activated Na^+ channels

(NALCN) in the vicinity of $K_{Na}1.1$ (Li et al., 2019). Another study has shown $K_{Na}1.1$ channels to be functionally coupled to AMPA (α-amino-3-hydroxy-5-methyl-4-isoxazolepropionic acid) receptors in both rat synaptic fractions and lamprey CNS lysates. Co-immunoprecipitation experiments confirmed the two channels were located in close vicinity of one another, and it was shown electrophysiologically that $K_{Na}1.1$ channels can be activated by Na^+ transients through AMPA receptors. AMPA and $K_{Na}1.1$ have a negative feedback relationship, which serves to regulate excitatory synaptic potentials (Nanou et al., 2008).

1.6 Amino isoforms of $K_{Na}1.1$

To date, five known isoforms in $K_{Na}1.1$ have been identified in rodents. The isoforms differ in their amino terminal region and arise as a result of alternative splicing of mRNA, which is detailed in Table 1.2. The channel is encoded for by upwards of 30 exons; following the third exon the coding region is shared between all five isoforms. Neuronal expression of the isoforms is likely controlled by distinct promoters (Brown et al., 2008).

Table 1.2: Five isoforms of $K_{Na}1.1$ that have been identified in mice, and the differences in their mRNA 5' transcripts.
Slack-A and Slack-Ax2 have a small first exon, 1a, located 13.8 bp upstream of the bigger first exon of Slack-B and Slack-Bx2, 1b. Slack-M lacks exons 1a or 1b and exon 2; with translation beginning just upstream of exon 3. $K_{Na}1.1$ contains upwards of 30 exons. The different mRNA features translate to disparities in the amino termini of the channel isoforms (Brown et al., 2008).

$K_{Na}1.1$ isoform	mRNA 5' transcript features
mSlack-A	114 bp 5'UTR before translation Exon 1a (93 bp), exon 2 (42 bp), exon 3
mSlack-Ax2	114 bp 5'UTR before translation Exon 1a (93 bp) linked directly to exon 3
mSlack-B	15 bp 5'UTR before translation Exon 1b (153 bp), exon 2 (42 bp), exon 3
mSlack-Bx2	15 bp 5'UTR before translation Exon 1b (153 bp) linked directly to exon 3
mSlack-M	1.2 kb 5'UTR before translation Exon 3

Two of the rodent $K_{Na}1.1$ subunit isoforms have been expressed and functionally characterised. Termed Slack-A and B, despite having the same unitary conductance, these isoforms with differing initiating sequences have distinct kinetic and structural properties (Brown et al., 2008). Slack-A channels have a smaller N-terminus than Slack-B and are activated rapidly. Slack-B channels on the other hand, activate much more slowly and are involved in generating rhythmic firing patterns in neurons; contributing to oscillatory currents generated during sleep. The Slack-A isoform enters subconducting states more frequently than Slack-B; which has a mean open time that is around six times longer than that of Slack-A (Brown et al., 2008; Kaczmarek, 2013). The N-terminus of Slack-A more closely resembles that of the $K_{Na}1.2$ channel, which also displays the fast activation kinetics and frequent entry into subconducting states observed in Slack-A channels (Bhattacharjee and Kaczmarek, 2005). The two isoforms of $K_{Na}1.1$ have differential expression in the CNS, with Slack-A having more widespread expression. Limited Slack-B immunoreactivity was detected in hippocampal regions and the olfactory bulb previously (Bhattacharjee et al., 2002) whereas, use of a non-specific pan-Slack antibody in the mouse brain showed more immunoreactivity in these regions than a Slack-B antibody alone (Brown et al., 2008).

1.7 Regulatory proteins of $K_{Na}1.1$

The large intracellular C-terminus of $K_{Na}1.1$ possesses a number of residues that enable interaction of the channel with cell signalling partners. These protein-protein interactions may contribute to the effects of GOF epilepsy-causing pathogenic variants on normal channel function, or be altered as a result of DEE-associated variants. It is thus important to understand the nature of these interactions as they may prove to be a useful therapeutic target.

1.7.1 Protein Kinase C

As discussed earlier, the C-terminus of $K_{Na}1.1$ has 13 consensus sites for phosphorylation by PKC, which potentiates activity of the rat $K_{Na}1.1$ channel. Alanine scanning experiments have revealed the serine residue rS407 in the rat $K_{Na}1.1$ channel sequence to be the most critical site for phosphorylation (hS426). rS407A $K_{Na}1.1$ channels expressed in *Xenopus* oocytes were insensitive to the PKC activator, 12-O-Tetradecanoylphorbol-13-acetate (TPA) (Barcia et al., 2012). Co-immunoprecipitation experiments have shown that $K_{Na}1.1$ subunits are localised in close proximity to muscarinic M1 receptors in the frontal cortex of rats. Furthermore, macroscopic

currents recorded from rat $K_{Na}1.1$ channels expressed in *Xenopus* oocytes were augmented upon activation of co-expressed M1 receptors with oxytremorine. The M1 receptor, which is widely distributed in the CNS, is a Gq-coupled G protein-coupled receptor (GPCR) and PKC is activated downstream in its signalling cascade (Santi et al., 2006). This modulatory effect of PKC on $K_{Na}1.1$ is controversial however, since phosphatidylinositol bisphosphate (PIP_2) is hydrolysed by G_q pathway activation, but has also been shown to potentiate $K_{Na}1.1$ currents (de los Angeles Tejada et al., 2012). Furthermore, a study looking at the human WT $K_{Na}1.1$ channel found the channel to be significantly inhibited by another PKC activator, Phorbol 12-myristate 13-acetate (PMA) (Milligan et al., 2014). It is possible that PKC potentiation of $K_{Na}1.1$ channels is specific to the rodent channel.

1.7.2 Protein Kinase A

Protein Kinase A (PKA) has a more indirect modulatory effect on the channel compared to PKC. As opposed to directly interacting with the C-terminus of the channel, PKA rapidly internalises $K_{Na}1.1$ channels expressed on the membrane of rat DRG primary nociceptive neurons, decreasing K_{Na} current without impacting the gating behaviour of $K_{Na}1.1$. This rapid internalisation is thought to contribute to the aberrant firing of nociceptive neurons in inflammatory pain states, when the PKA pathway is activated upstream by inflammatory substances such as prostaglandin E2. Suppression of $K_{Na}1.1$ using siRNAs increases excitability of DRG primary nociceptors, confirming the role of $K_{Na}1.1$ in preventing hyperexcitability (Nuwer et al., 2010).

1.7.3 Phosphatidylinositol bisphosphate

WT rat $K_{Na}1.1$ channels expressed in *Xenopus* ooctyes can be activated by exogenous application of two isoforms of PIP_2; $PI_{(3,4)}P_2$ and $PI_{(4,5)}P_2$. Furthermore, modulation of endogenous PIP_2 levels using inhibitors reduces the activity of $K_{Na}1.1$. Mutation of rK339 on the RCK1 domain, which is conserved in the human $K_{Na}1.1$ channel (hK358), almost completely abolished PIP_2 activation of the channel and is the putative site for PIP_2 binding (de los Angeles Tejada et al., 2012).

1.7.4 Phactr1

$K_{Na}1.1$ has been shown in rats to be co-localised with Phactr1, a protein with high expression in cerebral cortical neurons, that recruits protein phosphatase 1 (PP1) (Ali

et al., 2020). WT $K_{Na}1.1$ currents recorded from HEK293-T (human embryonic kidney) cells are suppressed by co-expressed phactr1, and it is hypothesised that this happens via PP1-mediated dephosphorylation of the channel. Mutation of rS407 (hS426), the critical PKC phosphorylation residue on the C-terminus of $K_{Na}1.1$, to alanine rendered the channel insensitive to suppression by Phactr1 (Ali et al., 2020). It has been postulated that when PKC translocates to the membrane and phosphorylates $K_{Na}1.1$ at rS407, Phactr1 is dissociated from the C-terminus along with PP1. This dissociation promotes the potentiation of $K_{Na}1.1$ current by PKC phosphorylation (Fleming et al., 2016).

1.7.5 Fragile-X Mental Retardation protein

Fragile X mental retardation protein (FMRP) is an mRNA-binding protein that interacts with a site on the C-terminus of $K_{Na}1.1$ and acts as a potent activator of the channel (Brown et al., 2010; Zhang, Y. et al., 2012). The protein acts by increasing $P_{o,max}$ and reducing likelihood of the channel entering into subconducting states in single channel recordings when $K_{Na}1.1$ is expressed in *Xenopus* oocytes. Furthermore, dissociated MNTB neurons from FMRP-/y mice lacking the protein show a decrease in K_{Na} current (Brown et al., 2010).

1.7.6 TMEM16C

TMEM16C is a transmembrane protein that is closely related to Ca^{2+}-activated Cl- channels, TMEM16A and TMEM16B, and small conductance, Ca^{2+}-activated non-selective cation channel TMEM16F. Unlike other members of the TMEM16 family however, TMEM16C is not a functioning ion channel when expressed alone. In rat DRG nociceptive neurons, TMEM16C is expressed alongside $K_{Na}1.1$, and directly interacts with the channel to potentiate it by increasing its Na^+-sensitivity. This interaction results in dampened nociceptive firing, which is confirmed by increased mechanical and thermal pain sensitivity in TMEM16C KO mice, as a result of reduced $K_{Na}1.1$ current size (Huang et al., 2013).

1.7.7 SCYL-1

Activated disease resistance protein 1 (ADR-1) mediated RNA editing of the 3' untranslated region (UTR) of SCYL-1 has been shown to potentiate SLO-2, the C. elegans equivalent of $K_{Na}1.1$, by promoting interaction of SCYL-1 with the C-terminus of the channel. ADR-1 is a transcriptional activator, and SCYL-1 is a transcriptional

regulator belonging to the SCY1-like family of kinase-like proteins. This results in increased probability of opening, an effect which is also seen when SCYL-1 and human $K_{Na}1.1$ are co-expressed in *Xenopus* ooctyes. Expression patterns of the two proteins do not largely overlap, although they are co-expressed in the hippocampus and cerebellum in the mouse brain. It is thus likely that the effects of SCYL-1 on $K_{Na}1.1$ activity are localised to specific cell types, and the regulatory protein is not an absolute requirement for channel function (Niu et al., 2020).

1.8 Gating mechanisms of potassium channels

The gating mechanism of $K_{Na}1.1$ is yet to be determined. Cryo-EM data for the structure of chicken $K_{Na}1.1$ has shown that the channel may exist in several different 'closed' conformations that are independent of Na^+-binding. However, one conformation was dependent on Na^+ concentration, and is believed to be the "open" conformation; the probability of channels existing in this conformation against intracellular Na^+ concentration showed a sigmoidal relationship (Hite and MacKinnon, 2017).

The opening and closing of K^+ channels in response to various stimuli, such as ligand binding, pH and voltage, is known as gating. An effective K^+ channel gate that maintains strict control of K^+ flux has recently been defined as one that is; A) sensitive to stimuli such as extra- and intracellular signalling, B) able to increase or decrease the energetic barrier to conduct K^+ ions and C) does not affect the structural integrity of the selectivity filter (Black et al., 2021). Channels move between active, deactivated and inactivated states. Inactivation of K^+ channels, which is usually stimulus-independent, happens either by fast, autoinhibitory "N-type" inactivation (Zagotta et al., 1990) or "C-type" inactivation which is mediated by structural changes within the selectivity filter (Cuello et al., 2010). It was previously accepted that K^+ channels such as the K_v subfamily, KcsA and K_{ir} channels share a common canonical mechanism of activation gating. A constriction point, or 'bundle-crossing', formed by the interface of four inner S6 helices sterically occludes the ion flux pathway in the "closed" state, and widens to enable conduction when the channel is "open". Voltage-sensing of channels was limited to the VSD, the activation gate located at the S6 bundle-crossing, and inactivation gate in the selectivity filter (Yellen, 1998). There is increasing evidence that

the gates of many K^+ channel classes do not conform to this steric mechanism however, leading to other 'non-canonical' mechanisms being described in the literature.

1.8.1 Hydrophobic gating mechanism

Hydrophobic gating is a concept first demonstrated using MD simulations to explain gating of prokaryotic mechanosensitive ion channel, MscS, and pentameric cys-loop ion channels such as nicotinic acetylcholine receptor subunits (nACHR) and their prokaryotic counterpart GLIC (Beckstein and Sansom, 2006; Zhu and Hummer, 2012). More evidence is emerging to suggest that other ion channels, including several K^+ channels, may be gated by reversible hydrophobic barriers to ion conduction within their pore forming regions. Water moves between liquid and vapour states upon interaction with pore-lining hydrophobic residues, and the vapour or "dewetted" state acts as a barrier against K^+ ion conduction (Figure 1.2). When opened in response to a stimulus the pore exists in a "wetted" state and is able to conduct K^+ ions. Dewetting can also result in collapse of the pore, physically preventing ion conduction (Aryal et al., 2014; Aryal et al., 2015; Jensen et al., 2010). Early models of hydrophobic nanopores demonstrated that wetting and dewetting transitions are dependent on hydrophobicity, transmembrane voltage and pore diameter, with nanopores becoming completely dewetted below 8-10 Å (Aryal et al., 2015). This mechanism may be able to explain gating of K^+ channels lacking a canonical S6 bundle-crossing gate.

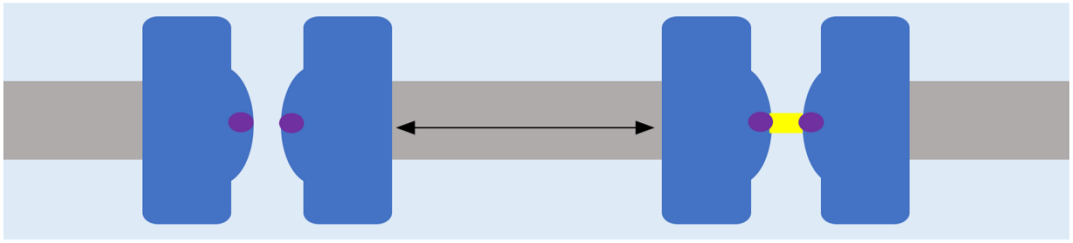

Figure 1.2: Schematic representation of the hydrophobic K^+ channel gating mechanism.
The de-wetting transition from the open (or "wetted"; left) to closed ("de-wetted"; right) channel conformation is enabled by hydrophobic pore-lining residues (purple). A vapour plug, shown in yellow, acts as a barrier to K^+ ion conduction. Water is shown in pale blue.

TWIK-1 (Tandem of pore domains in a Weak Inward rectifying K^+ channel-1), a member of the K2P subfamily, was shown to have a hydrophobic gate located within the inner pore using MD simulations of the crystal structure. Two pore-lining leucine residues were identified that form a hydrophobic barrier, and their involvement was validated by electrophysiological characterisation of hydrophilic substitutions (Aryal et

al., 2014). MthK, a Ca^{2+}-activated prokaryotic K^+ channel, may also possess a hydrophobic barrier to ion conduction formed by an alanine residue. The residue is in fact located in the equivalent position to one of the leucine residues implicated in hydrophobic gating of TWIK-1. Again, mutation of this residue to hydrophilic asparagine or aspartate results in increased conductance and P_o (Shi et al., 2011).

$K_{Ca}1.1$ channels lack an S6 bundle-crossing, and the recently resolved cryo-EM structures of *Aplysia californica* $K_{Ca}1.1$ in the absence and presence of Ca^{2+} indicated that the pore of BK channels remains physically open in the absence of Ca^{2+}-binding, in the "closed" conformation (Tao et al., 2017; Hite et al., 2017). Furthermore, the upper pore-forming region remained accessible to quaternary ammonium cations both in the closed and open conformations (Wilkens and Aldrich, 2006), implying that there is not a steric gate. It was later shown using atomistic simulations that the deep pore region of $K_{Ca}1.1$ undergoes hydrophobic dewetting transitions in Ca^{2+}-free conditions, as hydrophobic contacts within the pore are disrupted and pore-lining valine and leucine residues are exposed. Mutations that affect hydrophobicity and polarity of the $K_{Ca}1.1$ pore impair hydrophobic gating. The deep pore region itself is not responsible for initiating dewetting transitions however. Rather, conformational changes are triggered by Ca^{2+}-binding and unbinding within the RCK domains on the C-terminus, alongside changes in transmembrane voltage detected by the VSD (Jia et al., 2018). $K_{Ca}1.1$ and TWIK-1 are two channels thought to possess a "true" hydrophobic barrier. K^+ flux is prevented directly by water in the vapour state, as opposed to by physical occlusion following collapse of the pore upon dewetting (Aryal et al., 2014; Jia, Z. et al., 2018).

1.8.2 Selectivity filter gating

Another mechanism has been proposed that encompasses channels lacking the features of the canonical gating mechanism, such as K2P, $K_{Ca}1.1$, MthK and hERG, in which activation gating arises at the selectivity filter (Heer et al., 2017; Wilkens and Aldrich, 2006; Schewe et al., 2016; Schewe et al., 2019; Nematian-Ardestani et al., 2020; Labro et al., 2018; Lolicato et al., 2017; Kopec et al., 2019). It has been proposed that the selectivity filter undergoes a conformational change as a result of allosteric coupling with the activation gate, facilitated by pore-lining transmembrane helices. This in turn lowers the energetic barrier to K^+ conduction, enabling outward ion flux (Kopec et al., 2019).

Compelling evidence of a selectivity filter gate in MthK has been demonstrated using MD simulations. The distance between highly conserved T59 threonine residues in the selectivity filter correlated strongly with variations in both K^+ conductance at the level of an alanine residue, A88, and distance between A88 residues in diagonally opposite subunits. A88 is thought to be an important constriction point in the activation gate of the channel. This finding implies that there is some coupling between the selectivity filter and the activation gate of the channel. It was then shown that T59 forms hydrophobic contacts with an isoleucine residue, I84, on the M2 (inner) pore-lining helix, which is part of the activation gate. Upon opening of the activation gate, the T59 residue maintains this contact whilst the M2 helix moves; thus widening the selectivity filter and reducing the high energetic barrier between T59 residues, enabling K^+ conduction (Kopec et al., 2019). Importantly, the same threonine residue is also thought to be critical in the gating of K2P channels, $K_{Ca}1.1$ and KcsA channels (Schewe et al., 2016; Nematian-Ardestani et al., 2020; Labro et al., 2018; Kopec et al., 2019).

Negatively-charged activator compounds provided further evidence of the selectivity filter gate of K2P, $K_{Ca}1.1$ and hERG channels. These compounds were shown to bind below the selectivity filter of the channels and increase channel activity. It was hypothesised that the negative charge on the compounds attracts K^+ ions and promotes binding to the K^+ occupancy sites within the selectivity filter (Schewe et al., 2019).

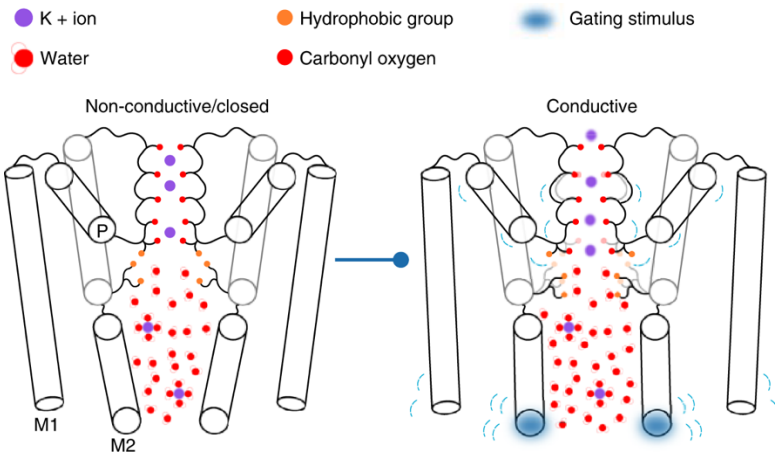

Figure 1.3: Schematic representation of a selectivity filter K^+ channel gating mechanism.
In the closed channel conformation, energetic barriers to ion conduction between selectivity filter-lining residues, particularly a threonine residue at position S4, prevent K^+ flux. An activating stimulus causes widening of the activation gate, which is allosterically coupled to the selectivity filter gate. The selectivity filter undergoes a conformational change and the energetic barrier is reduced, enabling outward K^+ conduction [Adapted from (Kopec et al., 2019)].

1.8.3 K_{Na}1.1 gating

Cryo-EM structures of the chicken K_{Na}1.1 channel in “closed” and “open” conformations were recently resolved. Compared to the closed conformations, the proposed open structure displayed expansion of the RCK1 lobes, which contribute to the gating ring structure, and displacement of S6 helices away from the pore as a consequence of this. In the closed, Na^+-unbound state however, the pore remains physically open and is wide enough in diameter to enable K^+ ion conduction (Hite and MacKinnon, 2017). This observation is similar to the finding that K_{Ca}1.1 channels remain physically open in both active and inactive conformations, and suggests that the channel is not gated sterically by an S6 bundle-crossing formed at cM333 as previously proposed (Hite et al., 2015). Other functional studies of K_{Na}1.1 and K_{Na}1.2 point away from a canonical S6 bundle-crossing as the primary mechanism of activation gating (Giese et al., 2017; Garg et al., 2013; Suzuki et al., 2016). For example, mutation of the human equivalent of the methionine located at the narrowest part of the ion conduction pathway, hM282 for K_{Na}1.2 and hM354 for K_{Na}1.1, to negatively-charged glutamine yielded currents that were indistinguishable from WT K_{Na}1.2 and K_{Na}1.1 currents when channels were expressed in *Xenopus* oocytes (Giese et al., 2017). Instead, it is possible that K_{Na}1.1 possesses a hydrophobic gate or a selectivity filter gate.

Hydrophobic leucine residues hL339 and hL342 in the pore-forming region of K_{Na}1.1 channels, in the upper S6 domains, have been implicated as possible residues involved in forming a hydrophobic gate in K_{Na}1.1, based on the equivalent pore-lining residues involved in the hydrophobic gating of MScS and TWIK-1 channels. hL339H and hL342W mutations resulted in increased P_o and constitutive activity of K_{Na}1.1 channels expressed in *Xenopus* oocytes (Giese et al., 2017). There is 20-22 Å distance between the two residues, and hydrophobic gating could only feasibly take place if the distance between the two residues decreased. In rat K_v1.2 channels however, isoleucine residues on S6 helices involved in hydrophobic gating have been shown to move closer together during dewetting transitions (Jensen et al., 2010). It is therefore possible that movement of S6 domains could enable hydrophobic gating in K_{Na}1.1 channels by reducing the distance between the two leucine residues. Previous work on K_{Na}1.2, the pore-forming region of which differs by only one residue to that of K_{Na}1.1, provides further confirmation that the K_{Na} channels are likely not gated by an S6 bundle-crossing. Mutations of hydrophobic pore-lining residues located in close proximity to the selectivity filter to glutamate and glutamine were found to stabilise the

open conformation, implying that these residues are important in maintaining stability of the closed conformation. It was proposed that hydrophobic interactions between L209 in the S5 helix and F240 on the pore-helix are important in gating of $K_{Na}1.2$ (Garg et al., 2013).

A number of channels proposed to gate at the selectivity filter have also been shown to possess a hydrophobic barrier, such as $K_{Ca}1.1$ and MthK, and it is possible that the two mechanisms overlap in some way, although this is unclear. $K_{Ca}1.1$ channels for example, depend on narrowing and reshaping of the pore-forming region to stabilise and maintain the dewetted state (Jia et al., 2018). It is uncertain as of yet whether $K_{Na}1.1$ is gated by a hydrophobic mechanism or selectivity filter mechanism alone, and both could be involved. Importantly, the conserved threonine residue that has been demonstrated to be critical for selectivity filter gating of MthK, K2P channels, KcsA and $K_{Ca}1.1$ channels (Schewe et al., 2016; Nematian-Ardestani et al., 2020; Labro et al., 2018; Kopec et al., 2019) is conserved in $K_{Na}1.1$ and this is deserving of further investigation.

1.9 *KCNT1* pathogenic variants in epileptic disorders

As mentioned previously, upwards of 60 distinct missense GOF pathogenic variants of *KCNT1* have been identified that are associated with severe epileptic encephalopathies. There are 24 recurrent mutations that cause both more and less severe phenotypes and six amino acid changes (G288S, A934T, R474H, R428Q and R398Q) accounted for 50% of the DEE-associated *KCNT1* pathogenic variants in a study of 248 patients (Bonardi et al., 2021).

EIMFS is a severe, pharmacoresistant DEE. EIMFS associated with *KCNT1* variants has a median age of onset of 1 month (Bonardi et al., 2021), after which seizure frequency increases. Characterised by migrating and polymorphous seizures, it is accompanied by other severe comorbidities such as developmental disorders (Coppola et al., 1995; Ohba et al., 2015), and delayed motor function (Kim et al., 2014). The severity of the disease is such that, following onset, patients may lose all earlier developed psychomotor skills (Passey et al., 2019). *KCNT1* pathogenic variants have been identified as the most frequent cause of EIMFS through several whole exome sequencing (WES) studies and are GOF, causing a large increase in $K_{Na}1.1$ current amplitude (Barcia et al., 2012; Kim et al., 2014). Half of a cohort of EIMFS patients had

KCNT1 pathogenic variants (Barcia et al., 2012). Most mutations causing EIMFS are *de novo*, however three separate cases have been found of somatic mosaicism (Ohba et al., 2015; McTague et al., 2018; Møller et al., 2015), meaning siblings could be susceptible to the disease, even if the parents are asymptomatic.

(AD)SHE is another DEE associated with *KCNT1* pathogenic variants, though is clinically a less severe disorder. It is characterised by motor seizures occurring during sleep and seizures are, like EIMFS, accompanied by cognitive disabilities. The median age of onset for (AD)SHE is 4.5 years old; later than that for EIMFS (Bonardi et al., 2021). Aside from *KCNT1*, (AD)SHE-causing pathogenic variants have been reported in genes encoding nACHRs. However, (AD)SHE resulting specifically from *KCNT1* variants is more severe, has a younger age of onset, and comorbidities are a defining characteristic separating it from other forms of the disorder (Heron et al., 2012).

Other DEEs arising from *KCNT1* pathogenic variants include status dystonicus (Gertler et al., 2019), Ohtahara syndrome (Martin et al., 2014) and Lennox-Gastaut (Jia et al., 2019), which are also accompanied by severe psychomotor and developmental defects. Ohtahara syndrome is one of the first epilepsies to appear from birth, along with EIMFS (Kim and Kaczmarek, 2014). There have also been reported cases of West syndrome, leukoencephalopathies and Brugada syndrome (Ohba et al., 2015). Brugada syndrome, a cardiac arrhythmia, is likely a consequence of $K_{Na}1.1$ expression in the autonomic nervous system (ANS). There is reportedly an increase in vagal activity prior to ventricular fibrillation and, furthermore, parasympathomimetic drugs exacerbate symptoms of the disorder (Shen and Zipes, 2014). Cardiac effects are being increasingly reported and *KCNT1* pathogenic variants were linked to systemic-to-pulmonary artery collateral-mediated heart disease, otherwise known as collateralopathy (Kawasaki et al., 2017; Kohli et al., 2020; Ikeda et al., 2021).

Missense *KCNT1* variants are always heterozygous, with one exception. One patient with Ohtahara syndrome had a homozygous *KCNT1* pathogenic variant due to uniparental disomy (Martin et al., 2014). The severity of phenotypes arising from heterozygous pathogenic *KCNT1* variants is such that homozygous patients would likely have poor survival. It was earlier suggested that location of the *KCNT1* pathogenic variant and the type of DEE caused could be related (Milligan et al., 2014). Whereas there is no pattern of localisation of EIMFS-causing variants on the channel structure, (AD)SHE-causing mutations appear to be clustered on the RCK2 domain (Bonardi et al., 2021). However, despite EIMFS and (AD)SHE having distinct clinical

phenotypes, G288S located on the S5 domain and R398Q located on RCK1 have since been reported to cause both disorders, and the same mutations can cause distinct phenotypes within the same family (Kim et al., 2014; Møller et al., 2015). In a genotypic analysis of 248 individuals with *KCNT1* variants, R398Q variants were seen in 9 families with (AD)SHE, and 5 individuals with EIMFS (Bonardi et al., 2021).

Animal models of the diseases are limited, though one group have studied the effects of EIMFS-causing mutation mR455H (hR474H), located on the RCK1 domain, in mice. Homozygous mice were not viable and only heterozygous mice could be studied (Quraishi et al, 2020). The mice displayed persistent interictal spiking and spontaneous seizure onset; though also had an increase in convulsing agent pentylenetetrazole (PTZ) sensitivity (Quraishi et al, 2020). Conversely to human patients however, the R455H mice did not display intellectual disabilities. A hY796H model in mice has also been studied (mY777H); though in this model homozygous mice survived and were studied due to a lack of epileptiform behaviour in heterozygous mice. mY777H mice displayed intellectual impairments reflective of those seen in patients with (AD)SHE, as well as increased seizures compared to WT mice. Seizure activity was consistent with that reported for human patients carrying the same *KCNT1* mutation, with interictal epileptiform discharge (IED) events localised to the anterior medial cortex (Shore et al, 2020).

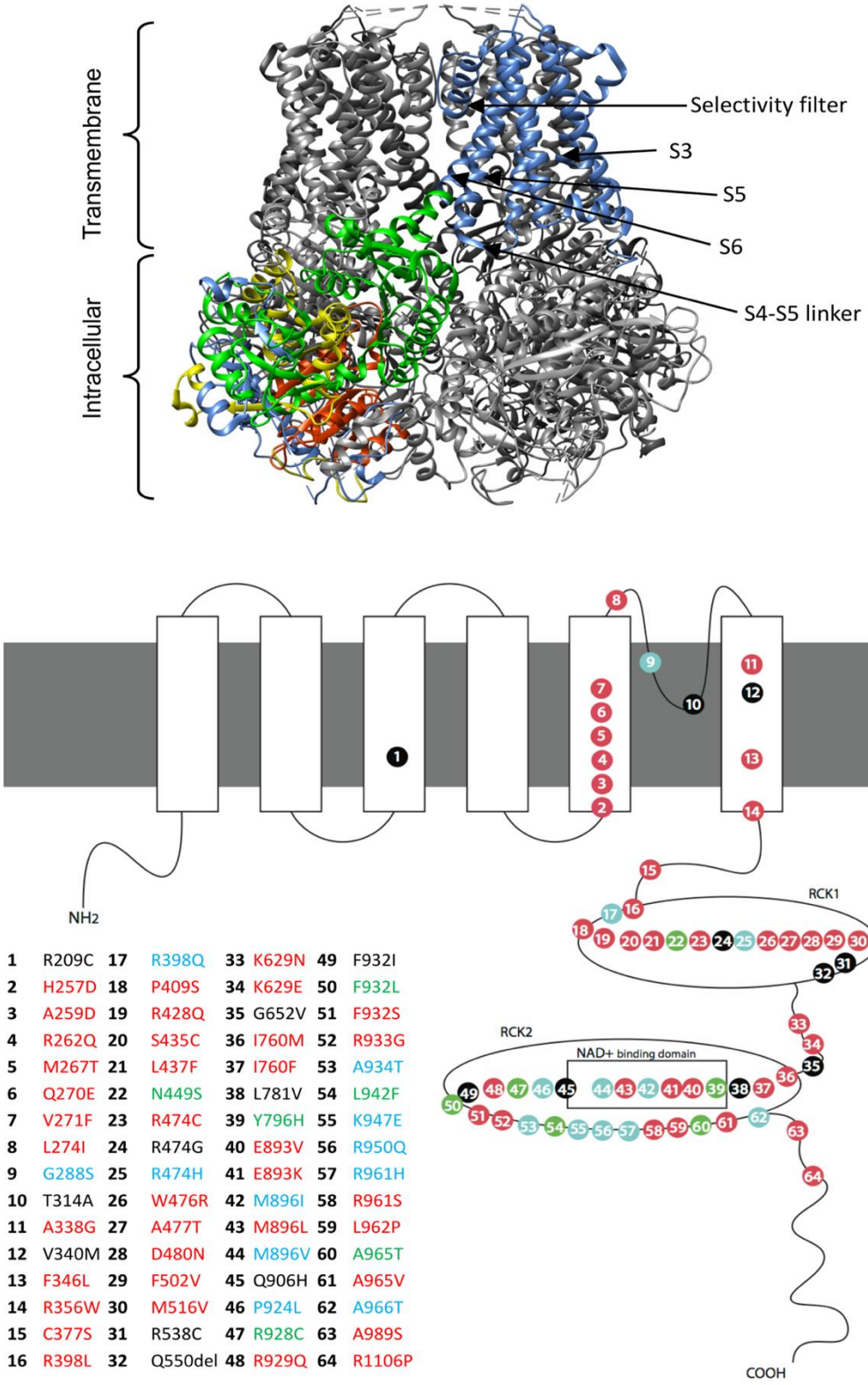

Figure 1.4: Structure of the open $K_{Na}1.1$ channel and location of pathogenic variants. The cryo-EM structure of the open chicken $K_{Na}1.1$ channel (Top) (PDB: 5U70 (Hite and MacKinnon, 2017) with functional domains in one subunit coloured. Blue: transmembrane segments 1-6, Green: RCK1, Yellow: RCK2 and Red: NAD+ binding domain [Figure prepared using UCSF Chimera]. Topological diagram of the $K_{Na}1.1$ channel and location of disease-causing amino acid substitutions (Bottom). Red: EIMFS- causing variant, Green: (AD)SHE-causing variant, Blue: variant associated with multiple phenotypes, Black: mutation causing a non-EIMFS or (AD)SHE DEE.

1.10 Mutations have varying effects on normal K_{Na}1.1 channel function

Since *KCNT1* pathogenic variants are highly pleiotropic, mutations have been reported to have varying effects on physiological function of the channel. Most of the reported DEE-causing *KCNT1* pathogenic variants, some of which are recurring, are missense mutations and result in GOF (Bonardi et al., 2021). To date, only one patient has been reported as harbouring a heterozygous LOF pathogenic variant, that impaired K_{Na}1.1 trafficking *in vitro*, and exhibited severe generalised seizures and delayed myelination (Evely et al., 2017; Vanderver et al., 2014). There are "hotspots" within the channel structure where clusters of pathogenic variants have been identified, as can be seen in Figure 1.3; this is particularly evident around the RCK domains and NAD^+ binding domain. Some variants are also found in the pore-forming region on the S5 and 6 helices however, and one has been reported on the S3 domain. Since the RCK1 and 2 domains and the S5-S6 pore-forming region are thought to have involvement with channel gating it is likely that clinical phenotypes that arise from the pathogenic *KCNT1* variants interfere with this in some way. Despite almost all patients being heterozygous, most efforts to functionally characterise the effects of *KCNT1* pathogenic variants on K_{Na}1.1 channels *in vitro* have used homomeric variant channels (Gertler et al., 2019; Milligan et al., 2014; McTague et al., 2018; Barcia et al., 2012; Kim et al., 2014; Tang et al., 2016; Mikati et al., 2015; Evely et al., 2017). Recently heterozygous *KCNT1* EIMFS-causing variants (Rizzo et al., 2016; Dilena et al., 2018) and DEE-causing variants of *KCNT2* in co-assembly with *KCNT1* have been studied in CHO cells (Mao et al., 2020).

1.10.1 Mutations located in the pore region

G288S is a pathogenic variant located within the pore-forming region of K_{Na}1.1 channels, on the S5 domain, and is one of the most recurring *KCNT1* pathogenic variants (Bonardi et al., 2021). It has been reported to cause a 6-10-fold increase in peak current amplitude recorded in whole cell experiments (Rizzo et al., 2016; Ishii et al., 2013). The variant causes a leftward shift in the conductance-voltage relationship, shifting the curve to more hyperpolarised potentials and resulting in increased activity at resting membrane potential (Rizzo et al., 2016). A proposed mechanism of GOF from *in silico* modelling, is the formation of a new hydrogen bond between G288S and G285 residues. Though it has been proposed that a negatively-charged, hydrophilic

aspartate residue exposed to the pore as a consequence could "trap" K^+ ions (Ishii et al., 2013), it is unlikely that this would lead to the increased outward current seen in this mutation. Increased hydrophilicity caused by the introduction of serine to the pore-forming region could however cause retention of water in the pore and destabilise the closed channel conformation, if $K_{Na}1.1$ does in fact possess a hydrophobic gate (Giese et al., 2017). This is not the only mutation identified as causing detrimental changes within the ion conduction pathway. EIMFS-causing hF346L in the pore-forming region has been proposed to destabilise the open state of the channel since the side chain of leucine is smaller than that of phenylalanine (McTague et al., 2018). Although, if this was the case, it would likely result in a lower P_o as opposed to GOF.

$K_{Na}1.1$ channels enter into frequent subconductance states when single channel behaviour is examined (Brown et al., 2010; Bhattacharjee et al., 2003); rG269S channels (hG288S) and other EIMFS-causing variants show a decrease in probability of entering into these subconducting states in single channel recordings (Barcia et al., 2012; Kim et al., 2014). In addition, Kim *et al* showed cooperative gating of rG269S and other EIMFS-causing variant channels; reporting simultaneous channel openings and increased activity in the cell-attached configuration when four or more channels were expressed in the same patch in *Xenopus* oocytes (Kim et al., 2014). In another study increases in Na^+-sensitivity and maximum probability of opening ($P_{o,max}$) were seen in single channel experiments using the same mutations in the rat $K_{Na}1.1$ channel (Tang et al., 2016). Since cell-attached configuration was used in the study by Kim *et al* (2014), intracellular Na^+ concentration would not have been controlled and therefore Na^+-sensitivity could not be measured in this study. Whole cell currents could be recorded in the absence of intracellular Na^+ when G288S channels were expressed in Chinese hamster ovary (CHO) cells (Rizzo et al., 2016), suggesting that the channels may be constitutively hyperactive.

1.10.2 Mutations located in the RCK domains

M516V is located in the RCK1 domain, which is likely where ion sensitivity and channel gating are coupled. Similarly to G288S, there is a leftward shift in the activation curve when hM516V is expressed in CHO cells, and activity in the absence of intracellular Na^+. Additionally, M516V $K_{Na}1.1$ subunits were shown to have lower levels of expression on the cell membrane, suggesting RCK1 folding and protein stability may be affected (Rizzo et al., 2016). This is not seen for hG288S subunits in the same

study, or for a number of other mutants studied in *Xenopus* oocytes, all which have no significant change in membrane expression levels from WT $K_{Na}1.1$ (Barcia et al., 2012).

Since EIMFS patients are usually heterozygous, Rizzo *et al* studied the behaviour of heteromeric channels; finding that heteromeric WT $K_{Na}1.1$ and M516V or G288S channels displayed current densities that were an intermediate between that of WT and mutant homomeric channels (2016). Two other EIMFS-causing variants, E893K and R950Q located at the end of the C-terminus also displayed intermediate current densities when co-expressed with WT $K_{Na}1.1$ subunits. Co-expressed mutant and WT assemblies exhibited less hyperpolarised activation curves, though the reported activation midpoint values were still negative (Dilena et al., 2018).

Despite the R428Q mutation showing increased Na^+-sensitivity in whole cell and single channel experiments (Tang et al., 2016), other mechanisms of GOF have also been proposed for this mutation involving the C-terminal site for PKC phosphorylation. PKC potentiates WT rat $K_{Na}1.1$ activity (Santi et al., 2006; Barcia et al., 2012). However, TPA, a PKC activator, was found to cause no increase in current amplitude when applied to the rat equivalent of R428Q expressed in *Xenopus* oocytes. It was proposed that this mutation is in a constitutively PKC phosphorylated-like state. The same effect was seen for another EIMFS-causing mutant, rA913T (hA934T) (Barcia et al., 2012). In contrast, another study using *Xenopus* oocytes found PMA to irreversibly inhibit hR428Q (Milligan et al., 2014), so it is unclear whether this effect is specific to the rat channel, and whether it is relevant to human patients.

Constitutive PKC phosphorylation of the rat channel may result from impaired protein-protein interactions with cytoplasmic binding partners of the channel; for example Phactr1. Mutant channels have been shown to have impaired association and dissociation with Phactr1, and consequently with PP1 (Fleming et al., 2016). Furthermore, rS407A channels expressed in HEK293-T cells, which have a non-functional site for PKC phosphorylation, are not suppressed by Phactr1 (Ali et al., 2020). It is thus possible that mutant channels are in a constitutively phosphorylated state as a result of impaired suppression by phactr1 and PP1 (Ali et al., 2020).

1.10.3 Mutations located on the NAD$^+$ binding domain

The cytoplasmic NAD$^+$ binding domain is involved in modulating Na^+-sensitivity of the channel (Tamsett et al., 2009). rY775H (hY796H) and rR907C (hR928C) located in this region were found to increase Na^+-sensitivity in single channel experiments, causing a leftward shift in the concentration-response relationship (Tang et al., 2016). R928C and another (AD)SHE-causing variant, M896I, are both located on the NAD$^+$ binding domain and both have been reported to have a faster time-to-peak compared to WT $K_{Na}1.1$ when studied in *Xenopus* ooctyes (Milligan et al., 2014).

(AD)SHE-causing Y796H, M896I and R928C, and EIMFS-causing P924L, similarly to mutants located on the RCK domains showed a reduced channel activity following addition of a PKC activator, PMA, when the mutants were expressed in *Xenopus* ooctyes (Milligan et al., 2014). The rat equivalent for R928C was studied under the same conditions however, and PMA had no significant effect on currents recorded from *Xenopus* oocytes, consistent with the reported effects of TPA on EIMFS-causing mutants (Barcia et al., 2012). The contrasting effects of PKC activators on rat and human WT and mutant $K_{Na}1.1$ channels can be therefore likely be explained by a species difference, and PKC phosphorylation may not be affected in human patients carrying DEE-causing pathogenic variants of *KCNT1.*

The exact role of the NAD$^+$ binding domain is unclear. NAD$^+$ binding to the domain is thought to potentiate activity of $K_{Na}1.1$ by decreasing the EC_{50} for activation by intracellular Na^+ (Tamsett et al., 2009), but there is a lack of information about how this domain interacts with the rest of the protein structure during channel gating. A number of pathogenic variants are located in this region however, and lead to large changes in channel activity. It is therefore likely that this region is important in gating and activation of $K_{Na}1.1$ and this is deserving of further investigation.

1.10.4 Co-assembly of $K_{Na}1.1$ with $K_{Na}1.2$

$K_{Na}1.2$, the closely related Na^+-activated K^+ channel encoded for by *KCNT2* differs from $K_{Na}1.1$ mainly in its N-terminus, but also by the presence of an Adenosine-5'-triphosphate (ATP) binding site on its C-terminus (Bhattacharjee et al., 2003). It was previously thought that $K_{Na}1.1$ was the only K_{Na} channel associated with DEEs, despite the fact that the two channels are known to co-assemble to form $K_{Na}1.1/1.2$ heteromers (Kaczmarek, 2013; Chen et al., 2009; Rizzi et al., 2016). Recently however, 8

pathogenic variants associated with DEEs have been identified in the *KCNT2* gene, highlighting that $K_{Na}1.2$ must also play an important role in normal physiology. Both GOF and LOF variants have been identified, unlike $K_{Na}1.1$ (Ambrosino et al., 2018; Mao et al., 2020; Alagoz et al., 2020; Inuzuka et al., 2020; Gururaj et al., 2017).

When expressed alone, $K_{Na}1.2$ produces almost undetectable current levels in CHO cells both with and without ATP (Gururaj et al., 2017; Chen et al., 2009; Mao et al., 2020). When $K_{Na}1.2$ is co-expressed with $K_{Na}1.1$ however, currents with larger amplitude than both channels expressed alone can be recorded (Chen et al., 2009; Mao et al., 2020). This may imply that its heteromerisation with $K_{Na}1.1$ is integral in the channel's role in normal physiology. It is also likely that the variant subunits would exert their effects on normal electrical behaviour of neurons when co-expressed with $K_{Na}1.1$ (Mao et al., 2020). By the same logic, it cannot be discounted that DEE-causing *KCNT1* variants may also be exerting their effects when variant $K_{Na}1.1$ channels co-assemble with $K_{Na}1.2$ subunits, which is deserving of further investigation.

One of the eight pathogenic variants identified in *KCNT2* is located in the N-terminus of $K_{Na}1.2$ (Mao et al., 2020). This is interesting since the N-terminus may play an important, though currently unknown, role in determining activation kinetics of the channel. This is evidenced by strikingly different activation kinetics between different isoforms of $K_{Na}1.1$ and between $K_{Na}1.1$ and $K_{Na}1.2$ that seemingly arise from their differing initiation sequences (Kaczmarek, 2013; Brown et al., 2008). It is therefore unexpected that no mutations leading to DEEs have thus far been identified in the N-terminus of $K_{Na}1.1$, though the possibility is now raised by the identification of a DEE-causing mutation in the N-terminus of $K_{Na}1.2$.

1.11 How $K_{Na}1.1$ mutations result in DEE phenotypes

1.11.1 $K_{Na}1.1$ mutations and hyperexcitability

The clinical phenotypes resulting from pathogenic variants of *KCNT1* are notably more severe than those resulting from other K^+ channelopathies. GOF mutations cause a marked increase in current amplitude when studied *in vitro*, but it is somewhat surprising that this leads to hyperexcitability and seizures, when in normal physiology K_{Na} current is important in maintaining RMP and in generation of AHPs (Franceschetti et al., 2003; Liu, X. and Stan Leung, 2004; Yang et al., 2007; Li et al., 2019; Martinez-Espinosa et al., 2015; Lee et al., 2019; Reijntjes et al., 2019).

Several mechanisms have been proposed for how hyperactive $K_{Na}1.1$ channels cause aberrant neuronal firing. One such hypothesis, is that $K_{Na}1.1$ channels carrying DEE-causing *KCNT1* variants expressed on inhibitory interneurons increase hyperpolarisation and dampen their inhibitory effect on excitatory interneurons, leading to increased excitation. A recent study utilising a mouse model of (AD)SHE-causing mY777H (hY796H) showed there to be a network increase in excitability and synaptic connectivity in dissociated neurons and cortical slices (Shore et al., 2020). These effects were underpinned by an increase in K_{Na} current at the subthreshold range of voltages both in non-fast- and fast-spiking GABAergic (gamma-aminobutyric acid) neurons, though it was most prominent in non-fast spiking neurons. As a result, in the current clamp configuration, a large increase in rheobase current was recorded in GABAergic neurons, and action potential generation was decreased in response to incremental current injections. This potentially subtype-specific effect was attributed to fast-spiking GABAergic neurons having a large subthreshold K^+ conductance, mediated by leak K^+ channels, and increases in K_{Na} current may therefore be less detrimental. No significant changes in glutamatergic neuron excitability were reported, though an increase in K_{Na} current was seen at depolarised voltages (+30-+50 mV). A number of factors may influence the differential effects of the mY777H variant on GABAergic and glutamatergic neurons, including expression of channels such as $K_{Na}1.2$ that form heteromultimers with $K_{Na}1.1$. Other possibilities are neuron-specific expression of different amino-terminal isoforms, or varying expression levels of co-localised Na^+ channels providing Na^+ for $K_{Na}1.1$ activation.

Another possibility is that mutant $K_{Na}1.1$ channels activate rapidly in response to action potentials, enabling more rapid recovery from action potentials. Voltage-gated Na^+ channels responsible for the upstroke of the action potential may become inactivated and re-primed at a faster rate, increasing the rate of high frequency firing and leading to hyperexcitability (Quraishi et al., 2019). Induced pluripotent stem cell (iPSC)-derived neurons have recently been engineered to express the *KCNT1* variant P294L (Quraishi et al., 2019) which causes EIMFS in patients (Milligan et al., 2014). The variant is located on the C-terminal of the channel, and results in an increase in whole cell current amplitude as well as prolonging the time-to-peak recorded from *Xenopus* oocytes. iPSC-derived neurons harbouring a homozygous P294L variant displayed a significant increase in the endogenous K_{Na} current seen in control neurons (Quraishi et al., 2019), in line with previous studies of the mutant channel expressed in *Xenopus* Oocytes (Milligan et al., 2014). The mutant neurons also had enhanced neuronal

outgrowth during differentiation. Multi-electrode arrays (MEA) were used to investigate the effect of the variant on neuronal activity within cultures. P294L-expressing neurons displayed a larger fast afterhyperpolarisation (fAHP) in comparison to control neurons, as well as a faster repolarisation slope. Spontaneous activity and bursts recorded from both control neurons and P294L neurons measured using MEAs demonstrated that variant neurons fire with more intensity and synchronicity compared to isogenic control neurons. These findings are contradictory to those seen in mY777H neurons, although the iPSC neurons used by Quraishi *et al* are likely immature glutamatergic neurons. In the dissociated mY777H neurons, which are more mature, hyperexcitability in glutamatergic neurons may have resolved (Shore et al., 2020).

1.11.2 Accompanying intellectual disorders resulting from KCNT1 mutations

As well as DEEs, *KCNT1* pathogenic variants are also associated with comorbidities including behavioural and psychiatric disorders, motor disorders and cognitive disabilities (Kim and Kaczmarek, 2014; Coppola et al., 1995; Ohba et al., 2015; Kim et al., 2014; Heron et al., 2012; Bonardi et al., 2021). Since (AD)SHE arising from pathogenic variants of other ion channel genes does result in intellectual disabilities (Heron et al., 2012), comorbidities can be attributed to *KCNT1* variants, rather than the seizure disorder. As discussed earlier, FMRP selectively interacts with the C-terminal domain of $K_{Na}1.1$. It is likely that $K_{Na}1.1$ interaction with FMRP is important in regulating its function in normal physiology, related to mRNA trafficking and development, and mutations in the C-terminal domain of $K_{Na}1.1$ may disrupt this (Brown et al., 2010; Kim and Kaczmarek, 2014).

$K_{Na}1.1$ channels play a role in intellectual function in normal physiology, evidenced by *KCNT1* KO mice. The null mice have impaired exploratory behaviour, procedural learning and motor learning, though their motor function control and working memory remain intact (Quraishi et al., 2020; Lu et al., 2015). It is hypothesised that loss of interactions of $K_{Na}1.1$ with binding partners such as FMRP may result in loss of neuronal plasticity, and it is these same protein-protein interactions that are likely impaired as a result of GOF variants in DEEs.

1.12 Pharmacological modulation of $K_{Na}1.1$ channels

Inhibition of hyperactive $K_{Na}1.1$ channels is the proposed treatment strategy for *KCNT1*-related DEEs, but the channels are pharmacologically distinct from other K^+ channels. The channels only have weak sensitivity to the non-selective K^+ channel blocker TEA^+ (tetraethylammonium ions); they are insensitive to 1 mM but have been shown to be inhibited reversibly by higher concentrations of 10-20 mM (Yang et al., 2006). DEEs resulting from mutation of *KCNT1* reported are mostly refractory, with conventional epilepsy drugs only temporarily alleviating symptoms. Antiarrhythmic drugs quinidine and bepridil have efficacy for inhibiting both WT and $K_{Na}1.1$ channels carrying pathogenic variants *in vitro* (Rizzo et al., 2016; Dilena et al., 2018; Milligan et al., 2014; Yang et al., 2006). A third antiarrhythmic drug, clofilium, has so far been found to inhibit WT $K_{Na}1.1$ (de Los Angeles Tejada et al., 2012). There is limited clinical data for use of quinidine as an effective treatment due to dose-limiting side effects, low potency and poor blood-brain-barrier (BBB) penetration (Numis et al., 2018; Mullen et al., 2018; Mikati et al., 2015; Bearden et al., 2014; Fitzgerald et al., 2019).

1.12.1 $K_{Na}1.1$ activators

There are four known exogenous agonists of $K_{Na}1.1$; antihelmintic compounds bithionol and niclosamide, antipsychotic compound loxapine, and riluzole, which is used to treat amyotrophic lateral sclerosis (ALS) (Yang et al., 2006; Biton et al., 2012). The mechanism of activation is unknown for all of the activators.

Whilst bithionol and riluzole both increase $K_{Na}1.1$ currents measured in HEK293 and CHO cells respectively, loxapine and niclosamide appear to have further effects on the voltage-dependence of the channel. Both compounds remove rectification, increasing $K_{Na}1.1$ current amplitude both in the inward and outward directions. It is likely that the compounds are in some way interfering with $K_{Na}1.1$ gating; possibly in-line with the effects of activators on other selectivity filter-gated channels. In K2P channels for example, activators such as arachidonic acid (AA) and PIP_2 cause similar changes in the voltage-dependence of TRAAK, TREK-1 and TREK-2. The activators convert the channels into ‘leak’ mode, removing outward rectification. It was hypothesised that this is due to the activated state of the channels being stabilised, shifting equilibrium away from the voltage-dependent step in the selectivity filter gating mechanism (Schewe et al., 2016). Though further investigation would be needed to draw parallels with $K_{Na}1.1$

activators, it is possible from the outset that activators of the channel could prove to be a useful tool in studying the gating mechanisms of $K_{Na}1.1$.

1.12.2 In vitro use of $K_{Na}1.1$ channel inhibitors and mode of action

Both quinidine and bepridil have been shown to significantly inhibit outwardly rectifying WT $K_{Na}1.1$ current. Bepridil is the most potent, causing reversible inhibition when applied to *Xenopus* oocytes, HEK293 and CHO cells expressing the channel with IC_{50} values ranging from 1-10 µM (Yang et al., 2006; Rizzo et al., 2016). Quinidine has IC_{50} values ranging from 82.1-140 µM in HEK293 cells, *Xenopus* oocytes and CHO cells (Yang et al., 2006; Rizzo et al., 2016; Gertler et al., 2019). Clofilium has been shown to inhibit $K_{Na}1.1$ whole cell currents in *Xenopus* oocytes with an IC_{50} of 109 µM, and slows the kinetics of channel activation (de Los Angeles Tejada et al., 2012). *Xenopus* oocytes may not be a reliable model for $K_{Na}1.1$ channel function and pharmacological modulation however, since they are very membrane and lipid-rich, so a higher concentration of drug is often required to evoke an effect (Yang et al., 2006).

Inhibition of a range of mutant $K_{Na}1.1$ channels carrying EIMFS and (AD)SHE-causing *KCNT1* variants by quinidine and bepridil has been evaluated in whole cell and single channel experiments, which is summarised in Table 1.3. Both drugs have been found to significantly and reversibly inhibit variant channels expressed in CHO cells, HEK293 cells and *Xenopus* oocytes (Milligan et al., 2014; McTague et al., 2018; Gertler et al., 2019; Dilena et al., 2018). In fact, when applied to EIMFS-causing hM516V and hG288S channels, bepridil was found to inhibit $K_{Na}1.1$ current at a significantly lower concentration (Rizzo et al., 2016), and the same was seen for quinidine inhibition of EIMFS-causing hR950Q and hE893K channels (Dilena et al., 2018). Heteromeric R950Q or E893K and WT $K_{Na}1.1$ channels expressed in CHO cells displayed intermediate sensitivity to quinidine inhibition (Dilena et al., 2018). Only one variant so far, EIMFS-causing hF346L located in the pore-forming region, has been reported as being insensitive to quinidine inhibition *in vitro* when expressed in *Xenopus* oocytes (McTague et al., 2018).

The mechanism of action of these drugs on $K_{Na}1.1$ channels is not currently known, and it is not fully understood why bepridil and quinidine appear to be more efficacious inhibitors of variant compared to WT $K_{Na}1.1$ channels. It has been postulated that bepridil and quinidine may be open channel blockers, and leftward-shifted activation of variant channels would potentiate their inhibition (Rizzo et al., 2016). Quinidine is

thought to interact with hydrophobic pore-lining residues when inhibiting other K^+ channels, such as hERG and $K_{v1.5}$ channels (Snyders and Yeola, 1995; Macdonald et al., 2018) and exerts its open-channel block by crossing the membrane in its neutral, unprotonated form. The structure of the hERG channel has recently been resolved by cryo-EM, and illuminated a hydrophobic pocket in the pore-forming region within which quinidine and other inhibitors are thought to bind (Wang and MacKinnon, 2017). It is possible therefore, that quinidine interacts with $K_{Na}1.1$ channels similarly.

Bepridil is primarily an L-type Ca^{2+} channel blocker, but also inhibits fast inward Na^+ current through voltage-gated Na^+ channels similarly to lidocaine (Li et al., 1999). However, since $K_{Na}1.1$ is expressed on cardiac myocytes and ASM cells as well as throughout the nervous system, it is possible that some of the antiarrhythmic effects of bepridil arise from inhibition of $K_{Na}1.1$ channels. Interestingly, both quinidine and bepridil are effective general treatments for Brugada syndrome (Antzelevitch and Patocskai, 2016). *KCNT1* pathogenic variants have been linked to Brugada syndrome (Ohba et al., 2015), so it is possible that the mechanism of both drugs for ameliorating ventricular tachycardia and fibrillation in this disease is due in part to inhibition of $K_{Na}1.1$ channels.

More recently small-molecule compounds have been identified that inhibit $K_{Na}1.1$ channels with low- and sub-micromolar potencies. VU0606170 was identified using a thallium-flux assay, a high-throughput fluorescence-based technique that utilises Tl^+ permeability through K^+ channels to detect active hits against heterologously expressed K^+ channels. WT $K_{Na}1.1$ channels were inhibited with an IC_{50} of 1.84 µM and EIMFS-causing mutant A934T channels with an IC_{50} of 1.16 µM. The compound was found to inhibit hERG but with lower potency than bepridil, and was inactive against $K_{Na}1.2$, $K_{Ca}1.1$, GIRK1/2, $K_v2.1$, TREK-1, $Ca_v3.2$ and $Na_v1.7$. Aberrant firing of cultured cortical rat neurons was also reduced by VU0606170 (Spitznagel et al., 2020). Compound 31 was derived from a hit identified in a rubidium-flux screen, similar in nature to the thallium-flux screen. This compound demonstrated *in vivo* efficacy, reducing seizure frequency in a mouse model harbouring the equivalent of an EIMFS-causing pathogenic variant, P924L (mP905L). Compound 31 inhibited WT $K_{Na}1.1$ with nanomolar and mP905L channels with low micromolar potency *in vitro* and was inactive against hERG, $Na_v1.5$, $Ca_v1.2$, I_{Ks}, $K_{Ca}1.1$ and $K_{Na}1.2$ (Griffin et al., 2021). The pore-forming regions of $K_{Na}1.1$ and $K_{Na}1.2$ are highly conserved, and the channels

share 78% sequence identity overall, so it is surprising that both VU0606170 and Compound 31 are selective for $K_{Na}1.1$.

1.12.3 Clinical use of $K_{Na}1.1$ inhibitors

Quinidine therapy in patients with pathogenic *KCNT1* variants has had variable outcomes. A recent study found >25% seizure reduction in 45% of patients, and another reported >50% reduction in only 20% of patients (Borlot et al., 2020; Fitzgerald et al., 2019). Despite decreasing macroscopic current to wildtype level when 300 µM quinidine was applied to *Xenopus* oocytes expressing the hY796H mutation; when used clinically there was no improvement in symptoms of (AD)SHE or accompanying developmental symptoms (Mikati et al., 2015). On the other hand, although quinidine was not as effective at reducing hK629N current *in vitro* when compared to inhibition other variants, an 80% reduction in seizure frequency in a patient carrying this EIMFS-causing variant was achieved with quinidine (Mikati et al., 2015). In another EIMFS patient, significant reduction of seizure frequency and accompanying developmental defects was reported following quinidine therapy (Bearden et al., 2014). Together this suggests that *in vitro* efficacy does not necessarily translate to clinical efficacy; the clinical and *in vitro* effects of quinidine and other drugs are summarised in Table 1.3. It is worth noting that all *in vitro* pharmacological studies to date aside from one, which found quinidine sensitivity of heteromeric assemblies to be intermediate between that of homomeric WT and variant $K_{Na}1.1$ channels (Dilena et al., 2018), have been carried out on homomeric mutant channels. This may explain some of the disparities between *in vitro* response and clinical responses in heterozygous patients to inhibitors.

Quinidine does not penetrate the BBB readily and may not reach therapeutically significant concentration in the CNS (Bearden et al., 2014; Mikati et al., 2015). $K_{Na}1.1$ is highly expressed in the CNS (Bhattacharjee et al., 2002; Rizzi et al., 2016) and as such, a drug that crosses the BBB is desirable. Varying serum concentrations have been reported; ranging from 1.23-14.8 µM in a study of 7 patients with *KCNT1*-related DEEs (Abdelnour et al., 2018). Quinidine has an IC_{50} of 100 µM *in vitro* (Yang et al., 2006; Rizzo et al., 2016; Gertler et al., 2019), so it is unsurprising that there has been low success rate in DEE patients. Furthermore, the therapeutic concentration range when the drug is used to treat arrhythmias is 6-15 µM, and toxicity is seen above 18.5 µM (Bearden et al., 2014). Cerebrospinal fluid (CSF) concentrations of quinidine have not been evaluated in patients being treated for *KCNT1*-associated DEEs. In a study of eight adult subjects however, unbound serum concentrations of quinidine ranged from

13-22%, and of this concentrations in the CSF ranged from 4-37% (Ochs et al., 1980). Subtherapeutic serum concentrations of quinidine were reported in over half of the patients in a study (Fitzgerald et al., 2019) and increasing serum concentration has been associated with off-target effects (Mullen et al., 2018).

Combination therapy with hepatic cytochrome P450 enzyme-inducers, such as phenobarbital and phenytoin, may induce quinidine metabolism and reduce serum concentrations of the drug by as much as 50% (Data *et al*, 1976). levels of quinidine were completely undetectable prior to discontinuation of concurrent phenobarbital administration in a patient with EIMFS resulting from two *KCNT1* variants, R356W and P724_L728 dup (Passey et al., 2019). Similarly, phenobarbital was found to significantly reduce serum quinidine concentration in two patients with EIMFS-causing *KCNT1* variants, G288S and A934T (Yoshitomi et al., 2019). Age was previously thought to be a determinant of quinidine effectiveness, since until recently all patients above the age of 4 were reportedly unresponsive to quinidine, regardless of serum concentration. It was hypothesised that in older patients, the BBB may be less permeable to quinidine, or that prolonged epilepsy symptoms worsen resistance of the channel to pharmacological modulation (Abdelnour et al., 2018). Another group reported the contrary, finding that patients below the age of 4 in their clinical cohort in fact responded less favourably to the treatment (Fitzgerald et al., 2019). In another study, a patient of the age of 12 diagnosed with Lennox-Gastaut syndrome resulting from a *KCNT1* variant, R209C, achieved almost complete seizure-freedom with quinidine (Jia et al., 2019).

Bepridil, quinidine and clofilium are not selective for $K_{Na}1.1$ channels since they bind to and inhibit a number of other ion channels, including those in the heart. Although only quinidine has been trialled therapeutically, all three compounds potently inhibit hERG channels at low- and sub-micromolar concentrations, and adverse cardiac effects may arise from their use in patients (Bearden et al., 2014). Quinidine for example, inhibits hERG channels expressed in HEK293 cells with an IC_{50} of 0.41 µM (Paul et al., 2002), compared to an IC_{50} of 100 µM for inhibition of $K_{Na}1.1$ (Yang et al., 2006; Rizzo et al., 2016; Gertler et al., 2019). In normal physiology hERG channels are involved in terminating cardiac action potentials, and inhibition can prolong the QT interval. Torsades de Pointes ventricular arrhythmia, characterised by “twisting” of the QRS segment of an electrocardiogram (ECG) can arise as a result of this and can lead to ventricular fibrillation and cardiac arrest (Finlayson et al., 2004). It is possible that this

could arise even when quinidine concentrations are subthreshold, with one case report finding no relationship between blood quinidine levels and propensity for prolonged QT interval (Fitzgerald et al., 2019).

Considering the proposed neuron subtype-specific effects of DEE-causing *KCNT1* variants (Shore et al., 2020), it may be useful to target specific cell types therapeutically. Specifically reducing subthreshold $K_{Na}1.1$ current in non-fast spiking GABAergic inhibitory interneurons could reverse the effects of pathogenic variants on membrane excitability and action potential generation whilst also reducing off-target effects. Gene therapy is one way this could be achieved; one group currently have produced antisense oligonucleotides (ASO) complementary to a target region within *KCNT1.* Intracerebroventricular injection of ASO into a homozygous *KCNT1* P924L mouse model reduced seizures and behavioural abnormalities, and increased survival. The ASOs function to degrade *KCNT1* mRNA or pre-mRNA by recruiting RNase H1 to the target, ultimately reducing *KCNT1* expression (Burbano et al., 2020)[pre-print, not peer-reviewed].

1.13 Outstanding questions and aims of the thesis

In view of the literature reviewed here, there are several unanswered questions surrounding GOF pathogenic variants of *KCNT1* that this thesis will aim to address. Firstly, understanding the underlying mechanisms of GOF pathogenic variants and more specifically in heteromeric assemblies of variant and WT $K_{Na}1.1$ subunits will be important for developing more effective treatments. Several mechanisms have been proposed for how mutations located across different functional regions of the channel protein exert their GOF (Tang et al., 2016; Rizzo et al., 2016; Dilena et al., 2018; Barcia et al., 2012; Kim et al., 2014; Ali et al., 2020). The overall result is usually the same however, and mutations located in distinct regions have similar proposed mechanisms. Secondly, understanding the mechanism of action of existing inhibitors of the channel will assist in development of novel inhibitors and improving the selectivity profile of future therapeutic interventions. The availability of high-resolution cryo-EM structures of the open and closed chicken $K_{Na}1.1$ channel (Hite et al., 2015; Hite and MacKinnon, 2017) will aid this. Determining how Na^+ interacts with the channel protein to activate $K_{Na}1.1$ and the gating mechanisms of the WT channel will be crucial both in terms of understanding how pathogenic variants cause GOF, and in developing perhaps more selective inhibitors of the channel.

General aims:

- ***To determine how the heteromeric assembly of mutant and WT K_{Na}1.1 subunits affects gating and inhibition of the channel***
- ***To determine how voltage and Na^+-sensing interact to gate K_{Na}1.1 and how DEE-causing pathogenic variants affect this***
- ***To determine how K_{Na}1.1 is activated by intracellular Na^+***
- ***To determine the mechanism of action of existing inhibitors of K_{Na}1.1 and use this to aid development of novel inhibitors***

Table 1.3: Pathogenic variants in *KCNT1* that have been studied in vitro or clinically with inhibitors, their location on the channel structure, and the associated clinical phenotype.

Pathogenic variant	CDS change	Location	Associated disorder	Pharmacological modulation *in vitro*	Clinical response to therapies	References
R209C	c.625C>T	S3 domain	Lennox-Gastaut	N/A	Clinically significant response to quinidine	(Jia et al., 2019)
A259D	c.776C>A	S4-5 linker	EIMFS	Quinidine significantly decreased current amplitude (300 µM)	No clinical response to quinidine	(Numis et al., 2018)
Q270E	c.808C>G	S5 domain	EIMFS	N/A	No clinical response to quinidine	(Madaan et al., 2018; Borlot et al., 2020)
					No clinical response to quinidine or ketogenic diet	
V271F	c.811G>T	S5 domain	EIMFS	Quinidine significantly decreased current amplitude (300 µM)	N/A	(McTague et al., 2018)
L274I	c.820C>A	S5 domain	EIMFS	Quinidine significantly decreased current amplitude (300 µM)	No clinical response to quinidine	(McTague et al., 2018; Borlot et al., 2020)
					Patient showed minimal response to ketogenic diet and no response to cannabidiol	
G288S	c.862G>A	S5 domain	(AD)SHE EIMFS	Bepridil significantly more potent compared to WT **IC_{50} for bepridil: 0.15±0.05 µM** No significant difference between inhibition of WT and mutant by quinidine **IC_{50} for quinidine: 67±19 µM** Inhibited by test compound 31 **IC_{50}: 221 nM**	Some patients have responded to quinidine, others have not	(Rizzo et al., 2016; Fitzgerald et al., 2019; Yoshitomi et al., 2019; Borlot et al., 2020; Griffin et al., 2021)
					No clinical response to quinidine, seizures worsened. Phenobarbital showed slight efficacy but discontinued due to drowsiness.	
					Three patients responded to quinidine, two out of the three had a marked response to ketogenic diet. The third had a marked response to cannabidiol.	
F346L	c.1038C>G	S6 domain	EIMFS	Completely insensitive to quinidine (300 µM) in *Xenopus* oocytes Inhibited by test compound 31 **IC_{50}: 1.77 µM**	N/A	(McTague et al., 2018; Griffin et al., 2021)
R356W/ P724_L728 dup	c.1066C>T c.2170_2184dup15	Bottom of S6 domain	EIMFS	N/A	Minor relief with quinidine. Interaction with phenobarbital, resulting in prolonged QTc interval.	(Passey et al., 2019)

Pathogenic variant	CDS change	Location	Associated disorder	Pharmacological modulation *in vitro*	Clinical response to therapies	References
R398Q	c. 1193G>A	RCK1 domain	(AD)SHE EIMFS	Quinidine significantly decreased current amplitude (300 µM)	No clinical response to quinidine	(Milligan et al., 2014; Borlot et al., 2020)
R428Q	c.1283G>A	RCK1 domain	EIMFS	Quinidine significantly decreased current amplitude (300µM)	Patient responded to phenobarbital and potassium bromide (later died of sudden cardiac arrest). Quinidine exacerbated seizures and was discontinued.	(McTague et al., 2018; Datta et al., 2019; Yoshitomi et al., 2019; Alsaleem et al., 2019; Borlot et al., 2020)
					Patient responded to quinidine in combination with other antiepileptic medications and ketogenic diet	
					>50% reduction in seizure frequency with quinidine, experienced ventricular tachycardia. Seizures unresponsive to phenobarbital, KBr, clonazepam, clobazam, levetiracetam.	
					Patient showed marked response to ketogenic diet, some response to cannabidiol and no response to quinidine.	
L437F	c.1309C>T	RCK1 domain	Epilepsy with status distonicus	**IC_{50} for quinidine: 66 µM**	N/A	(Gertler et al., 2019)
R474C	c.1420C>T	RCK1 domain	Focal epilepsy	N/A	23% reduction in seizure frequency with quinidine; not considered successful. No clinical response to conventional epilepsy therapeutics, methyl prednisolone pulse therapy, and ketogenic diet.	(Yoshitomi et al., 2019)
R474G	c.1420C>G	RCK1 domain	Multifocal seizures	N/A	Clinically significant response to phenobarbital	(Datta et al., 2019)
R474H	c.1421G>A	RCK1 domain	EIMFS	N/A	No clinical response to quinidine	(Fitzgerald et al., 2019; Borlot et al., 2020; Takase et al., 2020)
					One patient responded to ketogenic diet, another showed no response to quinidine	
					Patient responded to tipepidine and dextromethorphan	
F502V	c.1504T>G	RCK1 domain	EIMFS	Quinidine significantly decreased current amplitude (300 µM)	Clinically significant response to quinidine	(McTague et al., 2018)

Pathogenic variant	CDS change	Location	Associated disorder	Pharmacological modulation *in vitro*	Clinical response to therapies	References
M516V	c.1546A>G	RCK1 domain	EIMFS	Bepridil significantly more potent compared to WT **IC_{50} for bepridil: 0.3±0.1 µM** No significant difference between inhibition of WT and mutant by quinidine **IC_{50} for quinidine: 46±12 µM**	N/A	(Rizzo et al., 2016)
K629N	c.1887G>C	RCK2 domain	EIMFS	Quinidine (300 µM) less effective than when used for Y796H, R428Q and WT	Clinically significant response to quinidine; 80% decrease in seizure frequency	(Mikati et al., 2015; Milligan et al., 2014)
Y796H	c.2386T>C	NAD^+ binding domain	(AD)SHE	**IC_{50} for quinidine: 38±12.89 µM** **IC_{50} for bepridil: 12.8±2.48 µM**	No clinical response to quinidine	(Mikati et al., 2015)
E893K	c.2677G>A	NAD^+ binding domain	EIMFS	More sensitive to quinidine than WT in CHO cells **IC_{50} for quinidine: 9.6±2.5 µM**	Clinically significant response to quinidine; 90% reduction in seizures	(Dilena et al., 2018)
M896K	c.2687T>A	NAD^+ binding domain	EIMFS	Quinidine significantly decreased current amplitude (300 µM)	Severe pulmonary vasculopathy resulting from clinical use of quinidine	(McTague et al., 2018)
M896I	c.2688 G>C	NAD^+ binding domain	SHE	Quinidine significantly decreased current amplitude (300 µM)	N/A	(Milligan et al., 2014)
P924L	c.2771C>T	C-terminus (next to NAD^+ binding domain)	EIMFS	Quinidine significantly decreased current amplitude (300 µM) Mouse orthologue inhibited by test compound 31 **IC_{50}: 1.012 µM**	N/A	(Milligan et al., 2014; Griffin et al., 2021)
R928C	c.2782C>T	C-terminus (next to NAD^+ binding domain)	(AD)SHE	Quinidine significantly decreased current amplitude (300 µM)	No clinical response to quinidine	(Milligan et al., 2014; Mullen et al., 2018)
A934T	c.2800G>A	C-terminus (next to NAD^+ binding domain)	EIMFS	Quinidine significantly decreased current amplitude (300 µM) Inhibited by test compound VU0606170. **IC50: 1.16 µM**	Clinically significant response to quinidine Seizure frequency initially decreased, but later increased with quinidine therapy. In combination with phenobarbital and KBr, phenobarbital hindered increase in quinidine serum levels	(Milligan et al., 2014; Yoshitomi et al., 2019; Patil et al., 2019; Spitznagel et al., 2020; Borlot et al., 2020)

Pathogenic variant	CDS change	Location	Associated disorder	Pharmacological modulation *in vitro*	Clinical response to therapies	References
					One patient showed a marked response to both ketogenic diet and cannabidiol. Another responded to quinidine and low glycemic index diet. A third patient showed no clinical response to quinidine or ketogenic diet	
R950Q	c.2849G>A	C-terminus	EIMFS	More sensitive to quinidine than WT in CHO cells **IC_{50} for quinidine: 24±5.7 µM**	No clinical response to quinidine. Significant reduction in seizure frequency in another patient with quinidine therapy.	(Dilena et al., 2018; Patil et al., 2019; Borlot et al., 2020)
					One patient showed some response to cannabidiol therapy, another showed a marked response to quinidine and some response to low glycemic index diet	
L962P	c.2885T>C	C-terminus	EIMFS	N/A	Some clinical response to ketogenic diet	(Borlot et al., 2020)
A966T	c.2896G > A	C-terminus	Combination of (AD)SHE and EIMFS phenotype	N/A	Complete and persistent response to phenobarbital in patient	(Cataldi et al., 2019)
R1114W/ del 550	c.3340 C>T c.1649-1651delAGC	End of C-terminus	EIMFS	Quinidine significantly decreased current amplitude of R1114W variant (300 µM) but not del 550 variant	No clinical response to quinidine	(Numis et al., 2018)

2 Materials and methods

2.1 Molecular Biology and Mutagenesis

2.1.1 Chemicals and reagents

All chemicals were obtained from Sigma-Aldrich unless otherwise stated (Dorset, UK). All DNA-modifying enzymes and compatible buffers were from New England Biolabs (Hitchin, UK), unless otherwise stated.

2.1.2 Plasmids used for mammalian expression (source)

- **pcDNA6-*KCNT1*** - 8.9 kb plasmid encoding for the full length α-subunit of $K_{Na}1.1$. The plasmid contains a gene conferring ampicillin resistance in *E. coli*. (Dr Jonathan D. Lippiat).
- **pEYFP-N1** - 4.7 kb plasmid encoding enhanced yellow fluorescent protein (EYFP), which was used to confirm successful transfections. The plasmid contains a gene that confers kanamycin resistance in *E. coli*. (Dr Jonathan D. Lippiat).
- **pcDNA3-hERG** - 6.6 kb plasmid encoding the full-length α-subunit of Kv11.1, more commonly referred to as hERG. The plasmid contains a gene conferring ampicillin resistance in *E. coli*. (Prof. Asipu Sivaprasadarao).

2.1.3 Subcloning of mutations into pcDNA6-KCNT1

Human constructs of pore mutations M354I, M354S, F346I and F346S, and EIMFS-causing mutations R428Q, M516V and G288S were created previously by Hattapark Dejakaisaya in a pBF-hSlo2.2 *Xenopus* oocyte expression vector. These constructs were subcloned into the pcDNA6-hSlo2.2 plasmid. Nucleotide sequence changes are shown in Table 2.1. Mutant constructs were digested using Bsu36I and BspEI restriction enzymes, both of which are compatible with buffer 3.1.

In order to confirm digestion reactions had been successful, fragments in the reaction mixture were separated by agarose gel electrophoresis. A 1% agarose gel was made using Tris-acetate-EDTA (TAE) containing 0.1 M EDTA, and 10 mg/ml ethidium bromide was added following cooling to enable visualisation of DNA under UV light. Purple loading dye (6x) (New England Biolabs, Hitchin, UK) was added to digestion reaction mixtures prior to loading in the gel. The gel was then submerged in TAE buffer

and 100 V applied for 20 minutes. Bands could be visualised under UV light, and relevant fragments excised from the gel.

DNA was extracted from the excised gel fragments using the Monarch® DNA Gel Extraction Kit (New England Biolabs, Hitchin, UK) according to the instructions in the kit (Thermoscientific, Loughborough, UK). All mutations were ligated into the pcDNA6-hSlo2.2 vector using T4 DNA ligase and T4 ligase buffer (New England Biolabs, Hitchin, UK).

2.1.4 Transformation of Escherichia coli

DNA was introduced into competent cells by heat shocking. The competent cell and cDNA mixture were incubated on ice for 30 minutes and placed into a heat-block at 42°C for 45 seconds before transferring onto ice for 2 minutes for recovery. The mixture was then used to inoculate agar plates containing 100 mg/ml ampicillin, and colonies grown in an incubator at 37°C for 15 hours. Where kanamycin-resistant plasmids were transformed, for example pEYFP-N1, an additional recovery step was included. SOC outgrowth medium (New England Biolabs, Hitchin, UK) was added to heat shocked cells, and the mixture incubated for 1 hour at 37°C prior to inoculating agar plates containing 100 mg/ml kanamycin. Following successful transformation, colonies were picked from agar plates and inoculated in LB Broth (Sigma-Aldrich, Dorset, UK) containing 100 mg/ml ampicillin, and grown overnight in a shake incubator at 37°C, to select for successfully transformed cells. Cloudiness was used as an indication that *E. coli* cells had successfully grown-up in the broth, and DNA could be extracted. DNA was extracted from LB Broth using a QIAprep Miniprep kit (Qiagen, Manchester, UK), according to the instructions included in the kit. Identity of miniprep DNA was confirmed by Sanger sequencing (GeneWiz, Takeley, UK).

Table 2.1: Changes in cDNA sequence for mutants subcloned from a pBF-hSlo2.2 expression vector into the pcDNA6-hSlo2.2 plasmid.
Successful subcloning was verified by Next Generation Sanger sequencing (GeneWiz, Takeley, UK).

Mutation	CDS change
Pore-lining mutations	
F346I	c.1036T>A
F346S	c.1037T>C
M354I	c.1062G>A
M354S	c.1061-2TG>GC
EIMFS-causing pathogenic variants	
G288S	c.862G>A
R428Q	c.1283G>A
M516V	c.1546A>G

2.1.5 Polymerase chain reaction

(AD)SHE-causing mutants Y796H, R928C, R398Q and M896I, Na^+-binding site mutants T922K, T922A, D839E, D839A, D898K, D898A, D884A, D884I, D884E, D884V, D884F, K885A and E920A, and selectivity filter mutant T314C were created using the the polymerase chain reaction (PCR), using the New England Biolabs site-directed mutagenesis method (New England Biolabs, Hitchin, UK). The guanine-cytosine (GC) content of the male and female human genome is 40.9% (Piovesan et al., 2019), although some genes are particularly GC-rich. *KCNT1* has a high GC content of 61% (NM_020822.3; (Benson et al., 2017)), which makes PCR reactions challenging. Due to the high GC content of the *KCNT1* sequence, pcDNA6-*KCNT1* (Dr Jonathan D. Lippiat), was used as a template to amplify short fragments of sequence flanking naturally-occurring restriction sites, which were then ligated into a small pJET1.2 blunt cloning vector (Thermoscientific, Loughborough, UK). These constructs were then used as templates for site-directed mutagenesis to introduce DEE-causing mutations or mutations to probe activation and gating mechanisms.

Using forward and reverse primers detailed in Table 2.2, Q5 polymerase was used to amplify a fragment, termed “Fragment 2” (Figure 2.1), containing naturally-occurring restriction sites for the enzymes SbfI and BsiWI (Figure 2.1 and Table 2.3) in which Y796H, R928C and M896I could be engineered. This fragment was also used to create Na^+-binding site mutants. For (AD)SHE-causing mutant R398Q and selectivity filter

mutant T314C, PrimeSTAR HS polymerase (Takara Bio Europe SAS, Saint-Germain-en-Laye, France) was used to amplify “Fragment 1” with restriction sites for enzymes Bsu36I and BspEI (Figure 2.1 and Table 2.3), since this polymerase enzyme proved to be more effective. The fragments were ligated into a small pJET1.2 blunt cloning vector using the CloneJET PCR cloning kit (Thermoscientific, Loughborough, UK). Q5 polymerase was then used to engineer Y796H, R928C and M896I mutations, using forward and reverse primers detailed in Table 2.2, and the protocol detailed in Table 2.5. PrimeSTAR HS polymerase (Takara Bio Europe SAS, Saint-Germain-en-Laye, France) was used to engineer the R398Q, T314C, and Na^+-binding site mutations using the forward and reverse primers detailed in Table 2.2, and the protocol detailed in Table 2.6.

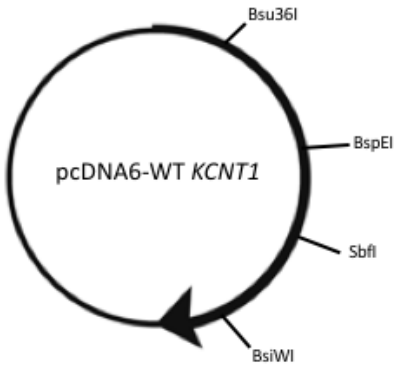

Figure 2.1: Schematic plasmid map showing restriction fragments amplified to carry out site-directed mutagenesis.
“Fragment 1”: 1.3 kb fragment including unique restriction sites Bsu36I and BspEI. “Fragment 2”: 1.04 kb fragment including SbfI and BsiWI. Fragments were ligated into pJET1.2 blunt cloning vector and used as templates for site-directed mutagenesis.

PCR reactions were assembled in 0.1 ml PCR tubes and, for Q5 site-directed mutagenesis, consisted of: 10 µl Q5 polymerase buffer (5x), 10 µl Q5 High GC enhancer (5x), 200 µM dNTP mix, ~5 ng template cDNA, 0.4 µM forward and reverse primer, 0.02 units/µl Q5 polymerase, and an appropriate volume of nuclease-free water to make the reaction up to 50 µl. For reactions replacing Q5 polymerase with PrimeSTAR HS polymerase (Takara Bio Europe SAS, Saint-Germain-en-Laye, France), reactions consisted of: 10 µl PrimeSTAR buffer (5x), 200 µM dNTP mix, ~5 ng template cDNA, 0.3 µM forward and reverse primer, 0.02 units/µl PrimeSTAR polymerase, and an appropriate volume of nuclease-free water to make the reaction up to 50 µl. DpnI was used at a concentration of 0.4 units/µl following the reactions to digest template cDNA in the PCR products and the products separated using agarose gel electrophoresis. Polynucleotide kinase was used to introduce phosphate groups to

the linear PCR products, enabling ligation with T4 DNA Ligase. Following ligation, the products were used to transform *E. coli.* The identity of miniprep DNA was then verified by Sanger sequencing (GeneWiz, Takeley, UK), before subcloning the fragment into the pcDNA6-*KCNT1* expression vector. The pJET vector containing the relevant fragment was digested with BsiWI and SbfI digestion enzymes for Y796H, R928C, M896I and the Na^+-binding site mutants, Bsu36I and BspEI enzymes for R398Q and T314C. T4 DNA Ligase was then used as described previously for subcloning of mutations from the pBF-*KCNT1* expression vector into the pcDNA6-*KCNT1* plasmid.

Table 2.2: Primers used to generate fragments and for site-directed mutagenesis reactions.
Nucleotide change in lower case. Oligonucleotide primers were designed using the New England Biolabs website (Hitchin, UK), ordered from Integrated DNA Technologies (Leuven, Belgium) and were reconstituted in nuclease-free water to make 100 µM stock solutions. Prior to PCR reactions, 10 µM stock solutions containing forward and reverse primer were made.

CDS change	Mutation	Primer sequence
Fragments used as templates for site-directed mutagenesis		
"Fragment 1"	Bsu36I forward	5′- CAAAAACCAAAGATCGA -3′
	BspEI reverse	5′- ATACATGCGCTGC -3′
"Fragment 2"	SbfI forward	5′- GGACAGTGGCC -3′
	BsiWI reverse	5′- GGCGGCCGTA -3′
(AD)SHE-causing pathogenic variants		
c.2386T>C Y796H	Y796H forward	5′- CGCCAAGCCCcACGGGTTCAA -3′
	Y796H reverse	5′- TCTTCATAGCTGTTGTGCTTGC -3′
c.2782C>T R928C	R928C forward	5′- TTCCAACATGtGCTTCATGCAGTTCC -3′
	R928C reverse	5′- GGGTGGGTGAGCTCCGTG -3′
c.2688G>C M896I	M896I forward	5′- AGGACTACATaGCGGACGCCAAG -3′
	M896I reverse	5′- CCTCGGCGCTCATGGTGC -3′
c.1193G>A R398Q	R398Q forward	5′- GCCCACCCCCaGCTCCAGGAC -3′
	R398Q reverse	5′- GTAGAACTCGTTCAGGAAGTCCATGAG -3′
Mutations for probing activation and gating mechanisms		
c.940-2ACC>TGC T314C	T314C forward	5′- CACCTTCTCCtgcGTGGGCTAC -3′
	T314C reverse	5′- ACGATGCAGAAGTAGAAG -3′
c.2765-6CC>AA T922K	T922K forward	5′- ACGGAGCTCAaaCACCCTTCCAACATG -3′
	T922K reverse	5′- GGTGATGCTGAGGCTGGG -3′
c.2692-4GAC>AAA D898K	D898K forward	5′- CTACATGGCGaaaGCCAAGACCATC -3′
	D898K reverse	5′- TCCTCCTCGGCGCTCATG -3′
c.2517C>A D839E	D839E forward	5′- TGCTGCTGGAaAACAAGCCCG -3′
	D839E reverse	5′- GCACGATGGGGTTCAGCTC -3′
	K885A forward	5′- GGTGGTGGACgcGGAGAGCACC -3′

c.2653-4AA>GC K885A	K885A reverse	5′- ACCAGGTTGTCCGCATAG -3′
c.2516A>C D839A	D839A forward	5′- CTGCTGCTGGcCAACAAGCCC -3′
	D839A reverse	5′- CACGATGGGGTTCAGCTC -3′
c.2650-1GA>AT D884I	D884I forward	5′- GGTGGTGGTGatCAAGGAGAGC -3′
	D884I reverse	5′- AGGTTGTCCGCATAGATG -3′
C2652C>A D884E	D884E forward	5′- TGGTGGTGGAaAAGGAGAGCA -3′
	D884E reverse	5′- CCAGGTTGTCCGCATAGATG -3′
c.2759A>C E920A	E920A forward	5′- ATCACCACGGcGCTCACCCAC -3′
	E920A reverse	5′- GCTGAGGCTGGGGAAGAG -3′
c.2650-1GA>TT D884F	D884F forward	5′- GGTGGTGGTGttCAAGGAGAGC -3′
	D884F reverse	5′- AGGTTGTCCGCATAGATG -3′
c.2651A>T D884V	D884V forward	5′- GTGGTGGTGGtCAAGGAGAGC -3′
	D884V reverse	5′- CAGGTTGTCCGCATAGATG -3′
c.2764A>G T922A	T922A forward	5′- CACGGAGCTCgCCCACCCTTC -3′
	T922A reverse	5′- GTGATGCTGAGGCTGGGG -3′
c.2693A>C D898A	D898A forward	5′- TACATGGCGGcCGCCAAGACC -3′
	D898A reverse	5′- GTCCTCCTCGGCGCTCAT -3′

Table 2.3: PCR protocol used to amplify fragment 2 containing SbfI and BsiWI restriction sites.
Q5 polymerase was used, with Q5 Buffer and GC enhancer.

Temperature	Time	Purpose
98°C	1 minute	Denaturation
98°C	20 seconds	Denaturation
55°C	20 seconds	Annealing
72°C	30 seconds	Extension
Stages 2-5 repeated for 28 cycles		
72°C	5 minutes	Extension
4°C	-	Holding temperature

Table 2.4: PCR protocol used to amplify fragment 1 containing Bsu36I and BspEI restriction sites.
PrimeSTAR HS polymerase was used, with PrimeSTAR HS buffer (Takara Bio Europe SAS, Saint-Germain-en-Laye, France).

Temperature	Time	Purpose
98°C	1 minute	Denaturation
98°C	10 seconds	Denaturation
55°C	15 seconds	Annealing
68°C	30 seconds	Extension
Stages 2-5 repeated for 28 cycles		
68°C	5 minutes	Extension
4°C	-	Holding temperature

Table 2.5: PCR protocol used to engineer Y796H, R928C, M896I and Na^+-binding site mutations in pJET1.2-Fragment 2.
When generating the mutations, a gradient for annealing temperature was set up, and 68°C was found to be the optimum annealing temperature. Q5 polymerase was used, with Q5 Buffer and GC enhancer.

Temperature	Time	Purpose
98°C	1 minute	Denaturation
98°C	20 seconds	Denaturation
68°C	20 seconds	Annealing
72°C	1 minute	Extension
Stages 2-5 repeated for 30 cycles		
72°C	5 minutes	Extension
4°C	-	Holding temperature

Table 2.6: PCR protocol used to engineer R398Q, Na^+-binding site and T314C mutations in pJET1.2-Fragment 1
When generating the mutations, a gradient for annealing temperature was set up, and 63°C was found to be the optimum annealing temperature. PrimeSTAR HS polymerase was used, with PrimeSTAR HS buffer (Takara Bio Europe SAS, Saint-Germain-en-Laye, France).

Temperature	Time	Purpose
98°C	1 minute	Denaturation
98°C	10 seconds	Denaturation
63°C	15 seconds	Annealing
68°C	1 minute 20 seconds	Extension
Stages 2-5 repeated for 30 cycles		
68°C	5 minutes	Extension
4°C	-	Holding temperature

2.2 Construction of concatemers

To model the genetic status of heterozygous patients carrying the (AD)SHE-causing variant Y796H, concatemeric channels were engineered utilising the WT $K_{Na}1.1$ channel cDNA in the pcDNA6 expression vector, and the Y796H mutant cDNA in pcDNA6 detailed in the previous section. Briefly, tandem dimers were engineered by joining the C-terminus of one subunit to the N-terminus of an adjacent subunit; omitting the respective stop and start codons and introducing a linker region between the two. The tandem dimers contain variable combinations of Y796H mutant and WT $K_{Na}1.1$ subunits, and could be used to transfect mammalian cells, producing tetrameric channels. Using the NEB insertion/deletion PCR method, monomers termed the 'recipient' and 'donor' subunits were created, referring to the first and second subunits respectively, and the donor was subcloned into the recipient using AgeI and XhoI restriction sites to produce the full-length tandem dimer (Figure 2.2). The recipient subunit consists of the channel without the stop codon, and the donor consists of a linker (GGGSGGGS), followed by the channel sequence lacking its start codon, and included a V5/His6 epitope tag on the C-terminus.

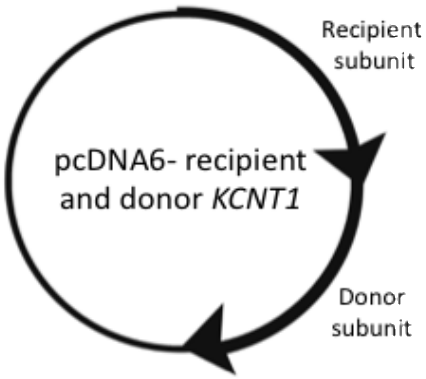

Figure 2.2: Schematic plasmid map showing full tandem dimer construct. Containing variable combinations of WT and Y796H *KCNT1* recipient and donor subunits.

2.2.1 Primers used for PCR

Primers for creating the tandem-dimer constructs using the NEB insertion/deletion PCR method were ordered and prepared as described previously for site-directed mutagenesis. The forward and reverse primers used for individual reactions are detailed in Table 2.7.

Table 2.7: Primers used for insertion/deletion PCR to engineer tandem-dimer constructs and later to modify the linker region (Integrated DNA Technologies Inc, Leuven, Belgium).
The primers were designed using the New England Biolabs site, and were reconstituted in nuclease-free water to make 100 µM stock solutions.

Construct	Primer sequence
Partial donor N-terminus	
Xho1 linker forward	5′-TTAACTCGAGGGCGGCGGCAGCGGCGGCGGCAGCCCACTCCCTGACG -3′
Xba1 Bsu36I reverse	5′- CGCCTCTAGACCTCAGGCTCGATC -3′
Partial donor C-terminus and V5-His6 tag	
Xba1 Kas1 forward	5′- TTAATCTAGAGGCGCCCAAGC -3′
BstBi reverse	5′- CTTACCTTCGAAGAGCTGTGTCTCGTC-3′
Recipient	
Kas1 forward	5′- CGGAGGCTGAGC -3′
Xho1 reverse	5′- CTAGACTCGAGCTGTGTCTCGTC -3′
Self-cleaving T2A peptide	
T2A site forward	5′-ACATGCGGGGACGTGGAGGAAAATCCCGGCCCACTCCCTGACGGGGCG -3′
T2A site reverse	5′-TAGAAGACTTCCCCTGCCCTCGCCGGAGCCCTCGAGCGGCCGCCACTG -3′
Long linker sequence	
Long linker forward	5′-GGTGGCTCTGGCGGTGGCGGATCGCCACTCCCTGACGGGGCG -3′
Long linker reverse	5′-TCCGCCTGAACCGCCACCACCTGACTCGAGCGGCCGCCACTG -3′

2.2.2 Construction of the donor monomer

The donor was created in two steps; first, a "partial donor" construct was created, consisting of an empty pcDNA6 vector containing just the linker and N-terminus of the channel, and the V5His6-tagged C-terminus. The NEB insertion/deletion PCR method was utilised to amplify a 339 bp fragment from pcDNA6-*KCNT1,* from the second codon to the unique Bsu36I restriction site, containing a linker (GGGSGGGS) and omitting the channel start codon. An XbaI restriction site was introduced at the 3' end, and a XhoI site introduced at the 5' end of the N-terminus of the WT K_{Na}1.1 channel.

In a separate reaction, a 434 bp fragment containing the C-terminus of the WT K_{Na}1.1 channel from the unique KasI restriction site to the last codon was amplified from

pcDNA6-*KCNT1*. XbaI was introduced at the 5' end, and BstBI at the 3' end. Both reactions were carried out using the primers detailed in Table 2.7, and the reaction protocol detailed in Table 2.8. The two fragments were ligated into the pJET1.2 blunt cloning vector described earlier (Thermoscientific, Loughborough, UK) and the products used to transform *E. coli*. Following verification by Sanger sequencing (GeneWiz, Takeley, UK), the fragments were subcloned into an empty pcDNA6-V5His6 vector using restriction enzymes XhoI and XbaI for the N-terminus fragment and XbaI and BstBI for the C-terminus fragment, and T4 DNA ligase. The remainder of the WT $K_{Na}1.1$ or the Y796H channel sequence could then be subcloned into the partial donor construct to produce the full donor plasmid, using restriction enzymes Bsu36I and KasI, and T4 DNA ligase as previously described.

Table 2.8: PCR protocol used to engineer the N-terminus and C-terminus of the donor sequence, and the C-terminus of the recipient sequence in pcDNA6 vector.
Q5 polymerase was used, with Q5 Buffer and GC enhancer.

Temperature	Time	Purpose
98°C	1 minute	Denaturation
98°C	20 seconds	Denaturation
59°C	20 seconds	Annealing
72°C	30 seconds	Extension
Stages 2-5 repeated for 26 cycles		
72°C	5 minutes	Extension
4°C	-	Holding temperature

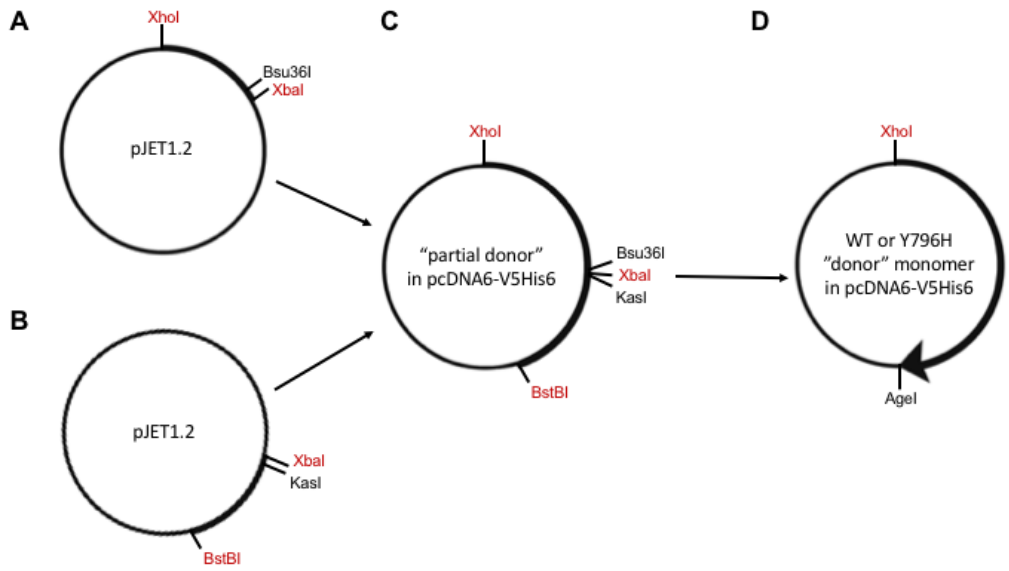

Figure 2.3: Schematic plasmid maps showing construction of *KCNT1* donor subunit, and the relevant naturally-occurring (black) and introduced (red) restriction sites at each stage.
A) 339 bp fragment containing *KCNT1* N-terminus and the linker region, ligated into pJET1.2 blunt cloning vector. **B)** 434 bp fragment containing *KCNT1* C-terminus and the linker region, ligated into pJET1.2 blunt cloning vector. **C)** 'Partial donor' plasmid comprised of the N-terminus **(A)** and C-terminus **(B)** fragments subcloned into an empty pcDNA6-V5His6 vector. The remainder of the channel sequence (without N- or C-termini) could then be subcloned into Bsu36I and KasI restriction sites from WT or Y796H pcDNA6-*KCNT1*. **D)** The full Y796H or WT donor monomer plasmid. XhoI and AgeI restriction sites were later used to subclone the donor into the recipient plasmid.

2.2.3 Construction of the recipient monomer

A 412 bp fragment containing the C-terminus of *KCNT1* from KasI to XhoI restriction sites was amplified from pcDNA6-*KCNT1* using PCR as described in Table 2.8, to insert a XhoI restriction site at the 3' end and omit stop codon. As with the donor monomer, the fragment was ligated into the pJET1.2 blunt cloning vector (Thermoscientific, Loughborough, UK) and the product used to transform *E.* coli. Using restriction enzymes KasI and XhoI, and T4 DNA ligase as previously described, the new C-terminus was subcloned into the pcDNA6-*KCNT1* sequence, replacing the existing C-terminus. The Y796H mutation could then be introduced into the recipient subunit using restriction enzymes SbfI and KasI.

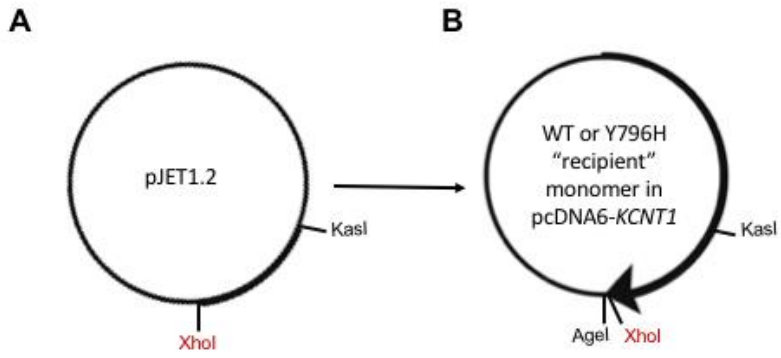

Figure 2.4: Schematic plasmid maps showing construction of *KCNT1* recipient subunit, and the naturally-occurring (black) and introduced (red) relevant restriction sites at each stage.
A) A 412 bp fragment containing the *KCNT1* C-terminus without stop codon and PDZ binding motif, ligated into pJET1.2 blunt cloning vector. **B)** Recipient monomer lacking stop codon and PDZ binding motif subcloned into pcDNA6-*KCNT1*; the Y796H mutation could be subcloned between naturally-occurring SbfI and KasI sites. The donor monomer detailed in Figure 2.2 was later subcloned into the AgeI and XhoI restriction sites.

2.2.4 Construction of the full tandem dimer sequence

Using AgeI and XhoI restriction enzymes and T4 DNA ligase as previously described, the donor sequence was subcloned into the recipient plasmid, fusing the two subunits together.

DNA was introduced into MAX Efficiency Stbl2 competent cells (Thermoscientific, Loughborough, UK), which are adapted for cloning unstable inserts and were selected due to their recombinase deficiency, by heat shocking. The competent cell and DNA mixture were incubated on ice for 30 minutes before heat shocking at 42°C for 25 seconds before transferring onto ice for 2 minutes for recovery. The mixture was then used to inoculate agar plates containing 100 mg/ml ampicillin, and colonies grown in an incubator at 30°C for >15 hours. Following successful transformation, colonies were picked from agar plates and inoculated in LB Broth (Sigma-Aldrich, Dorset, UK) containing 100 mg/ml ampicillin in ddH_2O and grown overnight in a shake incubator at 30°C. Cloudiness was used as an indication that *E. coli* cells had successfully grown-up in the broth, and DNA could be extracted. DNA was extracted from LB Broth using a QIAprep Miniprep kit (Qiagen, Manchester, UK), according to the instructions included in the kit. Identity of miniprep DNA was confirmed by Sanger sequencing (GeneWiz, Takeley, UK).

2.2.5 Introduction of T2A self-cleaving site and longer linker into tandem dimers

Following characterisation, two different approaches were taken to optimise the tandem dimer constructs; lengthening the linker region to 16 amino acids to increase flexibility (SGGGGSGGGGSGGGGS), and introduction of a *Thosea asigna* virus 2A (T2A) self-cleaving peptide sequence into the linker region. 'Self-cleaving' refers to ribosomal skipping over the prolyl-glycyl peptide bond at the C-terminus of the peptide, as opposed to true cleavage. This breaks the link between the tandem dimer subunits, whilst retaining subunit stoichiometry (Liu et al., 2017).

Both modifications were carried out in the donor subunit, using the NEB insertion/deletion method, and the 'partial donor' sequence as a template. The primers are detailed in Table 2.7, and the protocol detailed in Table 2.9. The remainder of the WT or Y796H channel sequence was subcloned into both of the new partial donor constructs to produce the full-length donor plasmids, using restriction enzymes Bsu36I and KasI, and T4 DNA ligase, as previously described. Finally, the new donor plasmids were subcloned into the original recipient subunit using restriction enzymes AgeI and XhoI.

In the text and figures, tandem dimers are named to indicate positioning of the WT and mutant subunits in the first or second position of the dimer. A hyphen between subunits indicates that the subunits are tethered, and a slash indicates a T2A site. For example, WT-YH describes a tethered tandem dimer with a WT subunit in the first position and Y796H in the second; WT/YH refers to the same subunit composition but with a T2A self-cleaving site between the subunits. Co-expressed subunits are indicated by a plus sign; for example, Y796H+WT refers to co-expressed WT and Y796H cDNA.

Table 2.9: PCR protocol used to introduce T2A or longer linker sequences into donor plasmid.
Q5 polymerase was used, with Q5 Buffer and GC enhancer.

Temperature	Time	Purpose
98°C	1 minute	Denaturation
98°C	20 seconds	Denaturation
63°C	20 seconds	Annealing
72°C	2 minutes	Extension
Stages 2-5 repeated for 28 cycles		
72°C	5 minutes	Extension
4°C	-	Holding temperature

2.3 Cell culture and transfection

HEK-293 cells expressing the human macrophage scavenger receptor (GripTite™ 293 MSR, Invitrogen) or CHO cells (gifted by Prof. Nikita Gamper) were cultured in Dulbecco's Modified Eagle's Medium (DMEM) containing Glutamax and supplemented with 10% (v/v) Foetal Bovine Serum (FBS), 50 U/ml penicillin and 0.05 mg/ml streptomycin (all from Thermoscientific, Loughborough, UK) and incubated at 37°C in air containing 5% CO_2. Cells were transiently transfected with wildtype or mutant plasmid using Mirus Bio TransIT-X2 transfection reagent (Geneflow, Lichfield, UK). For homomeric expression and concatemers 1.5 µg plasmid was used per 35 mm well at approximately 60% confluence. For heteromeric co-expression 0.75 µg of each construct was used. A pEYFP-N1 plasmid encoding EYFP (0.04 µg) was co-expressed as a marker of transfection; cells that fluoresced green when visualised with an epifluorescence microscope were likely to express the channel of interest since channel DNA was in excess of EYFP DNA in the transfection mixture. For electrophysiological experiments cells were plated onto borosilicate glass cover slips and used 2-4 days later.

2.3.1 Creating a stable HEK293 cell line

A HEK293 cell line was engineered that stably overexpressed one of the heteromeric concatemer constructs. HEK293 cells were transfected with 0.75 µg WT/YH plasmid using Mirus Bio TransIT-X2 as detailed above in a 35 mm well at 60% confluence, and following 24 hours of incubation cells were seeded into 10 cm petri dishes after 24 hours and cultured in DMEM containing 10 µg/ml blasticidin (InvivoGen, Toulouse,

France) as a selective pressure. Fresh media and blasticidin were added to the cells every 3-4 days over the course of two weeks, until visible colonies formed. Individual colonies were trypsinised and selected using gentle scraping and aspiration with a pipette tip, and transferred into wells of a 24-well plate containing media and 100 ng/µl blasticidin. Colonies were expanded into cell culture vessels of increasing size, and eventually characterised using whole cell electrophysiology to confirm stable expression of the channel of interest.

2.4 Electrophysiology

2.4.1 Solutions

- **Whole cell intracellular (pipette) solution** (mM) – 100 K-Gluconate, 30 KCl, 10 Na-Gluconate, 29 Glucose, 5 EGTA and 10 HEPES, pH 7.3 with KOH
- **Whole cell extracellular (bath) solution** (mM) – 140 NaCl, 1 $CaCl_2$, 5 KCl, 29 Glucose, 10 HEPES and 1 $MgCl_2$, pH 7.4 with NaOH
- **Nominally Na^+-free intracellular solution** (mM) – 100 K-Gluconate, 30 KCl, 10 $C_5H_{14}ClNO$ (choline chloride), 29 Glucose, 5 EGTA and 10 HEPES, pH 7.3 with KOH
- **40 mM Na^+ intracellular solution** (mM) – 100 K-Gluconate, 30 KCl, 40 Na-Gluconate, 5 EGTA and 10 HEPES, pH 7.3 with KOH
- **Whole cell intracellular (pipette) solution for hERG currents** (mM) – 100 K-Gluconate, 40 KCl, 2 $MgCl_2$, 10 EGTA and 10 HEPES, pH 7.2 with NaOH (Helliwell, 2008)
- **Whole cell extracellular (bath) solution for hERG currents** (mM) – 137 NaCl, 1.8 $CaCl_2$, 4 KCl, 10 Glucose, 10 HEPES and 1 $MgCl_2$, pH 7.3 with NaOH (Helliwell, 2008)

2.4.2 Whole cell electrophysiology

Macroscopic currents from CHO or HEK293-MSR cells transiently transfected with WT or mutant cDNA were obtained using the whole cell configuration of the gigaseal patch-clamp technique 2-4 days post-transfection, at room temperature (20-22°C). Glass micropipettes of 1.5-2.5 MΩ resistance were pulled from thin-walled, filamented borosilicate glass capillaries (Harvard Apparatus Ltd, Edenbridge, Kent, UK) using the Narishige PP- 830 pipette puller, and fire-polished before filling with experimental solutions.

Pipette and bathing solutions used are described above. Following establishment of a >2 GΩ seal, the cell membrane was ruptured to achieve the whole cell configuration. Currents were measured using a HEKA EPC 10 amplifier (HEKA electronic, Lambrecht, Germany) with 2.9 KHz low-pass filtering and 10 kHz digitisation. An Ag-AgCl electrode connected to the bath solution using a KCl-agar bridge was used as a reference. Data was collected and analysed using Patchmaster, and Fitmaster software (HEKA electronic, Lambrecht, Germany) for offline analysis. The liquid junction potentials between intracellular and extracellular solutions were calculated according to the stationary Nernst-Planck equation and used to correct reported $V_{0.5}$ values. This was 14.39 mV for 10 mM intracellular Na^+, 14.33 mV for the nominally Na^+-free solution and 14.61 mV for 40 mM intracellular Na^+.

In order to determine I-V relationships, the voltage protocol consisted of 400 msec steps from -100 to +80 mV in 10 mV increments, from a holding potential of -80 mV. Series resistance for whole cell recordings was <6 MΩ and recordings were compensated >65%.

2.4.3 Whole cell electrophysiology to study hERG channels

For analysis of hERG tail currents upon repolarisation to -80 mV, the whole cell configuration was used as previously described. In order to evoke large tail currents, cells were held at −80 mV, and 4 s depolarising pulses to +40 and then −50 mV were applied at 0.2 Hz (Helliwell, 2008). Peak tail currents were measured individually using HEKA Fitmaster offline analysis (HEKA electronic, Lambrecht, Germany) to avoid contamination by capacitance spikes.

2.5 Pharmacological modulation of the channel

2.5.1 Compounds used

Table 2.10: **Compounds used to study pharmacological modulation of $K_{Na}1.1$.** All compounds were made up as a 10 mM stock in DMSO, except for quinidine and bepridil which were made up as 100 mM and 30 mM stocks respectively. The final drug concentrations were obtained by diluting the stock solution in the whole cell bath solution on the day of experiments.

Compound	Supplier
Quinidine	Sigma-Aldrich, Dorset, UK
Bepridil	Sigma-Aldrich, Dorset, UK
Test compounds (BC1-17 and 12.1-4)	Chembridge Corp., San Diego, CA
Antrafenine dihydrochloride	Insight Biotech,
Candesartan cilexetil	Bioserv, Sheffield, UK
Nelfinavir mesylate	Bioserv, Sheffield, UK
Regorafenib	Bioserv, Sheffield, UK
Atorvastatin	Bioserv, Sheffield, UK
Dihydro tachysterol	Bioserv, Sheffield, UK
Lifitegrast	Cambridge Bioscience Ltd, Cambridge, UK
Terconazole	Sigma-Aldrich, Dorset, UK
Indinavir sulphate hydrate	Bioserv, Sheffield, UK
Niclosamide	Sigma-Aldrich, Dorset, UK
Loxapine succinate	Sigma-Aldrich, Dorset, UK

2.5.2 Experimental procedure for studying $K_{Na}1.1$ inhibition

Drugs were applied by continuous gravity perfusion into the bath for 2 minutes, following establishment of the whole cell configuration. Control solution was perfused to wash out the drugs at the end of the experiment. Only recordings that did not display any rundown prior to perfusion with drug solutions were included in the analysis.

Voltage ramps were applied at 0.2 Hz; voltage was stepped from a holding potential of -80mV to -100mV, then ramped to +40 mV or 0 mV over 500 ms and stepped back to the holding potential following this.

2.6 WST-1 cytotoxicity assay

A colorimetric WST-1 assay was used to assess possible cytotoxicity of test compounds. The assay involves cleavage by cellular mitochondrial dehydrogenases of a slightly red-coloured tetrazolium salt, WST-1 (Water-soluble tetrazolium-1, or 4-[3-(4-Iodophenyl)-2-(4-nitro-phenyl)-2H-5-tetrazolio]-1,3-benzene sulfonate), to formazan, which is dark red in colour. A decrease in cell viability results in a reduction in mitochondrial dehydrogenase activity, thus reducing cleavage of WST-1 and reducing the amount of formazan produced. This reduction can be quantified using a spectrophotometer to measure absorbance (Berridge et al., 2005).

Non-transfected HEK293-MSR cells were seeded at a density of $5x10^4$ cells/ well in a 96-well plate and incubated overnight at 37°C in 5% CO_2. Following exposure to three different concentrations of inhibitor for 24 hours, WST-1 reagent (Source Bioscience, Nottingham, UK) was added and cells were incubated for a further 2 hours. Inhibitor concentrations were chosen to compare with effects of individual compounds on $K_{Na}1.1$ current in electrophysiological experiments. Cells were also treated with 10% (v/v) DMSO and blasticidin (InvivoGen, Toulouse, France) at a concentration of 10 µg/ml as positive controls. Absorbance at 450 nm (reference 650 nm) was measured using the Flexstation 3 microplate reader (Molecular Devices, Wokingham, UK). Cell viability was calculated as a percentage of the absorbance value measured from untreated cells.

2.7 Western Blotting

2.7.1 Buffers

- **Lysis buffer** – Pierce RIPA buffer (Thermoscientific, Loughborough, UK), cOmplete™ Mini protease inhibitor cocktail (7x), Pierce universal nuclease (10,000x) (Thermoscientific, Loughborough, UK)
- **Sample buffer** – NuPAGE LDS sample buffer (4x) (Thermoscientific, Loughborough, UK), 100 µM 1,4-dithiothreitol (DTT)
- **Running buffer** – 25 mM Tris base, 192 mM glycine, 0.1% (w/v) SDS, pH 8.3
- **Transfer buffer** – 25 mM Tris base, 192 mM glycine, 0.05% (w/v) SDS, 10% (v/v) methanol, pH 8.3
- **PBS-T** – Phosphate buffered saline, 0.05% (v/v) Tween-20
- **Blocking buffer** – PBS-T, 5% (w/v) non-fat dried milk

2.7.2 Cell lysis and protein extraction

HEK293-T cells or CHO cells transfected with WT-WT or WT/WT cDNA were grown to 90% confluency in a 6-well plate. Cells were washed twice with ice-cold PBS and lysed with 200 µl lysis buffer at 4°C. The lysate was collected and sonicated on ice for a total of 15 seconds in 5 second pulses, before centrifuging for 20 minutes at 12,000 RPM at 4°C. The supernatant was used immediately or stored at -20°C for later use.

2.7.3 SDS-PAGE gel electrophoresis

20 µl total cell lysate was added to sample buffer and incubated at room temperature for 30 minutes. A 10% Mini-PROTEAN® TGX™ Precast Protein Gel (Bio-Rad, Hemel Hempstead, UK) was used, and run in a Mini-PROTEAN Tetra Vertical Electrophoresis Cell (Bio-Rad, Hemel Hempstead, UK). The gel was submerged in running buffer at room temperature, and 5 µl Color Prestained Protein Standard (New England Biolabs, Hitchin, UK) was pipetted into the first well. 30 µl of each total lysate sample was loaded into the following wells, and 160 V was applied for 45 minutes, or until the dye fronts had reached the bottom of the gel.

2.7.4 Electrophoretic transfer

The separated proteins were transferred onto a 0.45 µm nitrocellulose membrane (Sigma-Aldrich, Dorset, UK) using the Mini Trans-Blot Module (Bio-Rad, Hemel Hempstead, UK) to carry out a wet tank transfer optimised for high molecular weight proteins. The membrane, sponges, and 6 pieces of thick card were soaked in cold transfer buffer for up to 15 minutes prior to assembling the transfer sandwich. The blotting cassette was assembled in the following order; anode, sponge, 3 pieces of card, membrane, gel, 3 pieces of card, sponge, cathode. The cassette was inserted into the Mini-PROTEAN Tetra Vertical Electrophoresis Cell (Bio-Rad, Hemel Hempstead, UK), covered with cold transfer buffer and run at 150 mA for 4 hours at 4°C. Successful transfer of proteins from the gel was confirmed by incubating the gel in QuickBlue Stain (Stratech, Ely, UK) at room temperature for 15 minutes.

2.7.5 Immunodetection

Following transfer, the membrane was incubated for 1 hour at room temperature with blocking buffer, to block non-specific binding sites. The membrane was then incubated

with a rabbit anti-V5 antibody (Biolegend, London, UK) diluted 1:5000 in blocking buffer at 4°C. The membrane was washed for 30 minutes with PBS-T prior to incubating for 1 hour at room temperature with a Horseradish peroxidase-conjugated (HRP) goat anti-rabbit secondary antibody (Genetex, Ely, UK) diluted 1:1000 in blocking buffer. After another 30 minute wash with PBS-T, a 1:1 mixture of SuperSignal West Pico PLUS Luminol/Enhancer and SuperSignal West Pico PLUS stable peroxide (Thermoscientific, Loughborough, UK) was pipetted over the membrane, and the blot was exposed and imaged for 10 minutes using a G:BOX XT4 chemiluminescence and fluorescence imaging system (Syngene, Cambridge, UK).

2.8 Analysis

Statistical analysis was performed using SPSS (IBM Analytics, Portsmouth, UK), with the chosen tests indicated in figure legends. $p<0.05$ was considered significant. Graphs were constructed using Origin Pro (OriginLab, Stoke Mandeville, UK), and all values are plotted as mean ± s.e.m.

2.8.1 Characterisation of epilepsy-causing mutations

Representative whole cell and excised inside-out current traces were plotted, and residual capacitance spikes removed in Origin Pro. Whole cell current-voltage relationships were averaged and divided by whole cell capacitance to give current density (pA/pF). Reversal potentials were obtained by fitting the linear part of current-voltage relationships around the reversal potential using linear regression and determining the voltage at which current was 0 nA. Conductance values (*G*) were obtained by dividing current amplitudes by the driving force for K^+ ions, calculated using the reversal potentials obtained for individual recordings:

$$\boldsymbol{G = I/(V_m - V_{rev})} \qquad \textbf{(Equation 1)}$$

The values were then plotted and fit with a Boltzmann function using least squares fitting:

$$\boldsymbol{G = \frac{G_{max} - G_{min}}{1 + e^{(V - V0.5)/k}} + G_{min}} \qquad \textbf{(Equation 2)}$$

which gave values for activation midpoint ($V_{0.5}$), G_{max}, G_{min}, and Slope factor (*k*). Data were normalised by dividing by G_{max} for each recording. Reported $V_{0.5}$ values were corrected for Liquid Junction Potential. Elementary gating charges (*z*) were derived from the slope of the Boltzmann fit of G-V curves, k=RT/zF. The zero-voltage free

energy of channel opening (ΔG_0) was calculated using parameters derived from the Boltzmann fits:

$$\Delta G_0 = zFV_{0.5} \qquad \textbf{(Equation 3)}$$

and expressed as kcal/mol. The closed-state destabilisation energy ($\Delta\Delta G_0$) was calculated as the difference in ΔG_0 between WT and mutant $K_{Na}1.1$ channels.

Currents were fit with a single exponential function at each voltage measured, yielding the activation time constant (τ):

$$I(t) = I_0 + I_{max}\,(1 - e^{-t/\tau}) \qquad \textbf{(Equation 4)}$$

where I_0 is the current offset, I_{max} is the steady-state current amplitude and τ is the time constant of activation.

2.8.2 Characterising inhibition of $K_{Na}1.1$

Compounds that were deemed active after perfusion of a single concentration (10 µM) were analysed further by concentration-response analysis:

$$\frac{G}{G_C} = \left(1 + \left(\frac{[B]}{IC_{50}}\right)^{H}\right)^{-1} + c \qquad \textbf{(Equation 5)}$$

where G is the conductance measured as the slope of the current between -60 and 0 mV evoked by the voltage ramp in the presence of the inhibitor, G_c is the control conductance in the absence of inhibitor, [B] is the concentration of the inhibitor, IC_{50} the concentration of inhibitor yielding 50% inhibition, H the slope factor, and c the residual conductance.

3 Functional characterisation of homomeric and heteromeric epilepsy-causing variants

3.1 Introduction

Several mechanisms have been proposed for how pathogenic variants may lead to GOF, such as changes in Na^+ sensitivity or increased $P_{o,max}$ (Tang et al., 2016; Rizzo et al., 2016; Dilena et al., 2018). Other studies have shown that pathogenic variants increase cooperative gating between channels in the same patch excised from *Xenopus* oocytes (Kim et al., 2014), reduce subconductance states (Barcia et al., 2012; Kim et al., 2014), or cause $K_{Na}1.1$ to be in a constitutively phosphorylated-like state, as a result of altered interactions with binding proteins such as Phactr1 (Ali et al., 2020). Amino acid changes are seen across the channel structure, mainly in the pore-forming region and intracellular C-terminus, on the RCK domains and NAD^+ binding domain. Mutations located in distinct regions of the channel structure have been shown to have similar effects. Although the variants may alter channel activity through different mechanisms, the overall effect is through GOF characterised by an increase in outward current amplitude, accompanied by a shift in the half-maximal activation voltage in the hyperpolarising direction.

Virtually all patients to date with DEEs resulting from pathogenic *KCNT1* variants are heterozygous, carrying only one mutated allele. There is a paucity of information in the literature describing the behaviour of heteromeric channels comprising variant and WT $K_{Na}1.1$ subunits. Most functional studies have been carried out by studying homomeric variant channels, but some recent efforts have been made to study the implications of heterozygous *KCNT1* variants (Rizzo et al., 2016; Dilena et al., 2018) or *KCNT2* variant subunits co-expressed with *KCNT1* (Mao et al., 2020) on channel function *in vitro*. These studies suggest that heteromeric channels display 'intermediate' characteristics, with current amplitudes and activation kinetics lying somewhere between WT and variant homomeric channels.

In terms of treating *KCNT1*-related DEEs, a better understanding is required of how the effects of all pathogenic variants converge on the $K_{Na}1.1$ channel gating mechanism and how this is altered in heteromeric assemblies of WT $K_{Na}1.1$ and mutant subunits. To probe this further, seven (AD)SHE or EIMFS-causing *KCNT1* variants have been chosen that have been previously reported. The variants selected have had different mechanisms proposed for how they exert their GOF effect and are

located in different domains across the $K_{Na}1.1$ protein structure (Figure 3.1). It was hypothesised that the GOF effect in heteromeric mutant and WT $K_{Na}1.1$ assemblies would have a common underlying mechanism regardless of the location of the amino acid substitution on the channel protein. Intracellular Na^+ is an absolute requirement for activation of the WT $K_{Na}1.1$ channel, and a number of variants reportedly alter the Na^+ sensitivity of the channel (Tang et al., 2016; Rizzo et al., 2016). The effects of removing intracellular Na^+ and the properties of unliganded channels were therefore examined.

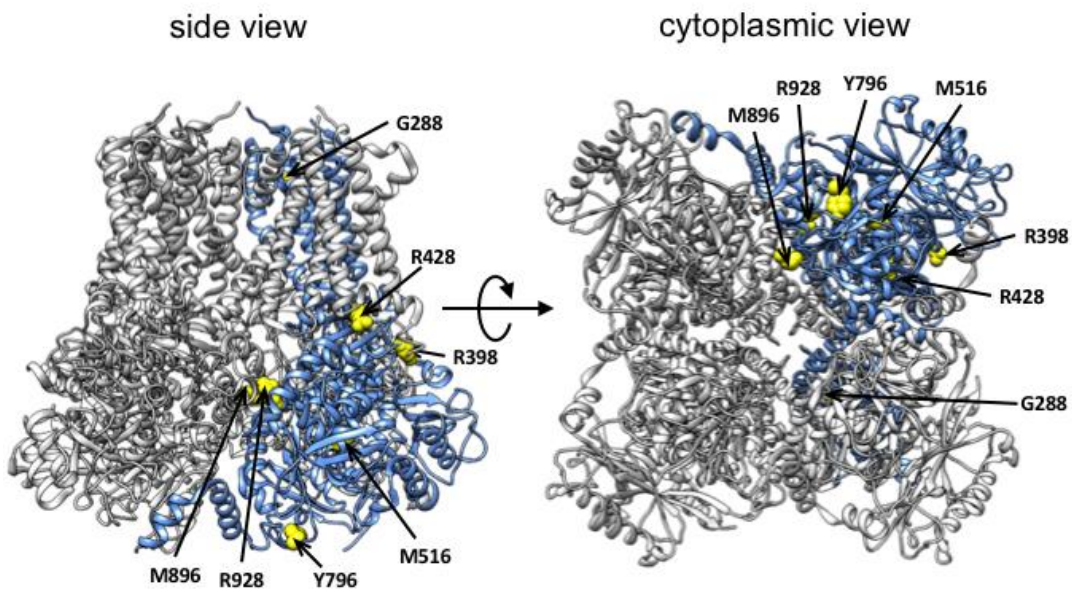

Figure 3.1: Location of amino acids associated with (AD)SHE or EIMFS examined in this chapter.
On the structure of the active chicken $K_{Na}1.1$ channel (PDB: 5U70). Amino acid residues indicated in yellow are the equivalent to disease-causing pathogenic variants on the human $K_{Na}1.1$ channel, one subunit indicated in blue [Figure prepared by Dr Jonathan D. Lippiat using UCSF Chimera].

3.1.1 Chapter hypothesis and aims

Hypothesis: GOF resulting from DEE-causing amino acid substitutions in arises as a result of a common mechanism, regardless of location of the amino acid substitution on the $K_{Na}1.1$ channel structure.

Aims:

- ***To investigate whether GOF in channels comprised of both mutant subunits alone and when co-expressed with WT $K_{Na}1.1$ subunits is due to a common mechanism***
- ***To examine the effects of removing intracellular Na^+ on kinetics and activation of homomeric and heteromeric mutant channels***

3.2 Results

3.2.1 All homomeric KCNT1 pathogenic variants increase macroscopic current in CHO cells

Macroscopic currents were recorded using the whole cell configuration from CHO cells expressing either WT $K_{Na}1.1$ or (AD)SHE or EIMFS-causing mutant channels. EIMFS-causing variants G288S, R428Q, and M516V, and (AD)SHE-causing variants Y796H, R928C, M896I, and R398Q were chosen. WT $K_{Na}1.1$ channels gave outward currents in response to a series of voltage steps from -100 mV to +80 mV from a holding potential of -80 mV with 10 mM intracellular Na^+, in line with previous characterisation (Yuan et al., 2003; Bhattacharjee et al., 2003; Joiner et al., 1998); and the current consisted of an instantaneous component followed by a slower, time-dependent component (Figure 3.2A and 3.2B). Non-transfected CHO cells yielded little outward current (1.49 ±0.67 pA/pF at +10 mV, n=8), with no time or voltage-dependence; implying very low endogenous activity. Similarly, in the nominally Na^+-free intracellular solution, negligible WT $K_{Na}1.1$ current was seen across the same voltage range (2.93 ±1.08 pA/pF at +10 mV, n=6); confirming that intracellular Na^+ is an absolute requirement for activation of the WT $K_{Na}1.1$ channel. Also in agreement with previous reports (Milligan et al., 2014; Rizzo et al., 2016; Dilena et al., 2018; Heron et al., 2012; McTague et al., 2018; Kim et al., 2014; Barcia et al., 2012; Gertler et al., 2019), each of the mutant $K_{Na}1.1$ channels examined resulted in large GOF with 10 mM intracellular Na^+ (Figure 3.2A-C). EIMFS-causing mutants caused a 6-7-fold increase in mean peak

current density at +10 mV (Figure 3.2B). (AD)SHE-causing mutants caused a 4-fold increase, except for Y796H, which resulted in a 6-fold increase (Figure 3.2B). From current-voltage relationships, mutations caused an increase in inward currents at membrane potentials negative to the reversal potential, as well as outward current. Both EIMFS and (AD)SHE-causing mutant channels displayed a shift in their activation midpoints towards more negative potentials when conductance-voltage values were fitted with a Boltzmann function (Figure 3.2C and Table 3.1). The zero-voltage activation energy change calculated for each EIMFS- or (AD)SHE-causing mutant channel was negative, unlike the positive value obtained with WT. The closed-state destabilisation energy ($\Delta\Delta G_0$), calculated by the difference between ΔG_0 values for WT and mutant $K_{Na}1.1$ channels, was high for all homomeric mutants (Table 3.1).

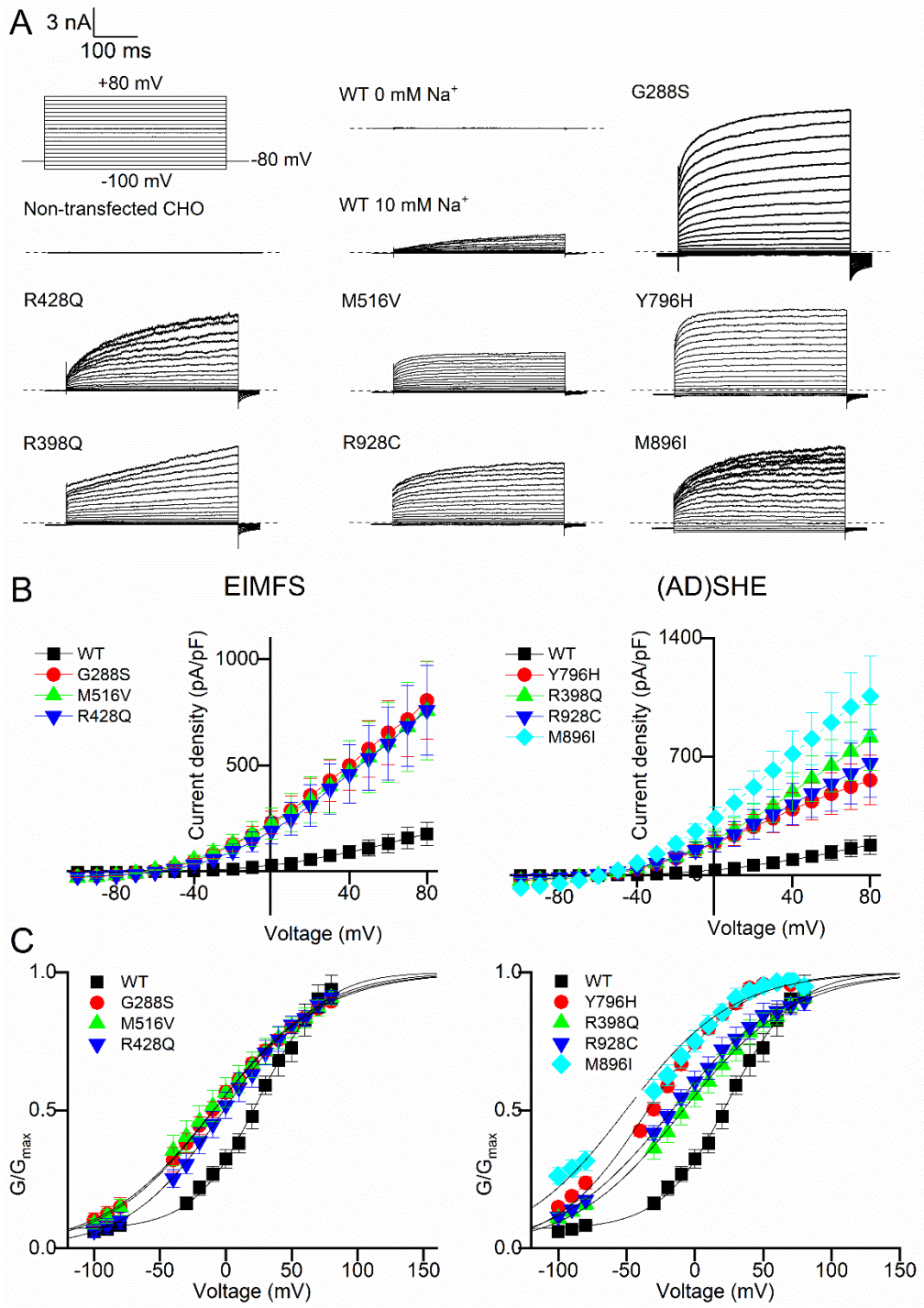

Figure 3.2: Functional characterisation of EIMFS and (AD)SHE-causing *KCNT1* variants.

A) Representative traces for whole cell currents from Non-transfected CHO cells (NT) and CHO cells transfected with WT and mutant human $K_{Na}1.1$, as indicated in response to 400 msec steps from -100 to +80 mV in 10 mV increments, from a holding potential of -80 mV. n= 5 to 9 cells for each mutation. **B)** Mean (±s.e.m.) current-voltage relationship for WT $K_{Na}1.1$ (n=6), EIMFS-causing mutant channels (n= 5-9 for each mutant, left) and (AD)SHE-causing mutant channels (n= 5-9 for each variant, right panel). **C)** Normalised mean (±s.e.m.) conductance-voltage relationship for WT $K_{Na}1.1$ (n=6), EIMFS-causing mutant channels (n= 5-9 for each mutant, left panel) and (AD)SHE- causing mutant channels (n= 5-9 for each mutant, right), fitted with Boltzmann functions.

3.2.2 Co-expressed WT $K_{Na}1.1$ and variant subunits yield currents displaying a mixture of WT and variant characteristics

Co-expression has been used in previous studies of $K_{Na}1.1$ and closely related $K_{Na}1.2$ to examine behaviour of heteromeric co-assemblies of WT and mutant subunits (Rizzo et al., 2016; Dilena et al., 2018; Mao et al., 2020). The EIMFS-causing mutations; G288S, R428Q and M516V, and (AD)SHE-causing mutations; Y796H, R928C, M896I and R398Q, were co-expressed with WT $K_{Na}1.1$ subunits in a 0.5:0.5 ratio, by plasmid mass, to model the genetic status of heterozygous patients.

Mean peak current densities at +10 mV recorded for all mutant+WT co-assemblies with 10 mM intracellular Na^+ were 3-4-fold larger than homomeric WT channels, regardless of whether the mutation was (AD)SHE or EIMFS-causing (Figure 3.3B and D; Figure 3.4B and D). Only G288S and M896I were significantly smaller at +10 mV than the homomeric mutant when co-expressed with WT $K_{Na}1.1$ subunits (Figure 3.3D and 3.4D). Furthermore, all heteromeric mutant assemblies except R398Q+WT exhibited a rightward shift in their activation midpoint derived from a Boltzmann fit of conductance values compared to homomeric mutant channels (Figure 3C, 4C and Table 1).

3.2.3 Mutant channels activate in the absence of intracellular Na^+

WT $K_{Na}1.1$ channels are primarily activated by intracellular Na^+, thus removing Na^+ from the pipette solution would enable any Na^+-independent activity of mutant $K_{Na}1.1$ channels to be detected. G288S and M516V, and two other EIMFS-causing variants, E893K and R950Q have been studied previously in the absence of intracellular Na^+ (Rizzo et al., 2016; Dilena et al., 2018), but no (AD)SHE-causing variants or other DEE-causing variants, including R428Q, have been studied in this way. All of the homomeric mutant channels examined yielded currents in a nominally Na^+-free solution, though current densities were reduced compared those recorded in the presence of intracellular Na^+. The decrease in mean peak current density at +10 mV was modest, with a 1-4 fold decrease for all mutants with the exception of R398Q, which showed a 13-fold decrease (Figure 3.3D and 3.4D). Activation midpoints obtained from Boltzmann analysis of the mutants were shifted rightwards by 15-60 mV compared to those measured in the presence of intracellular Na^+ for all mutants (Figure 3.3B, 3.4B and Table 3.1). The activation midpoints became positive for all mutants except Y796H in the absence of Na^+ (Table 3.1). Zero-voltage free energy values for

homomeric variants also became positive, and there was a reduction in $\Delta\Delta G_0$ values (Table 3.1).

For all co-expressed mutant and WT $K_{Na}1.1$ subunits, mean peak current density recorded at +10 mV was decreased 7-34 fold in the absence of intracellular Na^+ compared to currents recorded with 10 mM intracellular Na^+ (Figure 3.3D and 3.4D). The size of the currents prevented Boltzmann analysis of most mutant+WT channels in the absence of intracellular Na^+. Two (AD)SHE-causing mutants, M896I and R928C, produced sufficiently large currents in the absence of Na^+ when co-expressed with WT $K_{Na}1.1$. The activation midpoint in both cases was more rightward than the homomeric mutant with 0 mM intracellular Na^+ (Figure 3.4C and Table 3.1).

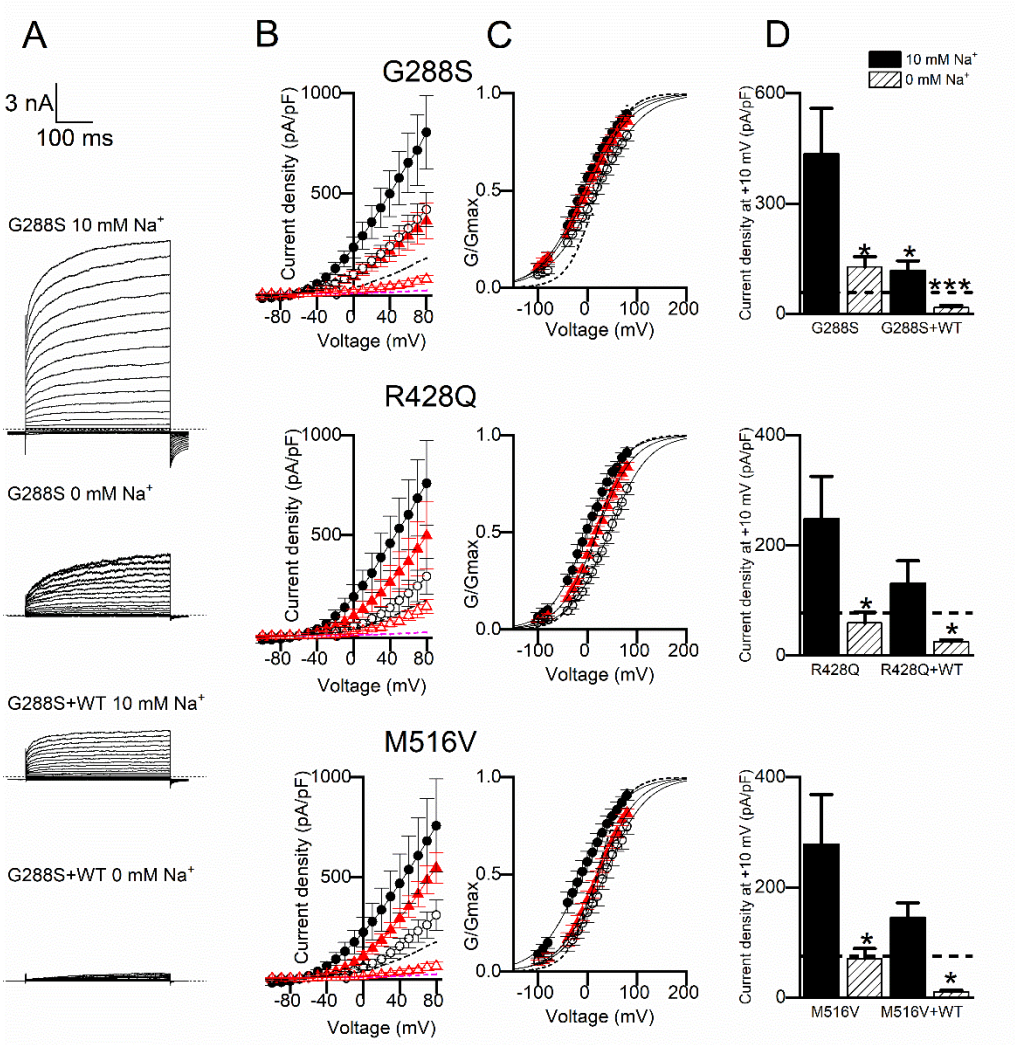

Figure 3.3: Functional characterisation of EIMFS-causing *KCNT1* variants in the presence and absence of intracellular Na^+.
A) Representative traces for homomeric G288S and heteromeric G288S+WT whole cell $K_{Na}1.1$ currents in response to 400 msec steps from -100 to +80 mV in 10 mV increments, from a holding potential of -80 mV in 10 mM and 0 mM intracellular Na^+, as indicated. Mean (±s.e.m.) current-voltage relationships **(B)** and conductance-voltage (**C)** relationships fitted with a Boltzmann function for EIMFS-causing mutants in 10 mM and 0 mM intracellular Na^+, and in the presence and absence of co-expressed WT $K_{Na}1.1$ (N=5-9 for all channel types). Black filled circle= homomeric mutant with 10 mM Na^+, black open circle= homomeric mutant with 0 mM Na^+, red filled triangle= heteromeric mutant+WT with 10 mM Na^+ and red open triangle heteromeric mutant+WT with 0 mM Na^+. WT $K_{Na}1.1$ indicated with dashed line. **D)** Mean peak current amplitude at +10 mV (±s.e.m.) for WT $K_{Na}1.1$ and mutant channels in 10 mM and 0 mM intracellular Na^+. Mean WT $K_{Na}1.1$ amplitude with 10 mM Na^+ indicated with dashed line. *p<0.05, **p<0.005, ***p<0.0005 compared to homomeric mutant with 10 mM Na^+, independent one-way ANOVA with Tukey's post-hoc test (N= 5-9 for each mutant).

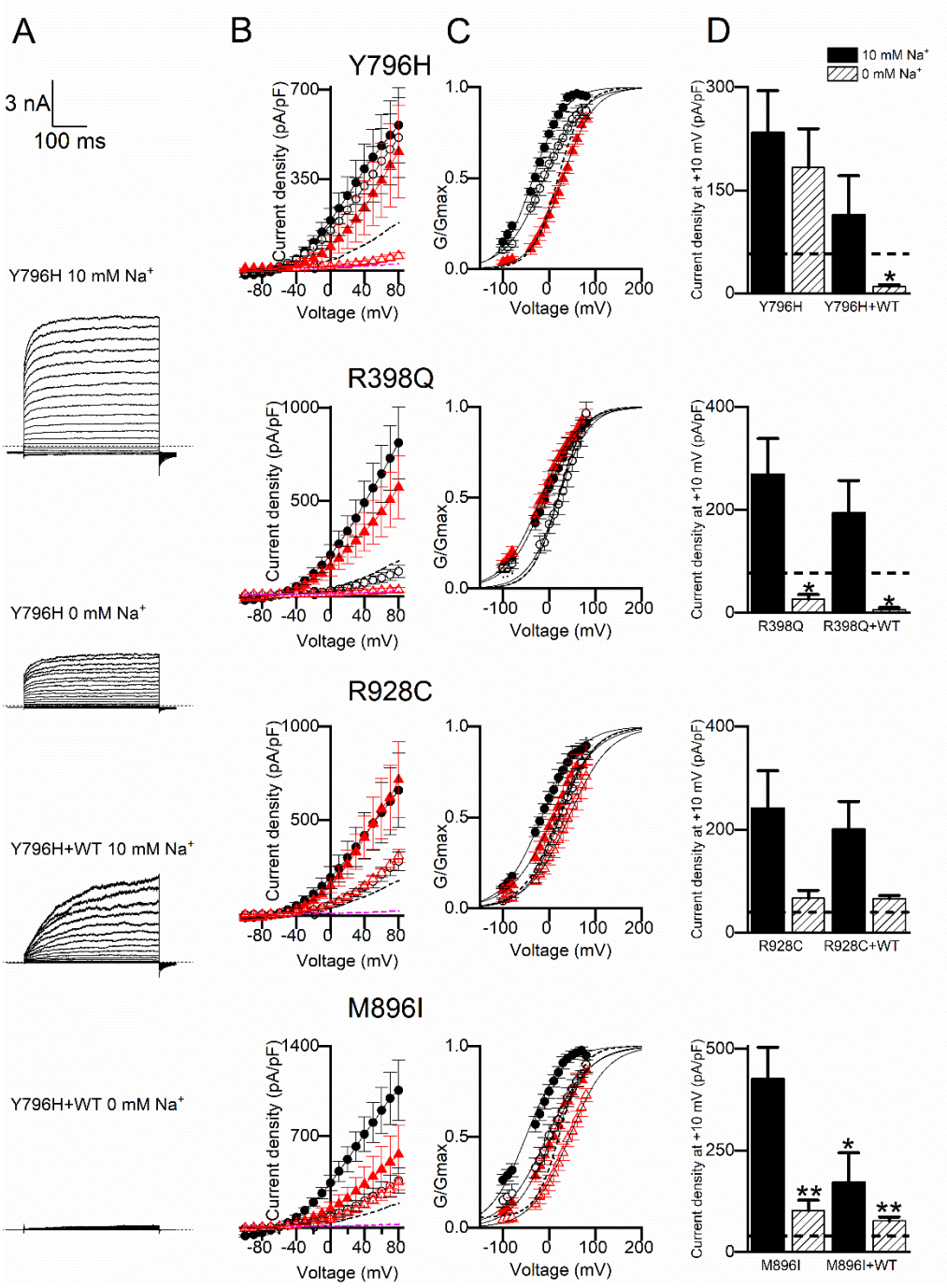

Figure 3.4: Functional characterisation of (AD)SHE-causing *KCNT1* variants in the presence and absence of intracellular Na^+.

A) Representative traces for homomeric Y796H and heteromeric Y796H+WT whole cell $K_{Na}1.1$ currents in response to 400 msec steps from -100 to +80 mV in 10 mV increments, from a holding potential of -80 mV in 10 mM and 0 mM intracellular Na^+, as indicated. Mean (±s.e.m.) current-voltage relationships **(B)** and conductance-voltage (**C)** relationships fitted with a Boltzmann function for (AD)SHE-causing mutants in 10 mM and 0 mM intracellular Na^+, and in the presence and absence of co-expressed WT $K_{Na}1.1$ (N=5-9 for all channel types). Black filled circle= homomeric mutant with 10 mM Na^+, black open circle= homomeric mutant with 0 mM Na^+, red filled triangle= heteromeric mutant+WT with 10 mM Na^+ and red open triangle heteromeric mutant+WT with 0 mM Na^+. WT $K_{Na}1.1$ indicated with dashed line. **D)** Mean peak current amplitude at +10 mV (±s.e.m.) for WT $K_{Na}1.1$ and mutant channels in 10 mM and 0 mM intracellular Na^+. Mean WT $K_{Na}1.1$ amplitude with 10 mM Na^+ indicated with dashed line. *p<0.05, **p<0.005, ***p<0.0005 compared to

homomeric mutant with 10 mM Na^+, independent one-way ANOVA with Tukey's post-hoc test (N= 5-9 for each mutant).

Table 3.1: Parameters derived from Boltzmann fit of WT, homomeric mutant, and co-expressed mutant+WT channels in the absence and presence of intracellular 10 mM Na^+.

Data are presented as mean ±s.e.m. $V_{0.5}$ is the half-maximal activation voltage, **p*<0.05, ***p*<0.005, ****p*<0.0005 compared to homomeric mutant with 10 mM $[Na^+]i$ (independent one-way ANOVA with Tukey's post-hoc test). Elementary gating charge, *z,* was derived from the slope of the Boltzmann curve, RT/zF. ΔG_0 is the zero-voltage free energy for channel opening: $\Delta \boldsymbol{G_0} = \boldsymbol{zFV_{0.5}}$ and is expressed as kcal/mol. $\Delta\Delta G_0$ is the closed-state destabilisation energy, calculated as the difference in mean ΔG_0 between WT and mutant $K_{Na}1.1$ channels (N= 5-9 for each mutant).

Channel	$V_{0.5}$ (mV)		*z*	ΔG_0 (kcal/mol)	$\Delta\Delta G_0$ (kcal/mol)
WT	7.38 ±4.35		1.01 ±0.13	0.15 ±0.10	-
G288S	-37.75 ±8.77		0.66 ±0.09	-0.58 ±0.18	0.73
G288S + WT	-11.76 ±4.18	*	0.59 ±0.04	-0.17 ±0.05	0.32
G288S 0 mM $[Na^+]_i$	-1.44 ±5.70	**	0.50 ±0.03	-0.02 ±0.07	0.17
Y796H	-39.99 ±2.27		0.92 ±0.08	-0.83 ±0.07	0.98
Y796H + WT	14.33 ±4.76	***	0.79 ±0.06	0.27 ±0.08	-0.12
Y796H 0 mM $[Na^+]_i$	-24.75 ±7.14		0.62 ±0.06	-0.36 ±0.11	0.51
R428Q	-14.61 ±6.19		0.73 ±0.03	-0.26 ±0.12	0.41
R428Q + WT	5.81 ±2.97	*	0.69 ±0.05	0.08 ±0.03	0.07
R428Q 0 mM $[Na^+]_i$	29.73 ±5.33	***	0.65 ±0.05	0.46 ±0.09	-0.31
M516V	-32.71 ±8.74		0.57 ±0.04	-0.42 ±0.11	0.57
M516V + WT	7.08 ±6.57	*	0.66 ±0.05	0.13 ±0.09	0.02
M516V 0 mM $[Na^+]_i$	23.42 ±7.17	**	0.65 ±0.04	0.35 ±0.10	-0.20
R398Q	-18.54 ±7.67		0.72 ±0.07	-0.32 ±0.13	0.47
R398Q + WT	-11.10 ±10.03		0.67 ±0.07	-0.20 ±0.13	0.35
R398Q 0 mM $[Na^+]_i$	11.91 ±3.91	*	0.91 ±0.10	0.28 ±0.13	-0.13
R928C	-36.23 ±4.11		0.64 ±0.12	-0.51 ±0.06	0.66
R928C + WT	-3.12 ±6.58	**	0.68 ±0.14	-0.07 ±0.09	0.22
R928C 0 mM $[Na^+]_i$	11.71 ±4.87	***	0.78 ±0.07	0.22 ±0.11	-0.07
R928C + WT 0 mM $[Na^+]_i$	26.72 ±6.51	***	0.65 ±0.13	0.37 ±0.13	-0.22
M896I	-37.70 ±5.90		0.96 ±0.10	-0.82 ±0.14	0.97
M896I + WT	-7.57 ±4.83	*	0.65 ±0.06	-0.09 ±0.05	0.24
M896I 0 mM $[Na^+]_i$	-12.55 ±5.58	*	0.78 ±0.15	-0.19 ±0.11	0.34
M896I + WT 0 mM $[Na^+]_i$	29.47 ±6.41	***	0.66 ±0.04	0.50 ±0.12	-0.35

3.2.4 The time constant of channel activation for WT and mutant $K_{Na}1.1$ channels is independent of both voltage and intracellular Na^+

To examine the effects *KCNT1* mutants may have on activation kinetics of the channel, a single exponential function was fitted to the currents at each voltage measured to yield the activation time constant (τ) (Figure 3.5A). Notably, although the channels have weak voltage sensitivity, the time constants for both WT and mutant channels were voltage-independent, with no significant difference across the whole voltage range (Figure 3.5B). The activation time constant of $K_{Na}1.1$ was not significantly altered by most mutations studied. An exception was (AD)SHE-causing $K_{Na}1.1$ mutation Y796H, which showed a 2-fold decrease in the time constant at +10 mV (Figure 3.5B and C). Another (AD)SHE-causing mutation, R398Q, could not be reliably fit with a single or double exponential function, but appeared to activate considerably more slowly than WT $K_{Na}1.1$ channels. This is consistent with characterisation of channels expressed in *Xenopus* oocytes showing this mutant to have a slower time-to-peak (Milligan et al., 2014). R928C (Figure 3.5A) and M896I currents could not be fit adequately with a single exponential function, and were better fit with two exponentials, giving a fast (τ_{fast}) and slow (τ_{slow}) time constant (Figure 3.5C).

Currents recorded from CHO cells expressing mutant $K_{Na}1.1$ channels in the absence of intracellular Na^+ were also fit with a single exponential function. As in the presence of Na^+ in the pipette solution, the τ values were voltage-independent. The τ values were also unchanged from those in the presence of Na^+, implying that removal of Na^+ from the intracellular solution does not affect the slowly activating, time-dependent component of channel activation (Figure 3.5C). The only exceptions to this were R928C and M896I (AD)SHE-causing mutations, which were fit with two exponential components in 10 mM Na^+. In the absence of Na^+ however, the currents were fit adequately with a single exponential function (Figure 3.5C).

All currents produced by co-expression of WT and mutant subunits were fit well with a single exponential, except for R398Q+WT, which could not be fit previously as a homomeric assembly. Aside from Y796H+WT, similar to homomeric mutant channels, the τ values obtained for all variant+WT heteromers were unchanged from WT $K_{Na}1.1$ channels across all voltages tested (Figure 3.5C). In the heteromeric assembly, both M896I and R928C were again better fit with a single exponential in both the absence and presence of intracellular Na^+. With 10 mM intracellular Na^+ the τ value was

reflective of the WT channel. In the absence of Na^+ it was faster and more reflective of the homomeric mutant, though this was only significant for M896I (Figure 3.5C).

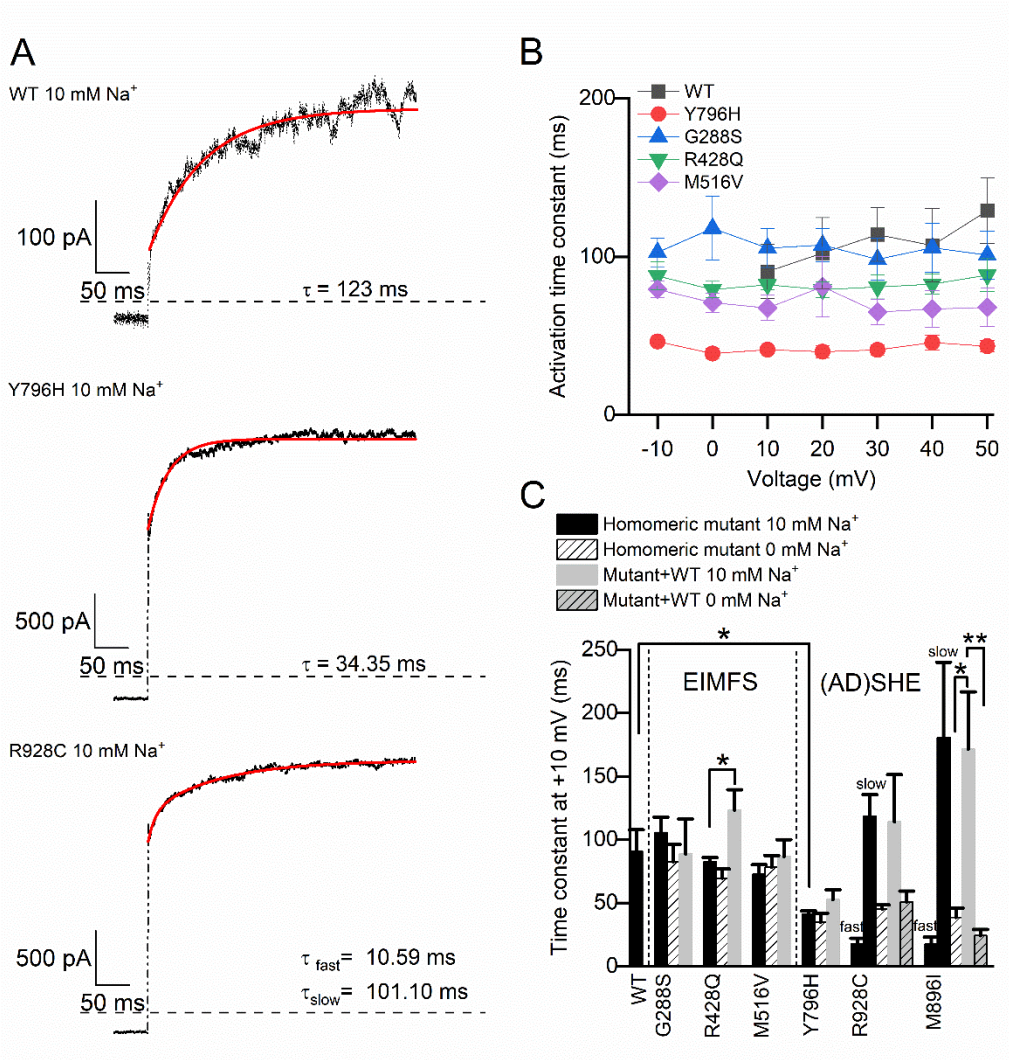

Figure 3.5: Activation time-course of WT and mutant $K_{Na}1.1$ in the presence and absence of intracellular Na^+.
A) Representative traces for WT and Y796H $K_{Na}1.1$ channels fitted with a single exponential function, and R928C $K_{Na}1.1$ with a bi-exponential function, recorded at +10 mV with 10 mM intracellular Na^+. **B)** Summary of mean (±s.e.m.) **τ** values derived from a single exponential fit of homomeric WT $K_{Na}1.1$, (AD)SHE-causing and EIMFS-causing mutants obtained at different voltages in 10 mM intracellular Na^+ (N= 5-9 for each mutant). **C)** Mean (±s.e.m.) **τ** values at +10 mV for EIMFS- and (AD)SHE-causing homomeric mutant and co-expressed mutant channels in 10 mM and 0 mM intracellular Na^+. Where R928C and M896I currents were fit with a bi-exponential function, τ_{fast} and τ_{slow} are indicated above the bars. *p<0.05, **p<0.005 independent one-way ANOVA with Tukey's post-hoc test compared to homomeric mutant with 10 mM Na^+ (n= 5-9 for each mutant).

3.2.5 Mutation of T314 alters selectivity filter gating but not Na^+-dependence of $K_{Na}1.1$

K2P channels that are gated at the selectivity filter also activate with a voltage-independent time constant, and lack a VSD despite being voltage-sensitive (Schewe et al., 2016), similarly to the results seen for $K_{Na}1.1$ channels. Mutation of a threonine at the cytoplasmic end of the selectivity filter motif that forms the intracellular-most K^+ binding site in these channels results in voltage- and ligand-independent channel currents (Schewe et al., 2016). The same residue is important in selectivity filter gating of a number of K^+ channels (Nematian-Ardestani et al., 2020; Schewe et al., 2016; Kopec et al., 2019; Lolicato et al., 2017; Schewe et al., 2019). The equivalent threonine residue in the $K_{Na}1.1$ selectivity filter motif is T314, and it was hypothesised that this may also be involved in selectivity filter gating. Mutation of the threonine to cysteine also resulted in voltage-independent currents, but these reversed close to 0 mV (Figure 3.6). Importantly, the Na^+-sensitivity of T314C $K_{Na}1.1$ remained intact since, like WT $K_{Na}1.1$, currents were recorded in the presence of 10 mM intracellular Na^+ but were negligible in the absence of intracellular Na^+ (Figure 3.6). Thus, the effects of mutating this potential selectivity filter gate were distinct from the effects of DEE-causing $K_{Na}1.1$ mutants on channel behaviour.

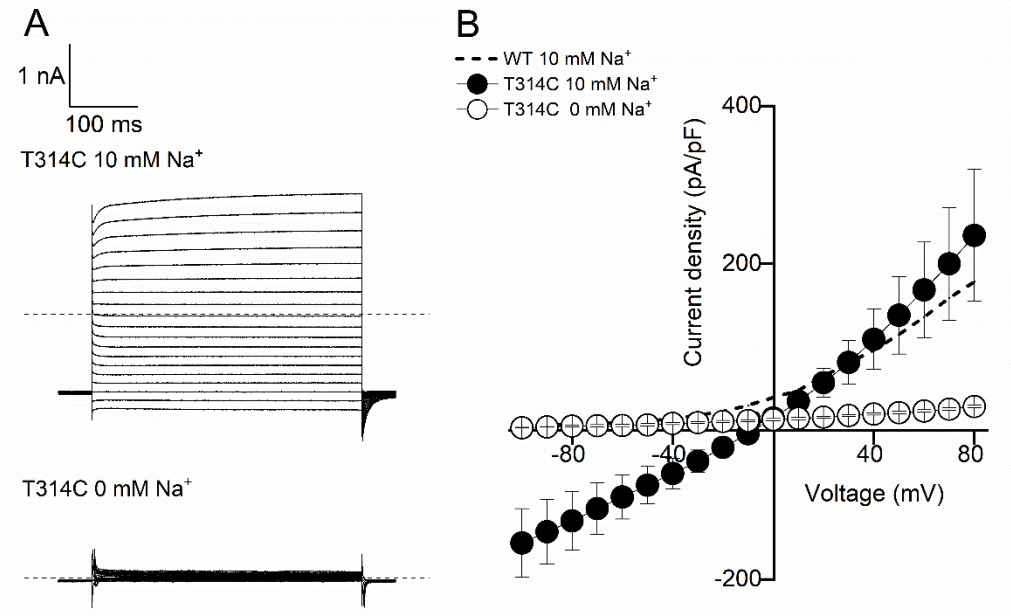

Figure 3.6: Mutation of a conserved threonine residue in the $K_{Na}1.1$ selectivity filter disrupts selectivity and voltage-activation, but not Na^+-activation.
A) Representative traces for T314C whole cell currents in response to 400 msec steps from -100 to +80 mV in 10 mV increments, from a holding potential of -80 mV in 10 mM and 0 mM intracellular Na^+. **B)** Mean (±s.e.m.) current-voltage relationships for T314C in 10 mM and 0 mM intracellular Na^+ (n=5). Mean WT $K_{Na}1.1$ current-voltage relationship indicated with dashed line.

3.3 Discussion

3.3.1 Functional characterisation of DEE-causing mutations

In excess of 60 known pathogenic *KCNT1* variants resulting in DEEs cause an increase in $K_{Na}1.1$ activity (Bonardi et al., 2021), despite being located in distinct regions of the channel structure. It was hypothesised that mutations cause GOF by a common mechanism. An increase in channel activity was observed for all EIMFS and (AD)SHE-causing variants evaluated, consistent with past efforts to characterise DEE-causing mutations (Milligan et al., 2014; Rizzo et al., 2016; Dilena et al., 2018; Heron et al., 2012; McTague et al., 2018; Kim et al., 2014; Barcia et al., 2012; Gertler et al., 2019). Left-shifted activation curves have been reported for four EIMFS-causing variants previously; G288S, M516V, E893K and R950Q (Rizzo et al., 2016; Dilena et al., 2018). The data here shows that this is not specific to EIMFS mutants, with all known (AD)SHE-causing variants having the same effect on activation midpoints obtained by Boltzmann analysis.

Unlike WT $K_{Na}1.1$ channels, each of the mutant channels yielded voltage-dependent currents in the absence of intracellular Na^+, though with depolarised activation curves compared to those in the presence of 10 mM intracellular Na^+. In terms of how the mutations may cause this Na^+-independent gating of the channel, Ca^{2+}-activated $K_{Ca}1.1$ channels may provide some clues. It has been previously proposed that the RCK domains of the $K_{Ca}1.1$ channel C-terminal act as a negative modulator of channel opening, and undergo a conformational change following Ca^{2+} binding to relieve the inhibition (Schreiber et al, 1999). Ca^{2+} binding to the RCK domains sets the Ca^{2+} dependent range of voltage-activation, via allosteric mechanisms. At strongly depolarised voltages, the channel can still open in the absence of Ca^{2+}, and the conformational changes induced by Ca^{2+} binding shift voltage dependence to the physiological range. $K_{Na}1.1$ channels may follow a similar ligand-dependent gating mechanism also, but with Na^+-binding inducing conformational changes within the RCK domains. This would explain how some of the mutations located on the RCK domains and NAD^+-binding domain could cause Na^+-independent channel opening, despite being located distally from the pore-forming region. This would also explain how, in the absence of Na^+, mutant channels are still opening, though within a more depolarised voltage range. It is possible that DEE-causing mutations destabilise the inactive, Na^+-unbound conformation and lower the energetic barrier coupled to the activation gate

opening, make it easier to open. Epilepsy-related *KCNT1* variants can possibly be considered as loss-of-function with respect to this autoinhibitory mechanism.

Similarly to MthK and other selectivity filter-gated channels, $K_{Na}1.1$ may possess a Na^+-dependent activation gate that is allosterically coupled to a selectivity filter gate. Na^+ binding to the RCK domains on the C-terminus lowers the energetic barrier for the channel moving from the inactive to active state, and in the absence of Na^+ the energetic barrier is high, explaining why no discernible WT $K_{Na}1.1$ current was recorded. The zero-voltage free energy values calculated for WT and mutant $K_{Na}1.1$ channels indicate that GOF mutations lower the energetic barrier for channel opening in the absence of intracellular Na^+, likely by destabilising the inactive conformation, and addition of Na^+ lowers this further. Negative ΔG_0 values indicate that the open channel conformation is more favourable, which is seen for all homomeric mutant channels in the presence of intracellular Na^+, in contrast to the WT $K_{Na}1.1$ channel. The hyperpolarising shift in activation midpoint values for mutant $K_{Na}1.1$ channels upon addition of Na^+ also reflects this. Heteromeric co-expressed assemblies of WT $K_{Na}1.1$ and mutant subunits behaved distinctly from homomeric mutant and WT channels with intermediate properties, and the ΔG_0 values were positive with 10 mM intracellular Na^+. It is thus likely that introducing WT $K_{Na}1.1$ subunits into the assembly raises the energetic barrier between the inactive and active channel states.

Secondary to conformational changes within the activation gate, selectivity filter-gated channels are proposed to undergo conformational changes in the selectivity filter as a result of allosteric coupling, leading to a reduction in the energetic barrier to K^+ conduction (Kopec et al., 2019). A threonine residue at the cytoplasmic end of the selectivity filter is proposed to be critical for selectivity filter gating of MthK, K2P, $K_{Ca}1.1$ and KcsA channels (Schewe et al., 2016; Labro et al., 2018; Kopec et al., 2019; Nematian-Ardestani et al., 2020), and this residue is conserved in $K_{Na}1.1$. Mutation of the equivalent residue in $K_{Na}1.1$, T314, to cysteine yielded voltage-independent currents that reversed around 0 mV, but retained Na^+-sensitivity in contrast to DEE-causing *KCNT1* mutations. This is consistent with Na^+ interacting with the protein structure to modulate the activation gate, as opposed to the selectivity filter gate, and with GOF DEE-causing *KCNT1* mutations generally affecting the activation gate. The Na^+- and voltage-independent time constants obtained by fitting $K_{Na}1.1$ currents with an exponential function likely reflect opening of the selectivity filter gate and resultant K^+ flux following Na^+ and voltage-activation. K2P channels also activate with a voltage-

independent time constant, and are voltage-dependent but lack a VSD similarly to $K_{Na}1.1$ (Schewe et al., 2016).

Further experiments would be required to determine the extent of the apparent selectivity changes caused by T314C. In terms of why the T314C mutant yielded currents reversing through 0 mV however, this is something that has been observed in mutants of the equivalent threonine in other K^+ channels previously and is thought to be related to the permeation mechanism (Kopec et al., 2018; Derebe et al., 2011). For example, a study assessing mechanisms of cation selectivity in tetrameric channels sought to identify differences in K^+ channels and a non-selective bacterial cation channel, NaK (Derebe et al., 2011). NaK has a similar amino acid composition in its selectivity filter (TVGDG) to K^+ channels (TVGYG), but can only coordinate K^+ ions at two sites. Based upon NaK, two channels named NaK2K and NaK2CNG-N were engineered to have altered selectivity filter K^+ coordination sites. NaK2K is modified to possess four binding sites, like physiological K^+ channels, and is K^+ selective. NaK2CNG-N is a mutant of the selectivity filter threonine in NaK2K, that only has three K^+ binding sites and is again non-selective. It was originally suggested that the lack of selectivity for NaK and NaK2CNG-N arose from the number of K^+ binding sites. Mutation of the conserved threonine in the MthK selectivity filter, leaving only three functional binding sites, had a similar effect on K^+ selectivity (Derebe et al., 2011). It was recently demonstrated using atomistic simulations however, that co-permeating water molecules in the selectivity filter reduce selectivity and conduction, and K^+ ions likely lose their hydration shell upon entering the selectivity filter (Kopec et al., 2018; Kopfer et al., 2014; Oster et al., 2019). NaK2CNG-N was found to have increased co-permeating water resulting from mutation of the selectivity filter threonine residue and had a water:ion ratio above 1, which enabled permeation of both K^+ and Na^+ ions with equal probability (Kopec et al., 2018). Electrophysiological studies examining mutation of the critical threonine residue to cysteine in other selectivity filter gated K^+ channels, such as K2P channels and KcsA, have largely used symmetrical K^+ solutions however, so changes to K^+ selectivity would not have been observed (Schewe et al., 2016; Nematian-Ardestani et al., 2020; Zhou and MacKinnon, 2004). It is, however, possible that T314C in the $K_{Na}1.1$ selectivity filter would have similar detrimental effects on K^+ selectivity and permeation, consistent with MthK and NaK2K.

EIMFS-causing mutants show reduced likelihood of entering into subconductance states when single channel behaviour is studied in *Xenopus* oocytes (Barcia et al., 2012; Kim et al., 2014). Subconductance levels occurring during closed to open

transitions have been reported in a number of K^+ channels. They are thought to arise from conformational changes within the selectivity filter, due to subconductance levels having different ion selectivity compared to the fully open state, but are tightly coupled to channel activation (Chapman and VanDongen, 2005; Chapman et al., 1997; VanDongen, 2004). Conservative mutations of selectivity filter-lining residues dramatically alter subconductance levels in K_{ir} channels (Lu et al., 2001). It is possible that the suppressed or abolished subconductance states seen in $K_{Na}1.1$ channels are secondary to the destabilising effects of mutants on the closed activation gate of the channel and increases in P_o. Consistent with this, reduced subconductance levels are also seen upon potentiation of WT $K_{Na}1.1$ channels by FMRP interaction with the C-terminus (Brown et al., 2010). Increased Na^+-sensitivity and shifted EC_{50} for Na^+-activation has also been reported for DEE-causing mutants, and a decrease in the energetic barrier for the channel moving from the inactive to active state would explain this observation. Increased cooperative gating between multiple channels expressed in the same patch in *Xenopus* oocytes could also be explained by a reduction in the energetic barrier (Kim et al., 2014).

Some of the mutants examined may also affect the selectivity filter gate, additionally to their effects on the activation gate. (AD)SHE-causing variant Y796H activated with a faster time constant than WT $K_{Na}1.1$. An increase in $P_{o,max}$ has been described for Y796H when the equivalent mutation in the rat $K_{Na}1.1$ channel was expressed in *Xenopus* oocytes. It is possible that a faster activation time constant may result from increased $P_{o,max}$. A faster time constant may arise from an increase in either the opening or closing rate constant, however an increase in $P_{o,max}$ is consistent only with an increase in the opening rate constant. It is unclear how Y796H would affect the selectivity filter gate, since it is located far from the pore-forming region of the channel. Consistent with this, (AD)SHE-causing variant R398Q was reported as having a decreased $P_{o,max}$ at 25 and 50 mM intracellular Na^+ (Tang et al., 2016), and we found this variant to activate very slowly, preventing reliable fitting with either a mono- or biexponential function. This variant was also previously described as having a slower time-to-peak in *Xenopus* oocytes (Milligan et al., 2014). Since the time constant of activation appears to be both voltage and Na^+-independent, we assume the Na^+-dependent activation step precedes this, and is fast and consequently undetectable. In the presence of intracellular Na^+, (AD)SHE-causing mutants R928C and M896I reveal a second time constant, τ_{fast}. These mutations may slow the Na^+-dependent activation of the channel, revealing this usually undetectable step. It is unclear to what degree this would contribute to the GOF effect of the mutations however.

3.3.2 Implications for targeting K_{Na}1.1 channels therapeutically

The results demonstrate that co-expressed heteromeric WT and mutant K_{Na}1.1 channel assemblies behave distinctly to homomeric mutant channels. Previous work characterising homomeric mutant channels should be interpreted with caution when postulating how changes may lead to epilepsy phenotypes, particularly describing the effects on neuronal excitability. For example, a recent study investigating the electrical firing properties of iPSC-derived neurons harbouring the EIMFS-causing P924L mutation focused on the homozygous mutation (Quraishi *et al*, 2019). The results here suggest that heteromeric channels have less severe shifts in activation kinetics and activity in the absence of intracellular Na^+, and thus will have distinct effects on neuronal excitability. Whilst the method of studying the heteromeric assembly has limitations, it may provide a more physiologically relevant model for studying the functional implications of DEE-causing *KCNT1* mutations on K_{Na}1.1 channel behaviour. This will also be advantageous for development of pharmacological interventions, where studying the inhibition of homomeric WT and mutant channels *in vitro* may be of limited clinical relevance.

Focus in the literature has been predominantly on the channel pore for inhibitors to target *KCNT1*-related epilepsies (Rizzo et al., 2016; Yang et al., 2006; de Los Angeles Tejada et al., 2012), which are accompanied by problems resulting from non-specificity (Mikati et al., 2015; Bearden et al., 2014; Fitzgerald et al., 2019). Information provided by studying the heteromeric assemblies here may be useful in determining other, more specific drug modalities. For example, in the absence of Na^+, both co-expressed mutant and WT subunits show a decrease in channel activity, resulting in similar or smaller current amplitudes to WT K_{Na}1.1 channels, and activation of the channels is shifted towards more depolarised voltages. Recent work has identified that hyperexcitability resulting from GOF mutations is a result of increased subthreshold K_{Na}1.1 activity specifically in GABAergic inhibitory interneurons (Shore et al., 2020). Na^+ antagonists targeting the Na^+-binding region of the channel could therefore prove to be effective, without there being residual channel activity. Alternatively, a negative allosteric modulator that uncouples the interaction between Na^+-binding and channel activation, or that affects the intrinsic closed–open transition, could act to suppress K_{Na}1.1, perhaps in a similar manner to modulators of K_{Ca}1.1 channels. For example, paxilline allosterically modulates K_{Ca}1.1 by preferentially occupying the closed state

and decreasing the equilibrium constant *L* described in the Horrigan–Aldrich allosteric model for channel gating, with the overall effect of suppressing current (Zhou and Lingle, 2014). *L* describes the intrinsic closed-to-open channel transition in the absence of Ca^{2+}, and no active VSD (Horrigan and Aldrich, 2002).

4 Validation, optimisation and characterisation of concatemeric channels

4.1 Introduction

Recent functional studies have used co-expression to study the implications of heterozygous *KCNT1* mutations (Rizzo et al., 2016; Dilena et al., 2018) or *KCNT2* mutations in co-assembly with *KCNT1* (Mao et al., 2020) on channel function *in vitro*. All of these studies, and the results from Chapter 3, suggest that heteromeric channels comprised of WT $K_{Na}1.1$ and variant subunits display "intermediate" characteristics between WT $K_{Na}1.1$ and mutant homomeric channels. It cannot be discounted however, that populations of homomeric WT and homomeric mutant channels are formed and are underlying the effects seen. There are sixteen possible combinations of subunit stoichiometries in a heterozygous population of WT and variant $K_{Na}1.1$ subunits. Following a normal distribution, $1/16^{th}$ of channels would be expected to be homomeric WT $K_{Na}1.1$ channels and $1/16^{th}$ would be homomeric variant channels. Additionally, it is possible that when studying the effects of removing intracellular Na^+, only currents produced by homomeric mutant channels would be recorded.

Concatemeric channels enable uniform subunit arrangements and relative expression levels to be controlled. Their construction involves covalent linkage of the C-terminus of one channel subunit to the N-terminus of the next; removing the respective 5' stop and 3' start codons from the subunit sequences (Sack et al., 2008). This approach has proven successful for studying the function and pharmacological modulation of numerous K^+ channels such as hERG or members of the K_v family (Wu et al., 2015; Sokolov et al., 2007). In fact, concatenated $K_{Na}1.1$ channels have successfully been expressed in *Xenopus* oocytes previously to study their sensitivity to changes in cell volume (Tejada et al., 2017).

As well as being useful for studying the behaviour of heteromeric channels, it is also desirable to create concatemeric constructs to be used in inhibitor screening experiments where channels with exactly half mutant and half WT $K_{Na}1.1$ subunits are required. Whilst all drug development efforts or studies of existing inhibitors in the literature thus far have been focused on inhibition of WT $K_{Na}1.1$ channels or homomeric mutant channels (Griffin et al., 2021; Rizzo et al., 2016; Dilena et al., 2018; Spitznagel et al., 2020; Milligan et al., 2014; McTague et al., 2018), neither are clinically relevant. Furthermore, for carrying out drug screening to develop inhibitors of the channel it is

useful to create stable mammalian cell lines that can be used for higher-throughput methods than manual whole cell patch clamp, such as fluorescence-based assays and automated planar electrophysiology. When creating stable cell lines expressing two separate plasmids, expression levels of the two constructs may vary greatly, whereas a concatemeric construct would ensure equal subunit expression.

A caveat of using concatemers to study heteromeric conformations of K^+ channels, is that their expression in HEK293 cells is limited, and the most successful expression has been seen in *Xenopus* oocytes (Steinbach and Akk, 2011). Since *Xenopus* oocytes are very membrane and lipid-rich however, higher drug concentrations are required to evoke responses, thus limiting their usefulness for pharmacological studies (Yang et al., 2006). Where possible, mammalian heterologous expression systems are desirable for this work. Some success has been reported in CHO cells (Wimmers et al., 2002; Wacker et al., 2012; Gao et al., 2017; Meisel et al., 2012; Sachyani et al., 2014). CHO cells have the additional benefit of negligible endogenous K^+ channel activity (Gamper et al., 2005) and may therefore be a suitable expression system for the study of $K_{Na}1.1$ concatemers.

4.1.1 Chapter hypothesis and aims

Hypothesis: Concatenated WT $K_{Na}1.1$ and mutant subunits will have activation and kinetic properties that are an intermediate of WT and mutant subunits alone. The resulting channels will be a useful model for the genetic status of patients carrying heterozygous pathogenic *KCNT1* variants.

Aims:

- ***To create normally functioning concatemeric channels***
- ***To determine whether channel properties are altered in concatemeric mutant and WT $K_{Na}1.1$ channels, and whether the channels are active in the absence of intracellular Na^+***

4.2 Results

4.2.1 Concatenation of K_{Na}1.1 subunits altered activation kinetics

Tandem dimer constructs, consisting of two adjacent K_{Na}1.1 subunits tethered together with a linker region (GGGSGGGS) between the C-terminus of one subunit and the N-terminus of the next, were used to transiently transfect CHO cells, since no successful expression was seen in HEK293-MSR cells, and macroscopic currents from the resulting tetrameric K_{Na}1.1 channels were recorded using the whole cell configuration. In the text and figures, tandem dimers are named to indicate positioning of the WT and mutant subunits in the first or second position of the dimer and a hyphen between subunits indicates that the subunits are tethered. For example, WT-YH describes a tethered tandem dimer with a WT subunit in the first position and Y796H in the second. In order to validate the concatemer constructs, YH-YH (double (AD)SHE-causing variant, Y796H) and WT-WT (double WT K_{Na}1.1) constructs were compared with currents recorded from CHO cells transfected with either Y796H or WT K_{Na}1.1 monomeric constructs. Current densities were as expected in response to a series of voltage steps from -100 mV to +80 mV from a holding potential of -80mV in the presence of 10 mM intracellular Na^+; YH-YH produced larger currents compared to WT-WT (334.61 ± 44.96 pA/pF, n=6, compared to 11.21 ± 3.10 pA/pF at +10 mV, n=5, Figure 4.1B). The two heteromeric constructs which had mutant and WT K_{Na}1.1 subunits in different orientations, WT-YH and YH-WT, produced currents that were an intermediate between WT-WT and YH-YH currents, as expected (Figure 4.1B).

Boltzmann analysis of conductance-voltage relationships revealed a leftward shift in the conductance-voltage relationship in the hyperpolarising direction for all tandem dimer constructs; parameters derived from this are summarised in Table 4.1. Both WT-WT and YH-YH constructs had more negative activation midpoints compared to channels formed by monomeric WT and Y796H subunits alone (Figure 4.1C). The calculated zero-voltage free energy difference between the closed and open state (ΔG_0) for YH-YH was similar to that for monomeric Y796H channels, but in contrast to WT K_{Na}1.1 channels the value for WT-WT channels was negative.

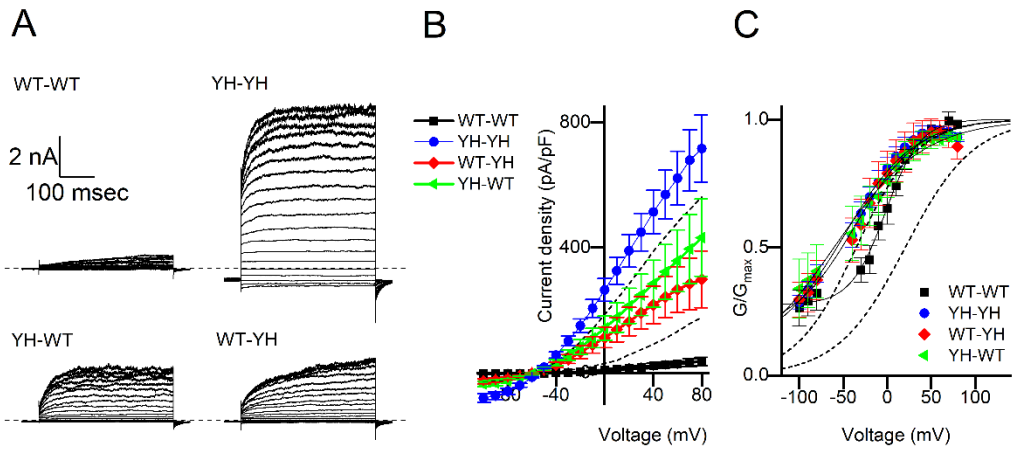

Figure 4.1: Validation of concatemeric $K_{Na}1.1$ channels.
A) Representative traces for whole cell currents from tethered homomeric and heteromeric tandem dimer constructs in response to 400 msec steps from -100 to +80 mV in 10 mV increments, from a holding potential of -80 mV. **B)** Mean (± s.e.m) current-voltage relationship for tethered homomeric and heteromeric tandem dimer constructs (n=5-9 for all channel types). Monomeric WT (black) and Y796H (red) indicated with dashed lines. **C)** Normalised mean (± s.e.m) conductance-voltage relationship for tethered homomeric and heteromeric tandem dimer constructs (n=5-9 for each variant) fitted with Boltzmann function. Monomeric WT $K_{Na}1.1$ and Y796H indicated with dashed lines**.**

4.2.2 Introduction of a T2A self-cleaving peptide sequence rectified the change in activation kinetics resulting from concatenation

In constructing tandem dimers, the N-terminus of the second ('donor') subunit is constrained. It is thus possible that a lack of flexibility could impact the gating kinetics. It was hypothesised that this constraint was the cause of the discrepancy in activation midpoint values and ΔG_0 values between the tandem dimers and their monomeric counterparts. The first approach to optimise the constructs was to introduce a longer linker region (16 amino acids) between the concatenated subunits, to increase flexibility. The channels expressed in CHO cells displayed negligible currents, even for the double Y796H mutant. It was uncertain how long the linker region needed to be however, since the N-terminus is lacking in cryo-EM structures of the channel (Hite et al., 2015; Hite and MacKinnon, 2017), and 16 amino acids may still not be sufficient.

Another approach used to rectify the altered activation kinetics seen in the tandem dimer constructs, was introduction of a self-cleaving viral oligopeptide sequence in the linker region between the recipient and donor subunits; T2A (*Thosea asigna* virus 2A) was chosen for this application (GSGEGRGSLLTCGDVEENPGP). 2A peptides have a common sequence on their C-terminus; GDVEXNPGP, and 'self-cleavage' refers to ribosomal skipping over the prolyl-glycyl peptide bond, which breaks the link between

the tandem dimer subunits whilst retaining subunit stoichiometry. Successful ribosomal skipping and translation results in the subunit upstream of the peptide having the whole sequence minus proline attached to its C-terminus, and the downstream subunit having a single proline attached to its N-terminus (Liu et al., 2017). In the text and figures, a slash indicates a T2A site. For example, WT/YH describes a tandem dimer with a WT subunit in the first position and Y796H in the second, with a T2A self-cleaving site between the subunits.

YH/YH and WT/WT constructs with a T2A site behaved similarly to monomeric Y796H and WT channels in response to a series of voltage steps from -100 mV to +80 mV from a holding potential of -80mV. In 10 mM intracellular Na^+, YH/YH produced 10-fold larger currents at +10 mV compared to WT/WT (Figure 4.2B and D). There was some discrepancy between the increase in current density from WT/WT for the two heteromeric concatemers. YH/WT caused a 2-fold increase, whereas WT/YH caused a 5-fold increase (Figure 4.2B and D). Both activation midpoint and slope values obtained by Boltzmann analysis of the conductance-voltage relationships for WT-WT and YH-YH constructs with a T2A site (Figure 4.2C) were not significantly different from those obtained for monomeric Y796H and WT channels; the parameters are summarised in Table 4.1. The activation midpoints derived from conductance-voltage relationships of the heteromeric variants were less negative upon introduction of the T2A site, though were still shifted in the hyperpolarising direction compared to homomeric WT channels (Figure 4.2C). When the currents were fit with a single exponential function to examine possible effects on $K_{Na}1.1$ activation kinetics, similarly to monomeric channels YH/YH channel activation proceeded with a fast time constant (Figure 4.2E). The τ values reported for the heteromeric tandem dimers more closely resembled the time constant of activation of WT/WT (Figure 4.2E).

Monomeric $K_{Na}1.1$ channels have a predicted weight of 142 kDa in western blot analysis. A successfully tethered concatemer was therefore predicted to yield a 284 kDa band, and a successfully cleaved construct with a T2A site expected to produce a 142 kDa band. Western blot analysis of WT-WT and WT/WT constructs expressed in both HEK293 and CHO cells indicated that the 284 kDa band produced by tethering WT $K_{Na}1.1$ subunits together is cleaved upon introduction of the T2A self-cleaving peptide sequence. The cleaved 142 kDa band obtained in both cell lines was faint however, and a distinct band indicating uncleaved protein remained visible. Consistent with no currents being successfully recorded from HEK293 cells for tethered concatemer constructs, no 284 kDa band was visible for HEK293 cells transfected with

the WT-WT construct (Figure 4.3). There was a significant amount of difficulty associated with producing western blots for these constructs, particularly when carrying out the transfer step, due to their very high molecular weights. Further optimisation and repeats would be needed to accurately draw conclusions from this. The apparent low efficiency of cleavage seen in the western blots is not consistent with the electrophysiological data, where introduction of the T2A site appears to completely rescue the effects of constraining the N-terminus on channel behaviour.

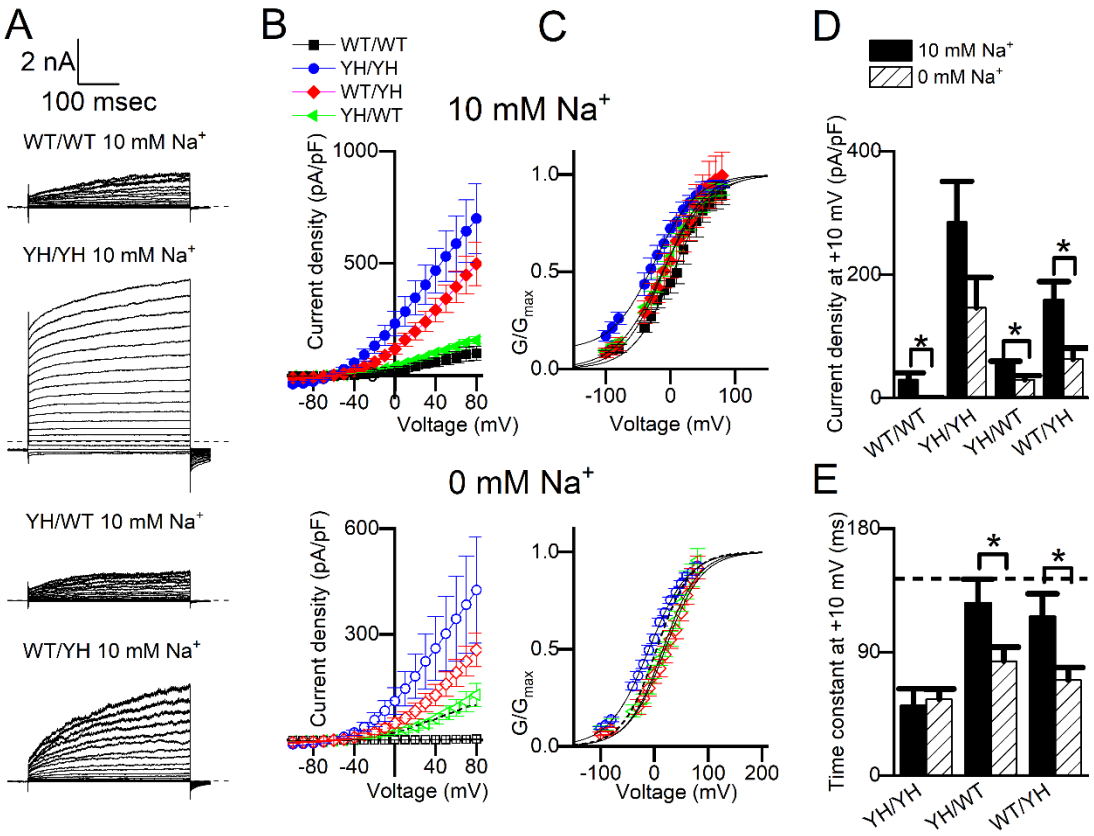

Figure 4.2: Optimisation of tandem dimers and effects of removing intracellular Na^+. **A)** Representative traces for whole cell currents from tethered homomeric and heteromeric tandem dimer constructs containing a T2A site in response to 400 msec steps from -100 to +80 mV in 10 mV increments, from a holding potential of -80 mV. **B)** Mean (± s.e.m) current-voltage relationship for homomeric and heteromeric tandem dimer constructs with a T2A site in 10 mM and 0 mM intracellular Na^+ (n=5-9 for all channel types). **C)** Normalised mean (± s.e.m) conductance-voltage relationship for homomeric and heteromeric tandem dimer constructs with a T2A site in 10 mM and 0 mM intracellular Na^+ (n=5-9 for each variant) fitted with Boltzmann function**. D)** Mean (± s.e.m) peak current amplitude at +10 mV for homomeric and heteromeric tandem dimer constructs in 10 mM and 0 mM intracellular Na^+. *p<0.05, one-tailed student's T-test to compare 0 mM and 10 mM (n=5-9 for each construct). **E)** Mean (± s.e.m) τ values at +10 mV for homomeric and heteromeric concatemers with a T2A site in 10 mM and 0 mM intracellular Na^+. *p<0.05, one-tailed student's T-test to compare 0 mM and 10 mM (n=5-9 for each construct). Mean WT/WT τ value with 10 mM Na^+ indicated with dashed line (n=5).

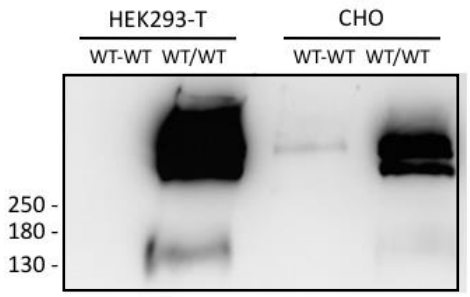

Figure 4.3: Western blot analysis of whole cell lysates from HEK293-T and CHO cells. Cells were transiently transfected with WT-WT and WT/WT constructs. Blots were probed with a rabbit anti-V5 primary antibody and goat anti-rabbit secondary antibody, and exposed for 10 minutes.

4.2.3 Heteromeric WT/ Y796H concatemers are active in the absence of intracellular Na^+

As in Chapter 3, possible variant-induced changes in Na^+ dependence were examined by removing intracellular Na^+ from the pipette solution. As expected, negligible current was yielded in CHO cells transfected with WT/WT in the nominally Na^+-free intracellular solution (Figure 4.2B and D), whereas large currents could still be recorded from YH/YH channels (Figure 4.2B and D). There was no significant decrease in the mean peak current density recorded from YH/YH channels at +10 mV with 0 mM intracellular Na^+ (Figure 4.2D). The heteromeric concatemers displayed residual activity in the absence of intracellular Na^+, though there was a significant 2-fold decrease in the mean peak current density recorded from YH/WT, and a 3-fold decrease for WT/YH (Figure 4.2B and D).

Boltzmann analysis of the conductance-voltage curve for YH/YH in the absence of intracellular Na^+ revealed a rightward shift of the activation midpoint by 20 mV (Figure 4.2C and Table 4.1). This is validated by the 15.19 mV shift in the depolarising direction seen for monomeric Y796H channels in the absence of Na^+ in Chapter 3 (Table 4.1). Both variations of the heteromeric assembly aligned closely in their conductance-voltage relationships in the absence of intracellular Na^+, with activation midpoints that were depolarised compared to those determined in the presence of intracellular Na^+. Both constructs displayed approximately a 20 mV rightward shift in the half maximal activation voltage in the absence of Na^+, though only YH/WT was statistically significant (Figure 4.2C and Table 4.1).

Currents recorded from CHO cells expressing the YH/YH tandem dimer construct in the absence of intracellular Na^+ were fit with a single exponential function, giving the

time constant of activation. As previously seen in the presence of Na^+ in the pipette solution, the τ value obtained from fitting the currents in the absence of Na^+ was the same across the full voltage range measured for all constructs. Furthermore, the τ value for YH/YH at +10 mV was unchanged from that in the presence of Na^+ (Figure 4.2E). Conversely, the time-dependent component of channel activation for both variations of heteromeric tandem dimer proceeded with a significantly faster time constant in the absence of Na^+ (Figure 4.3D).

Table 4.1: Parameters derived from Boltzmann fit of WT, homomeric variant, and concatemer channels in the absence and presence of intracellular Na^+.
Data are presented as mean ±s.e.m. Values for monomeric WT $K_{Na}1.1$ and Y796H from Chapter 3 are included for reference. $V_{0.5}$ is the half-maximal activation voltage, ***p*<0.005 compared to WT/WT, independent one-way ANOVA with Tukey's post-hoc test to compare constructs. #*p*<0.05, one-tailed student's T-test to compare 0 mM and 10 mM Na^+ (n=5-10 for each variant). Elementary gating charge, *z,* is derived from the slope of the Boltzmann curve, which is RT/zF. ΔG_0 is the zero-voltage free energy for channel opening: $\Delta \boldsymbol{G_0} = \boldsymbol{zFV_{0.5}}$ and is expressed as kcal/mol. and $\Delta\Delta G_0$ is the closed-state destabilisation energy, calculated as the difference in ΔG_0 between WT (or WT-WT and WT/WT for tethered and cleaved constructs) and variant $K_{Na}1.1$ channels (n=5-10 for each variant).

Channel	$V_{0.5}$ (mV)		*z*	ΔG_0 (kcal/mol)	$\Delta\Delta G_0$ (kcal/mol)
WT	**7.38 ±4.35**		1.01 ±0.13	0.15 ±0.10	-
WT-WT	-15.72 ±1.69		1.46 ±0.16	-0.55 ±0.11	-
WT/WT	-2.74 ±6.29		0.89 ±0.06	-0.10 ±0.11	-
Homomeric Y796H	**-39.99 ±2.27**		0.92 ±0.08	-0.83 ±0.07	0.98
YH-YH	-50.84 ±3.41		0.92 ±0.16	-1.05 ±0.21	0.50
YH/YH	-42.19 ±7.97	**	0.82 ±0.12	-0.76 ±0.13	0.66
YH/YH 0 mM $[Na^+]_i$	-22.13 ±3.41	#	0.72 ±0.05	-0.36 ±0.05	0.26
WT/YH	-16.42 ±8.97		0.71 ±0.09	-0.28 ±0.16	0.18
WT/YH 0 mM $[Na^+]_i$	4.20 ±7.71		0.75 ±0.04	0.06 ±0.13	-0.15
YH/WT	-21.51 ±5.43		0.80 ±0.08	-0.42 ±0.13	0.32
YH/WT 0 mM $[Na^+]_i$	1.55 ±7.84	#	0.80 ±0.08	0.02 ±0.14	-0.12

4.2.4 WT/YH could be stably expressed in HEK293 cells

A HEK293 cell line was created that stably expressed the WT/YH concatemer construct, that could be used in future for screening inhibitors of the channel in higher-throughput assays. To confirm expression of the construct, whole cell electrophysiology was used, and yielded currents closely resembling those recorded following transient transfection of CHO cells with the same construct (Figure 4.4).

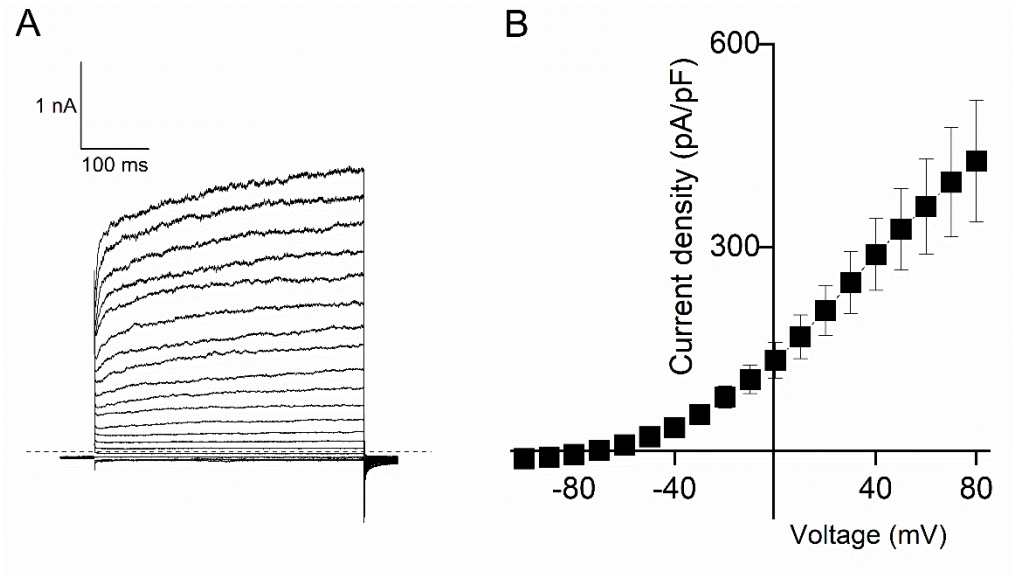

Figure 4.4: Characterisation of stable WT/YH HEK293 cell line.
A) Representative trace for whole cell current in response to 400 msec steps from -100 to +80 mV in 10 mV increments, from a holding potential of -80 mV. **B)** Mean (± s.e.m) current-voltage relationship for HEK293 cell line stably expressing WT/YH tandem dimer construct with T2A site (n=5).

4.3 Discussion

4.3.1 Concatenation of K_{Na}1.1 subunits altered activation kinetics

It was hypothesised that concatenation of K_{Na}1.1 subunits could be used to create a model for studying behaviour of channels reflective of heterozygous patients carrying only one variant DEE-causing allele; which make up the majority of patients. Concatemeric channels were created by joining the C-terminus of one K_{Na}1.1 subunit to the N-terminus of another. The original homomeric WT-WT and YH-YH concatemer constructs lacking a self-cleaving site activated with starkly different kinetics to WT and Y796H channels. This was particularly evident in the WT-WT construct, which had an activation midpoint value in the negative voltage range. The ΔG_0 value for WT-WT was negative, indicating that tethering of WT subunits results in a channel that favours the active state, in contrast to WT K_{Na}1.1 channels.

It is postulated that these changes arise as a result of constraining the N-terminus of the donor subunit. Of the five amino terminal isoforms of the channel identified in rodents, two have been functionally characterised; Slack-A and Slack-B. The only disparity in the sequence of these isoforms, is that the N-terminus of Slack-A is 20 amino acids shorter than that of Slack-B (Brown et al., 2008). Slack-A channels expressed in HEK293 cells display more rapid activation kinetics, not dissimilar to those recorded from WT-WT concatemeric channels. Additionally, K_{Na}1.2 channels

possess an N-terminus with high sequence homology to that of Slack-A, and also activate with similar, fast activation kinetics (Brown et al., 2008). It is unclear how exactly the N-terminus contributes to the gating kinetics of the channel, and there are likely other structural determinants.

Introduction of a self-cleaving T2A peptide sequence between the two subunits rectified the changes in activation kinetics, and the behaviour of the homomeric concatemers closely aligned with normal homomeric WT $K_{Ka}1.1$ and Y796H channels when expressed in CHO cells. The WT/WT and YH/YH constructs had near-identical activation midpoints and slope values to the homomeric WT and Y796H channels and displayed similar activation kinetics. ΔG_0 values for WT/WT and YH/YH and the $\Delta\Delta G_0$ for YH/YH were all consistent with their monomeric counterparts. Heteromeric channels however, displayed distinct activation midpoints, current densities and kinetics from the two homomers. The discrepancy in current densities between the two heteromeric constructs is potentially due to the WT $K_{Na}1.1$ subunit in the YH/WT construct having a proline residue on its N-terminus following cleavage, or the C-terminus of the Y796H subunit upstream of the cleavage site having the remainder of the peptide sequence attached. Though introduction of the self-cleaving T2A peptide into the sequence seems effective in electrophysiological experiments, the 'cleavage' is not 100% efficient (Chng et al., 2015; Liu et al., 2017). It should be taken into consideration when interpreting the results that there may still be a small population of channels expressed composed of subunits that remain tethered together. This was reflected in western blot analysis of the WT-WT and WT/WT constructs, though this data is preliminary and requires further optimisation and repeats. It is possible that cleaved subunits have bound together during western blot analysis. It is also noteworthy that western blotting detects the total protein in the cell whereas patch clamp detects only channels expressed on the plasma membrane; cell surface biotinylation may be useful in future to confirm expression of cleaved subunits.

Another possibility is that following the ribosomal skipping event, the ribosome falls off and only the first protein, upstream of the peptide, is translated. There are other self-cleaving 2A peptides, named after the virus from which they were derived; E2A (equine rhinitis A virus), F2A (foot and mouth disease virus) and P2A (porcine teschovirus) are other 2A viral oligopeptides. P2A and T2A are reported as the most efficient across a wide range of cell types (Chng et al., 2015; Liu et al., 2017). For this particular application, it may be useful to compare efficiencies with different 2A peptides between the $K_{Na}1.1$ subunits. It would perhaps be useful to quantify the cleavage efficiency and

relative protein expression in western blots for the constructs. Due to the very high molecular weight of the protein and the resulting challenges that arise with protein transfer however, doing this with accuracy may not be possible.

Studying co-expressed $K_{Na}1.1$ subunits instead of using concatemers is not without limitations however. The resulting population of channels is likely a mixture of heteromeric WT/mutant channels, and homomeric WT and mutant channels; and all channels will have their own activation kinetics. Co-expression provides a more physiologically relevant population of channels but creating the concatemer constructs validates the results seen upon co-expression of WT $K_{Na}1.1$ and mutant subunits.

4.3.2 Kinetic properties in heteromeric channels

Y796H, a *KCNT1* variant associated with the less severe disorder, (AD)SHE was focused on for creating the concatemeric constructs. Despite causing a less severe phenotype, this mutant caused the most discernible changes to normal $K_{Na}1.1$ gating behaviour when studied in a homomeric assembly. In particular, the homomeric mutant resulted in a faster time constant for activation. The tau value for heteromeric concatemers was, as with co-expression, more similar to that of WT/WT channels. The introduction of WT $K_{Na}1.1$ subunits into the tetrameric assembly may suppress the effects of the Y796H mutation on the time constant of activation, and thus the maximal probability of opening of the channel. When intracellular Na^+ was omitted, as the influence of the WT subunits was removed, the tau value became more reflective of the Y796H subunits in the heteromeric assembly. Whilst this was not seen in the co-expressed WT/Y796H assembly studied previously since heteromeric currents were too small to be accurately fitted in the absence of Na^+, it is consistent with the two (AD)SHE-causing variants that could be fitted.

Homomeric YH/YH channels facilitated activation gating in the absence of intracellular, producing currents that were still larger than WT/WT channels in the presence of Na^+. Conversely to co-expressed Y796H and WT $K_{Na}1.1$ subunits previously examined, currents could still be recorded for YH/WT and WT/YH channels in the absence of intracellular Na^+, and the activation kinetics were an intermediate between WT and Y796H homomeric channels. It is possible that in the co-expressed population, WT homomeric channels were predominant, and the contribution of true heteromeric channels was small. Concatemeric channels, in agreement with homomeric mutant channels and the two (AD)SHE-causing variants that produced large currents in the

absence of Na^+ when co-expressed with WT subunits, activated at more depolarised voltages in the absence of Na^+. The shift was to the same degree as that seen for homomeric Y796H channels, approximately 20 mV, but this resulted in considerably more positive activation midpoints in the heteromeric channels. Y796H amino acid substitutions in the tandem dimer constructs lowered the activation barrier between inactive and active states, indicated by the zero-voltage free energy (Table 4.1), in agreement with monomeric Y796H channels examined previously. Introduction of WT $K_{Na}1.1$ subunits into the tandem-dimer constructs increased the activation barrier again, reflected in both more positive $\Delta\Delta G_0$ values and activation midpoints for both combinations of heteromeric concatemer.

One of the concatemeric constructs, WT/YH, was used successfully to create a stable cell line expressing equal amounts of WT $K_{Na}1.1$ and Y796H subunits; reflective of patients carrying heterozygous DEE-causing variants. There were no problems with expression of the self-cleaving WT/YH construct in HEK293 cells for this purpose. The tethered concatemer constructs could not be expressed in HEK293 cells previously; perhaps since the construct was too large to be successfully trafficked to the plasma membrane. An advantage of using the heteromeric construct to produce stable cell lines for this purpose, is that cells stably expressing homomeric Y796H channels would likely have poor survival, since transient expression of this mutant consistently resulted in poor cell health due to its large GOF. The concatemer constructs engineered here will be valuable in future for single channel studies, but also for use in developing novel inhibitors of the channel. The HEK293 cell line stably expressing WT/YH can be utilised in high throughput fluorescence-based assays and automated patch clamp electrophysiology to screen potential drug hits.

5 Pharmacological modulation of $K_{Na}1.1$ channels

5.1 Introduction

5.1.1 Clues to mechanisms of inhibition of $K_{Na}1.1$ by existing drugs

DEEs arising from pathogenic variants of *KCNT1* are mostly refractory, and there is a lack of clinically efficacious inhibitors of the channel. Quinidine, bepridil and clofilium, the three known inhibitors of the channel, all have off-target effects resulting in part from non-selectivity and inhibition of cardiac cation channels (Rizzo et al., 2016; Yang et al., 2006; de Los Angeles Tejada et al., 2012). All three drugs are potent inhibitors of hERG (Paul et al., 2002). The hERG channel current is responsible for termination of the cardiac action potential, and inhibition can induce Torsades de Pointes ventricular arrhythmia and subsequently prolong the QT interval (Finlayson et al., 2004). There is an unmet need for more potent, selective inhibitors of $K_{Na}1.1$ that will ameliorate the increased current size resulting from GOF mutations; that do not inhibit hERG channels.

Though the mechanism of inhibition of $K_{Na}1.1$ has not been studied in depth in the literature, inhibition of hERG channels by the three antiarrhythmic drugs has been characterised. A phenylalanine residue located in the pore-forming region, F656, has been identified as a common determinant of hERG inhibition by quinidine, bepridil and clofilium (Kamiya et al., 2006; Perry et al., 2004; Macdonald et al., 2018). Other residues have also been identified within the pore-forming region; S631 for quinidine (Yang et al., 2004), Y652 for clofilium (Perry et al., 2004), and T623, S624 and V625 for bepridil (Kamiya et al., 2006). The drugs interact with the aromatic side chains of these residues to block the largely hydrophobic inner pore vestibule from the intracellular side. This leads to the hypothesis that quinidine and bepridil also inhibit $K_{Na}1.1$ channels via the intracellular pore vestibule.

5.1.2 Use of Cryo-EM structures to identify channel inhibitors

Recent advances in structural biology that have enabled determination of high resolution cryo-EM channel structures have opened up more possibilities for computer-aided drug discovery (CADD). High-throughput screening involves the expensive and labour-intensive process of carrying out experiments with whole compound libraries. Virtual high-throughput screening has greatly reduced the library size for physical

experiments, predicting likely candidates using *in silico* methods (Lin et al., 2020). Molecular docking can be used to predict the binding between compounds and the target protein, assigning scores to compounds in a virtual library (Lin et al., 2020; Yu and MacKerell, 2017). The structure of the chicken $K_{Na}1.1$ channel was one of the earliest ion channel structures to be elucidated using cryo-EM, at 4.5 Å (Hite et al., 2015) and was later resolved at higher resolution; the inactive conformation at 4.3 Å, and the open state 3.8 Å (Hite and MacKinnon, 2017). The structures of the chicken $K_{Na}1.1$ channel in open and closed conformations may therefore be utilised to carry out virtual high-throughput screening and identify novel inhibitors of the human $K_{Na}1.1$ channel that may have therapeutic potential.

5.1.3 Chapter hypothesis and aims

Hypothesis: Existing inhibitors of $K_{Na}1.1$ block the intracellular pore vestibule, similarly to their inhibition of the hERG K^+ channel. The chicken cryo-EM structure can be used to identify novel inhibitors of the channel.

Aims:

- ***To identify the binding site of quinidine and bepridil and designate a target for in silico screening***
- ***To use the cryo-EM structure of $K_{Na}1.1$ to identify novel inhibitors of the channel***
- ***To use a previously developed concatemeric construct to investigate inhibition of heteromeric WT/mutant $K_{Na}1.1$ channels***

5.2 Results

5.2.1 Two residues were identified as possible binding sites from the cryo-EM structure of the chicken $K_{Na}1.1$ channel

The pore-forming region of the channel was modelled by Dr Jonathan Lippiat using SwissDock (Figure 5.1), based on the recently resolved cryo-EM structure for chicken Slo2.2 (Hite and MacKinnon, 2017). The model consists of the S5 and 6 domains, and the pore loop of each subunit in the tetramer. Two residues were identified by *in silico* docking as possible binding sites for bepridil and quinidine in the closed conformation: cF325 and cM333 (hF346 and hM354). M354 is the proposed narrowest part of the

pore-forming region (Hite and MacKinnon, 2017). In the open conformation however, the drugs were only predicted to bind to the phenylalanine residue.

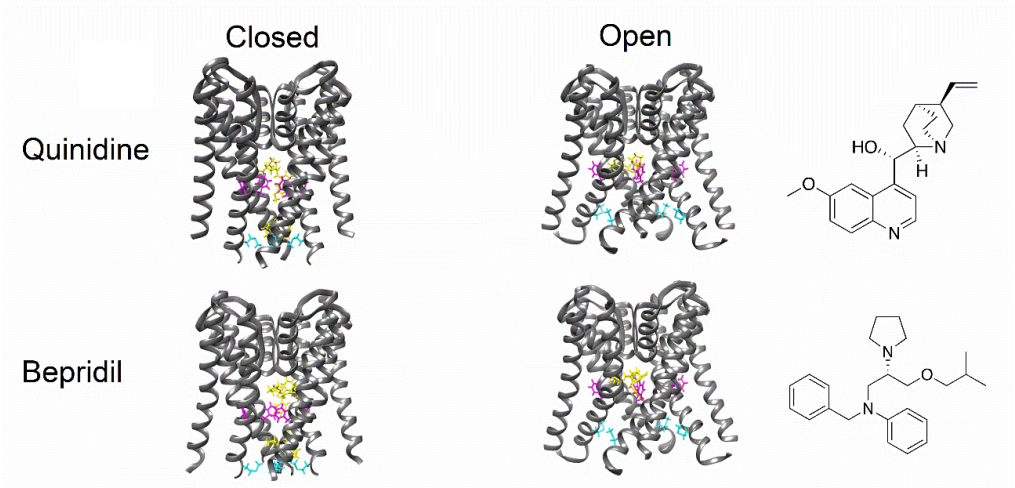

Figure 5.1: *In silico* docking model showing quinidine and bepridil binding to two possible pore-lining residues in the closed channel conformation, and one residue in the open conformation.
Work carried out by Dr Jonathan Lippiat. F346 (magenta) and M354 (cyan) side chains are highlighted on each of the four channel subunits, and one molecule of quinidine or bepridil (yellow) for each of the two possible residues. Side view of the S5 and S6 domains (grey) with other parts of the channel structure removed for clarity.

5.2.2 Pore mutants resulted in a GOF similar to that seen in epilepsy-causing mutations

A phenylalanine residue at position 346 or a methionine residue at position 354 in the human $K_{Na}1.1$ channel were mutated to either serine or isoleucine, and the mutant channels expressed in HEK293-MSR cells. In response to a series of voltage steps from -100 to +80 mV from a holding potential of -80 mV (Figure 5.2A), both phenylalanine mutations displayed a large increase in macroscopic current amplitude (Figure 5.2B and C). Furthermore, F346I in particular showed a loss in the outward rectification that normally arises as a result of the weak voltage dependence of the channel. This effect is akin to that seen as a result of epilepsy-causing mutations in Chapter 3, for example Y796H. M354 mutations did not have a significant effect on normal channel function however (Figure 5.2B and C).

To ensure that any potential changes in quinidine and bepridil efficacy were not as a result of increased channel activity in the F346 mutants, (AD)SHE-causing mutation Y796H was included in the study as a comparison. This mutation was previously shown to have a large GOF effect when expressed in CHO cells (Chapter 3), and this was consistent when the channel was expressed in HEK293-MSR cells (Figure 5.2A, B

and C). Importantly, this mutation is located far from the pore-forming region (Heron et al., 2012), and would therefore not interfere with the proposed binding region for the inhibitors.

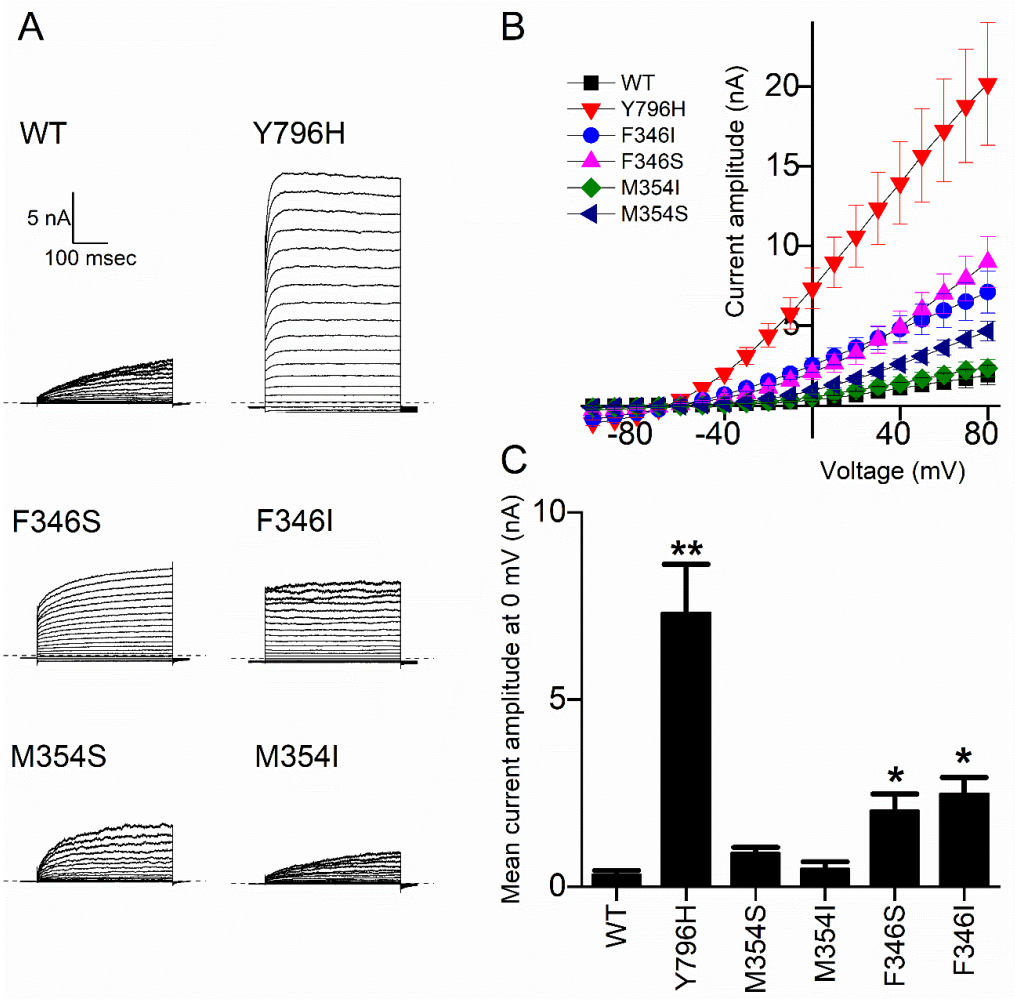

Figure 5.2: Functional analysis of mutant $K_{Na}1.1$ channels used.
A) Representative whole cell currents **B)** mean (± s.e.m., n=5-9 cells) current-voltage relationships for HEK293-MSR cells transfected with wild-type (WT), pore mutant (F346S, F346I, M354S, M354I) or (AD)SHE-causing mutant (Y796H) $K_{Na}1.1$. **C)** Mean (± s.e.m) peak current amplitude at 0 mV for WT and mutant channels. *p<0.05, **p<0.005 compared to WT, independent one-way ANOVA with Games-Howell post-hoc test.

5.2.3 A pore-lining phenylalanine residue may be involved in inhibition by quinidine and bepridil

Inhibition of the pore mutants by quinidine and bepridil were evaluated. Perfusion of a series of increasing concentrations of quinidine (3 µM-1 mM) or bepridil (0.3-100 µM) onto HEK293-MSR cells expressing WT $K_{Na}1.1$ channels for two minutes produced concentration-dependent inhibition of outward current, consistent with that previously reported for the channel. The IC_{50} values were 124.99 ± 34.52 µM (n=5) and 6.36 ±

2.12 μM (n=5) for quinidine (Figure 5.3B) and bepridil (Figure 5.3C), respectively. Inhibition was almost complete at the highest concentration used for both drugs, though residual current may be due to endogenously expressed channels that are not inhibited by quinidine and bepridil (Jiang et al., 2002; Yu and Kerchner, 1998). The mean peak current measured in endogenous channels at +80 mV was 151.76 ± 18.08 pA (n=8). To avoid contamination of recordings with endogenous current, the slope of the current-voltage relationship between -60 and 0 mV was used for analysis, since there is very little endogenous activity seen in this voltage range.

Mutation of F346 to both isoleucine or serine resulted in approximately a 10-fold reduction in potency of quinidine. M354 mutations on the other hand, had no significant effect on quinidine inhibition (Figure 5.3B). The effects of pore mutations on bepridil inhibition were more modest, with approximately a 5-fold reduction in potency for both phenylalanine mutations (Figure 5.3C). (AD)SHE-causing mutation Y796H yields large currents and loss of rectification similar to that seen in F346 mutants but caused a 3-fold increase in the potency of quinidine (Figure 5.3B). Conversely, there was no significant change in bepridil inhibition of Y796H compared to WT $K_{Na}1.1$ (Figure 5.3C).

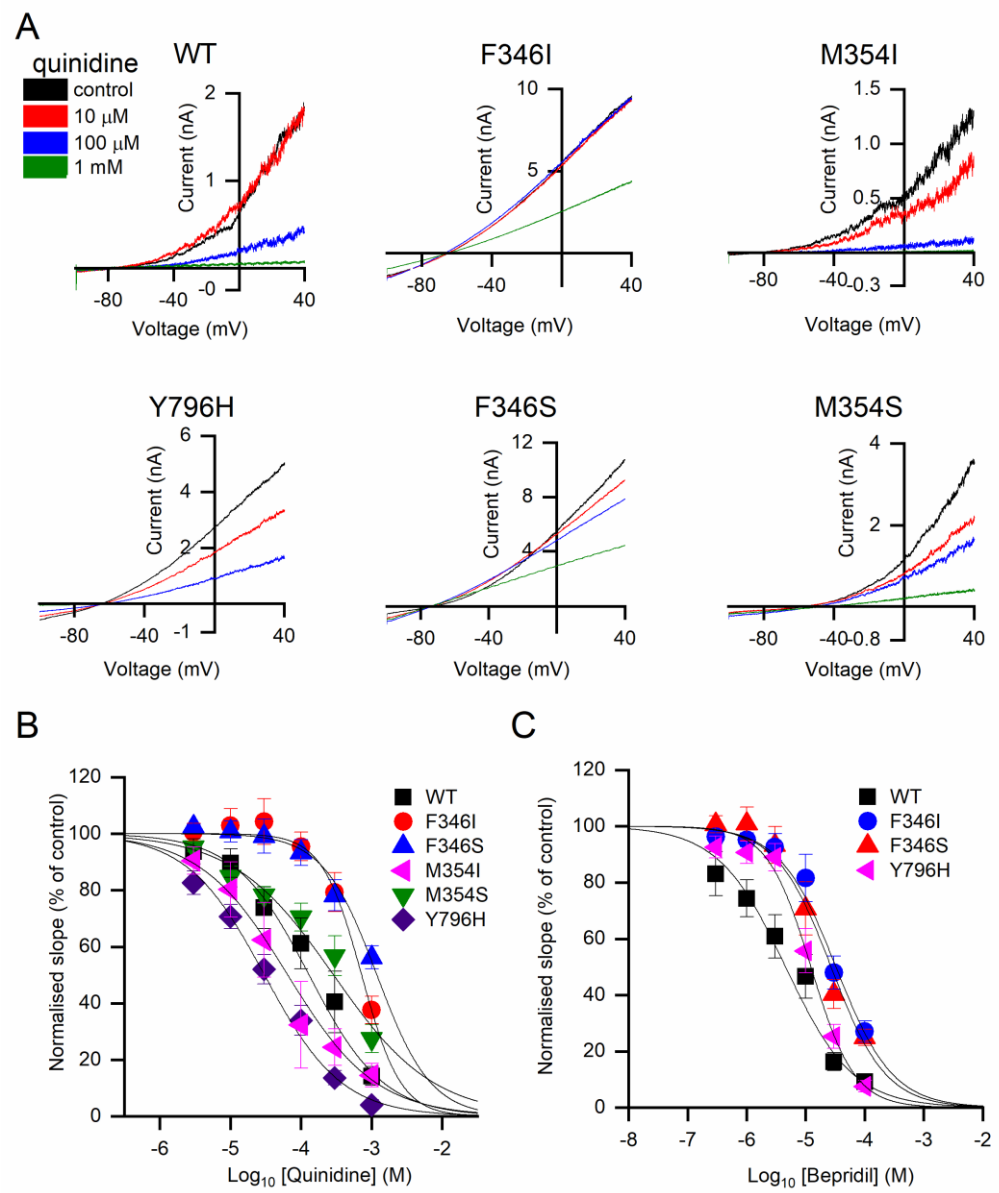

Figure 5.3: Concentration-inhibition analysis of wild-type and mutant $K_{Na}1.1$ channels by quinidine and bepridil.
A) Representative currents in response to voltage ramps from cells expressing WT or mutant $K_{Na}1.1$ following perfusion of increasing concentrations of quinidine as indicated. **B)** Mean (± s.e.m.) concentration-dependent inhibition of wildtype and mutant $K_{Na}1.1$ channels in response to 3 µM to 1 mM quinidine. Mean (± s.e.m.) IC_{50} for WT, 124.99 ± 34.52 µM (n=5 cells); F346I, 736.08 ± 94.09 µM (n=5); F346S, 1.23 ± 0.19 mM (n=4); M354I, 99.23 ± 49.61 (n=5); M354S, 247.16 ± 19.96 µM (n=5); Y796H, 38.00 ± 12.89 µM (n=5). **C)** Mean (± s.e.m.) concentration-dependent inhibition of wildtype and mutant $K_{Na}1.1$ channels in response to 0.3 µM to 100 µM bepridil. IC_{50} for WT, 6.36 ± 2.12 µM (n=5); F346I, 35.91 ± 11.01 µM (n=4); F346S, 23.43 ± 5.17 µM (n=5).

5.2.4 6 compounds with higher potency than quinidine identified by virtual high-throughput screening

Having identified the inner pore vestibule as a target for $K_{Na}1.1$ inhibitor binding, this region was used by Dr Rachel Johnson to conduct virtual high-throughput screening. Using the minimal pore structure of the chicken channel in the open state, a library of 100,000 compounds from the Chembridge small molecule library were docked into the identified region. Additionally, compounds that had a similar structure to bepridil were identified and docked into the structure. A ranked list of potential inhibitors of the channel was yielded from each of the virtual screening methods, based on binding affinity and the score assigned when docking. 17 of the compounds from this list were then selected for *in vitro* validation using whole cell electrophysiology (Table 5.1 and Figure 5.4A).

Six of the compounds were selected for further functional analysis, since at 10 μM they inhibited WT $K_{Na}1.1$ channels expressed in HEK293-MSR cells >40% and were deemed active (Figure 5.4A). Furthermore, to validate the inner pore vestibule as the site of inhibition, the six compounds were applied to cells expressing the F346S mutation at a concentration of 10 μM. A significant reduction in inhibition was seen for all of the compounds. IC_{50} values derived from concentration-response curves for each of the six compounds (Figure 5.4B and C) ranged from 0.6-7.4 μM when inhibiting the WT $K_{Na}1.1$ channel (Table 5.2); compared to values of 124.99 ± 34.52 μM (n=5) and 6.36 ± 2.12 μM (n=5) for quinidine and bepridil, respectively.

To further probe the effectiveness of the compounds, inhibition of (AD)SHE-causing mutation Y796H was studied; since inhibition of epilepsy-causing mutations is desirable in a clinical setting. BC7 and BC14, however, were significantly less potent when applied to Y796H channels (Figure 5.6 and Table 5.2). A number of commercially available structural analogues of BC12 were also studied, though at 10 μM none of these compounds were active against WT $K_{Na}1.1$ (Figure 5.7A and B).

Table 5.1: Compounds selected for validation.
Top-scoring compounds identified through virtual high-throughput screening or bepridil overlay (#), tested at 10 μM for inhibition of $K_{Na}1.1$. Virtual high-throughput screening carried out by Dr Rachel Johnson. *Compounds that demonstrated >40% inhibition and were further characterised. The predicted H-bonds use the amino acid sequence in the chicken $K_{Na}1.1$ structure (PDB: 5U70).

BC ID	PubChem ID	Chembridge ID	M.W.	cLog P	Docking score	Predicted H-bond
1	42211371	10226003	433.5	2.1	-8.731	E326 (hE347) T293 (hT314) x2
2	42170356	18717381	450.5	2.611	-8.841	T293 (hT314) S392 (hS313)
3	45198665	32500723	489.5	1.76	-9.151	T293 (hT314) x2
4	72869676	38250229	360.4	2.9	-8.88	T293 (hT314) x2
5*	42481567	38627778	491.5	4.154	-9.607	T293 (hT314) F291 (hF312)
6#*	1283470	5143781	413.3	4.81	-7.44	T293 (hT314)
7#*	2272824	5214461	412.2	7.05	-7.189	T293 (hT314) x2
8#	1376211	5422905	359.5	6.26	-7.246	-
9#	5341073	5574034	423.3	6.67	-7.28	T293 (hT314)
10	5342180	5690314	459.5	6.64	-9.022	F291 (hF312) T293 (hT314) x2
11	56902153	60526468	324.4	3.21	-9.074	F291 (hF312)
12*	1330052	7040211	467.4	5.37	-8.732	F291 (hF312) T293 (hT314) x2
13*	2185932	7364411	253.3	3.906	-8.891	F291
14*	1243440	7942343	455.5	5.214	-8.891	-
15	72922744	84082349	359.4	1.15	-8.638	F291 (hF312) T293 (hT314) x2
16	70780443	90931265	327.4	1.83	-8.74	F291 (hF312)
17	25249672	9273389	260.4	3.085	-8.861	F291 (hF312)

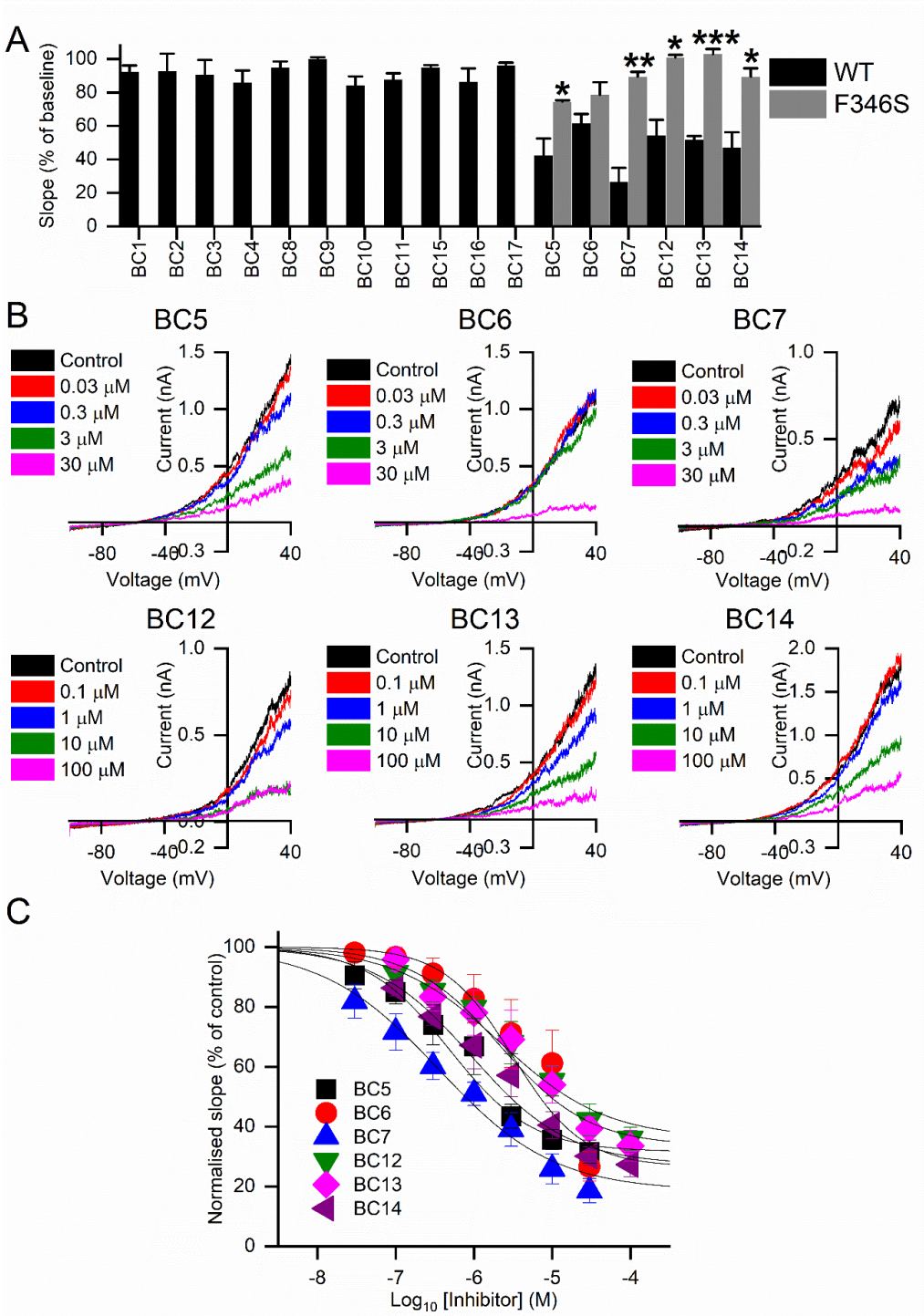

Figure 5.4: Functional evaluation of top-scoring molecules from *in silico* docking. **A)** Mean (± s.e.m., n = 3 to 4 cells) WT $K_{Na}1.1$ conductance measured as the slope of the current evoked by a voltage ramp to +40 mV, relative to baseline, in the presence of 10 µM test compound. Those that were active (right of dashed line) were also tested with the F346S $K_{Na}1.1$ pore mutant (*p<0.05, **p<0.005, ***p<0.0005, Student's T-test.). **B)** Representative traces and **C)** mean (± s.e.m., n= 5 to 7 cells) concentration-inhibition plots for active inhibitors.

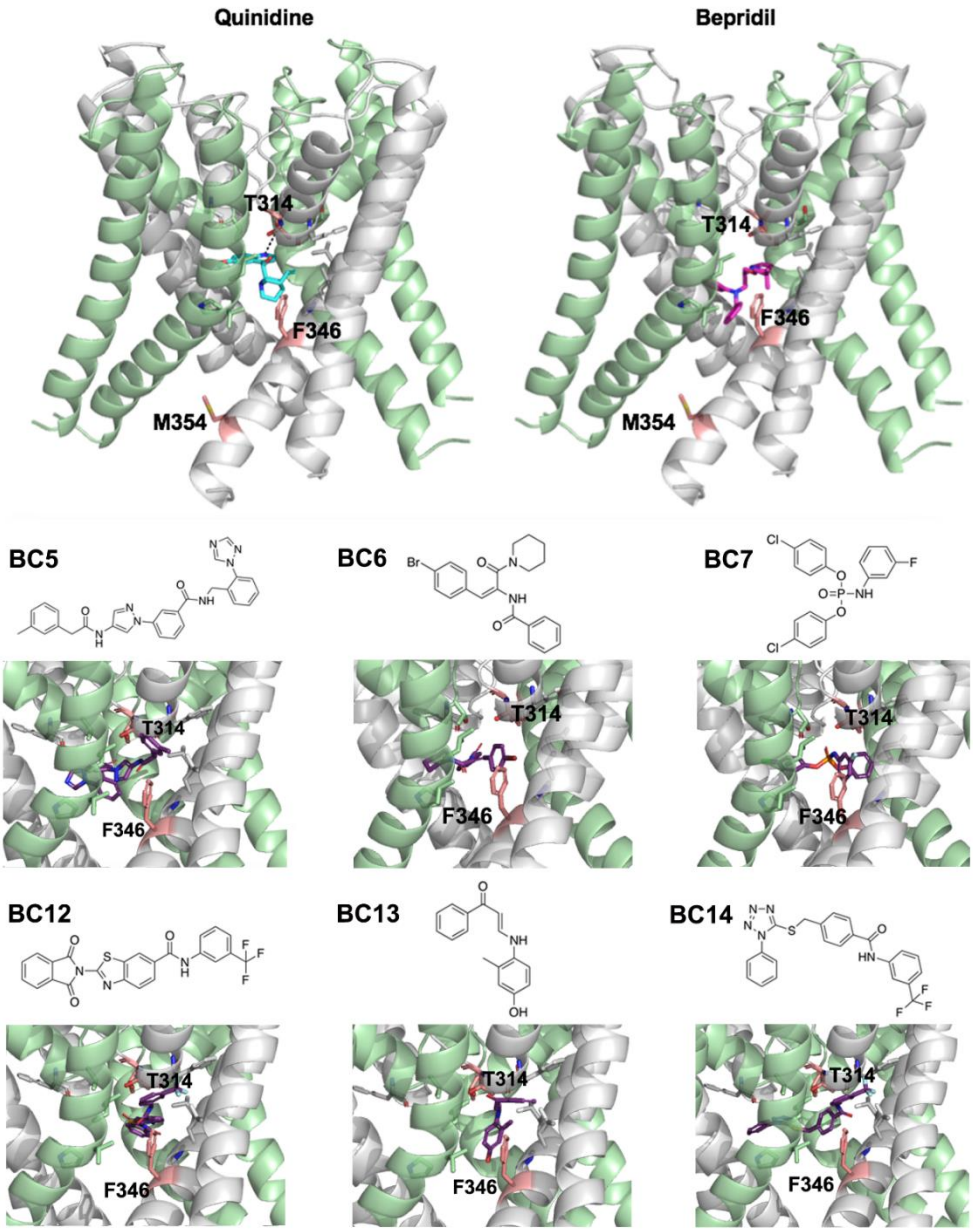

Figure 5.5: Chemical structures of 'active' inhibitors (magnenta) and their docked poses in the K_{Na}1.1 pore domain.
Work carried out by Dr Rachel Johnson and Dr Stephen Muench. Side chains at positions equivalent to the human isoform are indicated (pink): T314 in the P-loop, and F346 and M354 in the S6 segment of human K_{Na}1.1.

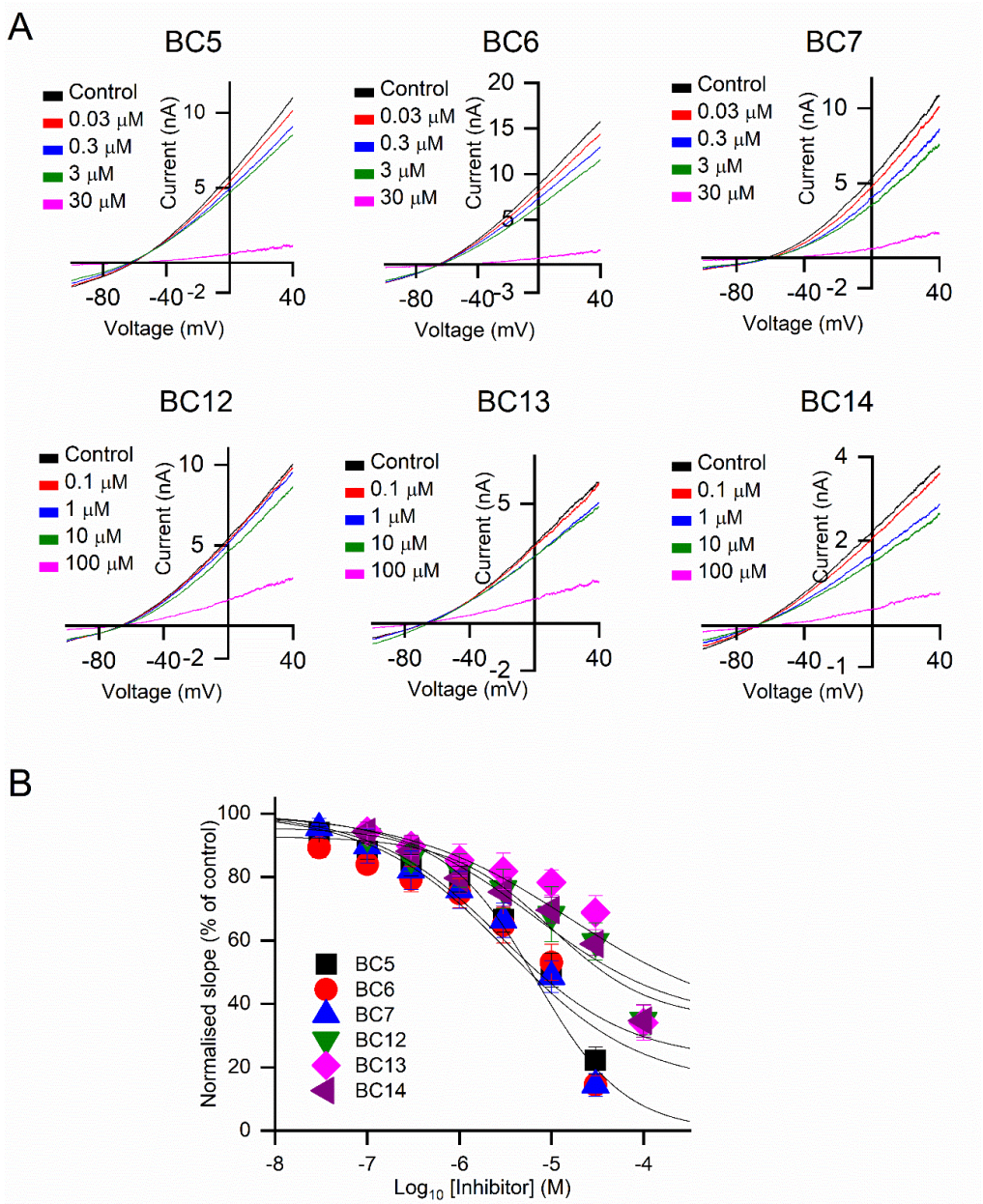

Figure 5.6: Functional evaluation of novel inhibitors with $K_{Na}1.1$ channels harbouring the epilepsy-causing mutation Y796H.
A) Representative traces and **B**) mean (± s.e.m., n= 5 to 7 cells) concentration-dependent inhibition by active inhibitors.

Table 5.2: **Summary table with mean (± s.e.m.) potencies of compounds.**
Inhibiting WT and Y796H $K_{Na}1.1$ (n= 5 to 7 cells). *p<0.05 vs potency with WT $K_{Na}1.1$ (Student's T-test).

Compound	WT $K_{Na}1.1$ IC_{50} (µM)	Y796H IC_{50} (µM)	
BC5	3.20 ± 1.16	3.61 ± 0.96	
BC6	7.41 ±1.90	3.88 ± 1.08	
BC7	0.63 ± 0.25	7.54 ±1.90	*
BC12	3.03 ± 1.12	13.72 ± 7.31	
BC13	4.29 ± 1.73	17.45 ± 7.04	
BC14	1.57 ± 0.39	7.55 ± 1.89	*
Quinidine	124.99 ± 34.52	38.00 ± 12.89	*
Bepridil	6.36 ± 2.12	12.80 ± 2.46	

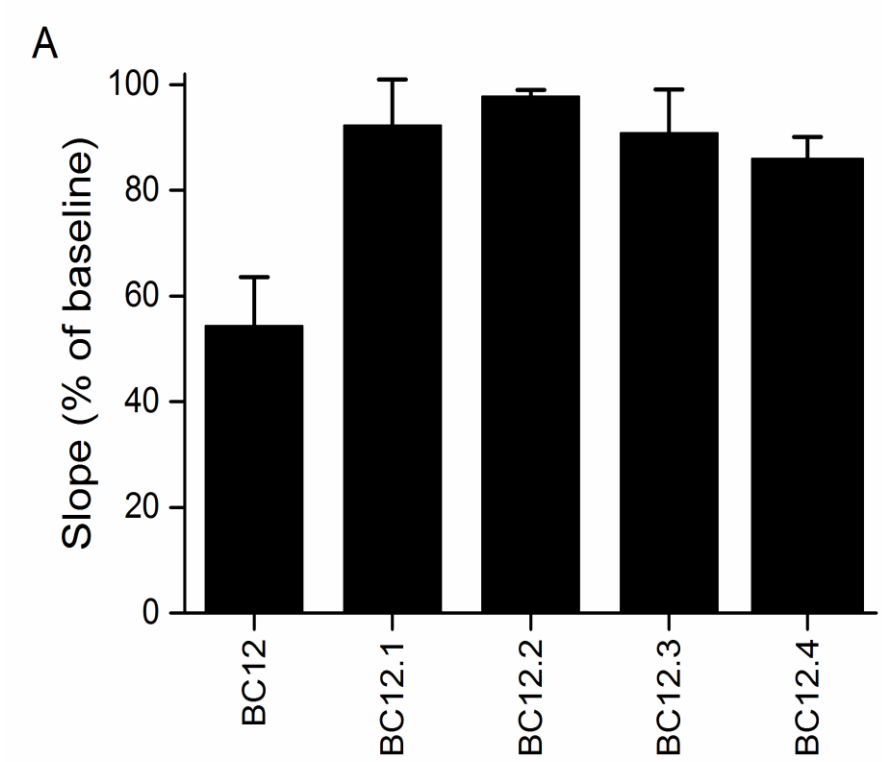

B

		cLogP	docking score
BC12	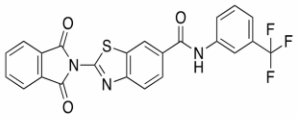	5.37	-8.73
BC12.1	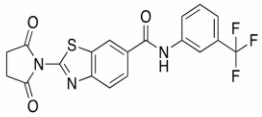	2.94	-8.77
BC12.2	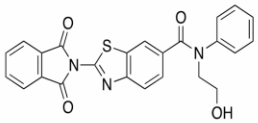	3.32	-6.12
BC12.3	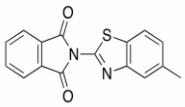	3.79	-5,60
BC12.4	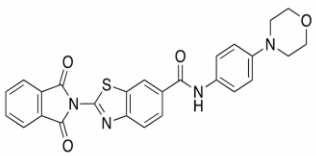	4.17	-3.79

Figure 5.7: Evaluation of BC12 analogue compounds.
A) Mean (± s.e.m., n=3) $K_{Na}1.1$ conductance, measured as the slope of the current evoked by a depolarising voltage ramp in the presence of 10 µM test compound relative to control solution. **B)** Chemical structures of compounds, their computed LogP (cLogP) and Glide docking score.

5.2.5 Toxicological assessment of the compounds

One of the biggest challenges clinically is the non-selectivity of the existing therapeutics for *KCNT1*-related DEEs, and their consequential inhibition of hERG channels. It was therefore important to study inhibition of hERG channels by the compounds. hERG channels have different activation kinetics to $K_{Na}1.1$ channels and inactivate at higher voltages leading to inward rectification. For this reason, a two-step pulse protocol is used, which enables recovery from inactivation and generates a large outward tail current (Witchel et al., 2002). The peak tail current was measured repeatedly every 20 seconds whilst perfusing the compounds into the bath (Figure 5.8A). BC5, BC6 and BC7, at a concentration of 10 μM, resulted in >80% reduction in the peak tail current. BC14 however, inhibited hERG by around 45%, and BC12 and BC13 by 10-20% (Figure 5.8B).

Finally, a WST cell viability assay was used to test for possible cytotoxicity of the compounds. Following 24 hours of exposure to different concentrations of compound, only BC7 (0.03-30 μM) displayed a concentration-dependent reduction in cell viability. BC5, BC6 and BC13 significantly decreased cell viability only at the highest concentration tested (30 μM for BC5, and 100 μM for BC6 and BC13), which is an order of magnitude higher than the IC_{50} values. BC12 and BC14 did not decrease cell viability at any concentration tested (Figure 5.8C). 10% (v/v) DMSO and 10 μM blasticidin were included as positive controls and caused approximately a 90% and 45% reduction in cell viability respectively.

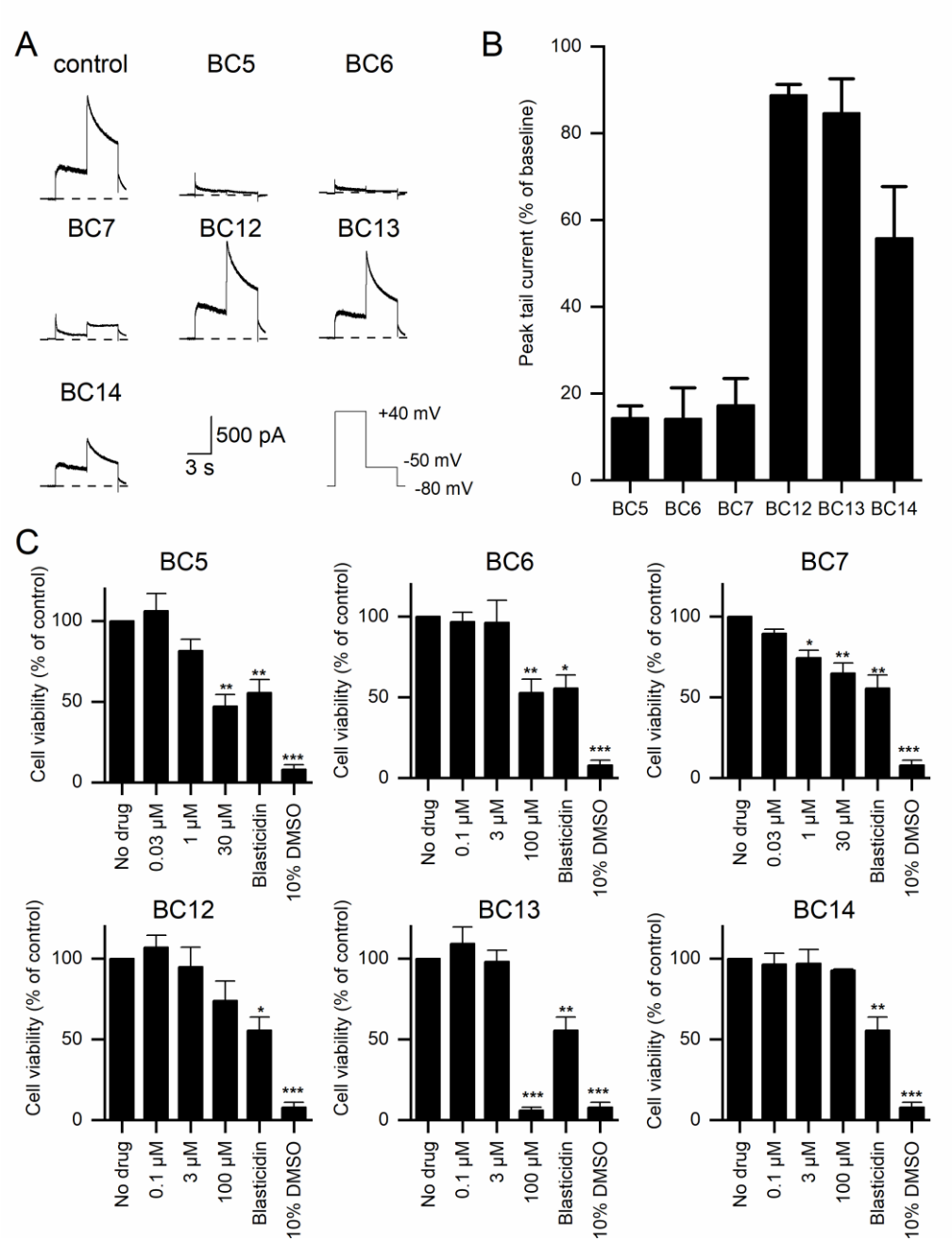

Figure 5.8: Preliminary toxicological assessment of $K_{Na}1.1$ inhibitors.
A) Representative hERG currents recorded from HEK293-MSR cells expressing hERG in the absence (control) and presence of 10 µM inhibitor, as indicated. **B)** Mean (± s.e.m., n=3) tail current at -50 mV remaining in the presence of each inhibitor. **C)** Cytotoxicity assays indicating mean (± s.e.m., n=3) viability of HEK293-MSR cells using WST reagent following 24h exposure to inhibitor at the indicated concentrations, with 10 µM blasticidin and 10% (v/v) DMSO as positive controls; *p<0.05, **p<0.005, ***p<0.0005, independent one-way ANOVA with Dunnett's post-hoc test.

5.2.6 Characterisation of FDA-approved inhibitors of $K_{Na}1.1$

Owing to the success of the *in silico* screen in identifying novel inhibitors of $K_{Na}1.1$, the same approach was used by Dr. Katie Simmons to dock the DrugBank database of compounds into the open channel pore model used earlier and filtered the results to include only FDA-approved compounds. Ten compounds predicted to occupy the pore-forming region were selected for in vitro screening, based upon commercial availability, clogP values (predicted octanol-water partition coefficient), and clinical status.

The WT/Y796H concatemer construct with a self-cleaving T2A site described in Chapter 4 was used to screen these inhibitors. This construct is reflective of the heterozygous phenotype in patients and is thus more physiologically relevant than screening against the WT $K_{Na}1.1$ or homomeric variant Y796H channel. The concatemer construct could not be expressed in HEK293-MSR cells however, so the CHO cell line was used for this work and has the additional advantage of low endogenous K^+ conductance. Rather than the previously used ramp protocol from -100 to +40 mV, for these experiments a ramp from -100 to 0 mV was applied (Figure 5.9A). With the exception of indinavir, dihydrotachysterol, liftegrast, and terconazole (Figure 5.9C), application of drugs at 10 μM reduced whole cell WT/Y796H currents and so were further evaluated to determine full concentration-response relationships. Four FDA-approved drugs, antrafenine, atorvastatin, nelfinavir mesylate and regorafenib inhibited WT/Y796H channels expressed in CHO cells with IC_{50} values ranging from 1.30-10.30 μM. Candesartan cilexetil was less potent, and higher concentrations were not attempted as it appeared to be similar to, or less potent than, quinidine (Figure 5.9B and Table 5.3).

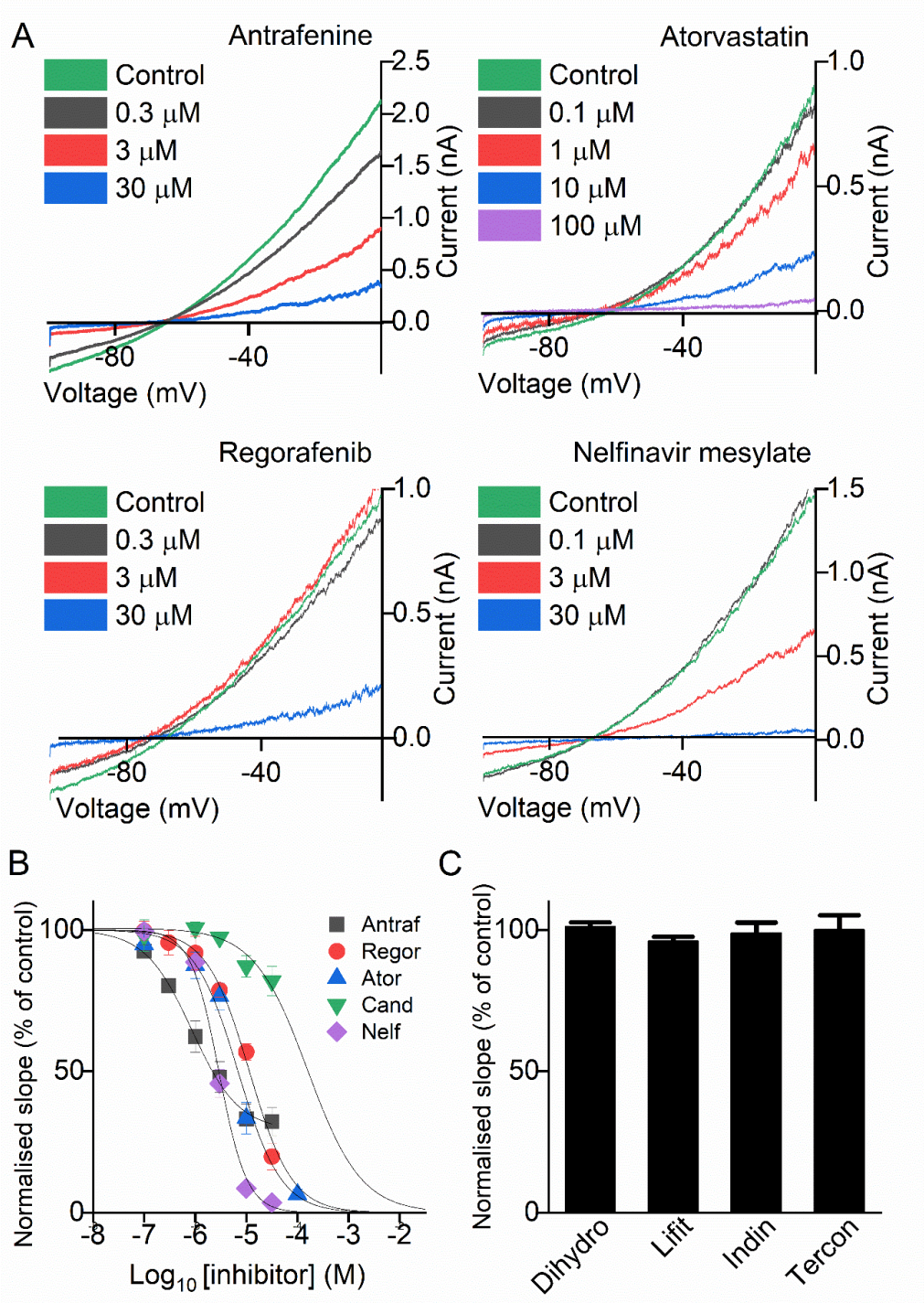

Figure 5.9: Functional evaluation of FDA-approved inhibitors with WT/Y796H concatemeric $K_{Na}1.1$ channels.
A) Representative traces and **B)** mean (± s.e.m., n= 5 to 6 cells) concentration-dependent inhibition by 'active' inhibitors; antrafenine (Antraf), regorafenib (Regor), atorvastatin (Ator), candesartan cilexetil (Cand) and nelfinavir mesylate (Nelf). **C)** Mean (± s.e.m., n = 3 to 4 cells) WT/Y796H $K_{Na}1.1$ conductance measured as the slope of the current evoked by a voltage ramp to +40 mV, relative to baseline, in the presence of 10 μM 'inactive' inhibitors; dihydrotachysterol (Dihydro), lifitegrast (Lifit), indinavir (Indin) and terconazole (Tercon).

Table 5.3: Mean (± s.e.m., n= 5 to 6 cells) potencies of FDA-approved compounds. Inhibiting WT/Y796H concatemeric $K_{Na}1.1$ channels.

FDA-approved drug	IC_{50} (μM)
Antrafenine	1.30 ± 0.20
Atorvastatin	7.54 ± 0.99
Nelfinavir mesylate	2.85 ± 0.30
Regorafenib	10.30 ± 1.25

5.3 Discussion

5.3.1 Identification as the inner pore vestibule as the binding region for KNa1.1 inhibitors

Mutation of a phenylalanine residue located in the intracellular pore vestibule of $K_{Na}1.1$ to either serine or isoleucine resulted in a reduction in potency of both quinidine and bepridil. It could not be discounted that the effects of F346I and F346S on inhibition were a result of the GOF effects seen for both mutants however, which likely arose due to introduction of hydrophobic and polar sidechains into the pore-forming region. Currents recorded from the epilepsy-causing pathogenic variant F346L also activate with large current amplitude and reduced outward rectification when channels are expressed in *Xenopus* oocytes (McTague et al., 2018). To rule this possibility out, inhibition of a mutant $K_{Na}1.1$ channel carrying (AD)SHE-causing pathogenic variant Y796H was examined. This mutant, which results in similar GOF effects to the F346 mutants, is located in the RCK domains on the C-terminus, distally to the intracellular pore vestibule, and did not result in the same loss of inhibitor efficacy.

The reduced efficacy of each of the test compounds identified from the *in silico* screen with F346S gave further confirmation that compounds inhibit by blocking the channel pore. F346L is an EIMFS-causing pathogenic variant, and is the only DEE-causing *KCNT1* mutation thus far that is reportedly insensitive to inhibition by quinidine (McTague et al., 2018). *Xenopus* oocytes are poor expression system for studying the pharmacology of $K_{Na}1.1$ channels due to being membrane and lipid-rich. Higher concentrations are required to evoke the same responses, which may explain the total insensitivity of this *KCNT1* variant to quinidine. More recently, reduced potency of novel small molecule inhibitor, Compound 31, with F346L was reported (Griffin et al., 2021).

Mutation of F346 does not wholly abolish quinidine and bepridil inhibition of the channel however, and there are likely other interactions involved. The residue is the equivalent of the phenylalanine residue in hERG channels that coordinates inhibition by quinidine, bepridil and clofilium, and for this channel other residues such as threonine and serine are also thought to be involved (Kamiya et al., 2006; Perry et al., 2004; Macdonald et al., 2018). Indeed, compounds BC5 and BC12 were predicted to form H-bonds with two other residues in the inner pore vestibule, cT293 (hT314) and cF291 (hF312); BC6 and BC7 were predicted to just bond to cT293, and BC13 just to cF291.

Gating of the channel is thought to arise in or near to the selectivity filter of the channel (Giese et al., 2017; Garg et al., 2013), so these inhibitors would likely block at the channel gate. Thus, we predict this mechanism of inhibition would have efficacy in all DEE-causing mutations; perhaps aside from F346L. The human equivalent of cT293 that some test compounds were predicted to H-bond with, T314, is predicted to be the critical selectivity filter residue involved in gating. Whilst this would be deserving of further investigation, mutation of the threonine to cysteine in Chapter 3 had detrimental effects on gating and permeability of the channel due to its role in selectivity filter gating. Currents yielded from whole cell characterisation of T314C expressed in CHO cells exhibited loss of voltage-dependence, and currents reversed around 0 mV.

5.3.2 Identification and functional characterisation of K_{Na}1.1 inhibitors

The pore-region model used for *in silico* screen was from the cryo-EM structure in the open state, so it was anticipated that the inhibitors would achieve similar or, as seen for the existing inhibitors with DEE-causing mutants, higher potency in inhibiting the Y796H mutant channel. This was not the case, however there is a significant amount of basal activity in the Y796H mutant. As a result, series resistance compensation may at times be incomplete and underestimate inhibition with lower concentrations of inhibitor. CHO cells may prove to be a better expression system for these experiments in future since the resulting Y796H currents are considerably smaller. The increase in potency of quinidine is consistent with previous reports of increased sensitivity of mutant K_{Na}1.1 channels to inhibition however (Rizzo et al., 2016; Dilena et al., 2018; Milligan et al., 2014).

The insensitivity of hERG channels to two of the compounds is promising, since existing therapeutics are potent inhibitors of this channel. In fact, quinidine inhibits

hERG with an IC_{50} of 0.41 μM (Paul et al., 2002), compared to reported values of 82.1 μM - 124.99 μM for $K_{Na}1.1$ (Yang et al., 2006; Rizzo et al., 2016). Two approaches were used by Dr Rachel Johnson to identify potential inhibitors *in silico*; bepridil overlay, in which structurally similar compounds to bepridil were identified computationally, and screening of a library of 100,000 compounds. The focus was on the latter approach, since bepridil and quinidine are both non-selective for $K_{Na}1.1$, which is one of the complications associated with their use. BC6 and BC7 were both identified using the bepridil overlay approach, and both inhibited hERG channels almost completely at 10 μM. It has been previously proposed that existing inhibitors of the channel directly block the inner pore vestibule of hERG channels, by crossing the membrane and inhibiting from the intracellular side (Kamiya et al., 2006; Perry et al., 2004; Macdonald et al., 2018). It was therefore hypothesised that inhibitors of $K_{Na}1.1$ would inhibit by the same mechanism. None of the compounds identified in the initial screen with a calculated LogP value of less than 3.2 successfully inhibited the channel, and it is possible that this is due to poor membrane permeability.

BC12 and 14, two of the more potent inhibitors identified, possess trifluoromethyl groups that are predicted to dock between the S5 helix and pore vestibule (Figure 5.4). It is a feature shared with compounds appearing in the literature more recently (Griffin et al., 2021); this group was important for the potency of Compound 31, pointing towards a pore-blocking mechanism for this inhibitor. None of the structural analogues of BC12 were found to be active against WT $K_{Na}1.1$ at 10 μM (Figure 5.7). This was particularly surprising for BC12.1, which retains the trifluoromethyl group possessed by BC12 and has an improved docking score compared to BC12. Based upon the earlier finding that no compounds with a cLogP value of <3.2 successfully inhibited the channel, the cLogP value of 2.94 for BC12.1 may limit its membrane permeability and subsequent inhibition of the channel.

Both BC6 and BC13 have potential pan assay interference (PAINS) properties, due to the presence of an α,β unsaturated carbonyl group. Upwards of 400 reactive molecules, usually part of larger chemical structures, are classified as PAINS and can lead to false positives and nonspecific effects in high throughput compound screens (Jasial et al., 2017). The α,β unsaturated carbonyl group is able to react and covalently bond with cellular structures due to being susceptible to nucleophilic addition. This may impact further development of these compounds and derivatives of them. The toxicological assessments for the novel small molecule compounds were preliminary, and neither the safety nor selectivity of the six compounds identified can be confirmed.

Prior to any *in vivo* experiments to assess effects of these inhibitors on neuronal firing and hyperexcitability, further selectivity screens would be needed to determine possible inhibition of other ion channels.

5.3.3 Identification and functional characterisation of FDA-approved inhibitors

DEEs resulting from *KCNT1* pathogenic variants are clinically very rare disorders so repurposing of FDA-approved compounds is a useful approach due to reduced costs associated with drug development. Furthermore, repurposing of existing drugs accelerates the process of getting the drug into clinical use due to there being pre-existing clinical data and information about tolerability. A repurposed drug can reach patients within 3-12 years compared to 10-15 years for a novel compound, and the success rate is up to 5 times higher (Roessler et al., 2021). Electrophysiological characterisation of drug hits identified from a preliminary thallium flux screen and *in silico* docking identified four FDA-approved compounds that had efficacy in inhibiting heteromeric WT/mutant $K_{Na}1.1$ channels, each with lower IC_{50} values than for inhibition of homomeric WT $K_{Na}1.1$ and Y796H channels with quinidine. As with the previously identified test compounds, these inhibitors are predicted to bind within the pore forming region of $K_{Na}1.1$.

Antrafenine, a piperazine derivative, was previously licensed as a therapeutic intervention for osteoarthritis due to its analgesic and anti-inflammatory effects. It is similar in efficacy to naproxen but has been overtaken by newer analgesic drugs. Its mode of action is not fully understood, though it is purported to inhibit prostaglandin synthesis through inhibition of cyclooxygenase-2 (COX-2) activity, yielding anti-inflammatory effects (Berry et al., 1983). Though antrafenine appears to be the most potent inhibitor of WT/Y796H $K_{Na}1.1$ identified in this screen, $K_{Na}1.1$ inhibition is likely not involved in its analgesic effects. $K_{Na}1.1$ has been implicated in sensory input regulation of neuropathic pain in rodents, but $K_{Na}1.1$ knock-out mice show no impairment in their sensitivity to inflammatory or acute pain models (Lu et al., 2015; Martinez-Espinosa et al., 2015). Induced neuropathic pain by spared nerve injury in WT mice, and chemotherapy in human patients (though with adverse effects) can be rescued by selective $K_{Na}1.1$ activator loxapine (Lu et al., 2015; Schmiedl et al., 2019). Furthermore, PKA activation downstream of prostaglandin rapidly internalises $K_{Na}1.1$ channels expressed in rat DRG primary nociceptive neurons. Excessive internalisation

and a resultant decrease in K_{Na} current is hypothesised to contribute to hyperalgesia in inflammatory pain states (Nuwer et al., 2010).

Regorafenib is currently in use as a multikinase inhibitor, targeting receptor tyrosine kinase, to treat metastatic colorectal cancer and more recently CNS tumours. It is one of the less potent $K_{Na}1.1$ inhibitors identified here, and as such adverse effects resulting from its strong antineoplastic properties may outweigh the benefits of its use for *KCNT1*-related epilepsies. The most common adverse effects associated with its use are hand and foot skin reaction, hypertension, diarrhoea, fatigue and hypertension; but thrombocytopenia, anaemia and anorexia have also been reported (Mercier and Voutsadakis, 2017; Wu et al., 2020; Krishnamoorthy et al., 2015; Giampieri et al., 2017). Although, two recent studies have found regorafenib to penetrate the BBB, which is desirable for treating *KCNT1*-related DEEs. Low levels of the drug and its active metabolites were detectable in three relapsed glioblastoma patients (Zeiner et al., 2019). Another study found the drug to have “moderate” CSF penetrance in one paediatric brain tumour patient, though less than 60% was unbound (Guntner et al., 2020).

One of the more potent FDA-approved compounds found to be an inhibitor of WT/Y796H $K_{Na}1.1$, is nelfinavir mesylate. This drug is an approved HIV drug, that potently inhibits HIV-1 protease. It has also recently been demonstrated to rescue SARS-Cov-2 infected vero-E6 cells from death, and potently inhibits cell fusion resulting from the SARS-Cov-2 spike glycoprotein (Musarrat et al., 2020). Despite being a potent inhibitor of WT/Y796H $K_{Na}1.1$, it has been described as an inhibitor of hERG channels with an IC_{50} of 11.5 μM, so prolongation of the QT interval has been reported as a result of its use as a HIV treatment (Anson et al., 2005). This may limit its use in treating *KCNT1*-related epilepsies; though in comparison to existing channel inhibitors quinidine and bepridil, its relative selectivity for $K_{Na}1.1$ compared to hERG is vastly improved. Since the IC_{50} for $K_{Na}1.1$ inhibition is 2.9 μM, it may be possible to use nelfinavir mesylate at a concentration that does not inhibit hERG channels.

Finally, atorvastatin inhibited the channel well, with an IC_{50} value of 7.54 ± 0.99 μM. This drug is a competitive inhibitor of 3-hydroxy-3-methyl-glutaryl-coenzyme A (HMG-CoA) reductase, an enzyme involved in cholesterol synthesis, and is a statin primarily used in the treatment of hyperlipidaemia and hypercholesterolaemia. The drug is also licensed as a preventative treatment for patients carrying risk factors for coronary heart disease. Atorvastatin has been described as an inhibitor of hERG channels with an IC_{50}

of 1.22 μM (Feng et al., 2018). The concentration-response relationship analysed in this study plateaus at around 60% inhibition, and has an upper asymptote of 20% inhibition however, meaning the IC_{50} may have been overestimated.

Antihypertensive drug candesartan cilexetil had very low activity in whole cell patch clamp experiments. Though a low concentration range was used, limiting the ability to fit the concentration-response relationship accurately, the potency appeared to be similar to that of quinidine. It was decided that higher concentrations would not be tested for this compound, as the low potency of quinidine is one of the biggest limiting factors for its use and a compound with similar potency is not desirable.

Test compounds identified in the earlier screen did not exhibit inhibition of $K_{Na}1.1$ if their cLogP value, the predicted octanol-water partition coefficient, was <3.2, possibly owing to poor membrane permeability. Antrafenine has a reported LogP of 6.3 (Wishart et al., 2006), implying that it is a highly lipophilic drug and will likely cross the BBB effectively. This feature is attractive since poor BBB penetration is a problem associated with quinidine treatment of *KCNT1*-related DEEs. LogP values reported for quinidine in the literature range from 2.6-3.44 (Wishart et al., 2006), and subtherapeutic concentrations have previously been reported in over 50% of patients in a study cohort (Fitzgerald et al., 2019). Some of the other drugs identified here may also be limited by their ability to accumulate in the brain however. Nelfinavir mesylate for example, is a substrate for P-glycoproteins, which could limit its accumulation in the brain despite its high logP value of 4.68 (Wishart et al., 2006). Inhibition of P-glycoproteins in mice has been shown to increase concentration of nelfinavir in the brain 37-fold however (Choo et al., 2000), and its high potency may mean that this is less of a limiting factor than for quinidine. Regorafenib is also a substrate for P-glycoprotein (Abcg2 and Abcb1a/1b) efflux pumps. Inhibition of these pumps has previously been proposed as a strategy to increase accumulation to treat metastases in the brain (Kort et al., 2015). Other drugs described here have higher potency and better tolerability however and would avoid the need for this.

An important structural feature of antrafenine and regorafenib is the presence of trifluoromethyl groups which are also present in some of the active test compounds, and their potency may be owing to this. All of the test compounds and FDA-approved inhibitors identified also possess a central amine group, which is likely important for hydrogen bonding to pore-lining residues, and is another feature shared by Compound 31 (Griffin et al., 2021). Though the mechanism of action of Compound 31 has not

been probed, the presence of a trifluoromethyl group along with the reduced potency of the inhibitor with F346L $K_{Na}1.1$ point towards a pore-blocking mechanism.

Whilst direct comparison of these drugs with quinidine is not possible since the characterisation was carried out using the WT/Y796H construct, quinidine has been tested both against homomeric Y796H and WT $K_{Na}1.1$ channels and inhibits the mutant channel more potently. We know from functional characterisation in Chapter 4 that the heteromeric channel behaves with intermediate characteristics and it is therefore unlikely that quinidine would prove to be more a more potent inhibitor of this channel compared to homomeric Y796H.

Overall, this work has identified potential therapeutic drugs that could be repurposed for treating *KCNT1*-related DEEs, or possible pharmacophores that could be starting points for developing potent and selective novel inhibitors. It has also highlighted the usefulness of cryo-EM structures of membrane proteins for computer-aided drug discovery. Despite the human structure of $K_{Na}1.1$ not being established, high sequence conservation with the chicken $K_{Na}1.1$ structure enabled this to be utilised in place of human $K_{Na}1.1$. The high success in finding active inhibitors of $K_{Na}1.1$ validates the use of protein structures very close to the human structure as a good approach when a 3D structure is not available.

6 Identification of the Na^+-activation mechanisms of $K_{Na}1.1$

6.1 Introduction

Intracellular Na^+ is an essential determinant of WT $K_{Na}1.1$ channel opening, and in normal physiology $K_{Na}1.1$ activity is coupled to persistent inward Na^+ currents through re-opening voltage-gated Na^+ channels or NALCN channels that increase local Na^+ concentration above that of the bulk cytosol (Hage and Salkoff, 2012; Li, P. et al., 2019). Transient currents through AMPA receptors located in the vicinity of $K_{Na}1.1$ have also been implicated as a Na^+ source for the channel, as part of a negative-feedback loop (Nanou et al., 2008). The mechanisms by which Na^+ ions interact with the channel protein to lead to its activation are poorly understood.

Previous work identified residues located in the $K_{Na}1.1$ RCK2 domain as a putative Na^+ binding site based upon a Na^+ coordination motif, DXRXXH, in Na^+-activated GIRK channels. rD818 and rH823 in $K_{Na}1.1$ were highlighted through a combination of molecular simulations and homology modelling. Neutralisation or mutation to a positively-charged residue of rD818 and, to a lesser degree, hH823 diminished $K_{Na}1.1$ Na^+-activation when the channels were expressed in *Xenopus* ooctyes. There was residual channel activity for both mutants (Zhang et al., 2010). In $K_{Na}1.2$, mutation of the equivalent aspartate residue in the human channel, hD757, to arginine abolished Na^+-activation, with functional expression confirmed by activation by niflumic acid (Thomson et al., 2015).

The structures of the chicken $K_{Na}1.1$ channel in the closed and active, sodium bound conformations have since been resolved by cryo-EM (Hite et al., 2015; Hite and MacKinnon, 2017), and the model of activation proposed by Zhang *et al* is not corroborated by this. The loop containing the DXRXXH coordination motif including the equivalent aspartate residue, cD812, is conserved between the chicken and rat $K_{Na}1.1$ channel but remains static between the two conformations.

Inhibition of hyperactive $K_{Na}1.1$ channels is the current proposed treatment strategy for DEEs arising from *KCNT1* pathogenic variants, and the results in Chapter 5 suggest that current inhibitors act on the intracellular pore-vestibule. Sequence conservation around the pore-forming region and selectivity filter with other K^+ channels, such as hERG, ensures non-selectivity of pore-blocking compounds. The structures of the C-

termini of $K_{Na}1.1$ and closely-related $K_{Na}1.2$ are distinct from other members of the SLO K^+ channel family due to the channels being Na^+-activated. In place of the Ca^{2+} bowl on the RCK domains of $K_{Ca}1.1$ channels that coordinates their activation by intracellular Ca^{2+} ions for example, $K_{Na}1.1$ has an extended αQ' helix across the assembly interface between adjacent RCK domains (Hite et al., 2015). Understanding how $K_{Na}1.1$ is activated by intracellular Na^+, and the residues involved in its activation may provide alternative inhibitor binding sites; circumventing the pore-forming region and improving selectivity.

6.1.1 Chapter hypothesis and aims

Hypothesis: The RCK2 domain coordinates Na^+-activation of $K_{Na}1.1$, and the cryo-EM structure of the chicken $K_{Na}1.1$ channel can be used to predict the residues involved in activation of the human channel.

Aims:

- ***To identify the residues involved in Na^+-dependent activation of human $K_{Na}1.1$ using the cryo-EM structure of the chicken $K_{Na}1.1$ channel***
- ***To functionally characterise the residues identified using whole cell electrophysiology***
- ***To propose an updated model for the molecular mechanisms of Na^+-activation of $K_{Na}1.1$***

6.2 Results

6.2.1 The cryo-EM structures of the inactive and active $K_{Na}1.1$ channel highlighted possible residues involved in Na^+-activation

The structure of the chicken channel in Na^+-saturating conditions, termed the "active" conformation, compared to the "closed" structure shows twisting of a loop on the RCK2 domain placing an aspartate residue, cD857, in the vicinity of a pocket of two negatively-charged aspartate and glutamate residues, and polar threonine. This movement places cD857 approximately 3.8 Å from cD871, 4.3 Å from cE893, and near to cT895. A lysine residue, cK885, moves to be approximately 3.4 Å from the conserved aspartate residue previously identified by Zhang *et al* (2010), cD812 (Figure 6.1). This suggests that the proposed Na^+-binding residue still plays a role in Na^+-

activation, but perhaps in stabilising the active state. The residues identified are conserved in closely related Na^+-activated $hK_{Na}1.2$ (Figure 6.2).

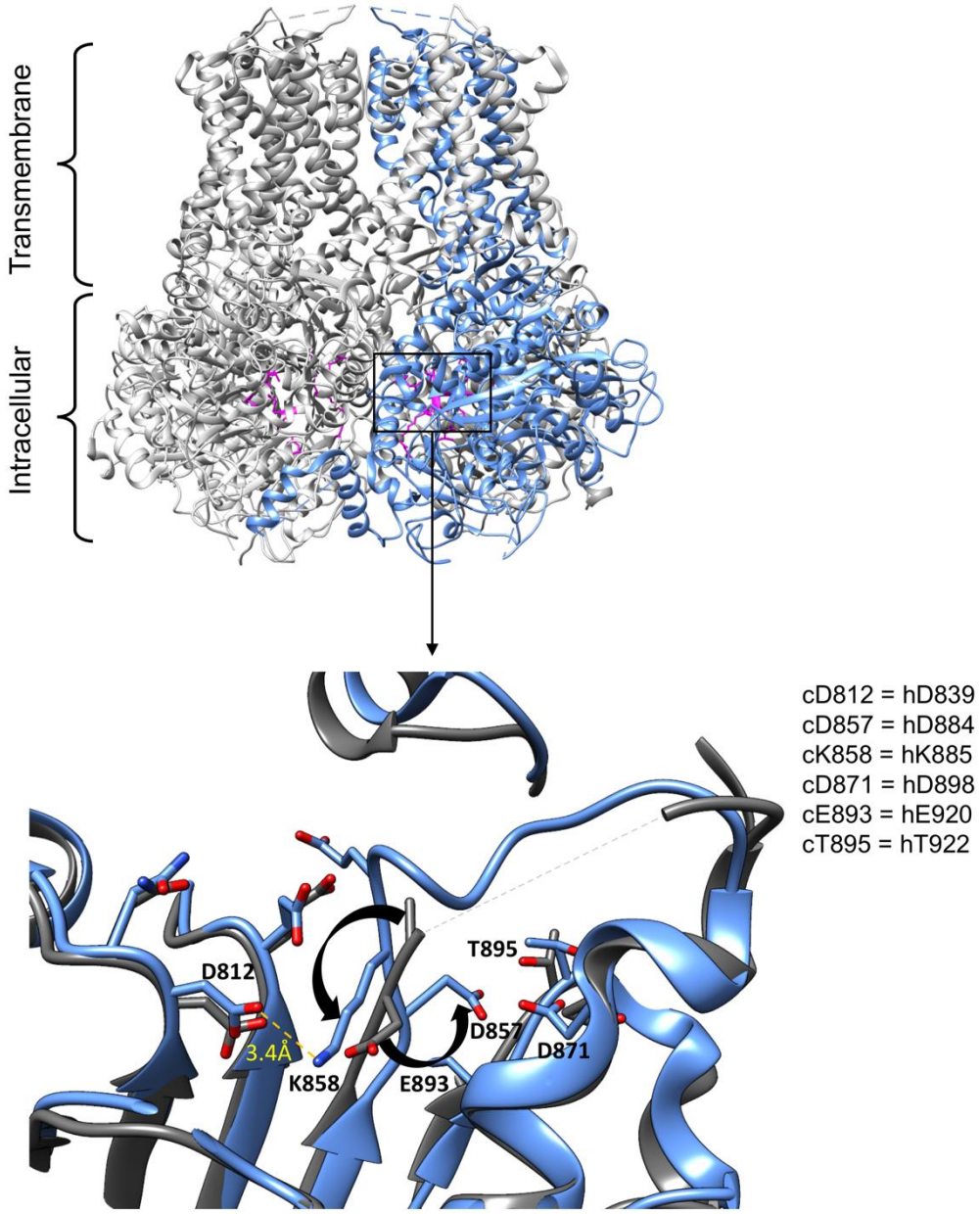

Figure 6.1: Overlaid inactive (grey) and active (blue) structures of chicken $K_{Na}1.1$ channel.
Key residues predicted to be involved in Na^+-activation of the channel indicated in magenta (top) with relevant distances between residues (bottom). The human equivalent of the identified residues indicated in the inset.

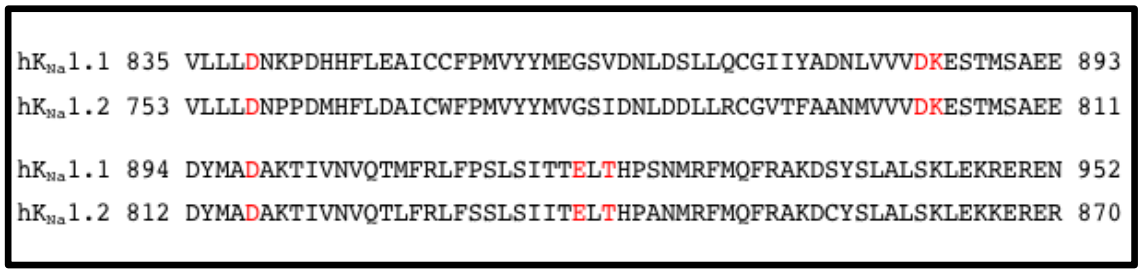

Figure 6.2: Sequence alignment of region of RCK2 domain predicted to coordinate Na^+-activation of $K_{Na}1.1$ with $K_{Na}1.2$.
Protein sequences of human $K_{Na}1.1$ (NM_020822.3; (Benson et al., 2017)) and human $K_{Na}1.2$ (NM_001287819.3; (Benson et al., 2017)) aligned using NCBI BLAST (Johnson et al., 2008). Residues of interest are highlighted in red, and amino acid numbers indicated to the left and right of each sequence.

6.2.2 Neutralisation of previously identified D839 results in loss of Na^+-activation

Guided by the cryo-EM structure of the chicken $K_{Na}1.1$ channel, a combination of mutagenesis and whole cell electrophysiology was used to validate the residues involved in Na^+-activation of the human $K_{Na}1.1$ channel. Firstly, the involvement of the aspartate residue previously identified as being important in Na^+-activation of the rat $K_{Na}1.1$ channel was confirmed by mutation of the equivalent residue on the human $K_{Na}1.1$ channel (D839) both to glutamate and alanine. The mutant constructs were overexpressed in CHO cells and characterised using whole cell electrophysiology. Substituting the aspartate with glutamate, to lengthen the sidechain without changing its charge, resulted in no change from WT $K_{Na}1.1$. The current-voltage relationships closely resembled the WT $K_{Na}1.1$ channel at 10 mM and 40 mM intracellular Na^+, and no currents were recorded in 0 mM intracellular Na^+, consistent with WT $K_{Na}1.1$ (Figure 6.3B). Consistent with the previous study which reported rD818A channels as being non-functional (Zhang, Z. et al., 2010), no currents could be recorded in the presence of 0, 10 and 40 mM intracellular Na^+ from D839A channels. Large, voltage-independent currents were yielded upon perfusion of 30 µM loxapine into the bath solution however, confirming its functional expression on the cell membrane (Figure 6.3B).

The anti-psychotic drug loxapine and anti-helminthic drug niclosamide are potent activators of WT $K_{Na}1.1$ with EC_{50} values of 4.4 µM and 2.9 µM respectively (Biton et al., 2012). Both drugs also remove voltage-dependence of $K_{Na}1.1$, resulting in linear current-voltage relationships and increased inward current at voltages negative to the reversal potential (Figure 6.3B). Initially, niclosamide was chosen to confirm functional expression of “inactive” mutant channels, since it is the more potent $K_{Na}1.1$ agonist.

CHO cells are believed to have little or no endogenous K^+ conductance (Gamper et al., 2005), but despite this a small current (58.96 ± 9.60 pA/pF at +10 mV, compared to 1.49 ±0.67 pA/pF at +10 mV in the absence of niclosamide, n=4 and 5 cells, respectively) could be recorded from non-transfected CHO cells when 30 µM niclosamide was perfused into the bath solution. Though this current is relatively small in comparison to the activated $K_{Na}1.1$ current (Figure 6.3B), this would be problematic for confirming functional expression of seemingly inactive $K_{Na}1.1$ channels. The identity of the K^+ current revealed by the activator is unknown, but preliminary experiments (not included) ruled out $K_{Na}1.1$, since the current was not inhibited by 10 µM bepridil. The reversal potential (-73.30 ± 0.85 mV, n=4) points to a K^+-selective channel, though no further efforts were made to characterise the current and its ion selectivity. Loxapine on the other hand did not activate this K^+ conductance in non-transfected CHO cells (Figure 6.3B). Although the two activators have similar potency, loxapine is more efficacious, evoking a higher maximal response when applied to CHO cells stably expressing $K_{Na}1.1$ (Biton et al., 2012). Loxapine is therefore more suitable for these experiments.

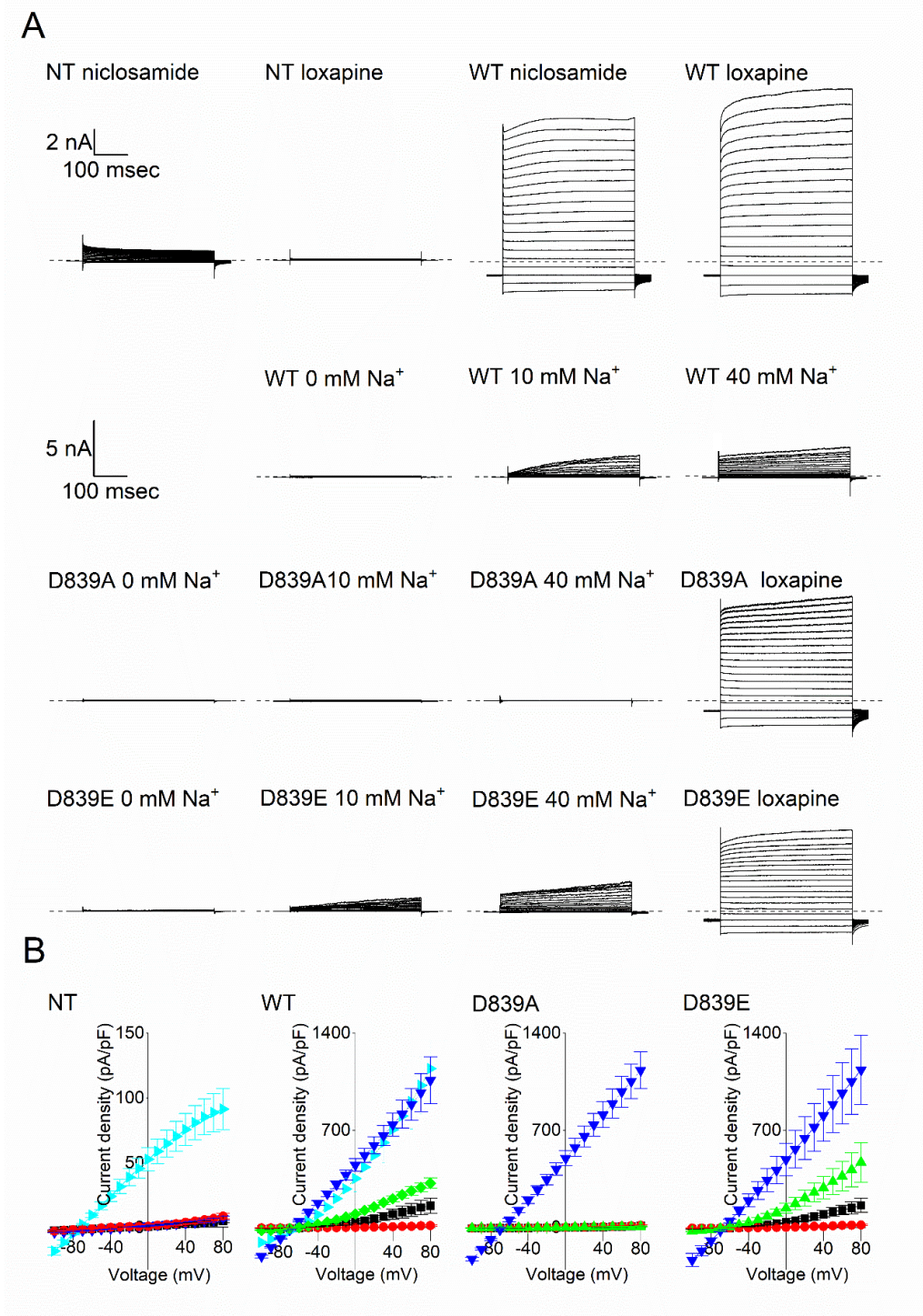

Figure 6.3: Mutational analysis of an aspartate residue previously predicted to coordinate Na^+-activation of $K_{Na}1.1$.
A) Representative traces for whole cell currents from Non-transfected CHO cells (NT) and CHO cells transfected with WT and mutant human $K_{Na}1.1$, as indicated in response to 400 msec steps from -100 to +80 mV in 10 mV increments, from a holding potential of -80 mV. n= 5 to 8 cells for each mutation. **B)** Mean (± s.e.m.) current-voltage relationships for NT cells, WT and mutant $K_{Na}1.1$ channels in the presence of 0 (red ●), 10 (black ■) and 40 (green ◆) mM intracellular Na^+, or 10 mM Na^+ and 30 µM loxapine (dark blue ▼). For NT CHO cells and WT $K_{Na}1.1$, 10 mM Na^+ and 30 µM niclosamide was also studied (cyan ▲).

6.2.3 Neutralisation of an aspartate residue locks the channel in the active conformation

Next, the human equivalent of the aspartate residue, cD857, that appears to move to the vicinity of the pocket of negatively-charged residues in the active channel structure was neutralised to alanine. This resulted in a GOF and loss of Na^+-dependence; large currents could be recorded from CHO cells expressing D884A channels in 0, 10 and 40 mM intracellular Na^+. No further activation was achieved by addition of 30 µM loxapine to the extracellular solution, though the activator still caused an apparent loss of voltage-dependence indicated by linear current-voltage relationships. Mutation of the same residue to valine, which has a slightly longer sidechain, had the same GOF effect (Figure 6.4B). Activation midpoints derived from conductance-voltage relationships fitted with a Boltzmann equation for D884A and D884V in 10 mM Na^+ were significantly hyperpolarised compared to WT $K_{Na}1.1$ (Table 6.1). When intracellular Na^+ was elevated to 40 mM however, the activation midpoints for D884A and D884V were not significantly different from WT $K_{Na}1.1$ currents recorded with the same Na^+ concentration. Whilst negligible current could be recorded for WT $K_{Na}1.1$ in 0 mM intracellular Na^+, notably the activation midpoints for D884A and D884V were not significantly different to the values for 10 and 40 mM Na^+.

Upon increasing the size of the sidechain substitution by mutating D884 to isoleucine and phenylalanine, or negatively-charged glutamate, the GOF effects were not seen. D884I had a similar activation midpoint to WT $K_{Na}1.1$ at both 10 mM and 40 mM intracellular Na^+, and current densities were similar to WT $K_{Na}1.1$. No discernible current could be recorded for D884E or D884F across all concentrations of intracellular Na^+ examined, despite their functional expression being confirmed by loxapine activation (Figure 6.3B).

The zero-voltage free-energy change coupled to channel opening was calculated from parameters derived from Boltzmann fits of G-V relationships. The value for WT $K_{Na}1.1$ channels is positive at 10 mM intracellular Na^+, but becomes negative when Na^+ is elevated to 40 mM. Both D884A and D884V have a negative ΔG_0 value across all concentrations of intracellular Na^+, indicating that the open state is more favourable. D884I on the other hand, has ΔG_0 values that are indistinguishable from WT $K_{Na}1.1$ both at 10 mM and 40 mM intracellular Na^+ (Table 6.1).

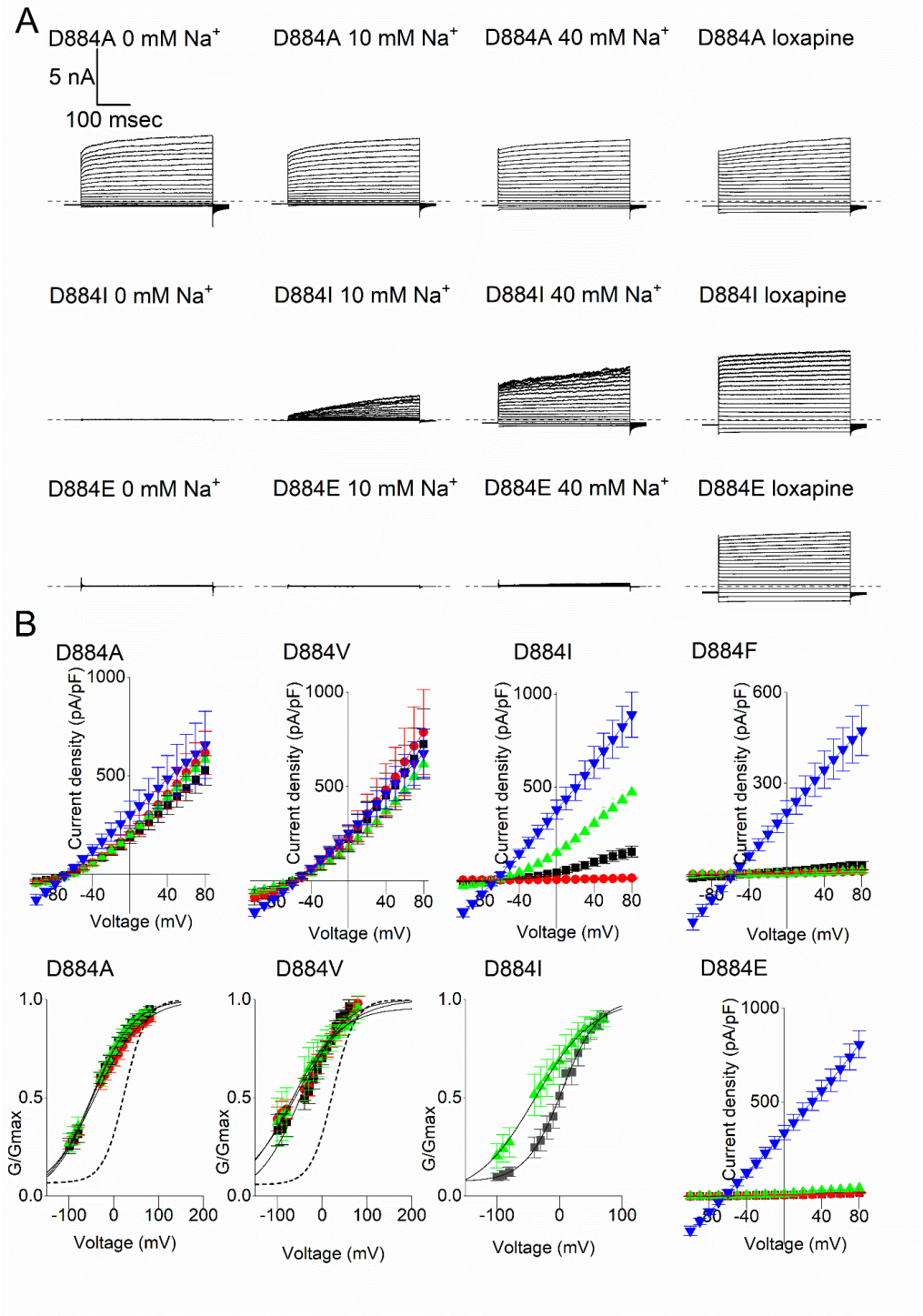

Figure 6.4: Probing the function of D884 in Na^+-activation of $K_{Na}1.1$.
A) Representative traces for whole cell currents in response to 400 msec steps from -100 to +80 mV in 10 mV increments, from a holding potential of -80 mV. n= 5 to 8 cells for each mutation. **B)** Mean (±s.e.m.) current-voltage relationships for mutations in the presence of 0 (red ●), 10 (black ■) and 40 (green ◆) mM intracellular Na^+, or 10 mM Na^+ and 30 µM loxapine (dark blue ▼). Mean (±s.e.m.) conductance-voltage relationships for D884A, D884V and D884I in the presence of 0 (red ●), 10 (black ■) and 40 (green ◆) mM intracellular Na^+. The G-V relationship for WT $K_{Na}1.1$ recorded with 10 mM intracellular Na^+ is indicated by a dotted line for comparison.

Table 6.1: Parameters derived from Boltzmann fit of WT and D884 mutant $K_{Na}1.1$ channels with 0, 10 and 40 mM intracellular Na^+.
Data are presented as mean ±SEM. $V_{0.5}$ is the half-maximal activation voltage, ***p*<0.005, ****p*<0.0005 compared to WT with 10 mM $[Na^+]i$. Independent one-way ANOVA with Tukey's post-hoc test. *z* is derived from the slope of the Boltzmann curve, which is RT/zF. ΔG_0 is the zero-voltage free energy for channel opening (n= 5 to 9 cells for each mutation).

Channel		$V_{0.5}$ (mV)		*z*	ΔG_0 (kcal/mol)
WT	**10 mM Na^+**	2.15 ±3.69		0.81 ±0.09	0.03 ±0.07
	40 mM Na^+	-46.63 ±8.06		0.75 ±0.14	-0.79 ±0.20
D884A	**0 mM Na^+**	-60.28 ±9.60		0.47 ±0.03	-0.63 ±0.09
	10 mM Na^+	-61.92 ±6.77	***	0.60 ±0.07	-0.80 ±0.07
	40 mM Na^+	-60.33 ±8.36		0.59 ±0.09	-0.77 ±0.05
D884V	**0 mM Na^+**	-46.99 ±11.08		0.51 ±0.10	-0.64 ±0.17
	10 mM Na^+	-61.08 ±3.23	**	0.59 ±0.06	-0.82 ±0.07
	40 mM Na^+	-60.86 ±4.89		0.57 ±0.08	-0.81 ±0.10
D884I	**10 mM Na^+**	0.23 ±6.78		0.92 ±0.02	0.00 ±0.12
	40 mM Na^+	-39.17 ±14.32		0.66 ±0.09	-0.64 ±0.23

6.2.4 Mutation of residues forming the "acidic pocket" results in loss of Na^+-activation

To examine whether the pocket of residues and positively-charged K885 play a role in the Na^+-activation of $K_{Na}1.1$, each residue was mutated to alanine in turn. In contrast to D884, negligible currents were yielded for all mutants studied with 0 mM or 10 mM intracellular Na^+. A small current could be recorded for K885A when intracellular Na^+ was elevated to 40 mM however, suggesting a decrease in Na^+-sensitivity of the channel. Functional expression of D898A, E920A and T922A was confirmed as previously by addition of 30 µM loxapine (Figure 6.5B).

T922 and D898 were also mutated to positively-charged lysine, as it was hypothesised that this may attract negatively-charged D884, forcing the channel into the "active" conformation, but no currents could be recorded for either mutant in 0, 10 and 40 mM Na^+. A double-mutant construct carrying both D898K and E920A was used to examine whether the effects seen were dependent on the number of negatively-charged or polar residues in the pocket, but again no currents could be recorded at any intracellular Na^+ concentration. When 30 µM loxapine was added to the extracellular solution, currents recorded from D898K, D898A and the double D898K/E920A mutant all show clear inward rectification at voltages positive to the reversal potential (Figure 6.5B).

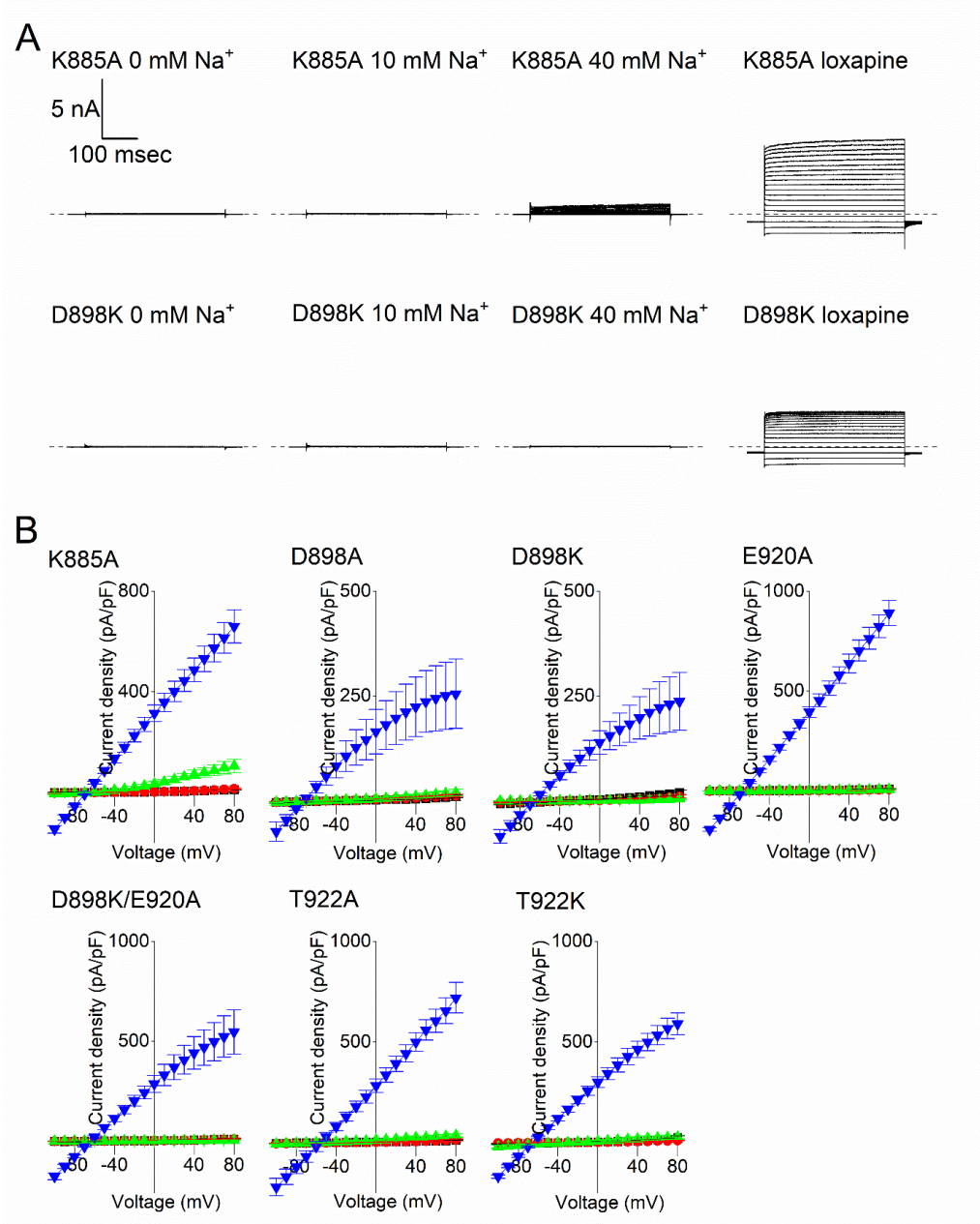

Figure 6.5: Mutational analysis of remaining residues predicted to be involved in Na^+-activation of $K_{Na}1.1$.
A) Representative traces for whole cell currents in response to 400 msec steps from -100 to +80 mV in 10 mV increments, from a holding potential of -80 mV. n= 5 to 8 cells for each mutation. **B)** Mean (±s.e.m.) current-voltage relationships for mutations in the presence of 0 (red ●), 10 (black ■) and 40 (green ◆) mM intracellular Na^+, or 10 mM Na^+ and 30 µM loxapine (dark blue ▼).

6.3 Discussion

6.3.1 D884 is unable to occupy the acidic pocket in the inactive conformation

In Na^+-free conditions, it is possible that D884 is unable to occupy the "acidic pocket" (Figure 6.6) of negatively-charged or polar residues; T922, E920 and D898. This leads to the "inactive" conformation as in the chicken cryo-EM structure being favoured, and addition of Na^+ ions may enable the aspartate residue to swing into the "active" conformation. Neutralisation of this aspartate residue to alanine or valine appears to result in the "active" conformation being favoured regardless of intracellular Na^+ concentration. This is indicated by the hyperpolarised activation midpoints that remain the same with 0, 10 and 40 mM Na^+, and negative ΔG_0 values. Increasing the length of the neutral sidechain substitution to phenylalanine may prevent the residue occupying the acidic pocket however. Likewise when the sidechain was lengthened to glutamate, which despite being negatively-charged, did not activate in response to any of the Na^+ concentrations tested. Neutralisation or reversing the charge of the negatively-charged residues forming the acidic pocket may prevent Na^+ ions occupying it, explaining why negligible currents were yielded at all Na^+ concentrations for these mutants.

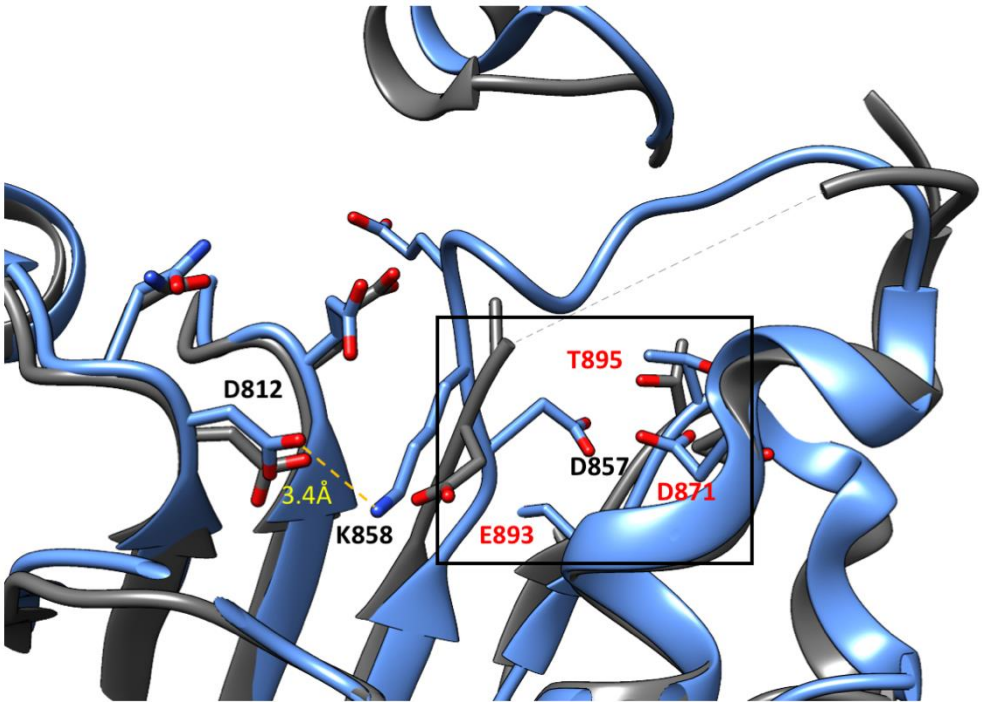

Figure 6.6: Residues involved in the "acidic pocket".
Overlaid inactive (grey) and active (blue) structures of chicken $K_{Na}1.1$ channel. Residues forming the acidic pocket indicated in red.

It is unclear whether the movements are related to the negative charges of the sidechains involved, with D884 being repelled from the acidic pocket until addition of Na^+ ions disrupts this, or whether it is related to the size of the sidechains. In support of the latter, mutation of D884 to neutral isoleucine, the sidechain of which is intermediate in length between valine and phenylalanine, yielded currents that were virtually identical to WT $K_{Na}1.1$ at all Na^+ concentrations tested. Isoleucine is similar in length to aspartate and may therefore be able to occupy the pocket normally. Indeed, mutations introducing positive and neutral charges into the acidic pocket, or the double D898K/E920A mutant which removed all negative charges, did not result in the same "locking" of the channel in the active conformation as D884A and D884V.

Although T922 is not negatively-charged, threonine residues have been reported as being an important determinant of Na^+ binding affinity in a number of Na^+-dependent transporter proteins. For example, a threonine is critical for coordination of Na^+ ions in the Na^+/di-carboxylate co-transporter, NaDC1. It was hypothesised that the residue does not directly interact with Na^+ via cation-dipole interactions, but rather is important for structure and positioning of other key residues in the binding site (Weerachayaphorn and Pajor, 2008). In others such as Na^+/aspartate symporter Gltph, glutamate transporter EAAT1 (excitatory amino acid transporter 1), BetP (Na^+-coupled betaine symporter) and LeuT (bacterial leucine transporter) the sidechain hydroxyl group or carbonyl backbone oxygens of threonine residues are critical for their Na^+ binding sites (Bastug et al., 2012; Khafizov et al., 2012; Yamashita et al., 2005). Mutation of T922 to alanine in $K_{Na}1.1$ may therefore affect Na^+ coordination in the acidic pocket either by preventing cation-dipole interactions or perhaps by affecting the ability of D898 and E920 to interact with Na^+ ions.

Mutation of one of the residues in the acidic pocket, D898, to either lysine or alanine resulted in clear inward rectification when currents were activated by loxapine. It is unclear how this may arise. The structure of the chicken $K_{Na}1.1$ channel highlighted a "funnel" through the gating ring that narrows as it approaches the pore-forming region, with a largely electronegative surface due to being lined by aspartate and glutamate residues (Hite et al., 2015). A similar electronegative funnel structure is present in $K_{Ca}1.1$ channels (Tao et al., 2017), and is accountable for the unusually high K^+ conductance of SLO channels; mutagenesis has shown that removal of the gating ring of $K_{Ca}1.1$ attenuates K^+ conductance (Budelli et al., 2013). D898 is positioned on a highly negatively-charged loop lining the inner surface of the $K_{Na}1.1$ gating ring and so

may contribute to the electronegative funnel. The negatively-charged residues act to attract K^+ ions and disruption of this by mutation of D898 may reduce K^+ conduction, leading to the slight inward rectification observed.

A number of factors may explain the selectivity of this proposed binding site for Na^+ over other ion species. Na^+ is a smaller ion compared to, for example K^+, and has a higher dehydration energy due to this. Other factors such as positioning and the number of binding residues within the site may also contribute. In BK_{Ca} channels, which possess Ca^{2+}-selective sites within the RCK domains, the Ca^{2+} selectivity is attributed to ionic radius. Other divalent cations with similar radii to Ca^{2+} are able to activate the channel, and smaller or larger ions have weaker activation efficiencies (Zhou et al., 2012).

It is worth noting that the residues identified here are in close vicinity to (AD)SHE-causing variants M896I and R928C, which face against the neighbouring subunit. These two variants in particular when characterised in Chapter 3 appeared to slow a usually undetectable Na^+-dependent time constant in $K_{Na}1.1$ currents when characterised in CHO cells using whole cell electrophysiology, introducing a “fast” tau value when the currents are fit with two exponential functions. Whilst it is unclear to what extent this affects the GOF phenotype, it is possible that this is due to the location of these residues on the channel structure.

6.3.2 The previously identified aspartate residue stabilises the active, Na^+-bound state

Consistent with our proposed model for Na^+-activation, mutation of both D839 and K885 to alanine had deleterious effects on activation of the channel, greatly reducing channel activation at the Na^+ concentrations tested. In the “active” Na^+-bound conformation of the chicken cryo-EM structure, the equivalent residue to K885 moves to 3.4 Å from the equivalent to D839, placing its cationic ammonium group within the acceptable distance (<4 Å) for salt bridge formation with the anionic carboxylate group of aspartate. Neutralisation of either residue would prevent formation of this salt bridge, thus reducing stability of the active conformation. Lengthening of the aspartate residue to glutamate, which retains the carboxylate group, seemingly had no effect since formation of a salt bridge would still be possible. The putative Na^+-binding residue identified previously is likely still involved in Na^+-activation of $K_{Na}1.1$ but has a more indirect role (Zhang, Z. et al., 2010).

Whilst no cryo-EM structure is available for $K_{Na}1.2$, the channel is highly homologous with $K_{Na}1.1$. The two channels share 78% sequence identity and most deviations are in the N-termini. All of the residues identified as having some involvement in our model of $K_{Na}1.1$ Na^+-activation are conserved in $K_{Na}1.2$ (Figure 6.2) so it is possible that the Na^+-activation mechanism of this channel is similar, with the conserved aspartate residue D757 identified (Thomson et al., 2015) again functioning to stabilise the active state.

6.3.3 The acidic pocket may provide a target for more selective inhibitors of $K_{Na}1.1$ to treat KCNT1-related DEEs

The results further implicate the RCK2 domain of $K_{Na}1.1$ in coupling Na^+-activation to channel opening. RCK1 and RCK2 domains of adjacent subunits in the $K_{Na}1.1$ channel tetramer interact at an assembly interface to form the octameric "gating ring" of $K_{Na}1.1$, which expands following Na^+-activation (Hite et al., 2015; Hite and MacKinnon, 2017). Results from Chapter 3 indicated that $K_{Na}1.1$ may possess a similar gating mechanism to MthK and other K^+ channels gated at the selectivity filter, which have an allosterically-coupled activation gate (Kopec et al., 2019). Interaction of Na^+ ions with the channel protein likely modulates the activation gate rather than the selectivity filter gate, and Na^+-induced conformational changes enable subsequent activation of the selectivity filter gate to enable K^+ conduction. Although the results do not pinpoint the exact locus for a "binding site" for Na^+ ions, they provide further insight into the sequence of events and possible conformational changes induced by Na^+-binding to the channel protein. Na^+ ions are too small to be resolved by cryo-EM but in future, MD simulations could be employed to gain further insight into the mechanisms of Na^+-induced activation. Ideally Na^+-sensitivity would be examined for each of the mutants using inside-out macropatches excised from *Xenopus* oocytes to obtain Na^+-response relationships. Rundown in excised-patch experiments is a common problem when studying $K_{Na}1.1$ channels however, and channels exhibit block by high intracellular concentrations of Na^+ which may also limit this.

In Chapter 3 and 4, removal of intracellular Na^+ was found to diminish current amplitude of both homomeric and heteromeric DEE-causing variant $K_{Na}1.1$ channels and shift the activation midpoints towards that of WT $K_{Na}1.1$. Previous work has also shown that EIMFS-causing variants G288S, M516V, E893K and R950Q activate with smaller current amplitudes in the absence of intracellular Na^+ (Rizzo et al., 2016; Dilena et al., 2018). It is therefore possible that an antagonist that impedes Na^+-

activation of variant channels could also diminish current amplitude and reduce hyperexcitability. The pocket of negatively-charged residues identified here may provide a novel target for inhibitors of the channel which have improved selectivity, by avoiding inhibition of the highly conserved pore-forming region.

7 General discussion and future perspectives

7.1 Functional characterisation of DEE-causing pathogenic variants

The work in this thesis has provided further information pertaining to the gating mechanisms of the WT $K_{Na}1.1$ channel, and how these are disrupted by DEE-causing pathogenic variants located in different regions of the channel structure and associated with different phenotypes. The effects of heteromeric co-assembly have been explored using two different methods. Results obtained from characterising both concatemeric and co-expressed heteromers highlighted that heteromeric WT and mutant $K_{Na}1.1$ channels behave distinctly to homomeric channels, and that previous characterisation of homomeric mutant channels should be interpreted with caution.

7.1.1 Mechanisms of $K_{Na}1.1$ channel gating and how DEE-causing variants disrupt this

The results in Chapter 3 provide compelling evidence for $K_{Na}1.1$ possessing a Na^+-dependent activation gate that is allosterically coupled to a selectivity filter gate. Na^+ ions appear to lower the energetic barrier for channel activation; no WT $K_{Na}1.1$ current was seen in the absence of intracellular Na^+, and smaller currents with rightward-shifted activation curves and more positive ΔG_0 values were yielded from GOF mutant channels under the same conditions. Additionally, increasing intracellular Na^+ to 40 mM in Chapter 6 yielded WT $K_{Na}1.1$ currents with hyperpolarised activation curves and a more negative ΔG_0 value compared to currents recorded in 10 mM intracellular Na^+. The results are in agreement with previous studies ruling out a canonical S6 helix bundle-crossing mechanism for $K_{Na}1.1$ and $K_{Na}1.2$ channel gating (Garg et al., 2013; Giese et al., 2017) and the cryo-EM structure of the channel which appears physically wide enough to conduct K^+ ions in the inactive conformation (Hite and MacKinnon, 2017). Using mutagenesis of the human $K_{Na}1.1$ channel an updated mechanism has been proposed for Na^+-activation of $K_{Na}1.1$ that better reflects the structural changes between the inactive and active cryo-EM structures of the chicken channel. The results in Chapter 6 implicate residues located within the RCK2 domain, which forms the gating ring of $K_{Na}1.1$ with an RCK1 domain in an adjacent subunit (Hite et al., 2015; Hite and MacKinnon, 2017), in Na^+-activation. Since Na^+ ions are too small to be

resolved by cryo-EM however, MD simulations would be useful to provide further insight into the exact locus for Na^+-binding in future.

Mutation of the conserved threonine residue that is critical in the selectivity filter gating of a number of other K^+ channels (Schewe et al., 2016; Labro et al., 2018; Kopec et al., 2019; Nematian-Ardestani et al., 2020) disrupted rectification and affected permeation and voltage-sensitivity, whilst retaining Na^+-sensitivity. This is further evidence for Na^+-binding modulating the activation gate, not the selectivity filter gate. The activation gate subsequently allosterically leads to widening of the selectivity filter gate. The Na^+ and voltage-independent time constants observed for both WT and mutant $K_{Na}1.1$ channel activation likely represent the time course of the selectivity filter gate widening to enable K^+ flux, following Na^+ and voltage-activation. This is a shared feature with other selectivity filter-gated K2P channels (Schewe et al., 2016). Further experiments would be required to confirm that the voltage-sensing mechanism of $K_{Na}1.1$ is similar to these voltage-sensitive selectivity filter gated channels that also lack a VSD. If the voltage-sensitivity of $K_{Na}1.1$ is indeed coupled to the electrochemical gradient, a shift in the activation midpoint for conductance-voltage curves would be observed with changes in reversal potential, achieved by altering the extracellular or intracellular K^+ concentration (Schewe et al., 2016).

$K_{Na}1.1$ channels are activated both by intracellular Na^+ and voltage but lack the canonical VSD that is found in other voltage-gated K^+ channels. Understanding the interactions of domains underlying WT $K_{Na}1.1$ gating is useful for determining the effects of pathogenic variants on $K_{Na}1.1$ function, and in developing new treatment modalities. The Horrigan-Aldrich model of gating for Ca^{2+} and voltage-activated $K_{Ca}1.1$ channels involves three equilibrium constants, and three allosteric factors that determine probability of channel opening (Horrigan and Aldrich, 2002); shown in Figure 7.1. The closed-open transition of the channel (C-O) is determined by the equilibrium constant *L,* which is weakly voltage-dependent and describes the closed to open transition in the absence of Ca^{2+}, and no active VSD. This module allosterically interacts with the Ca^{2+} unbound-bound transition by allosteric factor *C.* The equilibrium constant for the Ca^{2+} unbound-bound transition ($X\text{-}X_{Ca}^{2+}$) for each of the four Ca^{2+} binding sites, with inactive VSDs, is *K.* The VSD resting-active transition is allosterically coupled to the $X\text{-}X_{Ca}^{2+}$ transition by allosteric factor *E,* and to the C-O transition by allosteric factor *D*. Activation of the VSD is determined by equilibrium potential *J* when the channel is closed and in the Ca^{2+}-unbound state (Horrigan and Aldrich, 2002). The

model assumes that there are four identical Ca^{2+} binding sites, and four identical voltage sensors in the tetrameric channel assembly.

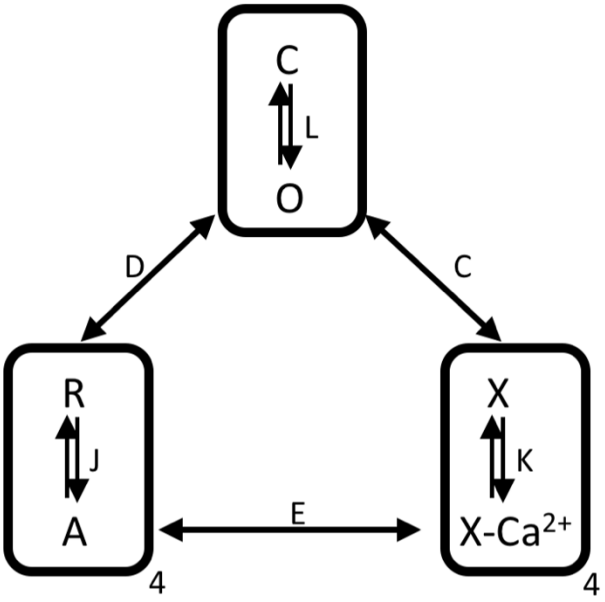

Figure 7.1: The Horrigan-Aldrich model of $K_{Ca}1.1$ channel gating.
Allosteric factors *C, D* and *E* describe the interactions between channel opening (C-O), Ca^{2+} binding (X-X_{Ca}^{2+}), and activation of the voltage sensor (R-A). The equilibrium constants for each process are *L* (C-O), *K* (X-X_{Ca}^{2+}) and *J* (R-A) (Horrigan and Aldrich, 2002).

$K_{Na}1.1$ channels lack the VSD that $K_{Ca}1.1$ channels possess; therefore a gating model that omits the R-A transition, along with its allosteric interactions, would better describe activation of $K_{Na}1.1$. The behaviour of each of the DEE-causing mutant channels in the absence of intracellular Na^+ suggests that the *L* value, the equilibrium constant for the open-closed transition in the absence of Na^+, underlies the voltage-dependent gating in $K_{Na}1.1$ and is higher in homomeric mutant channels. The increase is to a lesser degree in heteromeric mutant and WT $K_{Na}1.1$ channels. The amino acid substitutions located across the channel structure result in GOF by destabilising the inactive unliganded channel conformation. The P_o-voltage curve for channels would be shifted leftward in the presence of increasing concentrations of Na^+ due to the allosteric interaction (described by *C*) between *L* and *K* (the equilibrium constant for the Na^+ unbound to bound transition). This provides an explanation for the rightward shift in activation curves in the absence of intracellular Na^+. A higher value of *L* corresponds with a higher P_o value at a given voltage, and so the P_o-voltage curve would be more rightward to begin with in WT channels, that have a lower *L* value. For heteromeric

channels, which likely have an intermediate *L* value due to the introduction of WT $K_{Na}1.1$ subunits, the leftward shift in the P_o-voltage relationship would be to less negative voltages. Individual parameters of the gating model could be defined experimentally in future by measuring gating and ionic currents at the extremes of Na^+-activation, to isolate individual components (Latorre et al., 2017). $K_{Na}1.1$ channels show considerable, and as of yet unexplained, rundown in single channel experiments both in the literature and in preliminary experiments attempted for this thesis however, possibly due to absence of important intracellular components. This makes obtaining global data to determine parameters of a gating model difficult, and would need to be optimised in future.

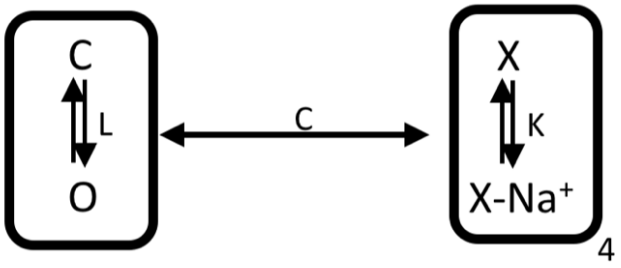

Figure 7.2: Proposed model for $K_{Na}1.1$ channel gating.
Allosteric factor *C* describes the interactions between channel opening (C-O) and Na^+-binding ($X\text{-}X_{Na}^+$). The equilibrium constants for each process are *L* (C-O) and *K* ($X\text{-}X_{Ca}^{2+}$).

In Chapter 3, some of the DEE-causing pathogenic variants were found to have effects on the selectivity filter gate, additionally to their destabilising effects on the activation gate. (AD)SHE-causing variant, Y796H, was found to decrease the time constant for channel activation, indicative of effects on the selectivity filter gate. A faster time constant may arise from an increase in either the opening or closing rate constant of the channel, but an increase in $P_{o,\,max}$ has previously been reported for this particular *KCNT1* pathogenic variant (Tang et al., 2016). Similarly, (AD)SHE-causing variant, R398Q, appeared to slow the time constant for channel activation, though this could not be quantified, and a decrease in $P_{o,max}$ was reported previously (Tang et al., 2016). An increase in $P_{o,\,max}$ as a result of an increase in the opening rate constant would result in a decrease in the time constant of activation; it is therefore speculated that it is the opening rate constant that is increased, since activation of mutant channels is shifted in the hyperpolarising direction. Values for opening and closing rate constants could be determined experimentally in future using mean-variance analysis to simultaneously measure $P_{o,\,max}$ and $\boldsymbol{\tau}$. This would involve repeatedly pulsing to a strongly positive voltage to estimate P_o from the mean-variance plots; as has been done previously for WT $K_{Na}1.1$ to estimate P_o as a function of intracellular Na^+

concentration (Horrigan and Aldrich, 2002; Latorre et al., 2017). The structural changes associated with DEE-causing pathogenic variants that lead to their effects on the activation gate, and for some variants the selectivity filter gate, are unclear at present.

7.1.2 Which method of studying heteromeric channel assembly is the most physiologically relevant?

One aim of this thesis was to create a model for studying behaviour of channels reflective of heterozygous patients carrying only one mutant DEE-causing allele, who make up the majority of patients. Concatemeric channels were created in Chapter 4 by joining the C-terminus of one $K_{Na}1.1$ subunit to the N-terminus of another, and a T2A self-cleaving peptide sequence introduced between the two subunits resolved problems arising from constraint of the N-terminus. The heteromeric concatemers yielded currents that were an intermediate between WT and mutant homomeric $K_{Na}1.1$ channels, that had distinct activation kinetics. Due to the self-cleaving peptide sequence, following translation separate peptides would be trafficked to the membrane and randomly co-assemble. Cells would express exactly half of each subunit type however, which is reflective of the genetic status of heterozygous patients.

Alongside the concatemers, co-expression with WT $K_{Na}1.1$ subunits was used to study the full range of (AD)SHE- and EIMFS-causing mutants in this study as heteromers in Chapter 3. Co-expression yields a more physiologically relevant population of channels. These heteromers, like concatemers, behaved distinctly from homomeric mutant and WT $K_{Na}1.1$ channels. Nevertheless, studying co-expressed subunits is not without limitations. The resulting population of channels is likely a mixture of heteromeric mutant channels, and homomeric WT and mutant $K_{Na}1.1$ channels. All resultant channels will thus have their own activation kinetics. Additionally, we do not know how many plasmids are taken up by cells when transfecting, and whether this is truly half of each subunit.

Both methods of studying heteromeric assemblies produced channels with current amplitudes that were an intermediate between homomeric WT and mutant $K_{Na}1.1$ channels, consistent with studies of G288S and M516V when co-expressed with WT $K_{Na}1.1$ subunits (Rizzo et al., 2016). Though no further functional characterisation was carried out in the aforementioned study, here it has been shown that the heteromeric assemblies for all the mutants display a shift in their activation threshold towards more depolarised potentials upon introduction of WT subunits. This is in accordance with two

other EIMFS-causing mutants, R950Q and E893K, which have previously been co-expressed with WT $K_{Na}1.1$ subunits (Dilena et al., 2018). The shift was more marked for Y796H co-expressed with WT in comparison to the YH/WT and WT/YH concatemers however, with approximately 30 mV difference between the two. This can likely be explained by contribution of WT $K_{Na}1.1$ homomeric channels present in the population of channels produced by co-expression; which cannot be controlled for by this method.

The work in this thesis was solely focused on characterising DEE-causing pathogenic variants of *KCNT1*, and demonstrates that heteromeric WT and mutant $K_{Na}1.1$ assemblies do not behave the same as homomeric mutant channels. $K_{Na}1.1$ channels are co-localised with $K_{Na}1.2$ in certain brain regions in rodents however (Chen et al., 2009; Rizzi et al., 2016; Bhattacharjee et al., 2002), and functional studies have demonstrated that both rat and human subunits co-assemble and produce currents with distinct properties to either homomeric channel alone. Heteromeric $K_{Na}1.1$ and $K_{Na}1.2$ channels have a distinct response to PKC modulation compared to their homomeric counterparts (Chen et al., 2009) and yield larger currents than those recorded from homomeric $K_{Na}1.1$ or $K_{Na}1.2$ channels (Chen et al., 2009; Mao et al., 2020). It would therefore be of clinical relevance to functionally characterise behaviour and inhibition of mutant $K_{Na}1.1$ channels carrying EIMFS and (AD)SHE-causing *KCNT1* variants in heteromeric co-assembly with WT $K_{Na}1.2$ subunits. Similarly, it has previously been suggested that heteromeric $K_{Na}1.1$ and $K_{Ca}1.1$ channels may occur, though this has not been explored in depth (Joiner et al., 1998).

7.2 Pharmacological modulation of $K_{Na}1.1$

Targeting hyperactive $K_{Na}1.1$ channels to treat *KCNT1*-associated DEEs currently poses a challenge due in part to dose-limiting side effects arising from non-selectivity, poor BBB penetration and low potency of existing inhibitors. A number of potent inhibitors of WT and mutant $K_{Na}1.1$ channels identified in Chapter 5 show clear therapeutic potential for *KCNT1*-associated epilepsies. The work in this thesis is an example of how cryo-EM structures of membrane proteins can be utilised for structure-based drug discovery, and there is large scope for future experiments relating to these compounds, all of which are more potent than quinidine, and potential new compounds.

An important next step for the FDA-approved compounds will be to characterise their potential effects on cultured primary neurons or iPSC-derived neurons harbouring DEE-causing *KCNT1* variants, such as the commercially available P924L iPSC-derived neurons (Quraishi et al., 2019). This would provide a good indication of the efficacy of the drugs for diminishing aberrant neuronal firing. Similarly, more mouse models of *KCNT1*-related epilepsies are being described in the literature (Shore et al., 2020; Quraishi et al., 2020), and would be useful for determining the effectiveness of the FDA-approved compounds for reducing hyperexcitability *in vivo.* The same experiments could be carried out for the novel small molecule inhibitors identified, but further development of the FDA-approved drugs is clearly advantageous due to reduced time and costs associated with repurposing of existing drugs (Shore et al., 2020; Quraishi et al., 2020). VU0606170, a recently described inhibitor was found to reduce the firing rate of hyperexcitable cultured cortical rat neurons (Roessler et al., 2021), and Compound 31 was found to reduce seizure frequency and interictal spikes in a mouse model harbouring the equivalent of an EIMFS-causing pathogenic variant P924L, mP905L (Griffin et al., 2021). Both of these studies are evidence for $K_{Na}1.1$ inhibition being an effective strategy to reduce hyperexcitability.

The high success rate achieved from *in silico* docking of libraries of compounds and manual patch clamp experiments is very promising, but there were large numbers of compound hits, both small molecules and approved drugs, that did not make it to the patch clamp screening stage. In future, higher throughput techniques would be useful to more efficiently screen larger compound libraries. Automated planar electrophysiology or fluorescence-based thallium or rubidium-flux assays would be well-suited for this application, and the WT/Y796H concatemer stable HEK293 cell line characterised in Chapter 4 can be utilised for this work. Identification of common structural or other features of active compounds in this thesis may also provide exclusion criteria and enable more stringent “shortlisting” of hits identified from *in silico* screens in future. For example, the observation that no compounds with a cLogP value of <3.2 were active, perhaps due to poor membrane permeability, or the importance of trifluoromethyl groups in potency of small molecule and approved inhibitors. FDA-approved drugs could be shortlisted based on known CNS activity, which would suggest BBB penetration. Additionally, the small molecule inhibitors identified may provide useful starting points for development of more potent or selective inhibitors.

7.2.1 Potential new inhibitor modalities

Although the work in this thesis was restricted to inhibition of the intracellular pore vestibule, advances in our understanding of the underlying mechanisms of GOF pathogenic variants may enable development of alternative drug modalities. For example, in light of the results in Chapter 3, the Na^+-binding region in the RCK2 domain may be a promising target for screening compounds in future. As discussed previously, removal of intracellular Na^+ in Chapter 3 both reduced current amplitude and shifted activation curves in the depolarising direction for heteromeric and homomeric mutant $K_{Na}1.1$ channels. Though further work may be required to pinpoint the exact locus for Na^+-binding to $K_{Na}1.1$, the residues identified in Chapter 6 may provide a target region for Na^+-binding site antagonists. Similarly, whether other regions of the channel protein can be targeted has yet to be studied. For example, the NAD^+ binding domain, where NAD^+ binds and potentiates WT $K_{Na}1.1$ activity (Tamsett et al., 2009), could be a possible target for modulatory drugs.

As well as providing insight into the mechanism of action of quinidine and bepridil, the results in this thesis suggest that Compound 31, a recently identified small molecule inhibitor, may also inhibit the intracellular pore vestibule of $K_{Na}1.1$ (Griffin et al., 2021). The compound possesses trifluoromethyl groups which are found to be important for its potency, and is a common feature with FDA-approved compounds antrafenine and regorafenib and small molecule inhibitors BC12 and 14. Additionally, the compound had particularly reduced potency with F346L compared to other DEE-causing variants (Griffin et al., 2021), which is a DEE-causing amino acid substitution of the same pore-lining residue found to be important for inhibition of $K_{Na}1.1$ by quinidine, bepridil and all of the small molecule inhibitors described in Chapter 5. The mechanism of action of another recently identified compound, VU0606170 is not known however, and this inhibitor is reportedly selective for $K_{Na}1.1$ channels over $K_{Na}1.2$, $K_{Ca}1.1$, GIRK1/2, $K_v2.1$, TREK1, $Ca_v3.2$ and $Na_v1.7$ (Spitznagel et al., 2020). Thus, it is possible that this molecule targets another domain of the channel that is less conserved with other ion channels.

$K_{Na}1.1$ has a number of cytoplasmic modulatory binding partners that could potentially be targeted therapeutically in future. For example, SCYL1 may potentiate $K_{Na}1.1$ channels in brain regions where the two proteins have overlapping expression (Niu et al., 2020), and FMRP and TMEM16C interact with the C-terminus of $K_{Na}1.1$ to potentiate channel activity (Zhang, Y. et al., 2012; Huang et al., 2013). Inhibiting the

physical or functional interaction of these proteins with the $K_{Na}1.1$ C-terminus may ameliorate hyperactive $K_{Na}1.1$ channel activity. Interaction with other binding proteins could perhaps be promoted to reduce $K_{Na}1.1$ activity. For example, Phactr1 is hypothesised to suppress rat $K_{Na}1.1$ channel activity via protein phosphatase 1-mediated (PP1) dephosphorylation of the channel (Ali et al., 2020). Suppression of $K_{Na}1.1$ by Phactr1 is disrupted by the introduction of two EIMFS-causing *KCNT1* pathogenic variants (Fleming et al., 2016).

7.3 Conclusion

To summarise, this body of work has provided evidence for a selectivity filter gating mechanism for the epilepsy-associated $K_{Na}1.1$ channel, allosterically coupled to an activation gate that is disrupted by DEE-causing amino acid substitutions located across the protein structure. Further information has been gained on the kinetic properties of heteromeric variant and WT $K_{Na}1.1$ channels. A model for Na^+-activation of human WT $K_{Na}1.1$ channels has been proposed that agrees with the cryo-EM structure of the chicken channel, and is supported by mutagenesis. The mechanism of action of existing inhibitors of $K_{Na}1.1$ has been elucidated, and used to guide identification of a number of novel and FDA-approved inhibitors with therapeutic potential that inhibit mutant and WT $K_{Na}1.1$ channels with low- and sub-micromolar potency. This work, and development of a cell line stably expressing a heteromeric (AD)SHE-causing variant and WT $K_{Na}1.1$ construct, has provided a solid foundation for further development of selective and potent inhibitors of $K_{Na}1.1$. Functional characterisation of DEE-causing *KCNT1* pathogenic variants in the absence of Na^+ alongside the proposed model for Na^+-activation has highlighted potential for the development of more selective inhibitors that circumvent the pore-forming region.

List of references

Abdelnour, E., Gallentine, W., McDonald, M., Sachdev, M., Jiang, Y.H. and Mikati, M.A. 2018. Does age affect response to quinidine in patients with KCNT1 mutations? Report of three new cases and review of the literature. *Seizure.* **55**, pp.1-3.

Alagoz, M., Kherad, N., Bozkurt, S. and Yuksel, A. 2020. New mutations in KCNT2 gene causing early infantile epileptic encephalopathy type 57: Case study and literature review. *Acta Biochim Pol.* **67**(3), pp.431-434.

Ali, S.R., Malone, T.J., Zhang, Y., Prechova, M. and Kaczmarek, L.K. 2020. Phactr1 regulates Slack (KCNT1) channels via protein phosphatase 1 (PP1). *FASEB J.* **34**(1), pp.1591-1601.

Alsaleem, M., Carrion, V., Weinstock, A. and Chandrasekharan, P. 2019. Infantile refractory seizures due to de novo KCNT 1 mutation. *BMJ Case Rep.* **12**(10).

Ambrosino, P., Soldovieri, M.V., Bast, T., Turnpenny, P.D., Uhrig, S., Biskup, S., Docker, M., Fleck, T., Mosca, I., Manocchio, L., Iraci, N., Taglialatela, M. and Lemke, J.R. 2018. De novo gain-of-function variants in KCNT2 as a novel cause of developmental and epileptic encephalopathy. *Ann Neurol.* **83**(6), pp.1198-1204.

Anson, B.D., Weaver, J.G., Ackerman, M.J., Akinsete, O., Henry, K., January, C.T. and Badley, A.D. 2005. Blockade of HERG channels by HIV protease inhibitors. *Lancet.* **365**(9460), pp.682-686.

Antzelevitch, C. and Patocskai, B. 2016. Brugada Syndrome: Clinical, Genetic, Molecular, Cellular, and Ionic Aspects. *Curr Probl Cardiol.* **41**(1), pp.7-57.

Aryal, P., Abd-Wahab, F., Bucci, G., Sansom, M.S. and Tucker, S.J. 2014. A hydrophobic barrier deep within the inner pore of the TWIK-1 K2P potassium channel. *Nat Commun.* **5**, p4377.

Aryal, P., Sansom, M.S. and Tucker, S.J. 2015. Hydrophobic gating in ion channels. *J Mol Biol.* **427**(1), pp.121-130.

Barcia, G., Fleming, M.R., Deligniere, A., Gazula, V.R., Brown, M.R., Langouet, M., Chen, H., Kronengold, J., Abhyankar, A., Cilio, R., Nitschke, P., Kaminska, A., Boddaert, N., Casanova, J.L., Desguerre, I., Munnich, A., Dulac, O., Kaczmarek, L.K., Colleaux, L. and Nabbout, R. 2012. De novo gain-of-function KCNT1 channel mutations cause malignant migrating partial seizures of infancy. *Nat Genet.* **44**(11), pp.1255-1259.

Bastug, T., Heinzelmann, G., Kuyucak, S., Salim, M., Vandenberg, R.J. and Ryan, R.M. 2012. Position of the third Na+ site in the aspartate transporter GltPh and the human glutamate transporter, EAAT1. *PLoS One.* **7**(3), pe33058.

Bearden, D., Strong, A., Ehnot, J., DiGiovine, M., Dlugos, D. and Goldberg, E.M. 2014. Targeted treatment of migrating partial seizures of infancy with quinidine. *Ann Neurol.* **76**(3), pp.457-461.

Beckstein, O. and Sansom, M.S. 2006. A hydrophobic gate in an ion channel: the closed state of the nicotinic acetylcholine receptor. *Phys Biol.* **3**(2), pp.147-159.

Benson, D.A., Cavanaugh, M., Clark, K., Karsch-Mizrachi, I., Lipman, D.J., Ostell, J. and Sayers, E.W. 2017. GenBank. *Nucleic Acids Res.* **45**(D1), pp.D37-D42.

Berridge, M.V., Herst, P.M. and Tan, A.S. 2005. Tetrazolium dyes as tools in cell biology: new insights into their cellular reduction. *Biotechnol Annu Rev.* **11**, pp.127-152.

Berry, H., Coquelin, J.P., Gordon, A. and Seymour, D. 1983. Antrafenine, naproxen and placebo in osteoarthritis: a comparative study. *Br J Rheumatol.* **22**(2), pp.89-94.

Bhattacharjee, A., Gan, L. and Kaczmarek, L.K. 2002. Localization of the Slack potassium channel in the rat central nervous system. *J Comp Neurol.* **454**(3), pp.241-254.

Bhattacharjee, A., Joiner, W.J., Wu, M., Yang, Y., Sigworth, F.J. and Kaczmarek, L.K. 2003. Slick (Slo2.1), a rapidly-gating sodium-activated potassium channel inhibited by ATP. *J Neurosci.* **23**(37), pp.11681-11691.

Bhattacharjee, A. and Kaczmarek, L.K. 2005. For K+ channels, Na+ is the new Ca2+. *Trends Neurosci.* **28**(8), pp.422-428.

Biton, B., Sethuramanujam, S., Picchione, K.E., Bhattacharjee, A., Khessibi, N., Chesney, F., Lanneau, C., Curet, O. and Avenet, P. 2012. The antipsychotic drug loxapine is an opener of the sodium-activated potassium channel slack (Slo2.2). *J Pharmacol Exp Ther.* **340**(3), pp.706-715.

Black, K.A., Jin, R., He, S. and Gulbis, J.M. 2021. Changing perspectives on how the permeation pathway through potassium channels is regulated. *J Physiol.* **599**(7), pp.1961-1976.

Bonardi, C.M., Heyne, H.O., Fiannacca, M., Fitzgerald, M.P., Gardella, E., Gunning, B., Olofsson, K., Lesca, G., Verbeek, N., Stamberger, H., Striano, P., Zara, F., Mancardi, M.M., Nava, C., Syrbe, S., Buono, S., Baulac, S., Coppola, A., Weckhuysen, S., Schoonjans, A.S., Ceulemans, B., Sarret, C., Baumgartner, T., Muhle, H., des Portes, V., Toulouse, J., Nougues, M.C., Rossi, M., Demarquay, G., Ville, D., Hirsch, E., Maurey, H., Willems, M., de Bellescize, J., Altuzarra, C.D., Villeneuve, N., Bartolomei, F., Picard, F., Hornemann, F., Koolen, D.A., Kroes, H.Y., Reale, C., Fenger, C.D., Tan, W.H., Dibbens, L., Bearden, D.R., Møller, R.S. and Rubboli, G. 2021. KCNT1-related epilepsies and epileptic encephalopathies: phenotypic and mutational spectrum. *Brain.*

Borlot, F., Abushama, A., Morrison-Levy, N., Jain, P., Puthenveettil Vinayan, K., Abukhalid, M., Aldhalaan, H.M., Almuzaini, H.S., Gulati, S., Hershkovitz, T., Konanki, R., Lingappa, L., Luat, A.F., Shafi, S., Tabarki, B., Thomas, M., Yoganathan, S., Alfadhel, M., Arya, R., Donner, E.J., Ehaideb, S.N., Gowda, V.K., Jain, V., Madaan, P., Myers, K.A., Otsubo, H., Panda, P., Sahu, J.K., Sampaio, L.P.B., Sharma, S., Simard-Tremblay, E., Zak, M. and Whitney, R. 2020. KCNT1-related epilepsy: An international multicenter cohort of 27 pediatric cases. *Epilepsia.* **61**(4), pp.679-692.

Brown, M.R., Kronengold, J., Gazula, V.R., Chen, Y., Strumbos, J.G., Sigworth, F.J., Navaratnam, D. and Kaczmarek, L.K. 2010. Fragile X mental retardation protein controls gating of the sodium-activated potassium channel Slack. *Nat Neurosci.* **13**(7), pp.819-821.

Brown, M.R., Kronengold, J., Gazula, V.R., Spilianakis, C.G., Flavell, R.A., von Hehn, C.A., Bhattacharjee, A. and Kaczmarek, L.K. 2008. Amino-termini isoforms of the Slack

K+ channel, regulated by alternative promoters, differentially modulate rhythmic firing and adaptation. *J Physiol.* **586**(21), pp.5161-5179.

Budelli, G., Geng, Y., Butler, A., Magleby, K.L. and Salkoff, L. 2013. Properties of Slo1 K+ channels with and without the gating ring. *Proc Natl Acad Sci U S A.* **110**(41), pp.16657-16662.

Burbano, L.E., Li, M., Jancovski, N., Jafar-Nejad, P., Richards, K., Sedo, A., Soriano, A., Rollo, B., Jia, L., Gazina, E., Piltz, S., Adikusuma, F., Thomas, P.Q., Rigo, F., Reid, C.A., Maljevic, S. and Petrou, S. 2020. Antisense oligonucleotide therapy for KCNT1 encephalopathy. *bioRxiv.* p2020.2011.2012.379164.

Cataldi, M., Nobili, L., Zara, F., Combi, R., Prato, G., Giacomini, T., Capra, V., De Marco, P., Ferini-Strambi, L. and Mancardi, M.M. 2019. Migrating focal seizures in Autosomal Dominant Sleep-related Hypermotor Epilepsy with KCNT1 mutation. *Seizure.* **67**, pp.57-60.

Chapman, M.L. and VanDongen, A.M. 2005. K channel subconductance levels result from heteromeric pore conformations. *J Gen Physiol.* **126**(2), pp.87-103.

Chapman, M.L., VanDongen, H.M. and VanDongen, A.M. 1997. Activation-dependent subconductance levels in the drk1 K channel suggest a subunit basis for ion permeation and gating. *Biophys J.* **72**(2 Pt 1), pp.708-719.

Chen, H., Kronengold, J., Yan, Y., Gazula, V.R., Brown, M.R., Ma, L., Ferreira, G., Yang, Y., Bhattacharjee, A., Sigworth, F.J., Salkoff, L. and Kaczmarek, L.K. 2009. The N-terminal domain of Slack determines the formation and trafficking of Slick/Slack heteromeric sodium-activated potassium channels. *J Neurosci.* **29**(17), pp.5654-5665.

Chng, J., Wang, T., Nian, R., Lau, A., Hoi, K.M., Ho, S.C., Gagnon, P., Bi, X. and Yang, Y. 2015. Cleavage efficient 2A peptides for high level monoclonal antibody expression in CHO cells. *MAbs.* **7**(2), pp.403-412.

Choo, E.F., Leake, B., Wandel, C., Imamura, H., Wood, A.J., Wilkinson, G.R. and Kim, R.B. 2000. Pharmacological inhibition of P-glycoprotein transport enhances the distribution of HIV-1 protease inhibitors into brain and testes. *Drug Metab Dispos.* **28**(6), pp.655-660.

Coetzee, W.A., Amarillo, Y., Chiu, J., Chow, A., Lau, D., McCormack, T., Moreno, H., Nadal, M.S., Ozaita, A., Pountney, D., Saganich, M., Vega-Saenz de Miera, E. and Rudy, B. 1999. Molecular diversity of K+ channels. *Ann N Y Acad Sci.* **868**, pp.233-285.

Coppola, G., Plouin, P., Chiron, C., Robain, O. and Dulac, O. 1995. Migrating partial seizures in infancy: a malignant disorder with developmental arrest. *Epilepsia.* **36**(10), pp.1017-1024.

Cuello, L.G., Jogini, V., Cortes, D.M. and Perozo, E. 2010. Structural mechanism of C-type inactivation in K(+) channels. *Nature.* **466**(7303), pp.203-208.

Dai, L., Garg, V. and Sanguinetti, M.C. 2010. Activation of Slo2.1 channels by niflumic acid. *J Gen Physiol.* **135**(3), pp.275-295.

Datta, A.N., Michoulas, A., Guella, I., Study, E. and Demos, M. 2019. Two Patients With KCNT1-Related Epilepsy Responding to Phenobarbital and Potassium Bromide. *J Child Neurol.* **34**(12), pp.728-734.

de los Angeles Tejada, M., Jensen, L.J. and Klaerke, D.A. 2012. PIP(2) modulation of Slick and Slack K(+) channels. *Biochem Biophys Res Commun.* **424**(2), pp.208-213.

de Los Angeles Tejada, M., Stolpe, K., Meinild, A.K. and Klaerke, D.A. 2012. Clofilium inhibits Slick and Slack potassium channels. *Biologics.* **6**, pp.465-470.

Derebe, M.G., Sauer, D.B., Zeng, W., Alam, A., Shi, N. and Jiang, Y. 2011. Tuning the ion selectivity of tetrameric cation channels by changing the number of ion binding sites. *Proc Natl Acad Sci U S A.* **108**(2), pp.598-602.

Dilena, R., DiFrancesco, J.C., Soldovieri, M.V., Giacobbe, A., Ambrosino, P., Mosca, I., Galli, M.A., Guez, S., Fumagalli, M., Miceli, F., Cattaneo, D., Darra, F., Gennaro, E., Zara, F., Striano, P., Castellotti, B., Gellera, C., Varesio, C., Veggiotti, P. and Taglialatela, M. 2018. Early Treatment with Quinidine in 2 Patients with Epilepsy of Infancy with Migrating Focal Seizures (EIMFS) Due to Gain-of-Function KCNT1 Mutations: Functional Studies, Clinical Responses, and Critical Issues for Personalized Therapy. *Neurotherapeutics.* **15**(4), pp.1112-1126.

Doyle, D.A., Morais Cabral, J., Pfuetzner, R.A., Kuo, A., Gulbis, J.M., Cohen, S.L., Chait, B.T. and MacKinnon, R. 1998. The structure of the potassium channel: molecular basis of K+ conduction and selectivity. *Science.* **280**(5360), pp.69-77.

Enyedi, P. and Czirják, G. 2010. Molecular background of leak K+ currents: two-pore domain potassium channels. *Physiol Rev.* **90**(2), pp.559-605.

Evely, K.M., Pryce, K.D. and Bhattacharjee, A. 2017. The Phe932Ile mutation in KCNT1 channels associated with severe epilepsy, delayed myelination and leukoencephalopathy produces a loss-of-function channel phenotype. *Neuroscience.* **351**, pp.65-70.

Feng, P., Zhao, L., Guo, F., Zhang, B., Fang, L., Zhan, G., Xu, X., Fang, Q., Liang, Z. and Li, B. 2018. The enhancement of cardiotoxicity that results from inhibiton of CYP 3A4 activity and hERG channel by berberine in combination with statins. *Chem Biol Interact.* **293**, pp.115-123.

Finlayson, K., Witchel, H.J., McCulloch, J. and Sharkey, J. 2004. Acquired QT interval prolongation and HERG: implications for drug discovery and development. *Eur J Pharmacol.* **500**(1-3), pp.129-142.

Fitzgerald, M.P., Fiannacca, M., Smith, D.M., Gertler, T.S., Gunning, B., Syrbe, S., Verbeek, N., Stamberger, H., Weckhuysen, S., Ceulemans, B., Schoonjans, A.S., Rossi, M., Demarquay, G., Lesca, G., Olofsson, K., Koolen, D.A., Hornemann, F., Baulac, S., Rubboli, G., Minks, K.Q., Lee, B., Helbig, I., Dlugos, D., Møller, R.S. and Bearden, D. 2019. Treatment Responsiveness in KCNT1-Related Epilepsy. *Neurotherapeutics.* **16**(3), pp.848-857.

Fleming, M.R., Brown, M.R., Kronengold, J., Zhang, Y., Jenkins, D.P., Barcia, G., Nabbout, R., Bausch, A.E., Ruth, P., Lukowski, R., Navaratnam, D.S. and Kaczmarek, L.K. 2016. Stimulation of Slack K(+) Channels Alters Mass at the Plasma Membrane by Triggering Dissociation of a Phosphatase-Regulatory Complex. *Cell Rep.* **16**(9), pp.2281-2288.

Franceschetti, S., Lavazza, T., Curia, G., Aracri, P., Panzica, F., Sancini, G., Avanzini, G. and Magistretti, J. 2003. Na+-activated K+ current contributes to postexcitatory

hyperpolarization in neocortical intrinsically bursting neurons. *J Neurophysiol.* **89**(4), pp.2101-2111.

Gamper, N., Stockand, J.D. and Shapiro, M.S. 2005. The use of Chinese hamster ovary (CHO) cells in the study of ion channels. *J Pharmacol Toxicol Methods.* **51**(3), pp.177-185.

Gao, H., Boillat, A., Huang, D., Liang, C., Peers, C. and Gamper, N. 2017. Intracellular zinc activates KCNQ channels by reducing their dependence on phosphatidylinositol 4,5-bisphosphate. *Proc Natl Acad Sci U S A.* **114**(31), pp.E6410-E6419.

Garg, P., Gardner, A., Garg, V. and Sanguinetti, M.C. 2013. Structural basis of ion permeation gating in Slo2.1 K+ channels. *J Gen Physiol.* **142**(5), pp.523-542.

Gertler, T.S., Thompson, C.H., Vanoye, C.G., Millichap, J.J. and George, A.L. 2019. Functional consequences of a KCNT1 variant associated with status dystonicus and early-onset infantile encephalopathy. *Ann Clin Transl Neurol.* **6**(9), pp.1606-1615.

Giampieri, R., Prete, M.D., Prochilo, T., Puzzoni, M., Pusceddu, V., Pani, F., Maccaroni, E., Mascia, R., Baleani, M.G., Meletani, T., Berardi, R., Lanzillo, A.M., Mariotti, S., Zaniboni, A., Cascinu, S. and Scartozzi, M. 2017. Off-target effects and clinical outcome in metastatic colorectal cancer patients receiving regorafenib: The TRIBUTE analysis. *Sci Rep.* **7**, p45703.

Giese, M.H., Gardner, A., Hansen, A. and Sanguinetti, M.C. 2017. Molecular mechanisms of Slo2 K+ channel closure. *J Physiol.* **595**(7), pp.2321-2336.

Goldman, D.E. 1943. POTENTIAL, IMPEDANCE, AND RECTIFICATION IN MEMBRANES. *J Gen Physiol.* **27**(1), pp.37-60.

Gonzalez, C., Baez-Nieto, D., Valencia, I., Oyarzun, I., Rojas, P., Naranjo, D. and Latorre, R. 2012. K(+) channels: function-structural overview. *Compr Physiol.* **2**(3), pp.2087-2149.

Griffin, A.M., Kahlig, K.M., Hatch, R.J., Hughes, Z.A., Chapman, M.L., Antonio, B., Marron, B.E., Wittmann, M. and Martinez-Botella, G. 2021. Discovery of the First Orally

Available, Selective KNa1.1 Inhibitor: In Vitro and In Vivo Activity of an Oxadiazole Series. *ACS Medicinal Chemistry Letters.* **12**(4), pp.593-602.

Guntner, A.S., Peyrl, A., Mayr, L., Englinger, B., Berger, W., Slavc, I., Buchberger, W. and Gojo, J. 2020. Cerebrospinal fluid penetration of targeted therapeutics in pediatric brain tumor patients. *Acta Neuropathol Commun.* **8**(1), p78.

Gururaj, S., Palmer, E.E., Sheehan, G.D., Kandula, T., Macintosh, R., Ying, K., Morris, P., Tao, J., Dias, K.R., Zhu, Y., Dinger, M.E., Cowley, M.J., Kirk, E.P., Roscioli, T., Sachdev, R., Duffey, M.E., Bye, A. and Bhattacharjee, A. 2017. A De Novo Mutation in the Sodium-Activated Potassium Channel KCNT2 Alters Ion Selectivity and Causes Epileptic Encephalopathy. *Cell Rep.* **21**(4), pp.926-933.

Hage, T.A. and Salkoff, L. 2012. Sodium-activated potassium channels are functionally coupled to persistent sodium currents. *J Neurosci.* **32**(8), pp.2714-2721.

Heer, F.T., Posson, D.J., Wojtas-Niziurski, W., Nimigean, C.M. and Berneche, S. 2017. Mechanism of activation at the selectivity filter of the KcsA K(+) channel. *Elife.* **6**.

Heginbotham, L., Lu, Z., Abramson, T. and MacKinnon, R. 1994. Mutations in the K+ channel signature sequence. *Biophys J.* **66**(4), pp.1061-1067.

Helliwell, R.M. 2008. Recording hERG potassium currents and assessing the effects of compounds using the whole-cell patch-clamp technique. *Methods Mol Biol.* **491**, pp.279-295.

Heron, S.E., Smith, K.R., Bahlo, M., Nobili, L., Kahana, E., Licchetta, L., Oliver, K.L., Mazarib, A., Afawi, Z., Korczyn, A., Plazzi, G., Petrou, S., Berkovic, S.F., Scheffer, I.E. and Dibbens, L.M. 2012. Missense mutations in the sodium-gated potassium channel gene KCNT1 cause severe autosomal dominant nocturnal frontal lobe epilepsy. *Nat Genet.* **44**(11), pp.1188-1190.

Hibino, H., Inanobe, A., Furutani, K., Murakami, S., Findlay, I. and Kurachi, Y. 2010. Inwardly rectifying potassium channels: their structure, function, and physiological roles. *Physiol Rev.* **90**(1), pp.291-366.

Hille, B. 2001. *Ion Channels of Excitable Membranes. 3rd Edition. Sinauer Associates Inc.* U.S.

Hite, R.K. and MacKinnon, R. 2017. Structural Titration of Slo2.2, a Na(+)-Dependent K(+) Channel. *Cell.* **168**(3), pp.390-399 e311.

Hite, R.K., Tao, X. and MacKinnon, R. 2017. Structural basis for gating the high-conductance Ca(2+)-activated K(+) channel. *Nature.* **541**(7635), pp.52-57.

Hite, R.K., Yuan, P., Li, Z., Hsuing, Y., Walz, T. and MacKinnon, R. 2015. Cryo-electron microscopy structure of the Slo2.2 Na(+)-activated K(+) channel. *Nature.* **527**(7577), pp.198-203.

Hodgkin, A.L. and Katz, B. 1949. The effect of sodium ions on the electrical activity of giant axon of the squid. *J Physiol.* **108**(1), pp.37-77.

Horrigan, F.T. and Aldrich, R.W. 2002. Coupling between voltage sensor activation, Ca2+ binding and channel opening in large conductance (BK) potassium channels. *J Gen Physiol.* **120**(3), pp.267-305.

Huang, F., Wang, X., Ostertag, E.M., Nuwal, T., Huang, B., Jan, Y.N., Basbaum, A.I. and Jan, L.Y. 2013. TMEM16C facilitates Na(+)-activated K+ currents in rat sensory neurons and regulates pain processing. *Nat Neurosci.* **16**(9), pp.1284-1290.

Ikeda, A., Ueda, H., Matsui, K., Iai, M. and Goto, T. 2021. Recurrent pulmonary hemorrhage in juvenile patients with KCNT1 mutation. *Pediatr Int.* **63**(3), pp.352-354.

Inuzuka, L.M., Macedo-Souza, L.I., Della-Ripa, B., Monteiro, F.P., Ramos, L., Kitajima, J.P., Garzon, E. and Kok, F. 2020. Additional observation of a de novo pathogenic variant in KCNT2 leading to epileptic encephalopathy with clinical features of frontal lobe epilepsy. *Brain Dev.* **42**(9), pp.691-695.

Ishii, A., Shioda, M., Okumura, A., Kidokoro, H., Sakauchi, M., Shimada, S., Shimizu, T., Osawa, M., Hirose, S. and Yamamoto, T. 2013. A recurrent KCNT1 mutation in two sporadic cases with malignant migrating partial seizures in infancy. *Gene.* **531**(2), pp.467-471.

Jasial, S., Hu, Y. and Bajorath, J. 2017. How Frequently Are Pan-Assay Interference Compounds Active? Large-Scale Analysis of Screening Data Reveals Diverse Activity Profiles, Low Global Hit Frequency, and Many Consistently Inactive Compounds. *J Med Chem.* **60**(9), pp.3879-3886.

Jensen, M., Borhani, D.W., Lindorff-Larsen, K., Maragakis, P., Jogini, V., Eastwood, M.P., Dror, R.O. and Shaw, D.E. 2010. Principles of conduction and hydrophobic gating in K+ channels. *Proc Natl Acad Sci U S A.* **107**(13), pp.5833-5838.

Jia, Y., Lin, Y., Li, J., Li, M., Zhang, Y., Hou, Y., Liu, A., Zhang, L., Li, L., Xiang, P., Ye, J., Huang, Z. and Wang, Y. 2019. Quinidine Therapy for Lennox-Gastaut Syndrome With KCNT1 Mutation. A Case Report and Literature Review. *Front Neurol.* **10**, p64.

Jia, Z., Yazdani, M., Zhang, G., Cui, J. and Chen, J. 2018. Hydrophobic gating in BK channels. *Nat Commun.* **9**(1), p3408.

Jiang, B., Sun, X., Cao, K. and Wang, R. 2002. Endogenous Kv channels in human embryonic kidney (HEK-293) cells. *Mol Cell Biochem.* **238**(1-2), pp.69-79.

Johnson, M., Zaretskaya, I., Raytselis, Y., Merezhuk, Y., McGinnis, S. and Madden, T.L. 2008. NCBI BLAST: a better web interface. *Nucleic Acids Res.* **36**(Web Server issue), pp.W5-9.

Joiner, W.J., Tang, M.D., Wang, L.Y., Dworetzky, S.I., Boissard, C.G., Gan, L., Gribkoff, V.K. and Kaczmarek, L.K. 1998. Formation of intermediate-conductance calcium-activated potassium channels by interaction of Slack and Slo subunits. *Nat Neurosci.* **1**(6), pp.462-469.

Kaczmarek, L.K. 2013. Slack, Slick and Sodium-Activated Potassium Channels. *ISRN Neurosci.* **2013**(2013).

Kameyama, M., Kakei, M., Sato, R., Shibasaki, T., Matsuda, H. and Irisawa, H. 1984. Intracellular Na+ activates a K+ channel in mammalian cardiac cells. *Nature.* **309**(5966), pp.354-356.

Kamiya, K., Niwa, R., Mitcheson, J.S. and Sanguinetti, M.C. 2006. Molecular determinants of HERG channel block. *Mol Pharmacol.* **69**(5), pp.1709-1716.

Kawasaki, Y., Kuki, I., Ehara, E., Murakami, Y., Okazaki, S., Kawawaki, H., Hara, M., Watanabe, Y., Kishimoto, S., Suda, K., Saitsu, H. and Matsumoto, N. 2017. Three Cases of KCNT1 Mutations: Malignant Migrating Partial Seizures in Infancy with Massive Systemic to Pulmonary Collateral Arteries. *J Pediatr.* **191**, pp.270-274.

Khafizov, K., Perez, C., Koshy, C., Quick, M., Fendler, K., Ziegler, C. and Forrest, L.R. 2012. Investigation of the sodium-binding sites in the sodium-coupled betaine transporter BetP. *Proc Natl Acad Sci U S A.* **109**(44), pp.E3035-3044.

Kim, G.E. and Kaczmarek, L.K. 2014. Emerging role of the KCNT1 Slack channel in intellectual disability. *Front Cell Neurosci.* **8**, p209.

Kim, G.E., Kronengold, J., Barcia, G., Quraishi, I.H., Martin, H.C., Blair, E., Taylor, J.C., Dulac, O., Colleaux, L., Nabbout, R. and Kaczmarek, L.K. 2014. Human slack potassium channel mutations increase positive cooperativity between individual channels. *Cell Rep.* **9**(5), pp.1661-1672.

Kohli, U., Ravishankar, C. and Nordli, D. 2020. Cardiac phenotypic spectrum of KCNT1 mutations. *Cardiol Young.* pp.1-5.

Kopec, W., Kopfer, D.A., Vickery, O.N., Bondarenko, A.S., Jansen, T.L.C., de Groot, B.L. and Zachariae, U. 2018. Direct knock-on of desolvated ions governs strict ion selectivity in K(+) channels. *Nat Chem.* **10**(8), pp.813-820.

Kopec, W., Rothberg, B.S. and de Groot, B.L. 2019. Molecular mechanism of a potassium channel gating through activation gate-selectivity filter coupling. *Nat Commun.* **10**(1), p5366.

Kopfer, D.A., Song, C., Gruene, T., Sheldrick, G.M., Zachariae, U. and de Groot, B.L. 2014. Ion permeation in K(+) channels occurs by direct Coulomb knock-on. *Science.* **346**(6207), pp.352-355.

Kort, A., Durmus, S., Sparidans, R.W., Wagenaar, E., Beijnen, J.H. and Schinkel, A.H. 2015. Brain and Testis Accumulation of Regorafenib is Restricted by Breast Cancer Resistance Protein (BCRP/ABCG2) and P-glycoprotein (P-GP/ABCB1). *Pharm Res.* **32**(7), pp.2205-2216.

Krishnamoorthy, S.K., Relias, V., Sebastian, S., Jayaraman, V. and Saif, M.W. 2015. Management of regorafenib-related toxicities: a review. *Therap Adv Gastroenterol.* **8**(5), pp.285-297.

Labro, A.J., Cortes, D.M., Tilegenova, C. and Cuello, L.G. 2018. Inverted allosteric coupling between activation and inactivation gates in K. *Proc Natl Acad Sci U S A.* **115**(21), pp.5426-5431.

Latorre, R., Castillo, K., Carrasquel-Ursulaez, W., Sepulveda, R.V., Gonzalez-Nilo, F., Gonzalez, C. and Alvarez, O. 2017. Molecular Determinants of BK Channel Functional Diversity and Functioning. *Physiol Rev.* **97**(1), pp.39-87.

Lee, J.H., Kang, M., Park, S., Perez-Flores, M.C., Zhang, X.D., Wang, W., Gratton, M.A., Chiamvimonvat, N. and Yamoah, E.N. 2019. The local translation of KNa in dendritic projections of auditory neurons and the roles of KNa in the transition from hidden to overt hearing loss. *Aging (Albany NY).* **11**(23), pp.11541-11564.

Lesage, F. and Lazdunski, M. 2000. Molecular and functional properties of two-pore-domain potassium channels. *Am J Physiol Renal Physiol.* **279**(5), pp.F793-801.

Li, P., Halabi, C.M., Stewart, R., Butler, A., Brown, B., Xia, X., Santi, C., England, S., Ferreira, J., Mecham, R.P. and Salkoff, L. 2019. Sodium-activated potassium channels moderate excitability in vascular smooth muscle. *J Physiol.* **597**(20), pp.5093-5108.

Li, Y., Sato, T. and Arita, M. 1999. Bepridil blunts the shortening of action potential duration caused by metabolic inhibition via blockade of ATP-sensitive K(+) channels and Na(+)-activated K(+) channels. *J Pharmacol Exp Ther.* **291**(2), pp.562-568.

Lin, X., Li, X. and Lin, X. 2020. A Review on Applications of Computational Methods in Drug Screening and Design. *Molecules.* **25**(6).

Liu, X. and Stan Leung, L. 2004. Sodium-activated potassium conductance participates in the depolarizing afterpotential following a single action potential in rat hippocampal CA1 pyramidal cells. *Brain Res.* **1023**(2), pp.185-192.

Liu, Z., Chen, O., Wall, J.B.J., Zheng, M., Zhou, Y., Wang, L., Ruth Vaseghi, H., Qian, L. and Liu, J. 2017. Systematic comparison of 2A peptides for cloning multi-genes in a polycistronic vector. *Sci Rep.* **7**(1), p2193.

Lolicato, M., Arrigoni, C., Mori, T., Sekioka, Y., Bryant, C., Clark, K.A. and Minor, D.L. 2017. K2P2.1(TREK-1):activator complexes reveal a cryptic selectivity filter binding site. *Nature.* **547**(7663), pp.364-368.

Lu, R., Bausch, A.E., Kallenborn-Gerhardt, W., Stoetzer, C., Debruin, N., Ruth, P., Geisslinger, G., Leffler, A., Lukowski, R. and Schmidtko, A. 2015. Slack channels expressed in sensory neurons control neuropathic pain in mice. *J Neurosci.* **35**(3), pp.1125-1135.

Lu, T., Ting, A.Y., Mainland, J., Jan, L.Y., Schultz, P.G. and Yang, J. 2001. Probing ion permeation and gating in a K+ channel with backbone mutations in the selectivity filter. *Nat Neurosci.* **4**(3), pp.239-246.

Macdonald, L.C., Kim, R.Y., Kurata, H.T. and Fedida, D. 2018. Probing the molecular basis of hERG drug block with unnatural amino acids. *Sci Rep.* **8**(1), p289.

Madaan, P., Jauhari, P., Gupta, A., Chakrabarty, B. and Gulati, S. 2018. A quinidine non responsive novel KCNT1 mutation in an Indian infant with epilepsy of infancy with migrating focal seizures. *Brain Dev.* **40**(3), pp.229-232.

Mao, X., Bruneau, N., Gao, Q., Becq, H., Jia, Z., Xi, H., Shu, L., Wang, H., Szepetowski, P. and Aniksztejn, L. 2020. The Epilepsy of Infancy With Migrating Focal Seizures: Identification of de novo Mutations of the KCNT2 Gene That Exert Inhibitory Effects on the Corresponding Heteromeric KNa 1.1/KNa 1.2 Potassium Channel. *Front Cell Neurosci.* **14**, p1.

Martin, H.C., Kim, G.E., Pagnamenta, A.T., Murakami, Y., Carvill, G.L., Meyer, E., Copley, R.R., Rimmer, A., Barcia, G., Fleming, M.R., Kronengold, J., Brown, M.R., Hudspith, K.A., Broxholme, J., Kanapin, A., Cazier, J.B., Kinoshita, T., Nabbout, R., Bentley, D., McVean, G., Heavin, S., Zaiwalla, Z., McShane, T., Mefford, H.C., Shears, D., Stewart, H., Kurian, M.A., Scheffer, I.E., Blair, E., Donnelly, P., Kaczmarek, L.K., Taylor, J.C. and Consortium, W. 2014. Clinical whole-genome sequencing in severe

early-onset epilepsy reveals new genes and improves molecular diagnosis. *Hum Mol Genet.* **23**(12), pp.3200-3211.

Martinez-Espinosa, P.L., Wu, J., Yang, C., Gonzalez-Perez, V., Zhou, H., Liang, H., Xia, X.M. and Lingle, C.J. 2015. Knockout of Slo2.2 enhances itch, abolishes KNa current, and increases action potential firing frequency in DRG neurons. *Elife.* **4**.

McTague, A., Nair, U., Malhotra, S., Meyer, E., Trump, N., Gazina, E.V., Papandreou, A., Ngoh, A., Ackermann, S., Ambegaonkar, G., Appleton, R., Desurkar, A., Eltze, C., Kneen, R., Kumar, A.V., Lascelles, K., Montgomery, T., Ramesh, V., Samanta, R., Scott, R.H., Tan, J., Whitehouse, W., Poduri, A., Scheffer, I.E., Chong, W.K.K., Cross, J.H., Topf, M., Petrou, S. and Kurian, M.A. 2018. Clinical and molecular characterization of KCNT1-related severe early-onset epilepsy. *Neurology.* **90**(1), pp.e55-e66.

Meisel, E., Dvir, M., Haitin, Y., Giladi, M., Peretz, A. and Attali, B. 2012. KCNQ1 channels do not undergo concerted but sequential gating transitions in both the absence and the presence of KCNE1 protein. *J Biol Chem.* **287**(41), pp.34212-34224.

Mercier, J. and Voutsadakis, I.A. 2017. A Systematic Review and Meta-analysis of Retrospective Series of Regorafenib for Treatment of Metastatic Colorectal Cancer. *Anticancer Res.* **37**(11), pp.5925-5934.

Mikati, M.A., Jiang, Y.H., Carboni, M., Shashi, V., Petrovski, S., Spillmann, R., Milligan, C.J., Li, M., Grefe, A., McConkie, A., Berkovic, S., Scheffer, I., Mullen, S., Bonner, M., Petrou, S. and Goldstein, D. 2015. Quinidine in the treatment of KCNT1-positive epilepsies. *Ann Neurol.* **78**(6), pp.995-999.

Milligan, C.J., Li, M., Gazina, E.V., Heron, S.E., Nair, U., Trager, C., Reid, C.A., Venkat, A., Younkin, D.P., Dlugos, D.J., Petrovski, S., Goldstein, D.B., Dibbens, L.M., Scheffer, I.E., Berkovic, S.F. and Petrou, S. 2014. KCNT1 gain of function in 2 epilepsy phenotypes is reversed by quinidine. *Ann Neurol.* **75**(4), pp.581-590.

Mironenko, A., Zachariae, U., de Groot, B.L. and Kopec, W. 2021. The Persistent Question of Potassium Channel Permeation Mechanisms. *J Mol Biol.* **433**(17), p167002.

Morais-Cabral, J.H., Zhou, Y. and MacKinnon, R. 2001. Energetic optimization of ion conduction rate by the K+ selectivity filter. *Nature.* **414**(6859), pp.37-42.

Mullen, S.A., Carney, P.W., Roten, A., Ching, M., Lightfoot, P.A., Churilov, L., Nair, U., Li, M., Berkovic, S.F., Petrou, S. and Scheffer, I.E. 2018. Precision therapy for epilepsy due to KCNT1 mutations: A randomized trial of oral quinidine. *Neurology.* **90**(1), pp.e67-e72.

Musarrat, F., Chouljenko, V., Dahal, A., Nabi, R., Chouljenko, T., Jois, S.D. and Kousoulas, K.G. 2020. The anti-HIV drug nelfinavir mesylate (Viracept) is a potent inhibitor of cell fusion caused by the SARSCoV-2 spike (S) glycoprotein warranting further evaluation as an antiviral against COVID-19 infections. *J Med Virol.* **92**(10), pp.2087-2095.

Møller, R.S., Heron, S.E., Larsen, L.H., Lim, C.X., Ricos, M.G., Bayly, M.A., van Kempen, M.J., Klinkenberg, S., Andrews, I., Kelley, K., Ronen, G.M., Callen, D., McMahon, J.M., Yendle, S.C., Carvill, G.L., Mefford, H.C., Nabbout, R., Poduri, A., Striano, P., Baglietto, M.G., Zara, F., Smith, N.J., Pridmore, C., Gardella, E., Nikanorova, M., Dahl, H.A., Gellert, P., Scheffer, I.E., Gunning, B., Kragh-Olsen, B. and Dibbens, L.M. 2015. Mutations in KCNT1 cause a spectrum of focal epilepsies. *Epilepsia.* **56**(9), pp.e114-120.

Nanou, E., Kyriakatos, A., Bhattacharjee, A., Kaczmarek, L.K., Paratcha, G. and El Manira, A. 2008. Na+-mediated coupling between AMPA receptors and KNa channels shapes synaptic transmission. *Proc Natl Acad Sci U S A.* **105**(52), pp.20941-20946.

Nematian-Ardestani, E., Abd-Wahab, F., Chatelain, F.C., Sun, H., Schewe, M., Baukrowitz, T. and Tucker, S.J. 2020. Selectivity filter instability dominates the low intrinsic activity of the TWIK-1 K2P K. *J Biol Chem.* **295**(2), pp.610-618.

Niu, L.G., Liu, P., Wang, Z.W. and Chen, B. 2020. Slo2 potassium channel function depends on RNA editing-regulated expression of a SCYL1 protein. *Elife.* **9**.

Numis, A.L., Nair, U., Datta, A.N., Sands, T.T., Oldham, M.S., Patel, A., Li, M., Gazina, E., Petrou, S. and Cilio, M.R. 2018. Lack of response to quinidine in KCNT1-related neonatal epilepsy. *Epilepsia.* **59**(10), pp.1889-1898.

Nuwer, M.O., Picchione, K.E. and Bhattacharjee, A. 2010. PKA-induced internalization of slack KNa channels produces dorsal root ganglion neuron hyperexcitability. *J Neurosci.* **30**(42), pp.14165-14172.

Ochs, H.R., Greenblatt, D.J., Lloyd, B.L., Woo, E., Sonntag, M. and Smith, T.W. 1980. Entry of quinidine into cerebrospinal fluid. *Am Heart J.* **100**(3), pp.341-346.

Ohba, C., Kato, M., Takahashi, N., Osaka, H., Shiihara, T., Tohyama, J., Nabatame, S., Azuma, J., Fujii, Y., Hara, M., Tsurusawa, R., Inoue, T., Ogata, R., Watanabe, Y., Togashi, N., Kodera, H., Nakashima, M., Tsurusaki, Y., Miyake, N., Tanaka, F., Saitsu, H. and Matsumoto, N. 2015. De novo KCNT1 mutations in early-onset epileptic encephalopathy. *Epilepsia.* **56**(9), pp.e121-128.

Oster, C., Hendriks, K., Kopec, W., Chevelkov, V., Shi, C., Michl, D., Lange, S., Sun, H., de Groot, B.L. and Lange, A. 2019. The conduction pathway of potassium channels is water free under physiological conditions. *Sci Adv.* **5**(7), peaaw6756.

Passey, C.C., Erramouspe, J., Castellanos, P., O'Donnell, E.C. and Denton, D.M. 2019. Concurrent Quinidine and Phenobarbital in the Treatment of a Patient with 2 KCNT1 Mutations. *Curr Ther Res Clin Exp.* **90**, pp.106-108.

Patil, A.A., Vinayan, K.P. and Roy, A.G. 2019. Two South Indian Children with KCNT1-Related Malignant Migrating Focal Seizures of Infancy - Clinical Characteristics and Outcome of Targeted Treatment with Quinidine. *Ann Indian Acad Neurol.* **22**(3), pp.311-315.

Paul, A.A., Witchel, H.J. and Hancox, J.C. 2002. Inhibition of the current of heterologously expressed HERG potassium channels by flecainide and comparison with quinidine, propafenone and lignocaine. *Br J Pharmacol.* **136**(5), pp.717-729.

Perry, M., de Groot, M.J., Helliwell, R., Leishman, D., Tristani-Firouzi, M., Sanguinetti, M.C. and Mitcheson, J. 2004. Structural determinants of HERG channel block by clofilium and ibutilide. *Mol Pharmacol.* **66**(2), pp.240-249.

Piovesan, A., Pelleri, M.C., Antonaros, F., Strippoli, P., Caracausi, M. and Vitale, L. 2019. On the length, weight and GC content of the human genome. *BMC Res Notes.* **12**(1), p106.

Quraishi, I.H., Mercier, M.R., McClure, H., Couture, R.L., Schwartz, M.L., Lukowski, R., Ruth, P. and Kaczmarek, L.K. 2020. Impaired motor skill learning and altered seizure susceptibility in mice with loss or gain of function of the Kcnt1 gene encoding Slack (K. *Sci Rep.* **10**(1), p3213.

Quraishi, I.H., Stern, S., Mangan, K.P., Zhang, Y., Ali, S.R., Mercier, M.R., Marchetto, M.C., McLachlan, M.J., Jones, E.M., Gage, F.H. and Kaczmarek, L.K. 2019. An Epilepsy-Associated KCNT1 Mutation Enhances Excitability of Human iPSC-Derived Neurons by Increasing Slack KNa Currents. *J Neurosci.* **39**(37), pp.7438-7449.

Reijntjes, D.O.J., Lee, J.H., Park, S., Schubert, N.M.A., van Tuinen, M., Vijayakumar, S., Jones, T.A., Jones, S.M., Gratton, M.A., Xia, X.M., Yamoah, E.N. and Pyott, S.J. 2019. Sodium-activated potassium channels shape peripheral auditory function and activity of the primary auditory neurons in mice. *Sci Rep.* **9**(1), p2573.

Rizzi, S., Knaus, H.G. and Schwarzer, C. 2016. Differential distribution of the sodium-activated potassium channels slick and slack in mouse brain. *J Comp Neurol.* **524**(10), pp.2093-2116.

Rizzo, F., Ambrosino, P., Guacci, A., Chetta, M., Marchese, G., Rocco, T., Soldovieri, M.V., Manocchio, L., Mosca, I., Casara, G., Vecchi, M., Taglialatela, M., Coppola, G. and Weisz, A. 2016. Characterization of two de novoKCNT1 mutations in children with malignant migrating partial seizures in infancy. *Mol Cell Neurosci.* **72**, pp.54-63.

Roessler, H.I., Knoers, N., van Haelst, M.M. and van Haaften, G. 2021. Drug Repurposing for Rare Diseases. *Trends Pharmacol Sci.* **42**(4), pp.255-267.

Sachyani, D., Dvir, M., Strulovich, R., Tria, G., Tobelaim, W., Peretz, A., Pongs, O., Svergun, D., Attali, B. and Hirsch, J.A. 2014. Structural basis of a Kv7.1 potassium channel gating module: studies of the intracellular c-terminal domain in complex with calmodulin. *Structure.* **22**(11), pp.1582-1594.

Sack, J.T., Shamotienko, O. and Dolly, J.O. 2008. How to validate a heteromeric ion channel drug target: assessing proper expression of concatenated subunits. *J Gen Physiol.* **131**(5), pp.415-420.

Salkoff, L., Butler, A., Ferreira, G., Santi, C. and Wei, A. 2006. High-conductance potassium channels of the SLO family. *Nat Rev Neurosci.* **7**(12), pp.921-931.

Santi, C.M., Ferreira, G., Yang, B., Gazula, V.R., Butler, A., Wei, A., Kaczmarek, L.K. and Salkoff, L. 2006. Opposite regulation of Slick and Slack K+ channels by neuromodulators. *J Neurosci.* **26**(19), pp.5059-5068.

Schewe, M., Nematian-Ardestani, E., Sun, H., Musinszki, M., Cordeiro, S., Bucci, G., de Groot, B.L., Tucker, S.J., Rapedius, M. and Baukrowitz, T. 2016. A Non-canonical Voltage-Sensing Mechanism Controls Gating in K2P K(+) Channels. *Cell.* **164**(5), pp.937-949.

Schewe, M., Sun, H., Mert, U., Mackenzie, A., Pike, A.C.W., Schulz, F., Constantin, C., Vowinkel, K.S., Conrad, L.J., Kiper, A.K., Gonzalez, W., Musinszki, M., Tegtmeier, M., Pryde, D.C., Belabed, H., Nazare, M., de Groot, B.L., Decher, N., Fakler, B., Carpenter, E.P., Tucker, S.J. and Baukrowitz, T. 2019. A pharmacological master key mechanism that unlocks the selectivity filter gate in K(+) channels. *Science.* **363**(6429), pp.875-880.

Schmiedl, S., Peters, D., Schmalz, O., Mielke, A., Rossmanith, T., Diop, S., Piefke, M., Thurmann, P. and Schmidtko, A. 2019. Loxapine for Treatment of Patients With Refractory, Chemotherapy-Induced Neuropathic Pain: A Prematurely Terminated Pilot Study Showing Efficacy But Limited Tolerability. *Front Pharmacol.* **10**, p838.

Shen, M.J. and Zipes, D.P. 2014. Role of the autonomic nervous system in modulating cardiac arrhythmias. *Circ Res.* **114**(6), pp.1004-1021.

Shi, N., Zeng, W., Ye, S., Li, Y. and Jiang, Y. 2011. Crucial points within the pore as determinants of K(+) channel conductance and gating. *J Mol Biol.* **411**(1), pp.27-35.

Shore, A.N., Colombo, S., Tobin, W.F., Petri, S., Cullen, E.R., Dominguez, S., Bostick, C.D., Beaumont, M.A., Williams, D., Khodagholy, D., Yang, M., Lutz, C.M., Peng, Y., Gelinas, J.N., Goldstein, D.B., Boland, M.J., Frankel, W.N. and Weston, M.C. 2020. Reduced GABAergic Neuron Excitability, Altered Synaptic Connectivity, and Seizures in a KCNT1 Gain-of-Function Mouse Model of Childhood Epilepsy. *Cell Rep.* **33**(4), p108303.

Snyders, D.J. and Yeola, S.W. 1995. Determinants of antiarrhythmic drug action. Electrostatic and hydrophobic components of block of the human cardiac hKv1.5 channel. *Circ Res.* **77**(3), pp.575-583.

Sokolov, M.V., Shamotienko, O., Dhochartaigh, S.N., Sack, J.T. and Dolly, J.O. 2007. Concatemers of brain Kv1 channel alpha subunits that give similar K+ currents yield pharmacologically distinguishable heteromers. *Neuropharmacology.* **53**(2), pp.272-282.

Spitznagel, B.D., Mishra, N.M., Qunies, A.M., Prael, F.J., 3rd, Du, Y., Kozek, K.A., Lazarenko, R.M., Denton, J.S., Emmitte, K.A. and Weaver, C.D. 2020. VU0606170, a Selective Slack Channels Inhibitor, Decreases Calcium Oscillations in Cultured Cortical Neurons. *ACS Chem Neurosci.* **11**(21), pp.3658-3671.

Steinbach, J.H. and Akk, G. 2011. Use of concatemers of ligand-gated ion channel subunits to study mechanisms of steroid potentiation. *Anesthesiology.* **115**(6), pp.1328-1337.

Suzuki, T., Hansen, A. and Sanguinetti, M.C. 2016. Hydrophobic interactions between the S5 segment and the pore helix stabilizes the closed state of Slo2.1 potassium channels. *Biochim Biophys Acta.* **1858**(4), pp.783-792.

Takase, C., Shirai, K., Matsumura, Y., Watanabe, T., Watanabe, A., Hirasawa-Inoue, A., Mizuguchi, T., Matsumoto, N., Sugai, K. and Hayashi, M. 2020. KCNT1-positive epilepsy of infancy with migrating focal seizures successfully treated with nonnarcotic antitussive drugs after treatment failure with quinidine: A case report. *Brain Dev.* **42**(8), pp.607-611.

Tamsett, T.J., Picchione, K.E. and Bhattacharjee, A. 2009. NAD+ activates KNa channels in dorsal root ganglion neurons. *J Neurosci.* **29**(16), pp.5127-5134.

Tang, Q.Y., Zhang, F.F., Xu, J., Wang, R., Chen, J., Logothetis, D.E. and Zhang, Z. 2016. Epilepsy-Related Slack Channel Mutants Lead to Channel Over-Activity by Two Different Mechanisms. *Cell Rep.* **14**(1), pp.129-139.

Tao, X., Hite, R.K. and MacKinnon, R. 2017. Cryo-EM structure of the open high-conductance Ca(2+)-activated K(+) channel. *Nature.* **541**(7635), pp.46-51.

Tejada, M.A., Hashem, N., Calloe, K. and Klaerke, D.A. 2017. Heteromeric Slick/Slack K+ channels show graded sensitivity to cell volume changes. *PLoS One.* **12**(2), pe0169914.

Thomson, S.J., Hansen, A. and Sanguinetti, M.C. 2015. Identification of the Intracellular Na+ Sensor in Slo2.1 Potassium Channels. *J Biol Chem.* **290**(23), pp.14528-14535.

Vanderver, A., Simons, C., Schmidt, J.L., Pearl, P.L., Bloom, M., Lavenstein, B., Miller, D., Grimmond, S.M. and Taft, R.J. 2014. Identification of a novel de novo p.Phe932Ile KCNT1 mutation in a patient with leukoencephalopathy and severe epilepsy. *Pediatr Neurol.* **50**(1), pp.112-114.

VanDongen, A.M. 2004. K channel gating by an affinity-switching selectivity filter. *Proc Natl Acad Sci U S A.* **101**(9), pp.3248-3252.

Villa, C. and Combi, R. 2016. Potassium Channels and Human Epileptic Phenotypes: An Updated Overview. *Front Cell Neurosci.* **10**, p81.

Wacker, S.J., Jurkowski, W., Simmons, K.J., Fishwick, C.W., Johnson, A.P., Madge, D., Lindahl, E., Rolland, J.F. and de Groot, B.L. 2012. Identification of selective inhibitors of the potassium channel Kv1.1-1.2((3)) by high-throughput virtual screening and automated patch clamp. *ChemMedChem.* **7**(10), pp.1775-1783.

Wang, W. and MacKinnon, R. 2017. Cryo-EM Structure of the Open Human Ether-à-go-go-Related K. *Cell.* **169**(3), pp.422-430.e410.

Weerachayaphorn, J. and Pajor, A.M. 2008. Threonine-509 is a determinant of apparent affinity for both substrate and cations in the human Na+/dicarboxylate cotransporter. *Biochemistry.* **47**(3), pp.1087-1093.

Whorton, M.R. and MacKinnon, R. 2011. Crystal structure of the mammalian GIRK2 K+ channel and gating regulation by G proteins, PIP2, and sodium. *Cell.* **147**(1), pp.199-208.

Wilkens, C.M. and Aldrich, R.W. 2006. State-independent block of BK channels by an intracellular quaternary ammonium. *J Gen Physiol.* **128**(3), pp.347-364.

Wimmers, S., Bauer, C.K. and Schwarz, J.R. 2002. Biophysical properties of heteromultimeric erg K+ channels. *Pflugers Arch.* **445**(3), pp.423-430.

Wishart, D.S., Knox, C., Guo, A.C., Shrivastava, S., Hassanali, M., Stothard, P., Chang, Z. and Woolsey, J. 2006. DrugBank: a comprehensive resource for in silico drug discovery and exploration. *Nucleic Acids Res.* **34**(Database issue), pp.D668-672.

Witchel, H.J., Milnes, J.T., Mitcheson, J.S. and Hancox, J.C. 2002. Troubleshooting problems with in vitro screening of drugs for QT interval prolongation using HERG K+ channels expressed in mammalian cell lines and Xenopus oocytes. *J Pharmacol Toxicol Methods.* **48**(2), pp.65-80.

Wu, W., Gardner, A. and Sanguinetti, M.C. 2015. Concatenated hERG1 tetramers reveal stoichiometry of altered channel gating by RPR-260243. *Mol Pharmacol.* **87**(3), pp.401-409.

Wu, Y., Fan, Y., Dong, D., Dong, X., Hu, Y., Shi, Y., Jing, J. and Li, E. 2020. Efficacy and safety of regorafenib as beyond second-line therapy in patients with metastatic colorectal cancer: an adjusted indirect meta-analysis and systematic review. *Ther Adv Med Oncol.* **12**, p1758835920940932.

Yamashita, A., Singh, S.K., Kawate, T., Jin, Y. and Gouaux, E. 2005. Crystal structure of a bacterial homologue of Na+/Cl--dependent neurotransmitter transporters. *Nature.* **437**(7056), pp.215-223.

Yang, B., Desai, R. and Kaczmarek, L.K. 2007. Slack and Slick K(Na) channels regulate the accuracy of timing of auditory neurons. *J Neurosci.* **27**(10), pp.2617-2627.

Yang, B., Gribkoff, V.K., Pan, J., Damagnez, V., Dworetzky, S.I., Boissard, C.G., Bhattacharjee, A., Yan, Y., Sigworth, F.J. and Kaczmarek, L.K. 2006. Pharmacological activation and inhibition of Slack (Slo2.2) channels. *Neuropharmacology.* **51**(4), pp.896-906.

Yang, B.F., Xu, D.H., Xu, C.Q., Li, Z., Du, Z.M., Wang, H.Z. and Dong, D.L. 2004. Inactivation gating determines drug potency: a common mechanism for drug blockade of HERG channels. *Acta Pharmacol Sin.* **25**(5), pp.554-560.

Yellen, G. 1998. The moving parts of voltage-gated ion channels. *Q Rev Biophys.* **31**(3), pp.239-295.

Yoshitomi, S., Takahashi, Y., Yamaguchi, T., Oboshi, T., Horino, A., Ikeda, H., Imai, K., Okanishi, T., Nakashima, M., Saitsu, H., Matsumoto, N., Yoshimoto, J., Fujita, T., Ishii, A., Hirose, S. and Inoue, Y. 2019. Quinidine therapy and therapeutic drug monitoring in four patients with KCNT1 mutations. *Epileptic Disord.* **21**(1), pp.48-54.

Yu, S.P. and Kerchner, G.A. 1998. Endogenous voltage-gated potassium channels in human embryonic kidney (HEK293) cells. *J Neurosci Res.* **52**(5), pp.612-617.

Yu, W. and MacKerell, A.D., Jr. 2017. Computer-Aided Drug Design Methods. *Methods Mol Biol.* **1520**, pp.85-106.

Yuan, A., Santi, C.M., Wei, A., Wang, Z.W., Pollak, K., Nonet, M., Kaczmarek, L., Crowder, C.M. and Salkoff, L. 2003. The sodium-activated potassium channel is encoded by a member of the Slo gene family. *Neuron.* **37**(5), pp.765-773.

Zagotta, W.N., Hoshi, T. and Aldrich, R.W. 1990. Restoration of inactivation in mutants of Shaker potassium channels by a peptide derived from ShB. *Science.* **250**(4980), pp.568-571.

Zeiner, P.S., Kinzig, M., Dive, I., Maurer, G.D., Filipski, K., Harter, P.N., Senft, C., Bahr, O., Hattingen, E., Steinbach, J.P., Sorgel, F., Voss, M., Steidl, E. and Ronellenfitsch, M.W. 2019. Regorafenib CSF Penetration, Efficacy, and MRI Patterns in Recurrent Malignant Glioma Patients. *J Clin Med.* **8**(12).

Zhang, Y., Brown, M.R., Hyland, C., Chen, Y., Kronengold, J., Fleming, M.R., Kohn, A.B., Moroz, L.L. and Kaczmarek, L.K. 2012. Regulation of neuronal excitability by interaction of fragile X mental retardation protein with slack potassium channels. *J Neurosci.* **32**(44), pp.15318-15327.

Zhang, Z., Rosenhouse-Dantsker, A., Tang, Q.Y., Noskov, S. and Logothetis, D.E. 2010. The RCK2 domain uses a coordination site present in Kir channels to confer sodium sensitivity to Slo2.2 channels. *J Neurosci.* **30**(22), pp.7554-7562.

Zhou, Y. and Lingle, C.J. 2014. Paxilline inhibits BK channels by an almost exclusively closed-channel block mechanism. *J Gen Physiol.* **144**(5), pp.415-440.

Zhou, Y. and MacKinnon, R. 2004. Ion binding affinity in the cavity of the KcsA potassium channel. *Biochemistry.* **43**(17), pp.4978-4982.

Zhou, Y., Morais-Cabral, J.H., Kaufman, A. and MacKinnon, R. 2001. Chemistry of ion coordination and hydration revealed by a K+ channel-Fab complex at 2.0 A resolution. *Nature.* **414**(6859), pp.43-48.

Zhou, Y., Zeng, X.H. and Lingle, C.J. 2012. Barium ions selectively activate BK channels via the Ca2+-bowl site. *Proc Natl Acad Sci U S A.* **109**(28), pp.11413-11418.

Zhu, F. and Hummer, G. 2012. Drying transition in the hydrophobic gate of the GLIC channel blocks ion conduction. *Biophys J.* **103**(2), pp.219-227.